ELECTRICAL ENGINEERING SERIES

Electrochemical Components

Marie-Cécile Péra, Daniel Hissel
Hamid Gualous and Christophe Turpin

ISTE WILEY

Electrochemical Components

Electrochemical Components

Marie-Cécile Péra
Daniel Hissel
Hamid Gualous
Christophe Turpin

Series Editor
Bernard Multon

ISTE

WILEY

First published 2013 in Great Britain and the United States by ISTE Ltd and John Wiley & Sons, Inc.

ISTE Ltd
27-37 St George's Road
London SW19 4EU
UK

www.iste.co.uk

John Wiley & Sons, Inc.
111 River Street
Hoboken, NJ 07030
USA

www.wiley.com

Library of Congress Control Number: 2013941766

British Library Cataloguing-in-Publication Data
A CIP record for this book is available from the British Library
ISBN: 978-1-84821-401-9

Printed and bound in Great Britain by CPI Group (UK) Ltd., Croydon, Surrey CR0 4YY

Table of Contents

Preface

"You can't store electricity! …"

Many of us have heard this phrase before, or indeed hear it regularly said still. At present, when there is a great deal of debate and reflection about the necessity of making a switch in our energy provision, this phrase is often even used as an excuse for the holders of one vision or another of that transition. Indeed, if electricity cannot be stored, we must at all times be able to balance supply and demand, and therefore we need to be able, to control either supply … or demand – or indeed both – in a highly dynamic way.

Yet this phrase is not entirely true. In fact, everyone knows this. On a daily basis, we all use objects, tools or mobile systems using an electrical supply (mobile telephones, laptop computers, portable electric tools, electrical vehicles, etc.). Thus, *de facto*, we know that electricity can be stored. Nevertheless, it is relatively difficult to store it, more difficult to store it over long periods of time, and more difficult still to store it in extreme environmental conditions.

Nevertheless, almost paradoxically, there are many technological solutions that can be envisaged in terms of electricity storage. In particular, we can cite electrochemical or electrostatic storage means (electrochemical accumulators, supercapacitors, etc.), but also magnetic means of energy storage (such as superconductors) or mechanical ones (such as flywheels). We can even envisage storing electricity by means of another energy vector, such as hydrogen. The purpose of this book is not to give an overview of all these means for the storage of electricity; rather, our aim here is to devote our attention to those methods of storage which are commonly used in hybrid systems, whether intended for stationary applications or use in transport.

Thus, after an introductory chapter – which cannot, however, be viewed as a complete *ab initio* introduction to the subject – reviewing the basics of

electrochemistry, Chapter 2 is given over to the storage of electricity in the form of hydrogen. While technological prototypes using this method are, as yet, limited, they should, in the future, come to play an increasingly significant role in storage for electrical grids or for supply of isolated sites. Electricity can be transformed into hydrogen by electrolysis of water. This is the technology which will be outlined and analyzed in Chapter 2.

Once hydrogen has been made by electrolysis and stored in *ad hoc* tanks, we have to be able to convert it back into electricity on demand. This can be done with another energy converter: a fuel cell. The description and usage of this technology will therefore be the subject of Chapter 3. Note that the complete combination of an electrolyzer, hydrogen storage facility and fuel cell can be viewed as what is known as a "hydrogen battery".

Such a system is unable to deliver significant dynamics in terms of storage and release of electricity. In hybrid systems, the time-delay is often prohibitive. Hence, we need to be able to supplement this solution with another, which is capable of dealing with the time requirements to meet storage/release of power needs. A supercapacitor is perfect for this role. Hence, a detailed study of supercapacitors is provided in Chapter 4.

While the storage systems touched upon in these three chapters (hydrogen batteries and supercapacitors) both exhibit potentially advantageous characteristics, which vindicate their usage in hybrid electrical systems, at present they are still relatively costly. In fact, the days of the electrochemical accumulator by no means appear to be numbered just yet. This will therefore be the topic of Chapter 5.

Finally, on the basis of the elements laid down in the previous chapters, Chapter 6 will focus on electrical hybridization of these storage systems, with a view to enhancing the performances (in terms of energy, lifetime, cost, etc.) of the new system thus formed.

Before getting to the heart of the matter, it is also useful to mention that the primary goal of this book is for use in teaching. It is intended for an audience of researchers, industrialists, academics, teachers, students, school students, etc., who are anxious to be informed, to gather information and to acquire the basic knowledge of physics and technology that will enable them to comprehend and appreciate these systems. Many exercises, along with corrected solutions, will therefore be provided to the reader throughout this manuscript. In addition, a carefully-considered list of pertinent bibliographical references is provided at the end of the book. We invite interested readers who wish to look more closely at the concepts evoked from a pedagogical angle in this book to refer to these other works.

Chapter 1

Basic Concepts of Electrochemistry used in Electrical Engineering

1.1. Introduction

The aim of this chapter is to lay down some basic concepts of electrochemistry which are necessary in order to understand the behavior of the electrochemical components described in this book. For a detailed presentation, the reader could be helped by referring to specialized books such as [DIA 96; LEF 09].

1.2. Brief description and principles of operation of electrochemical components

1.2.1. *Principle of operation [TUR 08]*

Every electrochemical component is made up of a positive electrode and a negative electrode, separated by an electrolyte which may be either liquid or solid (see Figure 1.1). Conventionally, with generators, it is the positive electrode from which the current originates when functioning in generator mode.

Generally speaking, an electrochemical component can operate as an electric generator or an electric load, or both if it has reversible function.

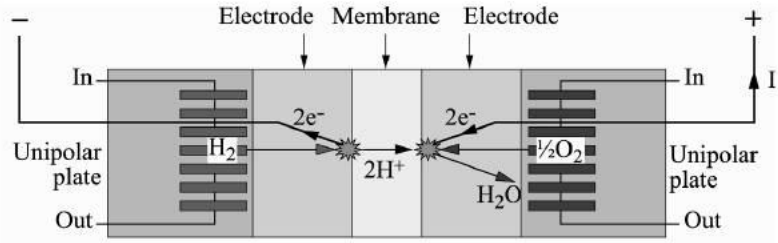

– electrode: $H_2 \leftrightarrow 2H^+ + 2e^-$; + electrode: $\frac{1}{2}O_2 + 2H^+ + 2e^- \leftrightarrow H_2O$

Global reaction: $H_2 + \frac{1}{2}\ O_2 \leftrightarrow H_2O$

a) Diagram of the principle of a proton exchange membrane (PEM) fuel cell (or a PEM water electrolyzer, if the direction of all the arrows is reversed)

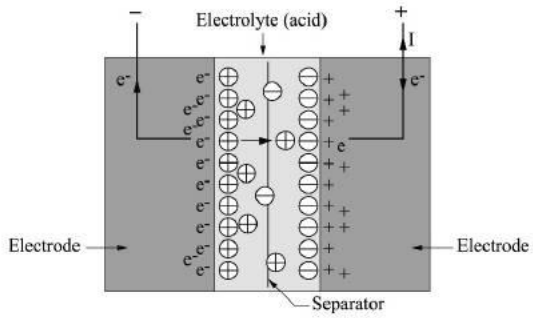

b) Diagram of the principle of a supercondenser (discharge)

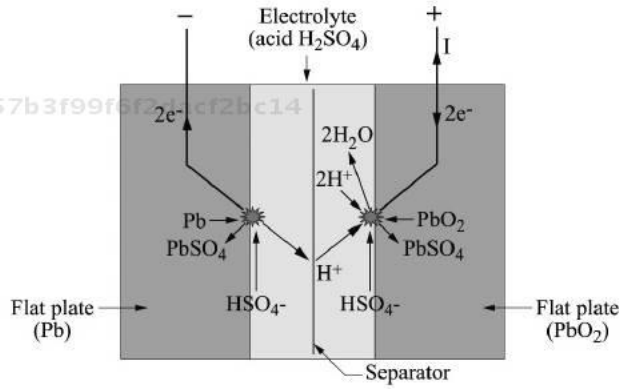

- electrode: $Pb + HSO_4^- = PbSO_4 + H^+ + 2e^-$

+electrode: $PbO_2 + HSO_4^- + 3H^+ + 2e^- = PbSO_4 + 2H_2O$

Global reaction: $Pb + PbO_2 + 2HSO_4^- + 2H^+ = 2PbSO_4 + 2H_2O$

c) Diagram of the principle of an acid/lead accumulator (discharge)

Figure 1.1. *Principle of operation of electrochemical components [TUR 08]*

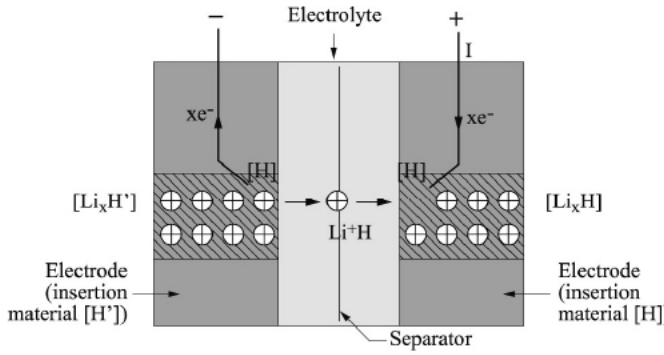

d) Diagram of the principle of a lithium-ion accumulator (discharge)

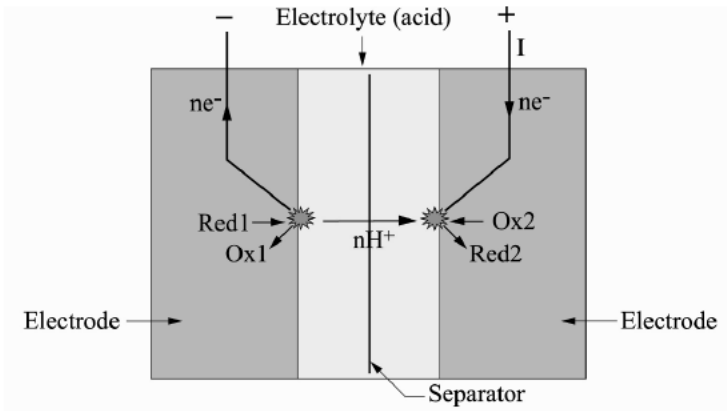

Red1/Ox1 and Red2/Ox2 pairs
(hypothesis: acid medium; the electrolyte is not involved in the reaction):

$$-\text{ electrode: } a_1(\text{Red}1) + nH_2O \leftrightarrow c_1(Ox1) + ne^- + nH_3O^+$$
$$+\text{ electrode: } c_2(Ox2) + ne^- + nH_3O^+ \leftrightarrow a_2(\text{Red}2) + nH_2O$$
$$\text{Global reaction: } a_1(\text{Red}1) + c_2(Ox2) \leftrightarrow c_1(Ox1) + a_2(\text{Red}2)$$

e) Diagram of the principle of an elementary cell in an electrochemical generator (discharge)

Figure 1.1. *(Continued) Principle of operation of electrochemical components [TUR 08]*

In short, the component is the site of an oxidation/reduction reaction which involves two "redox" pairs. More specifically, each electrode is the site of oxidation (loss of electrons) or reduction (gain of electrons) depending on the direction of the current flowing through the component (Figure 1.1e). The n electrons released by the oxidation reaction occurring in an electrode circulate from that electrode to the other via the external electrical circuit. Simultaneously to this circulation of

electrons, and in the same direction, the n ions from the electrode being oxidized circulate toward the other electrode through the electrolyte. Thus, the reduction reaction is able to take place on the other electrode.

The electrodes need to be good electrical conductors. The electrolyte has to be a good ion conductor and a good electron insulator, in order to avoid any short-circuits between the two electrodes. In the case of a liquid electrolyte, a separator is usually used to electrically insulate the two electrodes. The reactions consume reactants and form products, which have to be respectively brought to and evacuated from the reaction area.

In addition, in any electrochemical component, at every interface between an electrode and the electrolyte, there is a spontaneous phenomenon of accumulation of opposite charges on both sides of that interface, which then constitutes a condenser, in the electrostatic sense of the term (Figure 1.2a). This phenomenon is referred to as a "double electrochemical layer". As local electrical polarization occurs over a depth ranging from a few dozen to a few hundred nanometers around that interface, the equivalent condensers may have very large values if the electrodes have a very large surface per volume (they are therefore dubbed supercapacitors). This phenomenon plays an important role in the dynamic behavior of the component.

Finally, the phenomena described above are accompanied by heat exchanges; the performances and lifetimes of the components are very sensitive to temperature. Hence, thermal aspects are of crucial importance for their implementation in electrical systems.

1.2.2. *Brief description of groups of components*

There is a wide variety of electrochemical components for the production and storage of electricity [TUR 08], some of which will be the subject of a more in-depth description later on in this book. Amongst other things, it is possible to distinguish the following "families" of electrochemical components:

– accumulators (Chapter 5);

– supercapacitors (Chapter 4);

– fuel cells (Chapter 3);

– metal air batteries;

– electrolyzers (Chapter 2);

– reversible fuel cells (or electrolyzers);

– redox flow accumulators.

In the case of an accumulator (lead–acid, nickel–cadmium etc.), the electrical energy supplied as it discharges comes from the transformation of the free energy (this term will be clearly defined in section 1.4) from a redox reaction involving reagents already present in the accumulator at each electrode (Figures 1.1c and 1.1e). There is consumption or production of species at the electrodes and transport of charges from one electrode to the other via the electrolyte on the one hand, and via the external electrical circuit on the other. The electrolyte itself may be involved in the reaction (Figure 1.1c). This causes a structural alteration of the materials which make up the accumulator, which should ideally be reversible and allow numerous cycles of charge and discharge. Unfortunately, this is not the case in practice, which leads to an alteration of the electrode's internal structure and limits the number of cycles to a few hundred or thousand. The Li-ion accumulator is a special case, in that the lithium is "simply" introduced into the insertion materials (Figure 1.1c), passing from one electrode to the other, assuming different equivalent degrees of oxidation, and sources of chemical and electrical potentials. There is no significant macroscopic structural alteration of the electrodes, which *a priori* ensures better stability of the properties over time and a greater mass power [RAN 98; ROB 04].

In supercapacitors, the energy storage makes optimum use of the phenomenon of the double electrochemical layer, by using very large surface area to volume ratios at the two interfaces between the electrodes and the electrolyte (Figure 1.1b). There is very little structural alteration of the materials or transport of species, which means we are able to obtain power performances far superior to those of accumulators, and achieve a very high number of cycles (> 100,000). Conversely, the mass energy is smaller, and only part of the energy stored is usable, because it is difficult to recover energy ($1/2CV^2$) at low voltage levels [CON 99].

For this reason, in certain supercapacitors, Faradaic reactions are also exploited, yielding a hybrid component (supercapacitor–accumulator), providing a compromise between energy and power, which may be advantageous for certain applications and which enables us to exploit all the energy stored in the double electrochemical layer of the "internal supercapacitor" using the voltage from the "internal accumulator". This type of hybrid component therefore offers interesting avenues for dedicated design in a system approach, but the technology has not yet reached maturity.

In the components discussed above, accumulators and supercapacitors, the energy is stored in the electrochemical component itself. Thus, it is notably characterized by its specific power and specific energy [CHR 00].

In addition, apart from the primary accumulators (which are, by definition, non-rechargeable), all these components instantly facilitate reversible functions in terms of power (charge or discharge) which, unfortunately, are often not symmetrical. This property is of crucial importance for their use in electrical systems.

The situation is entirely different with fuel cells. A fuel cell does indeed experience a redox reaction which converts chemical energy into electrical energy, but the reagents are stored in tanks outside of the cell (Figure 1.1a). It is only truly characterized by its mass and volume powers. The energy that it is capable of supplying depends on the volume of the reservoirs and the nature of the fuel. Thus, there is no direct relation between the stored energy and the power supplied. In addition, theoretically, the fuel cell experiences no structural modification by the principle of its operation (there is no transport of species from one electrode to the other). Nevertheless, it is the site of various degradation phenomena, influenced by the conditions in which it operates, which limit its lifetime [LAR 00; STE 00].

Certain fuel cells can carry their fuel along with them, and therefore are halfway between a fuel cell as defined above and an accumulator. Such is the case, in particular, for metal–air batteries, which directly consume the metal fuel (zinc, aluminum, etc.) that their negative electrode is made of, by reaction with oxygen (contained in the air or purified), which transforms it into metal oxide stored in the battery. The consequence of this is that as it discharges, the component may become heavier and be deformed by the fixation of oxygen. In order to prevent this situation, which could render the component unusable, the metal oxide formed by the reaction must be regularly evacuated by circulation of the liquid electrolyte before it precipitates. To recharge the component, we have to replace its negative electrode when it is consumed. Note that it is possible to recycle the metal oxide recovered by electrolyzing it to re-create the metal to make the negative electrode. For very low-power applications, the metal–air battery is equivalent to a very long-lasting primary accumulator (very slow discharge when protected from oxygen) and with quasi-instantaneous recharge. This type of battery, which is less common, will not be discussed in Chapter 3.

Electrolyzers can be viewed as the dual components of the corresponding fuel cells (Figure 1.1a). This is true, in particular, of water electrolyzers and metal oxide electrolyzers. They employ the reverse redox reactions to those involved in the corresponding fuel cells, and function as receivers of electrical energy and thermal energy. The reagent for the positive electrode must be regularly supplied, and the by-products evacuated and stored (which is not often the case with the oxygen that is produced). Thus, the electrolyzers can refill the reservoirs that are emptied by the fuel cells – this property might be particularly advantageous in an electrical system. The electrolyzers are really components for storage of electric energy in the form of synthesized chemical compounds (gases, metals, etc.) – granted, with lesser efficiencies than accumulators but with good potentials for mass storage [MIL 07].

In general, fuel cells and electrolyzers cannot offer power-reversible function. As they are designed to be electricity generators and receivers, respectively, operating

them respectively as receivers and generators – even temporarily – can accelerate their aging and breakdown. Indeed, the redox reactions, which are in principle reversible, are generally not symmetrical, and optimal use of them – particularly in catalytic terms – may be very different depending on whether the cell is charging or discharging. This remark is particularly accurate in the context of fuel cells and electrolyzers, but can be extended to accumulators, where the conditions of charging and discharging are not at all symmetrical. Nevertheless, reversible fuel cells (or electrolyzers) are the subject of research, because they could present a particularly promising potential.

Finally, there are redox flow batteries which result from the hybridization of the functions of an accumulator and a fuel cell. Two reservoirs contain the liquid reagents at different levels of oxidation, which are brought in to react in a reversible fuel cell core. In these power-reversible devices, which represent a viable solution for heavy-duty storage of high-energy, high-power electricity, the energy stored and the power are unrelated, and there is no structural alteration of the component. In the principle of its operation, the device is comparable to reversible pumping/turbining groups exploiting two dams, as is the combination of an electrolyzer, storage of reagents and a fuel cell.

There is a wide variety of redox pairs and technologies within these broad categories, which means we have a very wide range of solutions to choose from, depending on the constraints of the technical specifications and of the system.

Following this brief overview, the rest of this chapter is given over to the formalization and expression in equation form of the main phenomena described above.

1.3. Redox reaction

As mentioned in section 1.2.1, a redox reaction involves a redox pair whose oxidized (or oxidizing) form is represented as Ox and the reduced (or reducing) form denoted as Red. These two species exchange electrons in accordance with equation [1.1]. In the oxidation direction, electrons are produced. In the reduction direction, the electrons are consumed. When we write a chemical equation, we do not express the quantity in terms of the number of molecules or ions, but rather the number of moles. Remember that a mole is equal to N, Avogadro's number ($N = 6.02214 \times 10^{23}$). Coefficients a and b are called stoichiometric coefficients: when n moles of electrons are exchanged, a moles of reducing species and b moles of oxidizing species are produced or consumed, depending on the direction of the reaction.

$$a\ \mathrm{Red} \underset{K_{red}}{\overset{K_{ox}}{\leftrightarrow}} b\ Ox + ne^- \qquad [1.1]$$

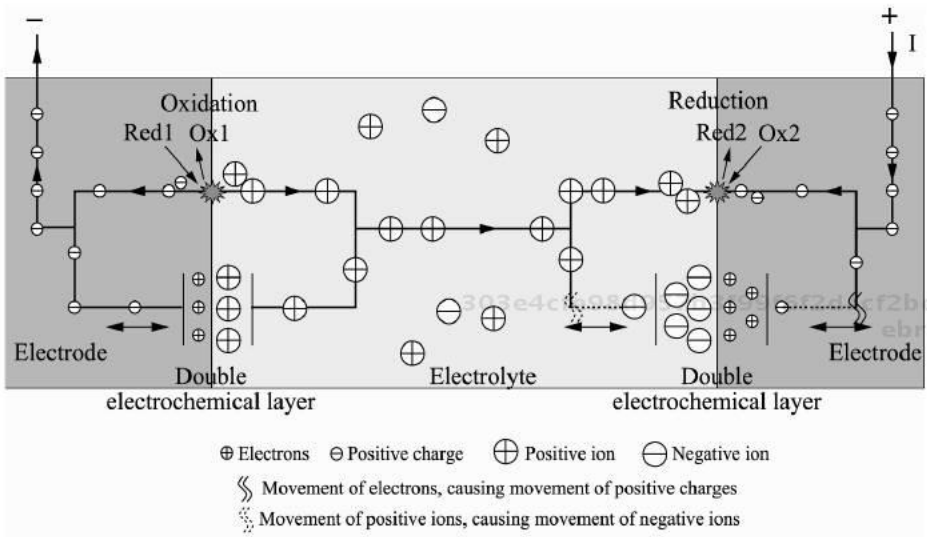

a) Redox and double layer phenomena in an electrochemical component

	Electrostatic supercapacitor	Electrochemical supercapacitor	Accumulator FC Electrolyzer
Majority physical phenomena	Double layer *	Double layer * + redox **	Redox **
Minority physical phenomena	Redox		Double layer *

* Electrostatic phenomenon ** Faradaic phenomenon

b) Predominant phenomena in electrochemical components (excluding thermal phenomena)

Figure 1.2. *Coupled electrostatic and Faradaic phenomena in an electrochemical component [TUR 08]*

In an electrochemical component, redox reactions occur at the interface between an electrode (which is an electron-conductive medium) and an electrolyte (which is an ion-conductive medium). Furthermore, in such a component, two electrodes are involved, as a cell is made up of two electrodes and an electrolyte. In addition, the

elements described hereafter may relate only to one electrode and to one half of the reaction, or indeed to the whole cell with its two electrodes, the two half reactions at each of the two electrodes and the balance reaction.

1.4. Chemical energy

1.4.1. *Enthalpy, entropy and free energy*

A system is said to be open if it exchanges energy and species with its environment, regardless of its form. The characteristic state function of the system is therefore the enthalpy, notated as H. When a chemical reaction occurs in the system at a given pressure and temperature, the enthalpy of the system changes, and that change is notated as ΔH. It is accompanied by a release or absorption of heat Q_{rev}:

– if the system releases heat, Q_{rev} is positive, and the reaction is said to be exothermic; and

– if the system absorbs heat, Q_{rev} is negative, and the reaction is said to be endothermic.

The heat produced or absorbed is expressed as a variation in the entropy of the system, which is said to be reversible:[1]

$$Q_{rev} = T\Delta S_{rev} \qquad [1.2]$$

Thus, we define the variation in free enthalpy or the variation in the Gibbs free energy ΔG as being the difference between the variation in enthalpy and the heat released or absorbed.

$$\Delta G = \Delta H - T\Delta S_{rev} \qquad [1.3]$$

The variation in free energy thus represents the energy released or consumed during the reaction which can be converted – into electrical energy in the case of discharge of an accumulator, for instance, or into chemical energy in the case of recharge.

1 The term "reversible" indicates that it is a heat exchange, with heat given to the medium when the reaction is exothermic, and taken away from it in the case of an endothermic reaction. It is not a question of loss, which corresponds to an irreversible phenomenon with heat given to the medium.

1.4.2. *Enthalpy, entropy and free energy of formation*

The variation in enthalpy at standard pressure during the course of the formation of a mole of a compound is called its enthalpy of formation. Hereafter in this chapter, it is denoted as Δh_f^0: the lowercase letter indicates that we are dealing with a mole of the substance; the superscript ^{0} reminds us that we are at standard pressure. In [ATK 96], the reader can find values of Δh_f^0 tabulated according to the temperature. If the reaction temperature T is different from that which is referenced T_{ref}, we can calculate the value of Δh_f^0 on the basis of its calorific capacity C_p for an isobaric transformation (meaning with no variation in pressure, as is the case in electrochemical components) [FEI 06].

$$\Delta h_f^0(T) = \Delta h_f^0(T_{ref}) + \int_{T_{ref}}^{T} C_p d\theta \qquad [1.4]$$

Similarly, the variation in entropy at standard pressure during the formation of a mole of a compound is called its entropy of formation. Hereafter in this chapter, it is denoted as Δs_f^0. Likewise for enthalpy, there are tables which show values for Δs_f^0 on the basis of the temperature. For a different temperature, we can calculate the value of Δs_f^0 as a function of the calorific capacity for an isobaric transformation C_p.

$$\Delta s_f^0(T) = \Delta s_f^0(T_{ref}) + \int_{T_{ref}}^{T} \frac{C_p}{\theta} d\theta \qquad [1.5]$$

Thus, we can deduce the free energy of formation at temperature T, $\Delta g_f^0(T)$, i.e. the energy which is "free" to be transformed into a form of energy other than the heat given off during the reversible reaction (e.g. electrical energy during discharge).

$$\Delta g_f^0(T) = \Delta h_f^0(T) - T\Delta s_f^0(T) \qquad [1.6]$$

1.5. Potential or voltage of an electrode

Between the electrode and the electrolyte a difference in potential exists, referred to as the absolute voltage of the electrode. In practice, we do not measure the potential of the electrode but rather a difference in potential in relation to a reference electrode defined during the phase of design and characterization of the

electrode. The electrode potential is thus defined in relation to a reference whose potential is zero.[2]

If the system is at electrochemical equilibrium at standard pressure $P_0 = 1$ bar, the potential of the electrode with zero current is the reversible redox potential E^0.

Consider a redox reaction during which n electrons are exchanged to form one mole of product [LAR 00]. Hence, the electrical charge exchanged is:

$$q = -nF \qquad [1.7]$$

where F is the charge of a mole of electrons.[3]

At standard pressure, the voltage at the limits of the system being the standard potential E^0, the electrical energy produced (during discharge of an accumulator, for example) or consumed (during charging of an accumulator, for instance) during the course of the formation of one mole of product is therefore:

$$W_{elec} = -E^0 \times nF \qquad [1.8]$$

If we consider that all of the Gibbs free energy is converted into electricity (when charging), or that all the electricity is converted into Gibbs free energy (when discharging), this means that the reaction is without loss, so:

$$W_{elec} = \Delta g_f^0 \qquad [1.9]$$

Thus, we get an expression of the standard potential:

$$E^0 = -\frac{\Delta g_f^0}{nF} \qquad [1.10]$$

1.6. Reversible potential of a cell

When we consider a whole cell inserted into an electrical circuit, the half redox reactions are no longer balanced, because the electrons and ionic species are exchanged between one electrode and the other. The electrodes are no longer at

---

2 The electrode with zero potential is the Normal Hydrogen Electrode (NHE). Experimentally, we choose an electrode for which we know the relative voltage in comparison to the NHE, tabulated for all temperatures.

3 F is known as the Faraday constant, expressed in Coulombs (C): $F = 96485$ C

thermochemical equilibrium and their potential is altered. At one electrode – the anode – electrons are produced by the oxidation reaction; at the other – the cathode – the electrons are captured by the reduction reaction. If the cell is functioning as a generator, it produces current in a load, and cedes electrical power to that load; this is what happens in a fuel cell battery or in an accumulator during discharge. The potential of the anode is then lesser than the potential of the cathode. If the cell is functioning as a receiver, it receives power from an electrical source, as happens in the case of an electrolyzer cell or an accumulator on charge. The potential of the anode is then greater than the potential of the cathode (Figure 1.3) [DIA 96].

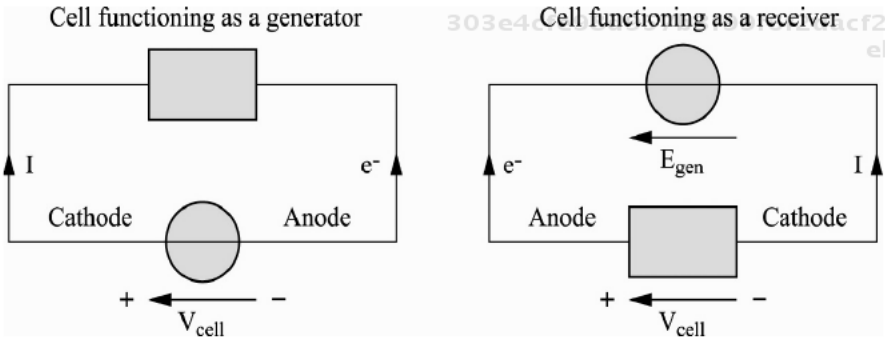

Figure 1.3. *Operation of a cell functioning as a generator (discharge of an accumulator) and as a receiver (charge of an accumulator)*

Thus:

– during charge, the potential of the anode is greater than that of the cathode; the positive electrode is the anode and the negative electrode the cathode;

– during discharge, the potential of the cathode is greater than that of the anode; the positive electrode is the cathode and the negative electrode the anode.

Hereinafter, so as to use identical equations to describe accumulators in charge or discharge mode, fuel cells or electrolyzers, we define the reversible potential, in standard conditions, of a cell, if it were at equilibrium and lossless, as being the difference between the highest electrode potential E^+ (positive electrode) and the lowest electrode potential E^- (negative electrode) [1.11] [TUR 08].

$$E^0_{rev} = E^+ - E^- \qquad [1.11]$$

The conditions of operation may well be different from standard conditions. The potential of the cell thus obeys the Nernst equation. The reversible potential of the cell is therefore calculated as follows:

$$E_{rev} = E^0 + \frac{RT}{nF} \ln \frac{\prod_j a_{j\text{reactants}}^{\nu j}}{\prod_i a_{i\text{products}}^{\nu i}} \qquad [1.12]$$

R is the ideal gas constant[4], T the temperature expressed in K, a_i the activity of species i and ν_i its stoichiometric coefficient. There are various values which can be used to express activity. For a species in its gaseous phase, the activity can be expressed as the partial pressure of the gas P_i (section 1.16) referenced in relation to standard pressure P_0 (or indeed the partial pressure expressed in bars). For a standard substance in the liquid phase, the activity can be taken as equal to 1. For species in an ideal solution, the activity is equal to the ratio of concentration of the species to the reference concentration of 1 mole/l^{-1} [ATK 96].

$$a_i = \frac{P_i}{P_0} \text{ for a species in the gaseous phase}$$
$$a_i = 1 \text{ for a pure substance or a solvent} \qquad [1.13]$$
$$a_i = \frac{[i]}{c_0} \text{ where } c_0 = 1 \text{ mole/l}$$

1.7. Faradaic current density and the Butler–Volmer equation

The electrochemical reactions at the electrodes give rise to charged species which move under the influence of the electrical field created by the difference in potential between the positive electrode and the negative electrode when a circuit connects the two electrodes. The electronic charges move into the electrodes and the ionic charges move into the electrolyte, with the electrode/electrolyte interface ensuring continuity between the two modes of conduction. Hence, the electrodes are no longer at electrochemical equilibrium.

As the reactions take place at the interface, a value that is frequently used for electrochemical components is the current density j, with I being the current of the cell and S the geometric surface area of the electrode. In view of the usual

4 $R = 8.314\,472$ J.mol^{-1}.K^{-1}.

dimensions of cells, the current density is often expressed in [A.cm^{-2}], but in the expressions given below, the unit used is that of the SI system [A.m^{-2}].

$$j = \frac{I}{S} \qquad [1.14]$$

Consider the notations of the redox reaction [1.1], with K_{ox} and K_{red} being the reaction constants respectively in the directions of oxidation and reduction [DIA 96].

The Faradaic current density of the electrode, i.e. the flow of electrons toward the electrode, is connected to the rate of appearance of the electrons v_o (in the direction of oxidation) and the rate of their disappearance v_r (in the direction of reduction):

$$j_f = nFv = nF\left(v_o - v_r\right) \qquad [1.15]$$

The reaction rates depend on the activities of the oxidizing and reducing species a_{Ox} and a_{Red} at the electrode/electrolyte interface, and on the reaction constants K_{ox} and K_{red}, where:

$$v_o = K_o a_{Red}^a \text{ and } v_r = K_r a_{Ox}^b \qquad [1.16]$$

$$K_o = k_o e^{\frac{\alpha_o nF}{RT}E} \text{ and } K_r = k_r e^{\frac{-\alpha_r nF}{RT}E} \qquad [1.17]$$

Thus, we can express the Faradaic current density j_f as a function of the electrode potential E, so that:

$$j_f = nF\left(k_o a_{Red}^a e^{\frac{\alpha_o nF}{RT}E} - k_r a_{Ox}^b e^{\frac{-\alpha_r nF}{RT}E}\right) \qquad [1.18]$$

α_o and α_r are the factors of symmetry of the electron transfer reaction or the transfer coefficient respectively in the oxidation and reduction directions. A coefficient equal to 0 means that we do not need to supply energy to the reagents in order for the reaction to take place. The coefficients vary in the interval [0,1]. With a first-order reaction, they are linked by the equation:

$$\alpha_o + \alpha_r = 1 \qquad [1.19]$$

Usually, we express equation [1.18] as a function of the overvoltage η, defined as the difference between the potential of the electrode and the thermodynamic potential:

$$\eta = E - E_{rev} \qquad [1.20]$$

This expression is known as the Butler–Volmer equation:

$$j_f = j_0 \left(\left(\frac{a_{red}}{a_{red,eq}} \right) e^{\frac{\alpha_o nF}{RT}\eta} - \left(\frac{a_{ox}}{a_{ox,eq}} \right) e^{\frac{-\alpha_r nF}{RT}\eta} \right) \qquad [1.21]$$

j_0 is called the exchange current density. At equilibrium, the Faradaic current is null because the rate of appearance of electrons is equal to the rate of disappearance of electrons. Each of these reaction rates can be interpreted as a current density $j_0 = \frac{v_{o,eq}}{nF} = \frac{v_{r,eq}}{nF}$. The activities $a_{i,eq}$ are the activities of the products at equilibrium or a long way from the reactional interface. We can show that the exchange current density is written:

$$j_0 = nFk_0^{\alpha_r} k_r^{\alpha_o} a_{red,eq}^{\alpha_r} a_{ox,eq}^{\alpha_o} = nFk^0 a_{red,eq}^{\alpha_r} a_{ox,eq}^{\alpha_o} \qquad [1.22]$$

where k^0 is the standard constant of rate of electron transfer for the redox reaction:

$$k^0 = k_0^{\alpha_r} k_r^{\alpha_o} \qquad [1.23]$$

The Butler–Volmer equation expresses the fact that two phenomena are involved. The first is the transfer of electronic charge. The second phenomenon is the transport of species, which manifests itself in the terms of activity of the species at the reactional interface, which may be different from those at equilibrium or far from the reaction site (see section 1.11).

1.8. Butler–Volmer equation for a whole cell

When the system is no longer at equilibrium, the reaction is favored in the direction of oxidation at the anode (production of electrons) and in the direction of reduction at the cathode (consumption of electrons). We can write a Butler–Volmer equation at each electrode:

At the anode:

$$j_{fa} = j_{0a}\left(\left(\frac{a_{a,red}}{a_{a,red,eq}}\right)e^{\frac{\alpha_{oa}nF}{RT}\eta_a} - \left(\frac{a_{a,ox}}{a_{a,ox,eq}}\right)e^{\frac{-\alpha_{ra}nF}{RT}\eta_a}\right) \quad [1.24]$$

At the cathode:

$$j_{fc} = j_{0c}\left(\left(\frac{a_{c,red}}{a_{c,red,eq}}\right)e^{\frac{\alpha_{oc}nF}{RT}\eta_c} - \left(\frac{a_{c,ox}}{a_{c,ox,eq}}\right)e^{\frac{-\alpha_{rc}nF}{RT}\eta_c}\right) \quad [1.25]$$

When the cell, formed by the association of an anode with a cathode, is in operation and there is a current flowing through it, the two current densities are, of course, connected. At the anode, the current is an oxidizing current, it is inbound (see Figure 1.3) and counted positively. At the cathode, the current is a reducing current, it is outbound, and is counted negatively. Let j_f represent the Faradaic current density of the cell:

$$\begin{aligned} j_f &= j_{fa} = j_{0a}\left(\left(\frac{a_{a,red}}{a_{a,red,eq}}\right)e^{\frac{\alpha_{oa}nF}{RT}\eta_a} - \left(\frac{a_{a,ox}}{a_{a,ox,eq}}\right)e^{\frac{\alpha_{rc}nF}{RT}\eta_a}\right) \\ j_f &= -j_{fc} = j_{0c}\left(-\left(\frac{a_{c,red}}{a_{c,red,eq}}\right)e^{\frac{\alpha_{oc}nF}{RT}\eta_c} + \left(\frac{a_{c,ox}}{a_{c,ox,eq}}\right)e^{\frac{-\alpha_{rc}nF}{RT}\eta_c}\right) \end{aligned} \quad [1.26]$$

In addition, the sign of the anodic and cathodic overvoltages is different depending on whether the cell is acting as a generator (discharge) or a receiver (charge). Also, in the interests of generality, we shall revert now to using the notation of the positive electrode and the negative electrode. The subscripts a and c are thus replaced by + and –. Hence, we have:

$$\begin{aligned} \eta_- &= E_- - E_{rev-} > 0 \\ \eta_+ &= E_+ - E_{rev+} < 0 \end{aligned} \quad [1.27]$$

Figure 1.4 shows the plot for the Faradaic current as a function of the potential of the electrodes in the case of an accumulator on charge or an electrolyzer. The negative electrode is the cathode, for which the current is counted positively, and the positive electrode is the anode, for which the current is counted negatively. The voltage at the cell terminals is the difference between the potential of the anode and the potential of the cathode. In the above plot, we considered the activity of the

reagents and the products at the electrodes to be identical to that at equilibrium or far from the electrodes; this issue will be discussed later on in section 1.11. In this case, the overvoltages are referred to as activation overvoltages (see section 1.9).

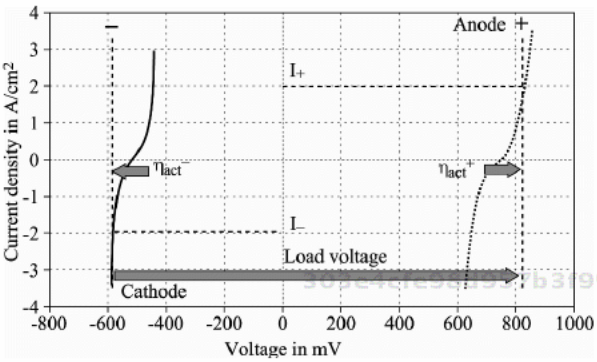

Figure 1.4. *Example of a cell of a charging accumulator or an electrolyzer for which all the symmetry coefficients are equal to 0.5, the exchange current densities 10 mA/cm $^{-2}$ and T = 330 K. [TUR 08]*

1.9. From the Butler–Volmer equation to the Tafel equation

The Butler–Volmer equations comprise two exponential terms. When the overvoltage η reaches a sufficiently high value, meaning that the current density is sufficiently great in comparison to j_{0-} and j_{0+}, the negative exponential term becomes negligible in comparison to the positive exponential term. Thus, the equation is simplified and becomes:

$$\begin{aligned} j_f &\approx j_{0-}\left(\left(\frac{a_{a,\text{reactant}}}{a_{a,\text{reactant,eq}}}\right)e^{\frac{\alpha_- nF}{RT}\eta_-}\right) \\ j_f &\approx j_{0+}\left(\left(\frac{a_{c,\text{reactant}}}{a_{c,\text{reactant,eq}}}\right)e^{\frac{\alpha_+ nF}{RT}\eta_+}\right) \end{aligned} \quad \text{for } j_f >> j_{0-}, j_{0+} \qquad [1.28]$$

In addition, if we discount the influence of transport of matter (see section 1.11) [SAI 04], then the ratios of the activities are equal to 1, and the equations become:

$$j_f = j_{0-}\left(e^{\frac{\alpha_- nF}{RT}\eta_{act,-}}\right) = j_{0+}\left(e^{\frac{\alpha_+ nF}{RT}\eta_{act,+}}\right) \qquad [1.29]$$

The corresponding overvoltages are called "activation overvoltages". This term should be viewed in the light of the "activated complex" theory [DIA 96]. In an elementary reactional stage, this theory postulates that there is an intermediary molecular state called the "transition state" or "activated complex", with a very short lifespan. In order to go from state A (e.g. oxidized state) to state B (e.g. reduced state), the reagent species thus needs to pass through an "activated complex" state AB*, whose energy is greater than A and B (Figure 1.5). Thus, in order for the state of oxidation of a species to change, the electron has to cross the "activation barrier" of the activated complex. In order for the oxidizing agent to reach its reduced form, it is necessary to supply the reduction energy ΔG^*_{red}. Similarly, in order for the reducing agent to reach its oxidized form, it is necessary to inject the oxidation energy ΔG^*_{ox}.

This enables us to offer a qualitative explanation for the inevitable loss of energy when a redox reaction occurs, i.e. when the cell emits or absorbs current.

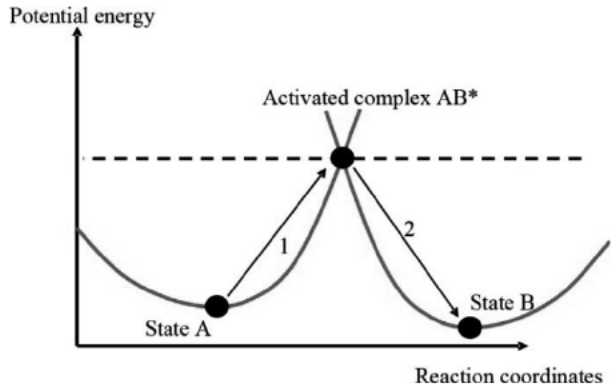

Figure 1.5. *Illustration of the activated complex theory. 1: increase of the potential energy and formation of the unstable activated complex; 2: the unstable activated complex loses some of its potential energy as kinetic energy [TUR 08]*

These equations are invertible, and we can easily express the anodic and cathodic activation overvoltages as a function of the Faradaic current density. In their inverted form, they are known as the Tafel equations:

$$\eta_{act,-} = \frac{\alpha_- nF}{RT} \ln\left(\frac{j_f}{j_{0-}}\right)$$
$$\eta_{act,+} = \frac{\alpha_+ nF}{RT} \ln\left(\frac{j_f}{j_{0+}}\right) \quad \text{for } j_f >> j_{0-}, j_{0+} \qquad [1.30]$$

They can also be expressed in a semi-empirical form:

$$\eta_{act,-} = A_{-} \ln\left(\frac{j_f}{j_{0-}}\right) \quad \text{for } j_f >> j_{0-}, j_{0+} \qquad [1.31]$$
$$\eta_{act,+} = A_{+} \ln\left(\frac{j_f}{j_{0+}}\right)$$

The A_{-}, A_{+} are called the Tafel slope respectively of the negative and positive electrodes.

1.10. Faraday's law

The exchange of electrons between two electrodes is due to redox reactions at the electrodes which consume reagents and form products. Faraday's laws can be used to calculate the flowrates of the reagents and products involved in the reactions. Let us return to the general form of the redox equation written at the negative electrode in the direction of oxidation and at the positive electrode in the direction of reduction. Balancing it so that the coefficients of stoichiometry of the reagents are equal to 1, we get:

At the anode:

$$\mathrm{Red}_a \rightarrow b_a \ Ox_a + n_a e^{-} \qquad [1.32]$$

At the cathode:

$$Ox_c + n_c e^{-} \rightarrow a_c \ \mathrm{Red}_c \qquad [1.33]$$

The current emitted or absorbed by the cell is the electronic charge emitted or absorbed per second; hence, it is equivalent to a molar flowrate of electrons via the Faraday constant F [5], which represents the charge of a mole of electrons in Coulombs:

$$I = q_{e-} F \qquad [1.34]$$

5 The Faraday constant is denoted as F, expressed in Coulombs (C) and its value is F = 96485 C.

For n_a moles of electrons, one mole of reagent is consumed at the anode. Thus, to produce one mole of electrons, $\frac{1}{n_a}$ moles of reagent Red_a have been consumed at the anode. Hence, in order to produce the molar flowrate of electrons q_{e-}, we consume a molar flowrate of reagent, q_{Red_a}:

$$q_{\mathrm{Red}_a} = \frac{q_{e-}}{n_a} = \frac{I}{n_a F} = \frac{j_f S}{n_a F} \quad [mols^{-1}] \qquad [1.35]$$

By applying the same reasoning at the cathode, we obtain Faraday's law for the anode and the cathode:

$$\begin{aligned} q_{\mathrm{Red}_a} &= \frac{I}{n_a F} = \frac{j_f S}{n_a F} \quad [mols^{-1}] \\ q_{Oxc} &= \frac{I}{n_c F} = \frac{j_f S}{n_c F} \quad [mols^{-1}] \end{aligned} \qquad [1.36]$$

These laws can also be written as the molar flowrate, by calculating the molar mass of the reagents:

$$\begin{aligned} \dot{m}_{\mathrm{Red}_a} &= \frac{I}{n_a F} M_{\mathrm{Red}_a} = \frac{j_f S}{n_a F} M_{\mathrm{Red}_a} \quad [gs^{-1}] \\ \dot{m}_{Oxc} &= \frac{I}{n_c F} M_{Oxc} = \frac{j_f S}{n_c F} M_{Oxc} \quad [gs^{-1}] \end{aligned} \qquad [1.37]$$

1.11. Matter transfer model: Nernst model

In order for a reaction to be able to happen continuously, the reagents need to be continuously supplied by way of matter transfer phenomena. Generally, the chemical species can move into the electrodes and the electrolyte in different ways [DIA 96]:

– by electrical migration, which consists of a movement into an electrical conductor of charged particles under the influence of an electric potential gradient;

– by diffusion, which consists of a movement of species – charged or neutral – under the influence of a concentration gradient. Thus, the species move from the

most concentrated area into the least concentrated area, to tend toward equilibrium; and

– by forced or natural convection, which consists of a movement of species under the influence of the movement of the medium in which they are present. This movement may be caused by a thermal or mechanical gradient.

Thus, the modeling of matter transport is a complex subject, governed by different phenomena, different boundary conditions, different media, etc.

Here, we intend to present Nernst's model of diffusion/convection. To begin with, we consider that the reaction occurs mainly at the interface between the electrode and the electrolyte (reaction surface). Thus, the reagents need to diffuse and reach that interface in order to react (Figure 1.13). Convection can be explained by the fact that, beyond a certain distance from the reactive zone, the concentration of reagent can be deemed to be constant and independent of the distance from the reactive zone. Consider an electrode. We wish to describe the profile of concentration of an electroactive species in stationary conditions. We suppose that the transport of matter occurs only in one direction x, which is perpendicular to the plane of the electrode.

The transport of matter is governed by Fick's law:

$$D_{Xi}\frac{\partial^2[X_i]}{\partial x^2}=\frac{\partial[X_i]}{\partial t} \qquad [1.38]$$

In a stationary regime, this law is written as:

$$D_{Xi}\frac{\partial^2[X_i]}{\partial x^2}=0 \qquad [1.39]$$

where D_{Xi} is the constant of diffusion of species X_i in the medium and is expressed in m^2s^{-1}. In an area sufficiently far removed from the reaction interface, $x \geq \delta_i$, where δ_i is the thickness of the diffusion zone, the concentration of species is not altered by the reaction happening at the electrode – it is a convection regime. Such is the case, for instance, in the channel in a fuel cell carrying a reagent. In this area, equation [1.39] has the following solution:

$$[X_i]=[X_i]_{eq} \text{ for } x \geq \delta_i \qquad [1.40]$$

In the stationary regime, the flow of species X_i, J_{X_i}, across the surface of the electrode S, is constant. The species X_i is consumed (or respectively produced) by the redox reaction, during the course of which n electrons are exchanged. The flow of the species X_i across the surface of the electrode S is thus regulated by Faraday's law.

$$J_{Xi} = \pm\frac{q_{Xi}}{S} = \pm\frac{j_f}{nF} \qquad [1.41]$$

The sign "–", or respectively "+", corresponds to a species consumed, or respectively a species produced.

In the zone of diffusion of the species X_i, of thickness δ_i, Fick's law is then written:

$$D_{Xi}\frac{d[X_i]}{dx} = -J_{Xi} \qquad [1.42]$$

At $x = \delta_i$, the boundary condition for the concentrations of reagents is:

$$[X_i](\delta_i) = [X_i]_{eq} \qquad [1.43]$$

This gives us the profile of concentration of reagents:

$$[X_i](x) = [X_{i,eq}] - \frac{J_{Xi}\delta_i}{D_{Xi}} + \frac{J_{Xi}x}{D_{Xi}} = [X_{i,eq}] - \frac{j_f(\delta_i - x)}{D_{Xi}nF} \qquad [1.44]$$

The concentration profile obtained by this model is linear in the diffusion zone, with an increasing slope for a consumed species and a decreasing one for a produced species, if the origin of the axis Ox is the reaction interface. Other types of models can be developed – particularly those of mixed diffusion, as several species can coexist in the same medium (for instance, air, a nitrogenous compound, oxygen, water vapor, in an H_2/air fuel cell).

1.12. Concept of limit current

The redox reactions at the electrodes influence the concentrations of the species. The stronger the current at an electrode, the more quickly the medium loses reagent and gains product. Indeed, the rate of disappearance of the reagents, related to the

kinetics of the reaction, increases in relation to the rate of diffusion of those reagents, which bring them to the reaction site. We define the limit current as an asymptotic value of the current for which the rate of disappearance of the products is equal to the rate of their transport. It is an asymptotic value because this situation would suppose that the redox reaction occurs with a zero concentration of reagents at the interface. In reality, in this situation, other reactions occur.

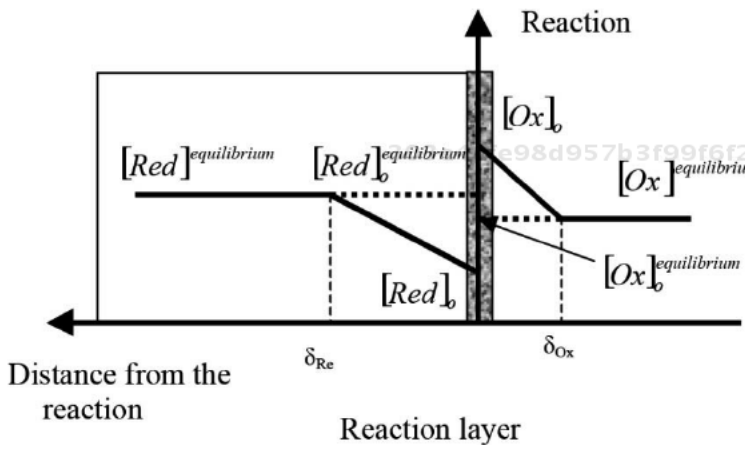

Figure 1.6. *Profile of concentration of reagent (here the reduced form) and product (here the oxidized form) from the equilibrium zone to the reactional zone [TUR 08]*

We express the limit current density by setting a zero concentration of reagent. If we use the hypothesis from Nernst's model, equation [1.44] gives us:

$$[X_i](0) = \left[X_{i,eq}\right] - \frac{j_{\lim}\delta_i}{D_{Xi}nF} = 0 \qquad [1.45]$$

$$j_{\lim} = \frac{D_{Xi}nF}{\delta_i}\left[X_{i,eq}\right] \qquad [1.46]$$

We can thus express the concentration at the reaction interface as a function of the limit current density:

$$[X_i](0) = \left[X_{i,eq}\right]\left(1 - \frac{j_f}{j_{\lim}}\right) \qquad [1.47]$$

1.13. Expression of the polarization curve

Figure 1.11 illustrates the evolution of the current density as a function of the potential of the electrodes (without taking account of diffusion) according to the Butler–Volmer equations.

Yet what interests an electrical engineer wishing to integrate an electrochemical component into a generator is its component as a whole cell, given that an electrode does not work on its own. The quasi-static function of such a component is therefore characterized by the polarization curve, i.e. the relation linking the difference in potential V_{cell} to the boundaries of the cell, defined by $V_{cell} = E^+ - E^-$, to the current or the average current density. We can obtain the polarization curve by deducing it on a pointwise basis from the curves $j_{f,i} = f(E_i)$, $i = a,c$, but from a practical point of view, it is preferable to look for an analytical or semi-analytical expression of the polarization curve by inverting the Butler–Volmer equations.

The inversion was performed in section 1.9, leading to activation overvoltages, when we can discount the influence of the variation in concentration of the species, i.e. the influence of diffusion. What about the expression which integrates this phenomenon of diffusion? Let us return to the expressions [1.28]:

$$\begin{aligned} j_f &\approx j_{0-}\left(\left(\frac{a_{-,reagent}}{a_{-,reagent,eq}}\right)e^{\frac{\alpha_- nF}{RT}\eta_-}\right) \\ j_f &\approx j_{0+}\left(\left(\frac{a_{+,reagent}}{a_{+,reagent,eq}}\right)e^{\frac{\alpha_+ nF}{RT}\eta_+}\right) \end{aligned} \quad \text{for } j_f >> j_{0+}, j_{0-} \qquad [1.48]$$

We can rewrite these expressions by expressing the activity of the species as a function of the limit currents defined in section 1.12:

$$\begin{aligned} j_f &\approx j_{0-}\left(\left(1-\frac{j_f}{j_{\lim,-}}\right)e^{\frac{\alpha_- nF}{RT}\eta_-}\right) \\ j_f &\approx j_{0+}\left(\left(1-\frac{j_f}{j_{\lim,+}}\right)e^{\frac{\alpha_+ nF}{RT}\eta_+}\right) \end{aligned} \qquad [1.49]$$

We invert the above expressions to express the overvoltages of the positive electrode and the negative electrode:

$$\eta_{-} = \frac{RT}{\alpha_{-} nF} \ln\left(\frac{j_f}{j_{0,-}}\right) - \frac{RT}{\alpha_{-} nF} \ln\left(1 - \frac{j_f}{j_{\lim,-}}\right)$$
$$\eta_{+} = \frac{RT}{\alpha_{+} nF} \ln\left(\frac{j_f}{j_{0,+}}\right) - \frac{RT}{\alpha_{+} nF} \ln\left(1 - \frac{j_f}{j_{\lim,+}}\right) \quad \text{for } j_f >> j_{0-}, j_{0+} \qquad [1.50]$$

In each expression, the hypotheses made enabled us to "separate" two terms corresponding to two closely coupled phenomena, which are the charge transfer and the transport of species. Thus, we recognize the first term, identified as an activation overvoltage $\eta_{i,act}$, related to charge transfer, shown in section 1.9. The second term is related to the phenomenon of transport of matter by diffusion; it is called the "concentration overvoltage", $\eta_{i,conc}$. The overvoltage of an electrode can therefore be written as the sum of an activation term and a concentration term:

$$\eta_i = \eta_{i,act} + \eta_{i,conc} \quad \text{for} \quad i = -,+ \qquad [1.51]$$

If we wish to express the overvoltages as a function of the current rather than of the current density, we need only replace j_f with $\frac{I_f}{S}$, where S is the surface area of the electrode. Within the cell, charges move around: ions within the electrolyte and electrons into the electrodes and connections. Hence, the cell is also subject to an Ohmic drop in voltage. We can use the notation r_{cell} for the corresponding surface resistance, expressed in Ωm^2 and R_{cell} for the Ohmic resistance of a cell, expressed in Ω.

Thus, we find an expression for the voltage of the cell as a function of the current density and the current.

When operating as a generator, for $j_f >> j_{0a}, j_{0c}$ and $I_f >> I_{0a}, I_{0c}$:

$$V_{cell}\left(j_f\right) = E_{rev} - \left|\eta_{a,act}\right| - \left|\eta_{a,conc}\right| - \left|\eta_{c,act}\right| - \left|\eta_{c,conc}\right| - r_{cell} j_f$$
$$V_{cell}\left(I_f\right) = E_{rev} - \left|\eta_{a,act}\right| - \left|\eta_{a,conc}\right| - \left|\eta_{c,act}\right| - \left|\eta_{c,conc}\right| - R_{cell} I_f \qquad [1.52]$$

When operating as a receiver, for $j_f >> j_{0a}, j_{0c}$ and $I_f >> I_{0a}, I_{0c}$:

$$V_{cell}\left(j_f\right) = E_{rev} + \left|\eta_{a,act}\right| + \left|\eta_{a,conc}\right| + \left|\eta_{c,act}\right| + \left|\eta_{c,conc}\right| + r_{cell} j_f$$
$$V_{cell}\left(j_f\right) = E_{rev} + \sum_{i,j} \eta_{i,j} + r_{cell} j_f \qquad [1.53]$$
$$V_{cell}\left(I_f\right) = E_{rev} + \left|\eta_{a,act}\right| + \left|\eta_{a,conc}\right| + \left|\eta_{c,act}\right| + \left|\eta_{c,conc}\right| + R_{cell} I_f$$

These expressions separate the overvoltages of the anode and the cathode. However, identifying these different terms and the parameters which govern them is no easy task. Even if we are able to perfectly characterize the behavior of each electrode with a half-cell experiment, we need to be certain that this behavior will not be modified when the electrode is used in a whole cell. In addition, from the point of view of an electrical engineer, who is the "user" of this component, the only possible characterization is often that for a complete cell or a collection of cells, it may prove very tricky to differentiate the contributions of each of the two electrodes. In this case, we prefer to adopt a model with non-dissociated electrodes, with ad hoc signs depending on the mode of operation:

$$V_{cell}\left(j_f\right) = E_{th} \pm \left|\eta_{act}\right| \pm \left|\eta_{conc}\right| \pm r_{cell} j_f \qquad [1.54]$$

We then define an exchange current j_0, a limit current $j_{\lim}$, and a factor of symmetry α for the whole cell. The activation- and concentration overvoltages are thus expressed in the form:

$$\eta_{act} = \frac{RT}{\alpha n F} \ln\left(\frac{j_f}{j_0}\right)$$
$$\eta_{conc} = -\frac{RT}{\alpha n F} \ln\left(1 - \frac{j_f}{j_{\lim}}\right) \qquad [1.55]$$

In order to reach these expressions, we remove an exponential term from the Butler–Volmer equations. The approximate expression for inversion of the equations is valid only if the current density is sufficiently high. This approximation is, of course, seen again after inversion of that expression: equations [1.55] are not correct for overly low values of current density and are not defined in 0. In order to avoid numerical instability, it is usual to add a term of "internal current" j_n into the expression of the activation overvoltage:

$$\eta_{activation} = \frac{RT}{\alpha n F} \ln\left(\frac{j_f + j_n}{j_0}\right) \qquad [1.56]$$

In addition, the use of this term enables us to take account of the fact that the measured no-load voltage of an electrochemical cell is not equal to the difference in thermodynamic potentials of the electrodes. Certain authors give it a physical interpretation expressing two parasitic phenomena: a leakage of electric current into the electrolyte, and the permeation of the reagents across the electrolyte (termed "cross-over") [LAR 00].

The polarization curve found by the earlier study only takes account of the quasi-static behavior of an electrochemical cell. Dynamic phenomena occur, causing the passage from one point on the polarization curve to another. One such phenomenon was described in section 1.2 – the double layer capacity. The second is the electrochemical impedance, relating to the variations in current density and in the concentrations of the species.

1.14. Double-layer capacity

In the dynamic regime, the alteration of the distribution of charges, linked to the double-layer phenomenon, creates a current density which is added to the Faradaic current density:

$$j(t) = j_f(t) + j_n(t) \qquad [1.57]$$

1.15. Electrochemical impedance

The double layer phenomenon means that the current of an electrode or a cell is not identical to the Faradaic current in the dynamic regime. Also, the expressions established above for the potential (or respectively the voltage) as a function of the Faradaic current are not capable of giving an account of the dynamic regime, because they express the behavior of an electrode (or respectively a cell) in steady-state conditions, with constant current or current density. By defining and calculating the electrochemical impedance, by way of certain hypotheses, we are able to give a "small-signal" description of the dynamic behavior of the cell and put forward equivalent electrical arrangements [DIA 96]. Certain elements for the calculation are outlined below.

Indeed, if we write Fick's law [1.38] in non steady-state conditions, the potential and the concentrations are time-dependent. If we consider a slight variation in Faradaic current $\Delta j_f(t)$ around a point of operation and the voltage response of the electrode $\Delta e(t)$, we can define an electrochemical impedance as:

$$Z_f = \frac{\Delta e(t)}{\Delta j_f(t)} \qquad [1.58]$$

By differentiating the current density, we obtain the following expression:

$$\Delta j_f(t) = \left(\frac{\partial j_f}{\partial E}\right)_{[\mathrm{Ox}],[\mathrm{Red}]} \Delta E(0,t) + \left(\frac{\partial j_f}{\partial [\mathrm{Ox}]}\right)_{E,[\mathrm{red}]} \Delta[\mathrm{Ox}](0,t) + \left(\frac{\partial j_f}{\partial [\mathrm{Red}]}\right)_{E,[\mathrm{Ox}]} \Delta[\mathrm{Red}](0,t) \quad [1.59]$$

The Laplacian expression for this is:

$$\Delta j_f(p) = \left(\frac{\partial j_f}{\partial E}\right)_{[\mathrm{Ox}],[\mathrm{Red}]} \Delta E(0,p) + \left(\frac{\partial j_f}{\partial [\mathrm{Ox}]}\right)_{E,[\mathrm{red}]} \Delta[\mathrm{Ox}](0,p) + \left(\frac{\partial j_f}{\partial [\mathrm{Red}]}\right)_{E,[\mathrm{Ox}]} \Delta[\mathrm{Red}](0,p) \quad [1.60]$$

Hence:

$$\left(\frac{\partial j_f}{\partial E}\right)_{[Ox],[\mathrm{Red}]} \Delta E(0,p) = \Delta j_f(p) - \left(\frac{\partial j_f}{\partial [Ox]}\right)_{E,[red]} \Delta[Ox](0,p) - \left(\frac{\partial j_f}{\partial [\mathrm{Red}]}\right)_{E,[Ox]} \Delta[\mathrm{Red}](0,p) \quad [1.61]$$

By setting:

$$R_t = \frac{1}{\left(\frac{\partial j_f}{\partial E}\right)_{[Ox],[\mathrm{Red}]}} \quad [1.62]$$

We get:

$$\frac{\Delta E(0,p)}{\Delta j_f(p)} = R_t - R_t\left(\frac{\partial j_f}{\partial [Ox]}\right)_{E,[red]} \frac{\Delta [Ox](0,p)}{\Delta j_f} - R_t\left(\frac{\partial j_f}{\partial [\mathrm{Re}d]}\right)_{E,[Ox]} \frac{\Delta [\mathrm{Re}d](0,p)}{\Delta j_f} \quad [1.63]$$

Thus, the electrochemical impedance can be written in the form of three terms:

$$Z_f = R_t + Z_{Ox}(p) + Z_{red}(p) \quad [1.64]$$

such that:

$$Z_{Ox}(p) = R_t \frac{\partial j_f}{\partial [Ox]} \frac{\Delta [Ox](0,p)}{\Delta j_f(p)}$$
$$Z_{red}(p) = R_t \frac{\partial j_f}{\partial [\mathrm{Re}d]} \frac{\Delta [\mathrm{Re}d](0,p)}{\Delta j_f(p)} \quad [1.65]$$

We call $\tau_X = \frac{\delta_X^2}{D_X}$ the time constant of diffusion of species X, where δ_X is the thickness of diffusion and D_X the diffusion constant from Fick's law. If we hypothesize that there is a transfer of matter in accordance with Nernst's model, we can demonstrate that Z_{ox} and Z_{red} can be put in the form [DIA 96]:

$$Z_{ox}(p) = R_t \frac{th(\tau_{ox} p)^{1/2}}{(\tau_{ox} p)^{1/2}}$$
$$Z_{red}(p) = R_t \frac{th(\tau_{red} p)^{1/2}}{(\tau_{red} p)^{1/2}} \quad [1.66]$$

R_t is called the charge transfer resistance, Z_{ox} and Z_{red} are the impedances of diffusion-convection linked to the oxidizing species and reducing species respectively. The nonlinear nature of these impedances means it is tricky to use them directly in models of complete electrical systems. Many studies have been carried out to find usable equivalent electrical arrangements [LAF 08; DEV 12].

1.16. Reagents and products in the gaseous phase: total pressure, partial pressure, molar fraction and mixture

This final section is given over to a recap of certain points concerning species in the gaseous phase, which we tend to encounter in electrolyzer cells and fuel cells. For the purposes of this book, we shall consider them to obey the ideal gas law (equation [1.67]) [ATK 96; FEI 06].

$$PV = nRT \qquad [1.67]$$

P is the pressure of the gas, expressed in Pascal[6]; V is the volume occupied by the gas, expressed in m^3; n is the number of moles; R the ideal gas constant; and T the temperature expressed in K.

Consider a mixture of ideal gases. As the i^{th} gas in the mixture is ideal, we can write:

$$P_i V = n_i RT \qquad [1.68]$$

V is the volume occupied by the mixture, n_i the total number of moles, and T the temperature of the mixture. P_i is the partial pressure of the i^{th} gas in the mixture. It can be interpreted as the pressure of the i^{th} gas if it were alone in the same volume V, at temperature T.

Consider n_{tot}, the total number of moles:

$$n_{tot} = \sum_i n_i \qquad [1.69]$$

A mixture of ideal gases is itself an ideal gas. Thus, for a mixture, where P_{tot} is the total pressure of the mixture:

$$P_{tot} V = n_{tot} RT \qquad [1.70]$$

We can therefore write, in accordance with equations [1.68]–[1.70]:

$$P_{tot} = \sum_i P_i \qquad [1.71]$$

---

6 10^5 Pa = 1 bar.

We define the molar fraction of the gas i by:

$$x_i = \frac{n_i}{n_{tot}} \qquad [1.72]$$

From equations [1.68], [1.70] and [1.72], we can write:

$$P_i = x_i P_{tot} \qquad [1.73]$$

1.17. Corrected exercises

1.17.1. *Calculation of the variation in enthalpy during the formation of a mole of water*

Consider a (H_2, O_2) fuel cell. During the course of the reaction, the oxygen and hydrogen are consumed and water is produced. The enthalpy of formation of the water varies in accordance with the equation where the (α_i) and (α_j) are the stoichiometric coefficients of the products and reagents respectively:

$$\Delta H = \sum_{products\, i} \alpha_i \Delta H_i - \sum_{reagents\, j} \alpha_j \Delta H_j$$

The variation in enthalpy depends on the temperature and the pressure. Let ΔH^0_{298} be the variation in enthalpy of formation of a mole of water in standard conditions (1 bar, 25°C). Below we give the values of the variation in enthalpy for the oxygen, the hydrogen and the water.

	ΔH^0_{298} [J.mol^{-1}]
H_2	0
O_2	0
H_2O	-285.83×10^3

Table 1.1. *Variation in enthalpy*

The variation in enthalpy at a pressure of 1 bar as a function of the temperature is written as:

$$\Delta H^0(T) = \Delta H^0_{298} + \int_{298}^{T} C_p d\theta$$

where C_p is the molar heat. The expression of C_p as a function of the temperature can be approximated by:

$$C_p(T) = \alpha + \beta T + \gamma T^2$$

	α [J.mol^{-1}.K^{-1}]	β [J.mol^{-1}.K^{-2}]	γ [J.mol^{-1}.K^{-3}]
H_2	29.038	-0.8356×10^{-3}	2.0097×10^{-6}
O_2	25.699	12.966×10^{-3}	-3.8581×10^{-6}
H_2O	30.33	9.6056×10^{-3}	1.1829×10^{-6}

Table 1.2. *Coefficient of the polynomial approximation of C_p [LAR 00]*

– write the balance equation for the reaction with the formation of one mole of water;

– write the variation in enthalpy for the formation of a mole of water;

– calculate the variation in enthalpy at 25°C;

– calculate the expression of the variation in enthalpy of a pure substance depending on the temperature as a function of the coefficients of the polynomial expression of C_p;

– calculate the expression of the variation in enthalpy for the formation of a mole of water as a function of the temperature.

Solution

Balance equation for the formation of one mole of water

$$H_2 + \frac{1}{2}O_2 \rightarrow H_2O$$

Expression of the enthalpy of formation of a mole of water

$$\Delta H_0 = \Delta H_{H_2O} - \Delta H_{H_2} - \frac{1}{2}\Delta H_{O_2}$$

Calculation of the enthalpy of formation of a mole of water at 298 K

$$\Delta H_0 = \Delta H_{H_2O} - \Delta H_{H_2} - \frac{1}{2}\Delta H_{O_2}$$
$$\Delta H_0 = -285.83\times10^3\, Jmol^{-1}$$

Calculation of the variation in enthalpy of a pure substance as a function of the temperature

$$\Delta H^0(T) = \Delta H^0_{298} + \int_{298}^{T} C_p d\theta$$
$$\Delta H^0(T) = \Delta H^0_{298} + \int_{298}^{T} \left(\alpha + \beta\theta + \gamma\theta^2\right) d\theta$$
$$\Delta H^0(T) = \Delta H^0_{298} + \alpha(T-298) + \frac{\beta}{2}\left(T^2 - 298^2\right) + \frac{\gamma}{3}\left(T^3 - 298^3\right)$$

Calculation of the enthalpy of formation of a mole of water as a function of the temperature

$$\alpha_{reaction} = \alpha_{H_2O} - \alpha_{H2} - \frac{1}{2}\alpha_{O2} = -11.5575$$

We use the notation $\beta_{reaction} = \beta_{H_2O} - \beta_{H2} - \frac{1}{2}\beta_{O2} = 3.9582\times10^{-3}$

$$\gamma_{reaction} = \gamma_{H_2O} - \gamma_{H2} - \frac{1}{2}\gamma_{O2} = 1.10225\times10^{-6}$$

We therefore have:

$$\Delta H^0(T) = \Delta H^0_{298}$$
$$+\alpha_{reaction}(T-298) + \frac{\beta_{reaction}}{2}\left(T^2 - 298^2\right) + \frac{\gamma_{reaction}}{3}\left(T^3 - 298^3\right)$$
$$\Delta H^0(T) = -282,571\cdot10^3 + \alpha_{reaction}T + \frac{\beta_{reaction}}{2}T^2 + \frac{\gamma_{reaction}}{3}T^3$$

1.17.2. *Calculation of the variation in entropy for the formation of a mole of water*

Consider an (H_2, O_2) fuel cell. During the reaction, the oxygen and hydrogen are consumed and water is produced. The entropy of formation of the water varies in accordance with the equation where the (α_i) and (α_j) are the stoichiometric coefficients of the products and reagents respectively:

$$\Delta S = \sum_{products\ i} \alpha_i \Delta S_i - \sum_{reactants\ j} \alpha_j \Delta S_j$$

The variation in entropy depends on the temperature and the pressure. Let ΔS^0_{298} be the variation in entropy of formation of a mole of water in standard conditions (1 bar, 25°C). Below we give the values of the variation in entropy of the oxygen, the hydrogen and the water.

	ΔS^0_{298} [J.mol^{-1}.K^{-1}]
H_2	130.684
O_2	205.138
H_2O	69.91

Table 1.3. *Variation in entropy*

The variation in entropy at the pressure of 1 bar as a function of the temperature is written as:

$$\Delta S^0(T) = \Delta S^0_{298} + \int_{298}^{T} \frac{C_p}{\theta} d\theta$$

where C_p is the molar heat. The expression of C_p as a function of the temperature can be approximated by:

$$C_p(T) = \alpha + \beta T + \gamma T^2$$

	α [J.mol^{-1}.K^{-1}]	β [J.mol^{-1}.K^{-2}]	γ [J.mol^{-1}.K^{-3}]
H_2	29.038	-0.8356×10^{-3}	2.0097×10^{-6}
O_2	25.699	12.966×10^{-3}	-3.8581×10^{-6}
H_2O	30.33	9.6056×10^{-3}	1.1829×10^{-6}

Table 1.4. *Coefficient of the polynomial approximation of C_p*

– write the balance equation for the reaction with the formation of one mole of water;

– write the variation in entropy for the formation of one mole of water;

– calculate the variation in entropy at 25°C;

– calculate the expression of the variation in entropy of a pure substance depending on the temperature as a function of the coefficients of the polynomial expression of C_p;

– calculate the expression of the variation in entropy for the formation of a mole of water as a function of the temperature.

Solution

Balance equation for the formation of one mole of water

$$H_2 + \frac{1}{2}O_2 \rightarrow H_2O$$

Expression of the entropy of formation of a mole of water

$$\Delta S_0 = \Delta S_{H_2O} - \Delta S_{H2} - \frac{1}{2}\Delta S_{O2}$$

Calculation of the entropy of formation of a mole of water at 298 K

$$\Delta S_0 = \Delta S_{H_2O} - \Delta S_{H2} - \frac{1}{2}\Delta S_{O2}$$

$$\Delta S_0 = -163,343 \text{ JK}^{-1}\text{mol}^{-1}$$

Calculation of the variation in entropy of a pure substance as a function of the temperature

$$\Delta S^0(T) = \Delta S^0_{298} + \int_{298}^{T} \frac{C_p}{\theta} d\theta$$

$$\Delta S^0(T) = \Delta S^0_{298} + \int_{298}^{T} \left(\frac{\alpha}{\theta} + \beta + \gamma\theta \right) d\theta$$

$$\Delta S^0(T) = \Delta S^0_{298} + \alpha \ln\left(\frac{T}{298}\right) + \beta(T - 298) + \frac{\gamma}{2}\left(T^2 - 298^2\right)$$

Calculation of the enthalpy of formation of a mole of water as a function of the temperature

$$\alpha_{reaction} = \alpha_{H_2O} - \alpha_{H2} - \frac{1}{2}\alpha_{O2} = -11.5575$$

We use the notation $\beta_{reaction} = \beta_{H_2O} - \beta_{H2} - \frac{1}{2}\beta_{O2} = 3.9582 \times 10^{-3}$

$$\gamma_{reaction} = \gamma_{H_2O} - \gamma_{H2} - \frac{1}{2}\gamma_{O2} = 1.10225 \times 10^{-6}$$

We therefore have

$$\Delta S^0(T) = \Delta S^0_{298} + \alpha_{reaction} \ln\left(\frac{T}{298}\right) + \beta_{reaction}(T - 298) + \frac{\gamma_{reaction}}{2}\left(T^2 - 298^2\right)$$

$$\Delta S^0(T) = -164,5715 + \alpha_{reaction} \ln\left(\frac{T}{298}\right) + \beta_{reaction} T + \frac{\gamma_{reaction}}{2} T^2$$

1.17.3. *Calculation of the variation in free energy during the formation of a mole of water*

Using the expressions of the enthalpy and entropy of formation of a mole of water obtained in the previous two exercises:

– Give the expression of the variation in the Gibbs free energy during the formation of a mole of water as a function of the temperature.

– Calculate the variation in the Gibbs free energy at 65°C. Calculate the reversible potential of a fuel cell functioning at 65°C.

– Calculate the variation in the Gibbs free energy at 200°C. Calculate the reversible potential of a fuel cell functioning at 200°C.

– What is the influence of the temperature on the performances of a fuel cell?

– Calculate the value obtained for the reversible potential at 800°C. Draw a conclusion about the validity of the expression obtained.

Solution

Calculation of the Gibbs free energy of formation of a mole of water as a function of the temperature:

$$\Delta G_0(T) = \Delta H_0 - T\Delta S_0$$

$$\Delta G_0(T) = -282{,}571.10^3 + T \times 164{,}5715$$

$$+\alpha_{reaction} T\left[1 - \ln\left(\frac{T}{298}\right)\right] - \frac{\beta_{reaction}}{2} T^2 - \frac{\gamma_{reaction}}{6} T^3$$

Calculation of the Gibbs free energy of formation of a mole of water at 65°C:

$$T = 65 + 273 = 338\,K$$

$$\Delta G_0(T) = -230{,}594 \text{ kJmol}^{-1}$$

Calculation of the potential of a fuel cell at 65°C:

$$E_{rev} = \frac{-\Delta G_0}{2F} = \frac{230.594 \times 10^3}{2 \times 96485} = 1.195\,V$$

Calculation of the variation in Gibbs free energy during the formation of a mole of water and the reversible potential at 200°C

$$\Delta G_0(T) = -208.132 \text{ kJmol}^{-1}$$

$$E_{rev} = \frac{-\Delta G_0}{2F} = 1.078\,V$$

The rise in temperature slightly decreases the reversible potential of the cell, but causes a more drastic decrease in the activation overvoltages because it improves the

kinetics of the reactions. On balance, the rise in temperature is favorable for the performances of the fuel cells.

Calculation of the variation in Gibbs free energy during the formation of a mole of water and the reversible potential at 800°C

$$\Delta G_0(T) = -105.005 \text{ kJmol}^{-1}$$

$$E_{rev} = \frac{-\Delta G_0}{2F} = 0.544\,V$$

The value obtained is much lower than the no-load voltage obtained at the limits of this type of fuel cells. This means that at 800°C, the polynomial approximation of C_p used is no longer valid.

1.17.4. *Calculation of the Nernst potential for a cell in a PEM fuel cell (PEMFC)*

Consider a cell in a hydrogen PEMFC, functioning at 65°C. Consider that water is produced in liquid form.

– write the balance reaction. Write the Nernst potential of the cell as a function of the activities of the species;

– carry out numerical application for a hydrogen pressure of 1 bar, oxygen pressure of 0.21 bar and a reversible potential equal to 1.195 V.

Solution

The balance reaction in a PEMFC is written:

$$H_2 + \frac{1}{2}O_2 \rightarrow H_2O$$

The reversible potential as a function of the activities:

$$E_{rev} = E^0 + \frac{RT}{nF} \ln \frac{\prod_j a_{jreagents}^{vj}}{\prod_i a_{iproducts}^{vi}}$$

The reagents are in gas form, so their activity is the partial pressure. The water is produced in liquid form, so its activity is equal to 1. Thus, we get:

$$E_{rev} = E^0 + \frac{RT}{2F}\ln\left(\frac{P_{H2}}{P_0}\right) + \frac{RT}{2F}\ln\left(\frac{P_{O2}}{P_0}\right)^{1/2}$$

$$E_{rev} = E^0 + \frac{RT}{2F}\ln\left(\frac{P_{H2}}{P_0}\right) + \frac{RT}{4F}\ln\left(\frac{P_{O2}}{P_0}\right)$$

Numerical application:

$$E_{rev} = 1.195 + \frac{8.314\times 338}{2\times 96485}\ln(1) + \frac{8.314\times 338}{4\times 96485}\ln(0,21)$$

$$E_{rev} = 1.184V$$

1.17.5. *Faraday equations for a Pb accumulator*

In the case of a discharging lead accumulator, we get the following equations:

At the anode:

$$Pb + HSO_4^- \rightarrow PbSO_4 + 2e^- + 2H^+$$

At the cathode:

$$PbO_2 + HSO_4^- + 3H^+ + 2e^- \rightarrow PbSO_4 + 2H_2O$$

– write the Faraday equations linking the battery current and the molar flowrate of Pb at the anode and the molar flowrate of Pb oxide at the cathode;

– write the Faraday equation for the consumption of the electrolyte.

Solution

In accordance with the reaction at the anode, half a mole of Pb is consumed with the production of one mole of electrons. We can write the molar flowrate of Pb as a function of the battery current I, with F being the Faraday constant:

$$\dot{n}_{Pb} = \frac{I}{2F}$$

Similarly, we can write the molar flowrate of PbO_2:

$$\dot{n}_{PbO2} = \frac{I}{2F}$$

Half a mole of electrolyte is consumed at the anode and half a mole of electrolyte is consumed at the cathode. Thus, we have:

$$\dot{n}_{PbO2} = \frac{I}{F}$$

1.17.6. *Calculation of the mass of water consumed by an electrolysis cell*

Calculate the amount of water consumed by an electrolysis cell, when that cell consumes 10 A of power. What volume of liquid water will be consumed in 24 h by an electrolyzer comprising 100 cells? The atomic molar mass of hydrogen is 1 g, and that of oxygen is 16 g.

Solution

From the reactions taking place at the electrodes of the electrolyzer, we know that half a mole of water is consumed per mole of electrons exchanged, so:

$$\dot{n}_{H_2O} = \frac{I}{2F}$$

In 24 hours, the mass of water consumed is:

$$m_{H_2O} = N_{cell} M_{H_2O} \frac{I}{2F} \Delta t = 100 \times (2 \times 1 + 16) \times \frac{10}{2 \times 96485} \times 3600 \times 24$$

$$m_{H_2O} = 8.06\ kg$$

Thus, the electrolyzer consumes 8 liters in 24 hours.

Chapter 2

Water Electrolyzers

2.1. Introduction

Water electrolysis is often presented as the inverse reaction to that which takes place in a fuel cell (or vice versa). This description is not incorrect, but it tends to overlook the numerous thermodynamic and technological differences which exist between a water electrolyzer and a fuel cell. In addition, water electrolysis is often confused with hydrolysis. Yet these are totally different chemical reactions. Hydrolysis consists of using a reaction with water (literally) to decompose a chemical substance[1], whereas water electrolysis consists of using an electrical current and heat to split water into hydrogen and oxygen: H_2O + electricity + heat → $H_2 + ½O_2$.

Water electrolysis is one possible solution for producing hydrogen (and oxygen), which is not currently considered a natural resource, although it is known to exist in the natural state at the bottom of the oceans[2], and the existence of terrestrial sources

1 Example of a hydrolysis reaction: production of hydrogen by hydrolysis of sodium borohydride $NaBH_4$, which is a white powder: $NaBH_4(s) + 2H_2O(l) \rightarrow 4H_2(g) + NaBO_2(s)$. There has been a great deal of research done on this reaction the world over, because it enables us to avoid storing hydrogen, which can be produced as and when required, for low-power applications (mobile applications such as telephones, computers, etc.) [AND 09].

2 Indeed there are natural sources of hydrogen at the bottom of the oceans. These are hydrothermal vents emitting pressurized gases containing 40–50% pure hydrogen. This hydrogen is produced by the reaction of seawater with the ferrous rocks ejected from the earth's mantle, at high temperature and in the absence of oxygen: $2Fe^{2+}_{\text{reactive mineral}} + 2H^{+}_{\text{water}} \rightarrow 2Fe^{3+}_{\text{mineral product}} + H_2$. These potentially very significant renewable sources are currently being evaluated [GOF 08; CHA 09; IFR 11].

of natural hydrogen has very recently been confirmed[3]. However, it is a far cry from the solution which is currently applied to mass-produce hydrogen. Because of the current economic costs, global hydrogen production is in fact based almost exclusively on fossil energies (see Figure 2.1), and therefore emits vast quantities of CO_2. Reforming of natural gas[4] is the procedure which is most commonly used. It seems that the 4% of world hydrogen production that comes from electrolysis can be divided into: 3% from electrolysis of caustic soda[5] and only 1% from water electrolysis. Hence, production of hydrogen by water electrolysis is, as yet, marginal.

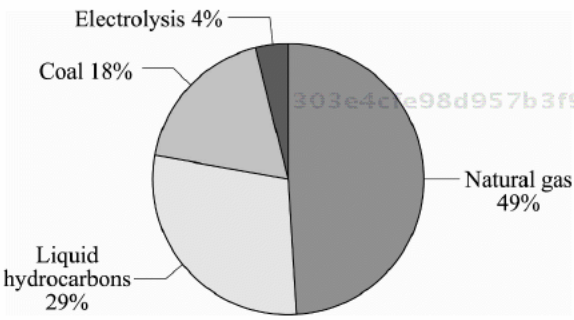

Figure 2.1. *World hydrogen production, estimated at 53 million tons[6] in 2010 [SUR 07; HGM 11]*

Water electrolysis requires deionized water, electricity and heat.

As regards the water, the overall balance in terms of environmental impact is potentially slight because its reuse in a fuel cell or in a hydrogen engine restores the same quantity of water as that used by electrolysis. If the sites of production and consumption of hydrogen are identical, as is the case in a "hydrogen battery"[7], it is

3 Announced in April 2013 by the New Energies Department of the French Petroleum Institute (IFPEN). The potential of these terrestrial sources of natural hydrogen remains to be evaluated, but could be very great.

4 Reforming of natural gas consists of decomposing the natural gas (methane) molecule CH_4, using steam: $CH_4 + H_2O \rightarrow CO + 3H_2$ in the presence of a nickel-based catalyst. Carbon monoxide in then converted into CO_2: $CO + H_2O \rightarrow CO_2 + H_2$.

5 Caustic soda electrolysis (better known as the chloralkali process) uses salt water (brine) to produce chlorine (Cl_2), caustic soda (NaOH) and hydrogen (H_2). The anodic and cathodic reactions are respectively: $Cl^- \rightarrow \frac{1}{2}Cl_2 + e^-$ and $Na^+ + H_2O + e^- \rightarrow NaOH + \frac{1}{2}H_2$.

6 This is around 595 billion Nm^3. A normal meter cube (Nm^3) is a unit of volume (1 m^3) occupied by a gas at 0°C and 1atm. There are 44.62 moles of gas in 1 Nm^3.

7 A "hydrogen battery" is a combination of an electrolyzer and a fuel cell to store and release electricity. This concept will be discussed later on in this chapter.

even possible to operate with a closed-loop cycle with a water tank. In spite of everything, mass development of electrolysis could raise the issue of where that water comes from.

As regards the electricity, it is its origin which will determine whether or not the production of hydrogen by electrolysis is damaging to the environment. With the current range of options for world electricity production (see Figure 2.2), mass production of hydrogen by electrolysis would produce a vast quantity of CO_2 because at present, two thirds of our electricity is produced from fossil energies. Thus, it seems large-scale development of electrolysis ought to be viewed in connection with the development of renewable energies which produce very little or no pollution, but are by nature intermittent and not uniformly distributed: hence, hydrogen appears to be an energy vector which would help rationalize the valorization of renewable energies.

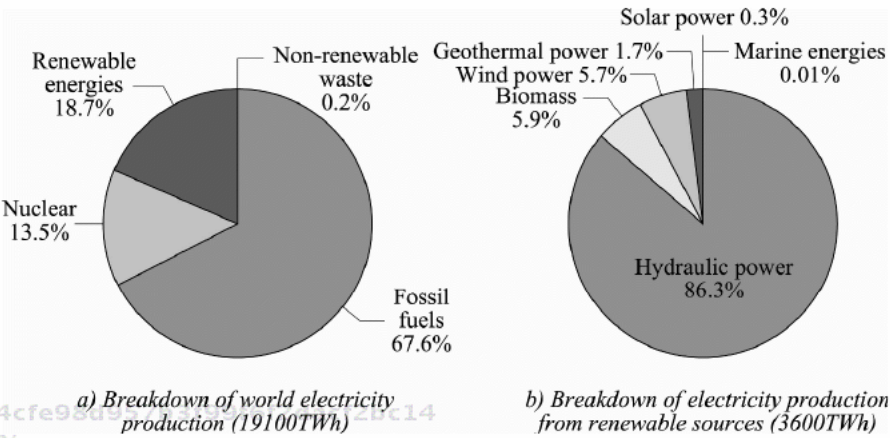

Figure 2.2. *World electricity production in 2008 [IEA 11; EIA 11]*

As regards the heat, it can be drawn from the extra heat generated by the irreversible reactions accompanying the process (low temperature electrolyzer technology), or may require an external heat source (high temperature electrolyzer technology). In this latter case, it seems particularly interesting to valorize the waste heat generated by a process to improve its efficiency (in a nuclear plant for example), or to use renewable energies to produce this heat.

In this chapter, we shall provide the reader with the key elements necessary to comprehend water electrolyzers: principle of operation, technological elements, elements for implementation, specification, characterization, modeling, and

examples of applications. The chapter will close with a number of points relating to the means of storage of the gases produced.

2.2. Principles of operation of the main water electrolyzers

The global reaction[8] that takes place in every water electrolyzer can be written:

$$H_2O + \text{electricity} + \text{heat} \rightarrow H_2 + \frac{1}{2}O_2 \qquad [2.1]$$

By injection of electrical energy and heat into the component, the water is decomposed into hydrogen and oxygen. More specifically, this is a redox reaction which takes place within the electrochemical component. Like all electrochemical components, an electrolyzer is made up of two electrodes (electron conductors) connected through an electrolyte (ionic conductor; electron insulator). Depending on the nature of the electrolyte, the reaction will be different at each electrode.

Three main water electrolyzer technologies can be distinguished[9]: alkaline technology, proton exchange membrane (PEM) technology and solid oxide (SO) technology. Note that these three technologies present numerous similarities respectively with the fuel cells (AFC, PEMFC and SOFC) discussed in Chapter 3.

There is no real "suffix" which exists to clearly denote an electrolyzer, in the same way that we add "FC" (for "Fuel Cell") at the end of each technology. However, it seems that the suffix "WE" (for "Water Electrolyser" or "Water

8 In the existing body of literature, it is common to find the following balance equation: $2H_2O$ + electricity + heat $\rightarrow 2H_2 + O_2$. It is equivalent to equation [2.1], because we think in terms of moles of products or reactants rather than in terms of molecules. The coefficient ½ does not mean that half a molecule of oxygen is produced when a molecule of water is consumed, but rather that half a mole (i.e. $N_A/2 = 3.0110684 \times 10^{23}$ molecules) of oxygen is produced when one mole (i.e. $N_A = 6.0221367 \times 10^{23}$ molecules) of water is consumed. Remember, N_A is Avogadro's number, which gives the quantity of elementary entities (ions, atoms, molecules) in a mole of matter.

9 Other technologies do exist, such as PCWE, named after the proton-conducting fuel cells (PCFCs) functioning between 400 and 600°C currently, with research as it currently stands; or phosphoric acid water electrolyzers (PAWEs) that are derived from PAFCs and function between 150 and 200°C, on which a number experiments have been carried out. At present, these technologies are marginal in comparison to the three technologies highlighted in this chapter, and for this reason we have chosen not to discuss them in detail in this book.

Electrolysis") is one of the most widely used forms: AWE; PEMWE[10]; and SOWE.[11] We shall use this notation system hereafter in this chapter.

This differentiation of technologies enables us to break down the global reaction (equation [2.1]) into two half-reactions taking place at the electrodes:

– Alkaline Water Electrolysis (AWE):

$$\begin{aligned} &\text{Cathode (-):} \quad 2H_2O + 2e^- \rightarrow H_2 + 2OH^- \\ &\text{Anode (+):} \quad 2OH^- \rightarrow H_2O + \frac{1}{2}O_2 + 2e^- \end{aligned} \qquad [2.2]$$

– PEM Water Electrolysis (PEMWE):

$$\begin{aligned} &\text{Cathode (-):} \quad 2H^+ + 2e^- \rightarrow H_2 \\ &\text{Anode (+):} \quad H_2O \rightarrow \frac{1}{2}O_2 + 2H^+ + 2e^- \end{aligned} \qquad [2.3]$$

– SO Water Electrolysis (SOWE):

$$\begin{aligned} &\text{Cathode (-):} \quad H_2O + 2e^- \rightarrow H_2 + O^{2-} \\ &\text{Anode (+):} \quad O^{2-} \rightarrow \frac{1}{2}O_2 + 2e^- \end{aligned} \qquad [2.4]$$

Regardless of the technology used for electrolysis, a reduction reaction always takes place at the cathode and produces hydrogen, and an oxidation reaction takes place at the anode, producing oxygen. The roles of the electrodes are indeed inverted in comparison to the function of a fuel cell, but the signs of the electrodes are not: it is still at the positive electrode where the oxygen is produced or consumed, and the negative electrode where the hydrogen is produced or consumed.

At this stage, the first difference between these three technologies relates to the nature of the charge carriers within the electrolyte, which lends its name to the particular technology, as with fuel cells: OH^- ions with AWE, H^+ ions with PEMWE and O^{2-} ions with SOWE. The second difference relates to the site of water consumption: it is at the cathode with AWE and SOWE, while water is consumed at the anode with PEMWE.

---

10 It is not uncommon in the existing body of literature to find the appellation "SPE water electrolyzer" (with SPE standing for Solid Polymer Electrolyte), particularly to denote this technology when it first appeared in the 1970s.

11 In the literature, the acronyms SOEC (Solid Oxide Electrolyzer Cell) or SOE also occur fairly regularly. The term high-temperature electrolysis (HTE) is fairly common, referring to the operating temperature of the component (typically 800°C) rather than to the nature of its electrolyte.

The third difference is the temperature at which these technologies operate. We speak of low-temperature electrolysis (under 100°C) for alkaline and PEM technologies, and high-temperature electrolysis (between 650°C and 1000°C) for solid-oxide technology. These operating temperatures are mainly conditioned by the ranges of operation of the electrolytes being used.

2.3. History of water electrolysis

The first step in gaining an objective view of a technology is to know its history. The history given here is an overview of bibliographical references [ALL1.1 11; ENC 08; KRO 06; HAL 1919; HAU 86; LEV 99; MIL 07; STO 10; TRA 99; TSI 12; WIK 13a; WIK2; WIK3; WIK4; WIK5; WIK6; ZOU 06].

The attribution of the discovery of water electrolysis is a matter for some debate, especially if we take account of the reaching of true appreciation of the phenomena which were being observed. However, the following three facts are unanimously agreed upon:

– 1789: Adriaan Paets van Troostwijk (1752–1837) and Johan Rudolph Deiman (1743–1808), Dutch, and respectively a trader and a doctor, used an electrostatic machine using friction to generate electricity on two electrodes in or within a Leyden jar (the ancestor of the capacitor) filled with water. This was the first experiment with water electrolysis.

– 1800: After having learned about the work of Alessandro Volta (1747–1827) on the invention of the first electric battery, William Nicholson (1753–1815) and Anthony Carlisle (1768–1840), two British chemists, attempted to reconstruct such a battery. During these tests, they discovered – by accident – that when the ends of the electrical conductors are submerged in water, the water is decomposed into hydrogen and oxygen. They had just performed the first form of water electrolysis with DC supply.

– In the same period around 1800 (some people say that it was a little later), Johann Wilhelm Ritter (1776–1810), a German chemist, physicist and philosopher, carried out the same experiment as W. Nicholson and A. Carlisle independently. Some think it was he who created the first electrolyzer (see Figure 2.3).

In the 1820s, Michael Faraday (1791–1867), a British physicist and chemist, clarified the principles of electrolysis, devoting a significant proportion of his activities to it. In 1834, he published the laws of electrolysis which today bear his name.

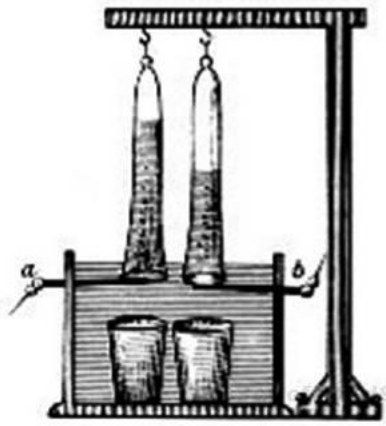

Figure 2.3. *The "electrolyzer" built by J.W. Ritter (drawing taken from [WIK4])*

In 1866, August Wilhelm von Hofmann (1818–1892), a German chemist, built his voltameter, which was able to electrolyze water. This device (see Figure 2.4) enabled the user to measure the amount of a product formed (or of a reactant consumed) throughout the duration of the experiment. More specifically, the goal is to work out the amount of electricity consumed during electrolysis by application of Faraday's law, using measured quantities of a product or reactant, supposing the Faradaic efficiency of the electrochemical reaction to be 100% (i.e. that there is no loss of electrons in parasitic processes).

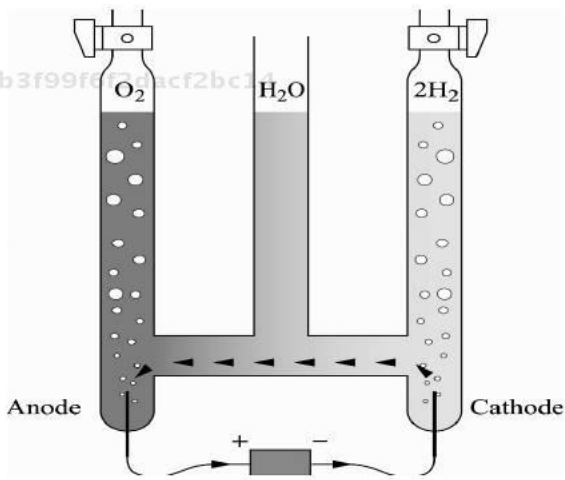

Figure 2.4. *Diagram of A.W. von Hofmann's voltameter (drawing taken from [WIK5])*

In 1868, Zénobe Théophile Gramme (1826–1901), a Belgian electrician and inventor, developed the Gramme dynamo (better known simply as "the Gramme machine"), which was the first ever industrial DC electrical generator. This invention, which marked the beginning of the modern electrics industry, would for a while render water electrolysis an affordable means of producing hydrogen, as the production of electricity using batteries was extremely expensive.

The first electrolyzer to generate oxygen was installed in 1885 in France in the laboratory of Arsène d'Arsonval (1851–1940) at the *Collège Royal de France*, who in 1894 would go on to found the *Ecole Supérieure d'Electricité* (Higher Electrical Engineering College) which would become "Supélec". The cylindrical electrodes were made of iron, and the electrolyte of potassium. The machine was capable of producing 150 liters per day.

In 1888, Dimitry Lachinov (also transliterated as Latchninoff) (1842–1902), a Russian physicist, electrician and inventor, began the industrial era in water electrolysis by developing the first machine using numerous bipolar electrodes, separated by sheets of parchment, in an iron tank, which was able to collect the pressurized gases. After running a variety of tests, he finally advocated the use of an alkaline solution for the electrolyte, as a basic solution is less corrosive than an acid solution for iron electrodes.

Between 1895 and the early 1920s, various devices and installations were deployed to produce hydrogen and oxygen by water electrolysis. These two gases are used in the manufacture of accumulators, as the Pb is welded using an oxyhydrogen flame. This high-temperature flame is also required in certain metallurgic procedures to melt refractive metals such as platinum. In 1902, there were over 400 industrial electrolyzers in usage.

In 1899, Dr O. Schmidt, in Zurich, presented the first industrial bipolar electrolyzer, based on the concept of the filter press and manufactured by Oerlikon. It used a 2.5V power supply. From 1902 onwards, it would be commercialized by Oerlikon.

In parallel, in 1900, Walther Hermann Nernst (1864–1941), a German physicist and chemist, developed the high-temperature electrolyte "YSZ", based on zirconium dioxide (Z_rO_2) stabilized by yttrium oxide (Y_2O_3) at a 15% mass ratio. The foundations were lain for high-temperature electrolyzers and batteries.

During the 1920s and 1930s, the electrolysis industry experienced significant growth. The main companies – Oerlikon, Norsk Hydro and Cominco – produced a great many installations exceeding 100 megawatts. They generally ran on hydroelectric power at a moderate cost, and were intended to produce hydrogen to

make ammonia for the fertilizer industry. The first very large scale installation (producing 27,900 Nm^3/h of hydrogen) would be built by Norsk Hydro in 1927 in Rjukan, Norway, based on filter press technology [SUN 12].

In the mid-1920s, two dates would mark a turning point for alkaline electrolyzers:

– 1924: Jacob Emil Noeggenrath invented the first electrolyzer to function at high pressure (up to 100 bars) and patented the design.

– 1926: Murray Raney (1885–1966), an American engineer, invented the procedure to produce what is now known as "Raney nickel". This is a fine gray powder of an alloy of nickel and aluminum, obtained by treating a piece of nickel–aluminum alloy with concentrated caustic soda. This opened the way for new electrodes for alkaline electrolysis.

However, it was not until 1948 that we would see the first pressurized industrial electrolyzer, developed by Ewald Arno Zdansky for the Swiss group Lonza, and 1951 saw the commercialization of the first high-pressure electrolyzer (30 bars) by the German company Lurgi, who had acquired Lonza's patent.

Similarly, it was only after the Second World War, in 1948, that Eduard Wilhelm Leonhard Justi (1904–1986), a German physicist, and August Winsel, a German inventor, produced the first Raney nickel electrodes, which significantly enhanced the performances of the cathode, which is the site of production of hydrogen. Such electrodes were first used in industrial electrolyzers in 1957.

In 1967, another significant advance in the design of alkaline electrolyzers was made by R.L. Costa and P.G. Grimes, who introduced the concept of "zero-gap" assembly of the electrodes; the objective was to reduce the resistance of the electrolysis cell by reducing the distance between the electrodes. 1978 saw the emergence in industry of first so-called "advanced" alkaline electrolyzers. What is meant by "advanced" is an alkaline electrolyzer which includes at least one of the following technological advances: high pressure, high temperature, zero-gap electrodes, new diaphragms or solid cells.

The 1960s would mark a turning point for water electrolyzers, because a new form of technology would emerge as part of two American space programs run by NASA:

– Project GEMINI (1962–1966), the second US program for manned space flight (with a two-seater spaceship), the aim was to develop and master extra-vehicular activity, which was not possible with the Mercury space capsule (Gemini's predecessor).

– APOLLO program (1961–1975), the aim of which was to land humans on the moon for the first time.

During these programs, PME fuel cells and electrolyzers were developed. These first solid membranes were made of sodium polystyrene sulfonate, and would be replaced by Nafion, which was discovered by DuPont in the same decade. Thus, it was in 1966 that the very first solid-polymer electrolyte (SPE) electrolyzer was built by General Electric (GE) for Project GEMINI to produce oxygen on board the spacecraft.

In the 1970s, military (submarine) and spatial applications, again relating to the production of oxygen on board, constituted the context of deployment of small PEM electrolyzers. It was around 1975 that development began with a view to applying the principles on a different scale – particularly for the purposes of storing electricity. The main developmental efforts to commercialize the technology are attributed to the Swiss company BBC (Brown Boveri Company) between 1976 and 1989, with the company becoming ABB (Asea Brown Boveri) in 1988 [STU 98]. The first electrolyzer created from these developments was deployed on a commercial scale in 1987 in Nyon, Switzerland, on the industrial site of the metallurgist Stellram SA [SCH 00]. It was capable of producing 20 Nm^3/h of hydrogen at a maximum pressure of 2 bars; its power consumption was around 100 kW. More recently, significant developments took place in Japan between 1993 and 2002 as part of the WE-NET program, aimed at storing renewable energies via hydrogen [RAS 03; ALL8.5 11]. Today, developments are continuing all over the world.

As regards HTE, while W.H. Nernst, in 1900, laid the foundations for the high-temperature electrolyte "YSZ" which is still very widely used today, it was only in the 1960s that developments of HTE began in earnest – once again driven by NASA in the context of its space programs.

Particularly significant work was done in Germany from the 1970s to the mid-1980s, with developments motivated by the idea of combining HTE with nuclear power plants. The high operating temperature electrolysis or "HotElly" project, conducted by the German companies Dornier Systems (Friedrichshafen) and Lurgi (Frankfurt), succeeded in developing HTE based on tubular elements functioning between 800 and 1000°C [DOE 82; DOE 85; QUA 86].

In parallel, in the United States, similar developments took place at the Westinghouse Electric Corporation in Pittsburgh [MAS 86].

With the exception of Japan, there was little research carried out on high-temperature electrolyzers during the 1990s. However, development has resumed since the beginning of this century, and is gathering momentum, more or less

everywhere in the world, with aims being to reduce the operating temperature and be able to use planar cells in an industrial context. In Europe, we can cite the "Relhy" project (Innovative Solid Oxide Electrolyser Stacks for Efficient and Reliable Hydrogen Production) in particular, one of the goals of which is to improve the lifetime of these components [REL 13]. One of the main advantages of this technology is that it rather naturally opens the way for co-generation of electricity and heat.

In conclusion, it is now over 120 years since the alkaline electrolyzer emerged, and over 50 years since PEM and SO electrolyzers were developed. While exact data are hard to come by, almost all (99%) of the current market for electrolyzers is dominated by alkaline technology. However, in recent years, PEM electrolyzers have noticeably gained ground. As was stated in section 2.1, water electrolysis accounts for a very marginal proportion (less than 1%) of worldwide hydrogen production.

For applications in mass production (thousands of kg per day) currently based on alkaline technology, the main reason for this situation is the cost of electricity, which constitutes a very significant part of the cost of each kg of hydrogen produced by water electrolysis. For small-scale applications (a few tens of kg per day), based essentially on PEM technology, it is the cost of investment in the electrolyzer which is currently too high. For intermediary hydrogen production applications between these two extremes, where the two technologies are in competition with one another, we unfortunately see a mix of the two situations. For further details, readers can refer, in particular, to [IVY 04; KRO 06; SAU 08; GEN 09; SUT 12].

2.4. Technological elements

Alkaline electrolysis is a mature technological solution, although technological developments continue, as we shall see. It is *the* technology used on the market today. In PEM electrolysis, there have been many developments which have been extrapolated from PEM fuel cells, and the technology has reached a level of maturity where it is commercially viable. Finally, HTE is still under development, as we shall show.

In this section, we aim to give readers the essential technological knowledge about each different form of technology. However, this discussion is by no means exhaustive.

2.4.1. *Alkaline technology*

To begin with, an alkaline electrolyzer is relatively simple (Figure 2.5a). It uses two electrodes (typically made of nickel), an electrolyte (typically potassium hydroxide at a concentration of 30%) and a separator (these used to be asbestos, but

are now nickel oxide). This separator, which is also known as a diaphragm, is necessary in order to avoid chemical recombination of the gaseous hydrogen and oxygen produced. It has to be impermeable to gases and to electrons, but must allow hydroxide ions (OH^-) and water to pass through. In practice, it will not be perfectly impermeable to the gases (with gaseous "crossover" phenomena occurring). On the one hand, this will be harmful in terms of the purity of the gases and, on the other, may cause safety problems. These phenomena therefore need to be very closely monitored in any electrolyzer.

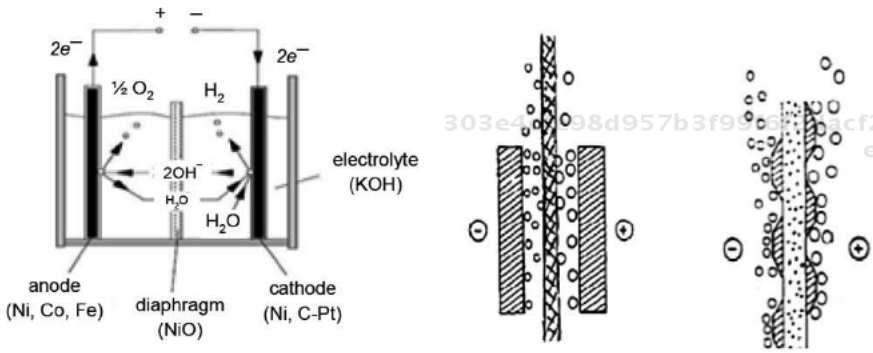

Figure 2.5. *Fundamental technological elements in alkaline electrolysis [STO 10b]*

Traditionally, the cells used were gap cells (Figure 2.5b), meaning that the electrodes were not resting against the separator. The gap between the electrodes is the distance that the ions have to travel through the electrolyte. A small gap has the advantage of limited Ohmic losses. Yet with this configuration, continuous gaseous films form in the spaces between the electrodes and separators, contributing to an increase in these Ohmic losses (greatly disturbed ion transport) [MIL 07]. The introduction of so-called "zero gap" cells (Figure 2.5c) significantly limited this issue. Indeed, with this second configuration, the electrodes, which are necessarily porous, are placed directly against the separator and the gases produced are evacuated behind the electrodes [MIL 07]. Hence, the Ohmic losses relating to ion transport are much reduced.

In practice, an alkaline electrolyzer will be made up of several cells. Two types of associations are found: parallel association (referred to as "monopolar" or "unipolar" – Figure 2.6a) and serial association (referred to as "bipolar" – Figure 2.6b). From the point of view of industrialization, the monopolar configuration is simple, affordable, and easy to manufacture and maintain. However, it uses (very) high electrical currents, causing significant Ohmic losses in the current feeders (connectors, wires, etc.). The bipolar filter-press-type configuration

can greatly reduce Ohmic losses in the current feeders, but requires greater mastery in the design and manufacture so as to prevent leakage of electrolyte and gas between the cells. It ultimately leads to greater compactness and higher current densities with lower levels of power supply needed. Thus, the bipolar configuration has gradually become more and more widely used instead of the monopolar configuration, which was very widely employed at the beginnings of alkaline electrolysis but which, today, is only used for certain low-power products.

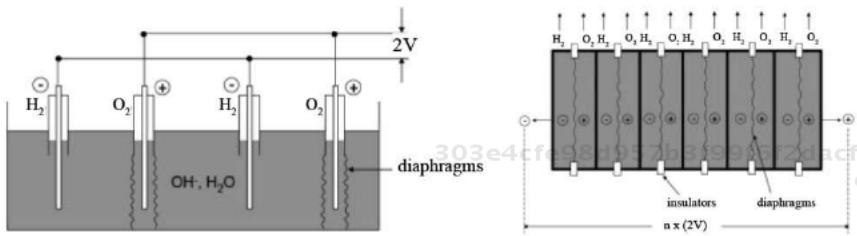

(a) Reservoir monopolar configuration (b) Filter-press bipolar configuration

Figure 2.6. *Possible configurations of the cells in an alkaline electrolyzer [SUN 12]*

Significant technological progress was made in the 1970s. The term "advanced alkaline electrolyzers" came into usage around this time. In fact, this term covers numerous technological advances [STO 10b]: zero-gap cells, new thin separators, new designs for assembly, better catalyzers, high-pressure function (up to 30 bars) and higher-temperature operation. They first began to be commercialized at the end of the 1970s. An often-repeated example of advanced design dating from the late 1970s is shown in Figure 2.7a. It should be noted that the distribution of electrolyte is done here by external piping which feeds fluid to each cell in parallel. Since then, designs have continued to evolve to integrate electrolyte distribution into the assembly, as illustrated in Figure 2.7b, which shows a diagram of the typical arrangement of a modern alkaline electrolyzer. Figure 2.8 offers two examples of modern commercial alkaline electrolyzers made by two flagship companies in the area of this technology.

Table 2.1 shows the characteristics of the different components in an alkaline electrolyzer: the electrodes, separator or diaphragm, electrolyte and bipolar plates.

Technological developments are still continuing today – even rather actively, one might say. Figure 2.9 gives an example of an industrial attempt to bring down the costs of materials and manufacture of an alkaline electrolyzer by using plastics with appropriate properties. The design has a square cross-section – which is sufficiently rare to be worthy of note. These principles are also in the process of evaluation by the same company with a circular design [SWA 08].

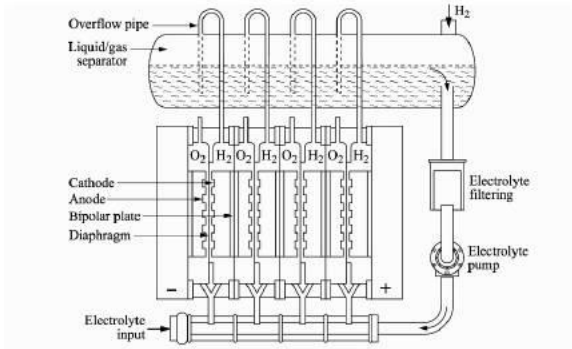

Figure 2.7. *Designs for different alkaline electrolyzers*

(a) HySTAT™-type alkaline electrolyzer from Hydrogenics; 10-15Nm³H₂/h; 10-25 bar (photo taken from [DEM 10])

(b) Two 200Nm³H₂/h alkaline electrolyzers each functioning at atmospheric pressure, from Norsk Hydro (photo taken from [KRU 02])

Figure 2.8. *Examples of commercial alkaline electrolyzers*

A major technological leap could be made by developing anionic membranes (which are conductive of hydroxide ions OH^-), which would mean we would no longer have to use a liquid electrolyte. By replacing the separator (diaphragm), which is porous and too vulnerable to pressure, this type of membrane should facilitate a significant rise in pressure (currently the best devices operate at around 30 bars). Certain industrial actors such as ACTA ENERGY are beginning to offer initial solutions, but these have yet to be proven.

Name	Role	Materials	Remarks/limitations
Electrode	Anode or cathode	– The electrodes need to be resistant to corrosion in the basic medium and must exhibit good electrochemical activity. – Nickel is the best material for electrodes: it offers good corrosion resistance in the basic medium, whilst still having good electrochemical activity and a reasonable cost. Future development might aim to replace it with nickel-based alloys. – Transition metals such as iron and copper are not sufficiently resistant to corrosion; noble metals, for their part, are too expensive. – Nickel, as a substrate of the electrodes, is itself a catalyst, but it is very advantageous to coat it with electro-catalysts (metal alloys, structured materials, noble metals), which greatly enhances the electrodes' electrochemical activity. – The electrodes must be porous in zero-gap cells so as to be able to evacuate the gas produced. – To help with the evacuation of the gas, it is useful to make physical alterations to the basic electrodes. We create slits or holes in them so as to facilitate the escape of gas bubbles. Thus, we speak of louvered electrodes, or finned or slit electrodes. The design of the electrodes has evolved a great deal over the years, and is very varied.	
Anode	– Reaction site for oxidation of water (creation of O_2)	– Substrate: nickel (+iron) – Catalysts deposited on the substrate: Ni/Co alloys, $NiCo_2O_4$, Ni_2CoO_4, Co_3O_4	– The combined effect of the corrosion and the high potential of the anode means that only nickel can be used as a substrate. – Deactivation of the nickel by formation of a hydride phase on its surface. An iron coating helps protect the nickel and also increases activity.
Cathode	– Reaction site for reduction of protons (creation of H_2)	– Substrate: mild steel (one of the most widely-used substances), nickel-plated steel, (+iron) – Catalysts deposited on the substrate: Ni/Co alloys, Ni/Mo alloys, possibly doped with TiO_2 or ZrO_2, C-Pt	– Raney nickel, which is nickel alloyed with other metals such as aluminum and zinc, is sufficient in terms of purity. – Deactivation of the nickel by formation of hydrides on its surface, worsened by the high concentration of hydrogen. An iron treatment is also effective in this case.
Separator/ diaphragm	– Separates the two gases produced to prevent them chemically recombining	– Organic materials: solid asbestos (< 100°C). – Composite materials: asbestos/polymer (< 100°C), potassium titanate/PTFE (120–150°C), zirconium/polymer (< 160°C), PAM (120–150°C), nickel/ceramic (<170°C). – Inorganic materials: IMET® (< 100°C), NiO (< 200°C).	– It needs to be chemically stable in a more or less severely basic medium.
Electrolyte	– Basic liquid electrolyte: transport of OH^- ions	– The most widely used material is potassium hydroxide (KOH) at 25-30% concentration at around 80°C. This is the best compromise in order to achieve good ion conductivity. – Sodium hydroxide (NaOH) can also be used.	– It must not be chemically decomposed by the operational voltages. – It must not be volatile, so it will not react with the gases being evacuated. – Possibility of improving ion transport by using additives to the electrolyte. These additives may also play a role in managing the bubbles by adjusting the affinity between the electrodes and the electrolyte. – In order to use a higher temperature, we need a more concentrated electrolyte so as to avoid evaporation (e.g. 40% at 160°C).
Bipolar plate	– Electrical serialization of the cells	- nickel-plated steel - plastic	

Table 2.1. *Characteristics of the main constitutive elements of an alkaline electrolyzer [JEN 08; STO 10b; ZEN 10; SUN 12]*

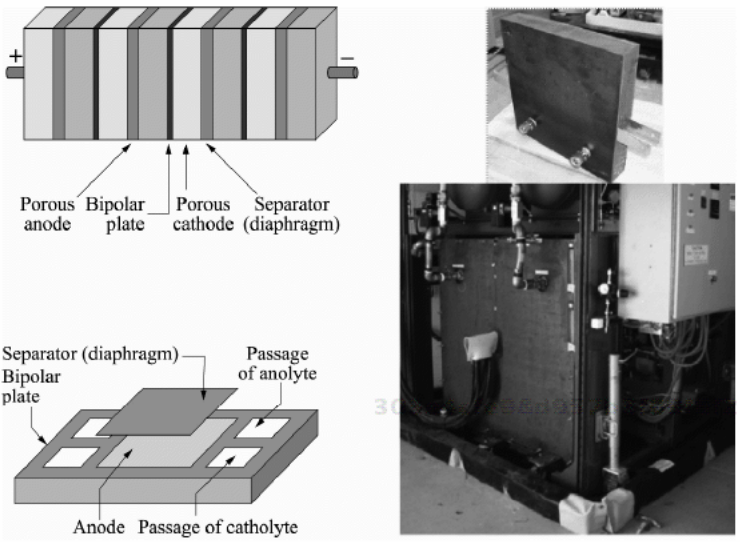

(a) Diagrams of the principle of an alkaline stack with a square cross-section (top) and a bipolar plate (bottom) (inspired by [BOU 06])[12]

(b) Prototypes of "plastic" alkaline electrolyzers from General Electric: 10gH_2/h (left); 1KgH_2/h (right) (photos taken from [BOU 06])

Figure 2.9. *Examples of recent developments of alkaline electrolyzers*

Another avenue is function at higher temperatures. At present, the operating temperature is typically around 80–90°C. The objective would be to take this figure up to 200°C so as to save on electrical consumption. This involves changing the materials, whose hardiness must be able to be proven, although certain industrialists, such as HYDROGENICS, claim a lifetime of at least 50,000 h for their current technology.

There are around twenty industrial manufacturers of alkaline electrolyzers the world over. Some of these are listed in Table 2.2.

2.4.2. *PEM technology*

Whilst alkaline technology, using a basic liquid electrolyte, soon began to develop significantly on an industrial level, the same is not true of acid electrolyte technology. The reason for this is simple: corrosion is far greater with a liquid acid electrolyte (typically H_2SO_4). It was not until proton-exchanger solid materials emerged in the mid 20th Century that acid technology began to develop – mainly in

12 Anolyte/catholyte: electrolyte placed in the anodic/cathodic compartment.

the context of space applications. Indeed, it was around this time that perfluorosulfonic acid membranes were discovered (NAFION – Dupont de Nemours). These materials are very stable, and are the only ones capable of withstanding the greatly oxidizing conditions imposed [MIL 07].

Name	Location	Capacity for hydrogen production in Nm^3/h	Maximum pressure (bar)
IHT (Industrie Haute Technologie)	Switzerland	3–760	32
ELT (Electrolyse Technik)	Germany	330–760	30
NEL Hydrogen (formerly Norsk Hydro)	Norway	10–485	15
GHW (Gesellschaft für Hochleistungwasserelektrolyseure)	Germany	12–500	30
WASSERELECTROLYSE HYDROTECHNIK HT	Germany	0.12–250	
TELEDYN ENERGY SYSTEMS	United States	2.8–56	10
CASALE CHEMICALS SA	Switzerland	0.5–100	
H2 NITIDOR	Italy	0.25–100	30
ACCAGEN SA	Switzerland	0.02-100	
IDROENERGY	Italy	10-80	8
HYDROGENICS (formerly Vandenborre/ Stuart Energy)	Belgium	10-60	25
ERRE DUE SPA	Italy	1-64	
H2 LOGIC	Denmark	> 21	
PIEL	Italy	7.6-18	18
AVALENCE LLC	United States	0.1-5	
SAGIM	France	0.1-5	10

Table 2.2. *Non-exhaustive list of industrialists in the field of alkaline electrolyzers [ALL-3.2.1 11; SMO 12]*

The design of a PEM-type electrolyzer is relatively simple. As Figure 2.10 illustrates, it comprises a stack of elementary cells connected in a series by bipolar plates. Each cell comprises two electrodes separated by a Proton Exchange Membrane (PEM). Each electrode is made up of a thin catalytic layer which is the site of the oxidation (anode) or reduction reaction (cathode), and layers of porous materials which act as current distributors/receivers depending on the electrode in question. In general, this porous material will be incompressible (titanium) at the anode and compressible (carbon) at the cathode in order to add mechanical flexibility when the whole ensemble is compressed.

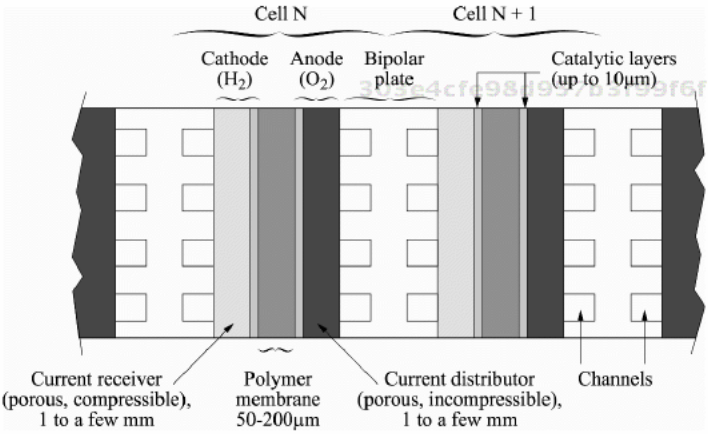

Figure 2.10. *Diagram of the internal constitution of a PEM electrolyzer stack*

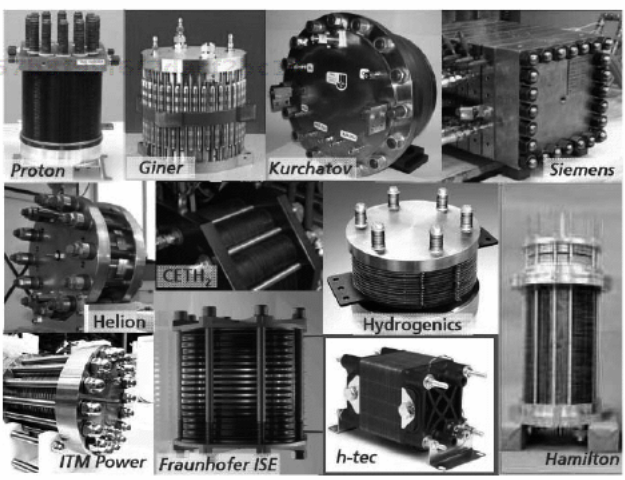

Figure 2.11. *Examples of PEM electrolyzer stacks (collage made by [SMO 12])*

Table 2.3 shows the characteristics of the different constituent parts in a PEM electrolyzer: the electrodes, the membrane and the bipolar plates. The PEM electrolyzer draws on all the significant developments to do with PEM fuel cell technology over the past 20 years, although the differences in terms of materials are fairly marked as regards the potentials of the positive electrode (anode) which are far higher than in fuel cell operation. For instance, carbon is not very durable as a support material for the anode; for this reason, it is essential to use a material such as titanium, which has the drawback of being very expensive and tending to become passive rather quickly.

Figure 2.11 illustrates a number of industrial designs for PEM electrolyzer stacks. The majority of stacks have circular cross-sections, but some are square.

The effort in terms of development seems to be greater than that for alkaline technology. Besides seeking to drive down costs and achieve a longer lifetime, two other objectives in terms of performances are envisaged:

– increased pressure ($\rightarrow$ 400 bars), in order to eliminate, or at least minimize, any mechanical compression before storage in pressurized tanks. In this case, it is primarily engineering problems which need to be resolved. While it is possible to directly increase the pressure of a stack up to a few dozen bars, it would seem preferable, for reasons of safety, to enclose the stack in a pressurization chamber, thereby facilitating a far greater rise in pressure [MIL 07];

– increased temperature ($\rightarrow$ 200°C) in order to decrease electrical consumption. However, this requires us to use new materials. These developments could benefit from the encouraging results obtained with "high-temperature" PEM fuel cells. One of the greatest sticking points is the need for a technological breakthrough regarding the membrane. Remember that the membranes currently used disintegrate rapidly when the temperature goes above 120°C, even if they have been reinforced. Materials such as PBI (polybenzimidazole) doped with phosphoric acid (H_3PO_4) to obtain good proton conductivity, or sPEEK (sulfonated poly(ether ether)ketone), seem promising.

Table 2.4 lists the characteristics of a number of commercial products with a more or less well established identity. At present, the commercial availability of PEM technology is nowhere near as advanced as that of alkaline technology, particularly in terms of very high capacities.

Laboratory electrolyzers producing several L/min use PEM technology. We can cite the following companies which commercialize such devices: SCHMIDLIN, MATHESON GAS, DOMNICK HUNTER, PEAK and CLAIND.

Name	Role	Materials	Remarks/limitations
Cathodic catalytic layer	– Reaction site for reduction of protons (creation of H_2) – Porous layer (to facilitate the evacuation of the gas produced)	– Catalysts: platinum (most widely used), palladium – Otherwise, support material for the catalyst: carbon, TiO_2	– The catalysts need to be resistant to the heavy acidity of the membrane – Nickel or cobalt can be used, but are only capable of limited performances. Complexes of cobalt or nickel with glyoxime bonds seem promising
Anodic catalytic layer	– Reaction site for oxidation of water (creation of O_2) – Porous layer (to facilitate the evacuation of the gas produced)	– Possible catalysts: iridium, ruthenium, their oxides and mixtures – I_rO_2 is the standard catalyst. It can be used in its pure state or mixed with other metals, precious or otherwise. Example of bimetallic catalyst: $Ir_xRu_{1-x}O_2$ – Active catalysts are stabilized by metal oxides, e.g. TiO_2, Ti_4O_7, SnO_2, Ta_2O_5, Nb_2O_5, etc. Thereby we obtain trimetallic catalysts, e.g. $Ir_1Ru_2O_x$ ($Ni_{0.1}Co_{0.1}$, $Fe_{0.1}$ or $Sn_{0.1}$) – The catalysts are not supported	– The catalysts need to be resistant to the heavy acidity of the membrane – Ruthenium is the best catalyst, but is unstable in the presence of O_2 – Platinum is a fairly poor catalyst for the oxidation of water – Carbon cannot be used, as the potential is greater than 0.9V
Polymer embrane	Twofold role: – Solid acid electrolyte: transport of H^+ ions – Separator for the two gases	– Perfluorosulfonic acid (PFSA) membranes not supported: Nafion® (most widely used), Fumapem®, Flemion®, Aciplex® – The PFSA membranes may be reinforced with Teflon to improve their mechanical strength: dimensionally stable membranes (DSM®)	– Possible addition of aniline (Nafion-PANI) to increase proton conductivity – Addition of SiO_2 or TiO_2 improves water retention and facilitates operation above temperatures of 100°C – Beyond 120°C, the PFSA membranes lose their mechanical strength (even those that are reinforced) – Issue of crossover of O_2 in high-pressure applications leading to the appearance of hydrogen peroxide, which is harmful to the electrode-membrane ensemble
Anodic current receiver (porous incompressible)	Fourfold role: – Mechanical strength when exposed to compression forces which need to be distributed in a homogenous manner – Collection of current for the reaction – Conduit of water to the anode – Porous layer (to facilitate the evacuation of the gas produced	– Porous titanium structures are most widely used: sintered titanium powder, sintered titanium felt, extruded titanium mesh	– Carbon cannot be used, as the potential is greater than 0.9V – Titanium rapidly becomes passive, which is unfavorable for the passage of the current. Surface treatments are needed in order to obtain long lifetimes – The porosity of the material has a very significant influence on the evacuation of the gases and on the streamlines
Cathodic current distributor (porous compressible)	Threefold role: – "Spring" effect against compression forces – Conduit of current for the reaction – Porous layer (to facilitate the evacuation of the gas produced)	– Paper or carbon-fiber felt treated with Teflon, which makes the carbon hydrophobic	– The porosity of the material plays a very significant influence on the evacuation of the gases and on the streamlines
Bipolar or separating plate	Fourfold role: – Mechanical rigidity in a filter-press stack – Conduit of water for an anode – Evacuation of gas for an anode (cell N) and a cathode (cell N+1) – Electrical serialization of the cells	– Solid titanium – Carbon-based systems (less sturdy). A metal reinforcement is needed on the anode side	– They include channels to decrease the charge losses in the stack

Table 2.3. *Characteristics of the main constitutive elements in a PEM electrolyzer [MIL 07; STO 10b; SUN 12; TSI]*

Name	Location	Capacity for hydrogen production in Nm^3/h	Maximum pressure (bar)
CETH2	France	5–40	14
AREVA Stockage d'Energie (formerly Helion Hydrogen Power)	France	1–40	50
PROTON ON SITE	United States	1–30	30
KOBELCO	Japan	> a few 10 Nm^3/h	
H-TEC	Germany	3.6	30
GINER Electrochemical Systems	United States	Lab-3	85
HYDROGENICS	Canada	1–2	7.9
ITM Power	England	> a few Nm^3/h	15
MITSUBISHI Corp.	Japan	1	8
CLAIND	Italy	0.5–1	15
TREADWELL	United States	0.2	75

Table 2.4. *Non-exhaustive list of industrialists for PEM electrolyzers [ALL 11c; SMO 12]*

2.4.3. *SO technology*

While both the aforementioned technologies have been commercialized (there are product lines using them), high-temperature electrolysis is still at the research and development stage. Thus, here, we shall only give an outline of this form of technology, which will undoubtedly evolve further in years to come.

A planar-design SO electrolyzer is fairly similar, in structural terms, to a PEM electrolyzer. Figure 2.12 shows the diagram of a typical layout of such a device. We see a sandwich-type structure, in which the solid electrolyte (a solid oxide which is a ceramic) is bordered on both sides by two porous electrodes (a ceramic is used for the anode and a ceramic/metal alloy (cermet) for the cathode). The interconnectors which serialize the cells are based on metallic materials. Depending on the design of the stack, channels are scored into the interconnectors or are replaced by "flow-fields" (pre-electrodes, so to speak), which are usually nickel-based.

Besides the planar structure, there are also tubular structures, but they are falling out of usage because their electrical performances are not as good.

Table 2.5 offers a fairly detailed description of the materials which are typically used. It should be stressed that high temperature poses the problem of expansion of the materials. Thus, the materials need to have compatible coefficients of thermal expansion. At present, the choice is fairly limited.

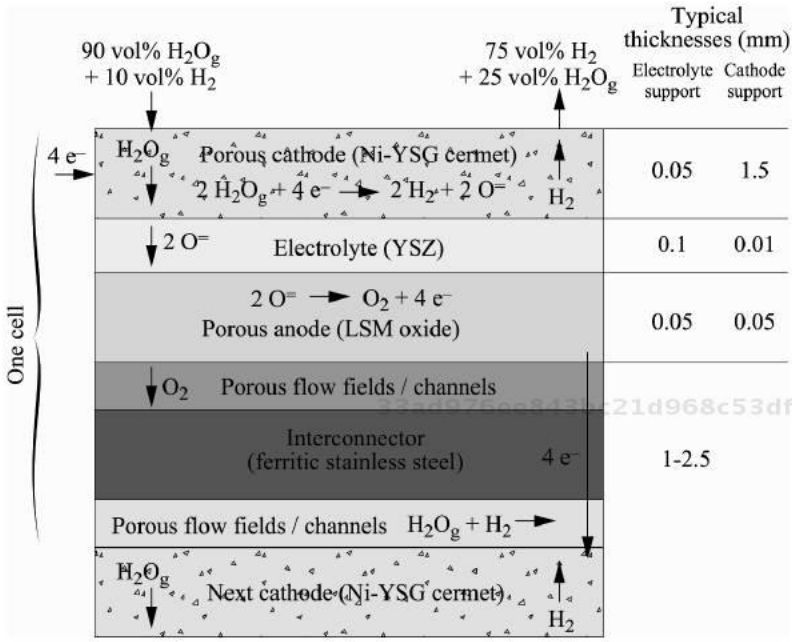

Figure 2.12. *Diagrammatic representation of the cross-section of a planar SO electrolyzer stack (inspired by [SUN 12])*

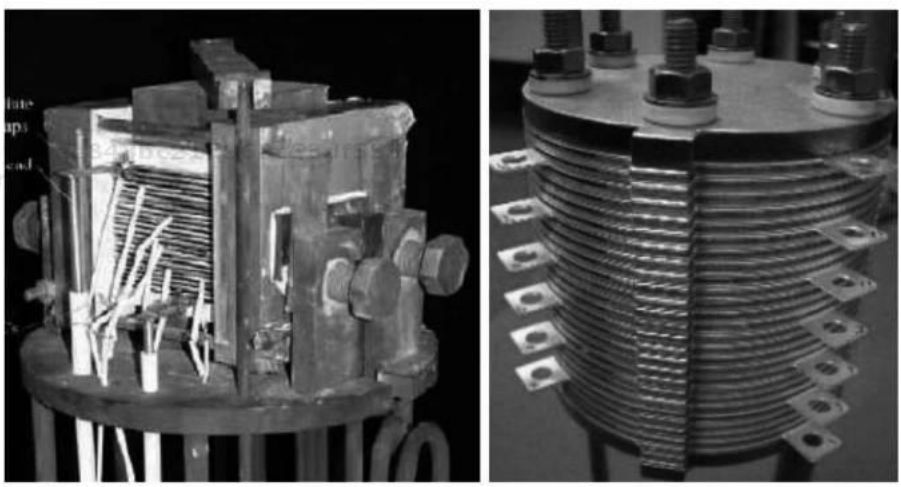

(a) CERAMATEC (photo taken from [LEF 11])

(b) University of Kyushu (photo taken from [SMO 12])

Figure 2.13. *Prototypes for 25-cell SO electrolyzers, planar designs*

There seem to be few industrial actors in this area. For instance, we can cite the American company CERAMATEC, or the Swiss company HT CERAMIX. Then we find institutes (CEA (France), EIFER (Germany), etc.) and university laboratories (RISO National Laboratory (Denmark), Kyushu University (Japan), Imperial College (England), etc.). Figure 2.13 gives two examples of planar SO electrolyzers made by two of these actors.

Name	Role	Materials	Remarks/limitations
Cathode	– Reaction site for reduction of protons (creation of H_2) – Porous layer (to facilitate the evacuation of the gas produced)	– Cermet – The material typically used is Ni-YSZ	– YSZ = Yttrium-Stabilized Zirconium – In order to limit oxidation of the nickel, a mixture of water vapor and hydrogen is injected. The proportion of water vapor chosen varies, typically between 50 and 90%
Anode	– Reaction site for oxidation of water (creation of O_2) – Porous layer (to facilitate the evacuation of the gas produced)	– Perovskite-type oxide – The materials typically used are LSM ($LaSr_XMn_{1-X}O_3$) or LSCF – Many other alternatives are possible	– LSM = Lanthanum strontium manganite – LSCF = Lanthanum cobalt strontium ferrite
Electrolyte	Twofold role: – Solid electrolyte: usually conductive of O^{2-} ions – Separator of the two gases	– Ceramic often based on zirconium – YSZ is the most commonly used – There are alternatives based on cerium or perovskites	– YSZ = Yttrium-Stabilized Zirconium – Proton-conductive solid electrolytes may be used
Interconnector	Twofold role: – Mechanical rigidity of the ensemble – Electrical serialization of the cells	– Ceramics and metallic materials have been investigated. These offer the advantage of greater mechanical toughness and a certain ease of manufacture – Noteworthy possible metallic materials are high-temperature nickel alloys and some ferritic stainless steels with high chrome content – The material selected is usually given a coating to improve its corrosion resistance	– In particular, the material must exhibit good corrosion resistance in air and in an H_2/H_2O_g mixture at 800°C
Flow field	Twofold role: – Conduit of water for an anode – Evacuation of oxygen for an anode and hydrogen for the cathode of the next cell	– Flow fields may be scored into the interconnector – The interconnectors may also be separate from the flow fields. In this case, the pre-cathode is usually made of nickel, and the pre-anode of Ni-Fe-Cr alloys	

Table 2.5. *Characteristics of the constitutive elements in a SO electrolyzer [DEM 07; SUN 12; LEF 11]*

Obviously, SO technology is in the process of development. Certainly, it can draw on all the developments made with SOFCs. However, the need arises to develop electrodes which are optimized for electrolyzer operation. In addition, a great deal of work needs to be done as regards the designs of the cell and stack. Durability also needs to be demonstrated: in particular, the aim is to improve the thermal cyclability of the materials. Certainly, we need to try to lower the operation temperature, much as we are seeking to do with SOFCs. Finally, at present, SO electrolyzers are incapable of functioning under significant pressure: hence we need to develop designs which can withstand pressure.

2.4.4. *Comparison of the three water electrolyzer technologies*

	Advantages	Disadvantages
AWE	– Industrially mature – Proven durability – Profitable (currently lowest cost with good/very good returns) – No noble catalyst – Able to function at high pressure (up to 30 bars) – Quick startup – Catalysts less sensitive than PEMWE technology to poisoning due to water quality	– Relatively low current densities (typically 0.4 A/cm², 1 A/cm² seemingly possible) – Problem of corrosion due to the nature of the electrolyte (KOH) – Fairly high maintenance costs – Safety a greater problem with high-pressure operation than PEMWE – *A priori* less resistant than PEMWE to fluctuations in electrical supply – particularly those fluctuations caused by photovoltaic and wind energy. However, this has yet to be confirmed – The procedure is more complex than that of PEMWE, because of the need to manage the electrolyte
PEMWE	– High purity of gases – High current densities (2 A/cm² commercially; 4 A/cm² seemingly possible) – Good efficiencies – Simple design of the cell – Possibility of operation at very high pressure (up to 400 bars) – Able to function with significant differences in pressure between the electrodes – Potentially robust against intermittent electrical function – Potentially low maintenance costs – Quick startup – No corrosion for auxiliaries in comparison to AWE	– Large initial outlay – Use of noble catalysts (Pt, IrO_2) because of the acidity of the membrane – Membrane costly – The manufacture process is more complex and more costly than with AWE – Long-term durability remains to be proven for commercial products
SOWE	– Low electricity consumption (high electrical efficiencies) – No noble catalyst – Potentially high current densities (3 A/cm²)	– Heat source required (although this may become an advantage if that heat would otherwise have been lost; in addition, heat is generally less expensive than electricity) – Very high operating temperature which is stressful for the materials – Slow startup – Durability remains to be proven – Cannot function under pressure – Elaborate process for separating the hydrogen from the water vapor

Table 2.6. *Compared advantages and disadvantages of each electrolyzer technology [MIL 07; STO 10b; LEF 11; RAL 11; SMO 12]*

2.4.5. *Specifications of a commercial electrolyzer*

The aim of this section is to give readers a description of the essential elements which are usually to be found on the technical specifications of a commercial electrolyzer with the most mature forms of technology – namely alkaline and PEM. These elements are:

– the pressure of hydrogen delivery and possibly oxygen delivery [barg]. The oxygen pressure may differ slightly;

– the nominal/maximum flowrate of hydrogen and possibly oxygen [Nm^3/h][13]. The flowrate of oxygen is equal to half that of hydrogen;

– the range of operation: this is usually expressed in % of the nominal hydrogen flowrate, e.g. 20–100%. Remember that this limitation is necessary in order to limit the impact of the phenomenon of crossover of the gases through the electrolyte, which is greatest at low current densities;

– the purity of the hydrogen produced, and possibly of the oxygen: this is expressed in %. The purity is often quoted before and after passage through the purification system, which may be optional. For instance: before, 99.9%; after: 99.998%. Sometimes, the content in terms of other substances is quoted (in ppm), such as that of O_2, N_2, etc. For example: $O_2 < 2$ ppm;

– the electrical energy consumed during full-capacity operation [kWh/Nm^3]. In general, it is specified whether the consumption of auxiliaries is included. However, as some auxiliaries are optional, it is sometimes rather tricky to obtain this value. Although it is indeed an energy, misuse of language means it is sometimes labeled as "electrical power consumed": this is not wrong if we suppose that function continues at that level of power for an hour;

– the electricity supply specifications: powerful electrolyzers will be connected to the three-phase 400 V 50–60 Hz grid; sometimes DC supply may be advocated. The total installed power will be expressed in kVA: it must be at least equal to the maximum flowrate [Nm^3/h] multiplied by the energy consumed at that rate [kWh/Nm^3]. In practice, it is oversized to a greater or lesser extent (typically 1.5–2 times the actual value) in order to allow for aging of the electrolyzer, which will consume increasing amounts of energy (the voltage increases over time for a given current). Sometimes, the electrical power of the auxiliaries is expressed separately;

– the specifications (T_{max}, water flowrate, water pressure, etc.) for cooling if a cooling system is not included;

– the characteristics of the water to be electrolyzed, particularly if a water purification system is not included. At the very least, the water needs to be

13 Conversion: 1 Nm^3/h = 0.0893 kg/h; 1 kg/h = 11.2 Nm^3/h.

demineralized: generally a conductivity of less than 1 µs/cm (or > 1 MΩ.cm for resistivity); sometimes an even lower conductivity value, <0.1 µs/cm (or >10 MΩ.cm for resistivity) is desired. Sometimes reference is made to international standards (ASTM Type II, Type I, etc.) defining water quality (conductivity, chloride content, sodium content, etc.). The input pressure of the water [bar] and its maximum temperature [°C] are also often specified. If a purification system is included, the specification "tapwater" is usually given;

– consumption of water [L/Nm^3] per Nm^3 of hydrogen produced;

– for an alkaline electrolyzer, the composition of the electrolyte and its quality [L]. For example: H_2O + 30% wt. KOH[14]; 300 L;

– information about the conditions of installation: indoor/outdoor; acceptable temperature range (e.g. –20°C; 40°C); the sizing; mass; maximum operating altitude, etc. Sometimes, the fluidic interfaces are specified;

– conformity to safety standards may also be specified.

Sometimes the number of stacks is given – almost certainly for the purposes of maintenance. However, the polarization curve is never given *a priori*.

By way of illustration, Figure 2.14 shows an example of a technical specification sheet for the series of alkaline electrolyzers HySTAT type V (cooling and water purification included) made by the Belgian-Canadian company HYDROGENICS.

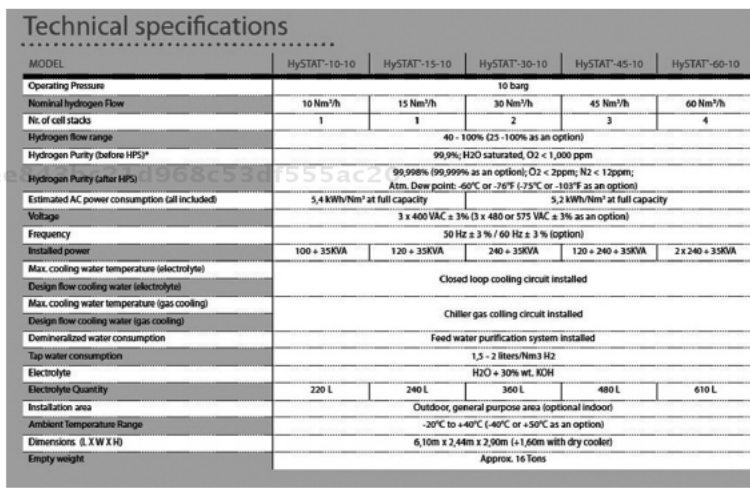

Technical specifications

MODEL	HySTAT"-10-10	HySTAT"-15-10	HySTAT"-30-10	HySTAT"-45-10	HySTAT"-60-10
Operating Pressure	10 barg				
Nominal hydrogen Flow	10 Nm³/h	15 Nm³/h	30 Nm³/h	45 Nm³/h	60 Nm³/h
Nr. of cell stacks	1	1	2	3	4
Hydrogen flow range	40 - 100% (25 -100% as an option)				
Hydrogen Purity (before HPS)*	99,9%; H2O saturated, O2 < 1,000 ppm				
Hydrogen Purity (after HPS)	99,998% (99,999% as an option); O2 < 2ppm; N2 < 12ppm; Atm. Dew point: -60°C or -76°F (-75°C or -103°F as an option)				
Estimated AC power consumption (all included)	5,4 kWh/Nm³ at full capacity		5,2 kWh/Nm³ at full capacity		
Voltage	3 x 400 VAC ± 3% (3 x 480 or 575 VAC ± 3% as an option)				
Frequency	50 Hz ± 3 % / 60 Hz ± 3 % (option)				
Installed power	100 + 35KVA	120 + 35KVA	240 + 35KVA	120 + 240 + 35KVA	2 x 240 + 35KVA
Max. cooling water temperature (electrolyte)	Closed loop cooling circuit installed				
Design flow cooling water (electrolyte)					
Max. cooling water temperature (gas cooling)	Chiller gas colling circuit installed				
Design flow cooling water (gas cooling)					
Demineralized water consumption	Feed water purification system installed				
Tap water consumption	1,5 - 2 liters/Nm3 H2				
Electrolyte	H2O + 30% wt. KOH				
Electrolyte Quantity	220 L	240 L	360 L	480 L	610 L
Installation area	Outdoor, general purpose area (optional indoor)				
Ambient Temperature Range	-20°C to +40°C (-40°C or +50°C as an option)				
Dimensions (L X W X H)	6,10m x 2,44m x 2,90m (+1,60m with dry cooler)				
Empty weight	Approx. 16 Tons				

Figure 2.14. *Technical specifications for the HySTAT type V series from HYDROGENICS (alkaline electrolyzer) [HYD]*

14 wt. = weight ratio.

2.5. Theoretical approach to an electrolyzer

2.5.1. *Energy-related elements*

2.5.1.1. *Thermodynamic elements*

As with any electrochemical component on charge, the electricity received can only be transformed into "chemical" energy[15] at the level of the free enthalpy (or Gibbs free energy) ΔG_d.[16] However, in order for hydrogen production to take place at the cathode and oxygen to be produced at the anode, it is necessary to reach the energy corresponding to the dissociation enthalpy of water ΔH_d. The energy complementary to the free enthalpy will be supplied by the environment in the form of heat equal to $T\Delta S_{d\,rev}$:

$$\Delta G_d + T\Delta S_{d\,rev} = \Delta H_d \qquad [2.5]$$

As regards the electrochemical reaction that takes place in an electrolyzer, it is therefore endothermic because it takes heat from the environment.

The free enthalpy ΔG_d is given by the following expression[17] representing the transformation of electrical energy first into heat, and then into chemical energy when the gases are finally produced:

$$\Delta G_d = E_{rev}\,2F \qquad [2.6]$$

The term $T\Delta S_{d\,rev}$ is called "(the reversible) entropic heat (of dissociation)". The qualifier "reversible", which is often omitted, is a term taken from the world of thermodynamics which denotes that it is theoretically possible to follow a reversible path to move from one mode of operation to another by way of a bidirectional heat exchange with the environment. In other words, if an electrolyzer were functioning in the opposite mode, i.e. as a fuel cell, it would then restore that entropic heat to the environment (as this time the reaction is exothermic).

The dissociation of the water takes place in the gaseous state. This means that if liquid water is injected into the electrolyzer, additional energy ΔH_{vapo} is required to vaporize the water during the reaction.

---

15 This refers to the chemical energy contained in the gases which will be produced. This energy necessarily passes through an intermediary situation in the form of heat.

16 The subscript "d" is used to represent "dissociation of water".

17 This equation linking the free enthalpy ΔG to the reversible voltage E_{rev} is better known in the form: $E_{rev} = -\Delta G_f/2F$, which implies operation in fuel-cell mode, and therefore transformation of the chemical energy first into heat and then finally into electrical energy when the current is supplied. The subscript "f" is used this time to denote "formation of water".

The typical values presented in the existing body of literature for thermodynamic values are those for standard ambient temperature and pressure (SATP) – i.e. 298 K (25°C) and 1 bar. These values are recapped in Table 2.7. The enthalpy of vaporization of the water ΔH_{vapo} is the difference between the two values of ΔH_d in Table 2.1: ΔH_{vapo} (25°C, 1 bar) = 44 kJ/mol in these conditions. If we now calculate the differences between the two values in this table for ΔG_d and $T\Delta S_{drev}$, we notice that the heat required for vaporization will largely be supplied by the environment via the entropic heat (35.5 kJ/mol, which is 81% of the required amount), in comparison with that provided by the electrical energy and free enthalpy (8.5 kJ/mol, 19% of the requirement). The higher the operating temperature, the greater the proportion of the heat needed to vaporize the water that will come from entropic heat (100% of the requirement at 100°C and 1 bar, so ΔH_{vapo} (100°C, 1 bar) = 40.65 kJ/mol).

State of the water injected into the electrolyzer	ΔH_d [kJ/mol]	ΔG_d [kJ/mol]	ΔS_d [kJ/mol/K]	$T\Delta S_{drev}$ [kJ/mol/K]
Liquid	285.8[18]	237.1	0.163	48.7
Vapor	241.8[19]	228.6	0.044	13.2
Difference between liquid and vapor	44	8.5	0.119	35.5

Table 2.7. *Thermodynamic values at 25°C and 1 bar*

The values of ΔG_d, $T\Delta S_{drev}$ and ΔH_d are dependent upon the operating temperature and pressure and on the state in which the water is injected into the electrolyzer. Figure 2.15 illustrates their dependence on temperature at atmospheric pressure.

It is important that Figure 2.15 be accompanied by certain comments. Indeed, the curves taken from [GON 12] seem to suggest that beyond 100°C, the enthalpy for vaporization of the water no longer needs to be supplied. This is only true if the water is injected into the electrolyzer as vapor (in terms of the component, it disappears from the balance; in terms of the overall procedure, we must not lose sight of it). If the water is injected in liquid form, as can clearly be seen from the curves taken from [STO 10b], then it needs to be supplied as entropic heat (caution: unlike the curve ΔH_d, the scenario is not traced as a dotted line for the curve representing the $T\Delta S_{drev}$, which would then be translated as ΔH_{vapo} (100°C[20], 1 bar) = 40.65 kJ/mol). Table 2.8 gives a numerical illustration of these arguments at 1000°C and 1 bar.

18 This corresponds to the HHV (Higher Heating Value) found in the literature.
19 This corresponds to the LHV (Lower Heating Value).
20 Strictly speaking, this is actually 99.63°C, as 100°C is at atmospheric pressure of 1.0133 bar.

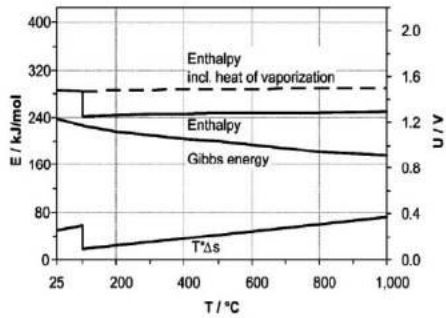

[STO 10b]

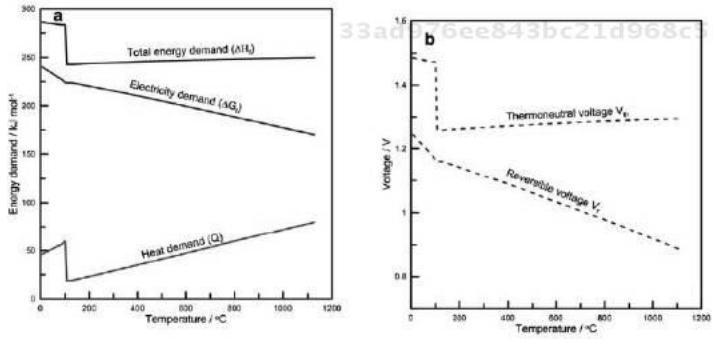

[GON 12]

Figure 2.15. *Dependence of thermodynamic values on temperature at atmospheric pressure*

State of the water injected into the electrolyzer	ΔH_d [kJ/mol]	ΔG_d [kJ/mol]	ΔS_d [kJ/mol/K]	$T\Delta S_{d\,rev}$ [kJ/mol/K]
Liquid	289.85	179.9	0.054	$+\Delta H_{vap}$ (100°C. 1bar) = 109.95
Vapor	249.2	179.9	0.054	69.3

Table 2.8. *Thermodynamic values at 1000°C and 1 bar*

NOTE.– For an electrolyzer operating at atmospheric pressure, the water will vaporize at 100°C. We need to bear in mind that the enthalpy of vaporization decreases with decreasing pressure, whereas the vaporization temperature increases, which complexifies the thermodynamic balances.

By increasing the temperature, we are able to achieve rather significant decreases (up to 25% between 25°C and 1000°C) in the direct electricity demand (ΔG_d) of the

reaction. This is particularly advantageous when we have an external heat source that is less expensive than electrical energy.

At this stage of the theoretical approach, only two modes of operation can be envisaged, depending on whether the water being electrolyzed is in liquid or vapor form. The electricity source supplies the free enthalpy. The other requirements in terms of heat (reversible entropy of reaction and, possibly, enthalpy of water vaporization) are fulfilled by an external heat source. The voltage at the terminals of an electrolysis cell for different cases is given in Table 2.9: at this stage, it can only be equal to the reversible voltage.

Nature of the water being electrolyzed	Temperature and pressure conditions	Voltage [V] at the terminals of an electrolysis cell: $E_{rev} = \frac{\Delta G_d}{2F}$
Liquid	25°C, 1 bar	1.229
	100°C, 1 bar	1.167[21]
	1000°C, 1 bar	0.932
Vapor	25°C, 1 bar	1.185
	100°C, 1 bar	1.167[22]
	1000°C, 1 bar	0.932

Table 2.9. *Some possible values of the voltages at the terminals of an "ideal" electrolysis cell ("ideal" meaning without irreversible losses)*

2.5.1.2. *Impact of irreversible losses*

In practice, as we shall see in detail in section 2.5.2, a "real" electrolyzer will require more electrical energy than just the free enthalpy ΔG_d to cater for the energy needs relating to the chemical kinetics of the reaction, the movements of the species and those of the charge carriers. The electrical power $P_{electrical}$ necessary for an electrolysis cell can be expressed as follows:

$$P_{electrical} = U_{cell}.I = \left(E_{rev} + \sum_i \eta_i \right).I = \left(\frac{\Delta G_d}{2F} + \eta_{activation} + \eta_{transport} + \eta_{Ohm} \right).I \qquad [2.7]$$

where U_{cell} is the real voltage of the electrolysis cell and the η_i values are the various overvoltages (in relation to the reversible voltage E_{rev}). $\eta_{activation}$, $\eta_{transport}$ and η_{Ohm}

21 Data taken from [MIL 07].
22 Estimated on the basis of [MIL 07].

are respectively the activation overvoltage (chemical kinetics), species transport overvoltage and Ohmic overvoltage (movements of the charge carriers).

In fine, this additional electrical power will be transformed into heat which will be released into the environment (the component itself to begin with). This time, the losses will be irreversible.[23] In other words, even if we were to reverse the function and have the component operate in fuel-cell mode, it is not possible to recover these losses from the environment.

Thus, although the electrochemical reaction as such remains endothermic, the overall thermal behavior of an electrolyzer could be exothermic because of these irreversible losses. This being the case, the component will need to be cooled in order to avoid any thermal runaway and preserve its integrity.

The heat liberated by these irreversible losses can be put to good use, to feed the component itself and satisfy all or part of the entropic heat requirement $T\Delta S_{rev}$ of the electrochemical reaction. It is for this reason that the electrical efficiency of an electrolyzer (a concept which we shall discuss later on) could be greater than that of a fuel cell, and even surpass 100% under certain considerations. Indeed, in a fuel cell, the irreversible losses, which are identical to those of an electrolyzer in terms of the nature of the phenomena involved, hamper electricity production.

Thus, in addition to the two modes of operation discussed in the previous section (2.5.1.1), there are two more possible modes as described in [STO 10b]. The entire collection of modes which are envisageable finally is shown in Table 2.10. Cases 2 and 4 correspond to the two previous cases, corrected by the presence of the irreversible losses, which contribute to feeding the entropic heat demands $T\Delta S_{rev}$. The two new cases are 1 and 3: they exploit only the heat generated by the inevitable irreversible losses; there is no external heat source (with the exception of a source to vaporize the water in case 3).

In a global approach, the first case corresponds to the function of the PEM and alkaline electrolyzers that are currently commercialized. They begin with liquid water and only require electrical supply. At normal operating temperatures below 100°C, the irreversible losses are such that the dissociation voltage $\Delta H_d/2F$ is attained with (very) low current densities. Put differently, these two technologies would systematically need cooling if operating at the current densities conventionally used for reasons of economic viability [MIL 07]. This first case could, to a certain extent, make sense for SO technology, for instance, in the case of exploitation of overproduction of renewable electricity (which would otherwise be

23 Thermodynamics engineers generally group these irreversible losses together, representing them with the term "irreversible entropic heat of reaction" (notated $T\Delta S_{irrev}$).

lost) facilitating operation at high current densities and enabling us to go beyond the dissociation voltage.

State of the water injected into the electrolyzer	***Minimum* electrical energy required | Voltage of a *corresponding* electrolysis cell** and origins of the energy required ΔH_d	
Liquid	CASE 1 (exothermic; $_{cell} \geq E_{tn}$): ΔH_d | $\Delta H_d/2F$ 285.8 kJ/mol | 1.481 V @ 25°C 283.5 kJ/mol | 1.469 @ 100°C[24] 289.9 kJ/mol | 1.502 V @ 1000°C ΔG_d, ΔH_{vapo} and $T\Delta S_{d\,rev}$ supplied by the electricity source directly to the reaction for ΔG_d and indirectly via the irreversible losses for the rest.	CASE 2 (endothermic; $U_{cell} \leq E_{tn}$): ΔG_d | $\Delta G_d/2$ F 237.1 kJ/mol | 1.229 V @ 25°C 225.2 kJ/mol | 1.167 @ 100°C[25] 179.9 kJ/mol | 0.932 V @ 1000°C ΔG_d supplied by the electricity source directly to the reaction. $T\Delta S_{d\,rev}$ supplied by the heat source and the electricity source (indirectly via the irreversible losses). ΔH_{vapo} supplied by the heat source and the electricity source (indirectly via the irreversible losses; below 100°C the electricity source will also contribute to around 20% via the free enthalpy).
Vapor	CASE 3 (exothermic; $U_{cell} \geq E_{tn}$): ΔH_d | $\Delta H_d/2F$ 241.8 kJ/mol | 1.253 V @ 25°C 242.8 kJ/mol | 1.258 @ 100°C[26] 249.2 kJ/mol | 1.291 V @ 1000°C ΔG_d and $T\Delta S_{drev}$ supplied by the electricity source respectively directly to the reaction and indirectly via the irreversible losses. ΔH_{vapo} supplied from outside of the electrolyzer system.	CASE 4 (endothermic; $U_{cell} \leq E_{tn}$): ΔG_d | $\Delta G_d/2$ F 228.6 kJ/mol | 1.185 V @ 25°C 225.2 kJ/mol | 1.167 @ 100°C[27] 179.9 kJ/mol | 0.932 V @ 1000°C ΔG_d supplied by the electricity source directly to the reaction. $T\Delta S_{d\,rev}$ supplied by the heat source and the electricity source (indirectly via the irreversible losses). ΔH_{vapo} supplied from outside of the electrolyzer system.

Table 2.10. *Four possible scenarios of operation for an electrolyzer (numerical illustrations at 1 bar pressure)*

24 Data taken from [MIL 07].
25 Data taken from [MIL 07].
26 Estimated on the basis of [MIL 07].
27 Estimated on the basis of [MIL 07].

Again in a global approach, the fourth case corresponds to the operation typically sought from SO technology, making use of a heat source and thus reducing electricity consumption. This is the case, for instance, with a nuclear power plant which produces extremely hot water vapor, and by which we wish to manage overproduction of electricity [HIN 04; PY 13]. In terms of a more renewable approach, the heat source could use concentrated solar power, and the electricity source photovoltaic solar power and/or wind power [DER 05]. Geothermal energy can also be envisaged, at least for vaporization and to heat the water to several hundred degrees [JON 92], etc. Note that this fourth case is possible with SO technology because the irreversible losses are considerably reduced, meaning the system can function below the dissociation voltage $\Delta H_d/2F$ with sufficiently high current densities[28] to be economically advantageous. For the reasons listed above, such operation is not, *a prion*, economically advantageous for PEM and alkaline technologies.

The second case is a variant of the fourth where the water would be injected in liquid form. For the same reasons, it only seems to be applicable for high-temperature technology.

The third case is a variant of the first. It remains fairly futuristic for PEM and alkaline technologies. It is possible for SO technology with high current densities.

In between all of these cases, there is a particular means of operation for which the electrolyzer exchanges no heat at all with the environment (the point of thermal equilibrium). This particular point corresponds to the rare case wherein all the irreversible losses generated by the component exactly cover the electrochemical reaction's needs in terms of entropic heat, or of heat for vaporization of the water. The voltage E_{tn} corresponding to this particular regime is equal to the equivalent voltage of dissociation of water:

$$E_{tn} = \frac{\Delta H_d}{2F} \qquad [2.8]$$

This is known as the "thermoneutral voltage/potential". Hence (theoretically) there is no longer any need for an external heat source and/or cooling system: the electricity source itself is sufficient.

Based on the same reasoning as for the previous four cases, thermoneutral function appears possible and pertinent only for SO technology operating at high

28 According to [LEF 11], the performances attained with the current state of the art are: 1 A/cm² at 800°C; 1.5 A/cm² at 850°C; and even 3 A/cm² at 950°C at thermoneutral voltage (rounded to ≈1.3 V).

temperature. Yet [LEF 11] advises readers to seek to operate their equipment at this point as far as possible. The drawback is that this immobilizes the operational current density; this only seems appropriate for highly stable electricity sources, which is not the case with renewable energies such as photovoltaic or wind power.

In closing this section, let us point out that it is naturally possible to switch from one mode of operation to another if we sweep a broad range of current densities. Take the well-known example where we wish to plot the voltage–current curve $U_{ELYZ}(I)$ of the component. This will afford us the opportunity to give an overview of the points discussed above:

– for PEM and alkaline technologies, we shall only have endothermic operation at very low current densities: the component draws heat from its environment (Figure 2.16). We can imagine that with high-power components, this mode of operation is not possible or cannot last for long. When this high current density is reached, the operation quickly becomes exothermic;

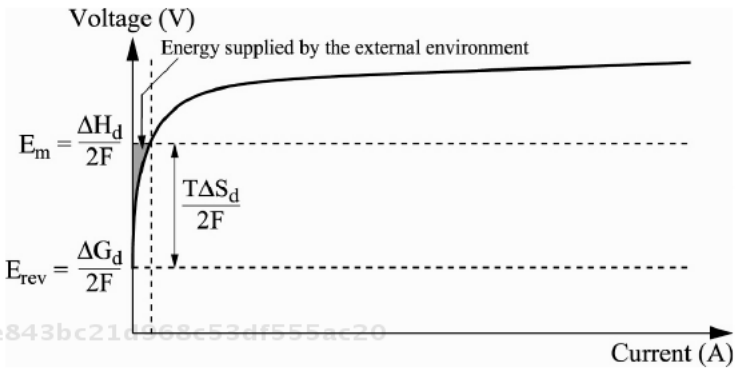

Figure 2.16. *Typical shape of the voltage–current curve for a PEMWE or AWE electrolyzer*

– for SO technology, endothermic operation will only be possible if heat is supplied by an external source because this zone covers a fairly broad range of current densities (Figure 2.17). Otherwise, the electrochemical reaction will take heat from the component itself, thereby cooling it to the point where it ceases to function. The heat supplied by the external source will progressively decrease and eventually disappear altogether at thermoneutral voltage $\Delta H_d/2$ F. Beyond this level of voltage, the component will need to be cooled.

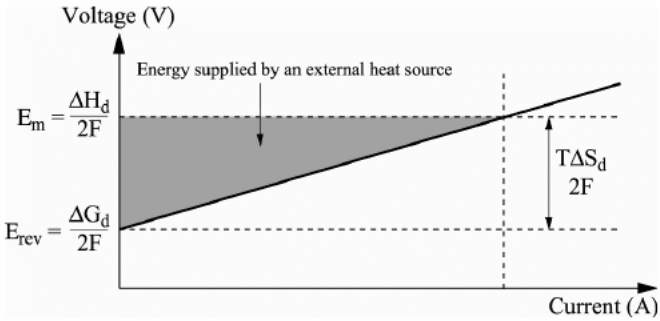

Figure 2.17. *Typical shape of the voltage–current curve of a SOWE electrolyzer*

2.5.1.3. *Efficiency of an electrolyzer*

As with all electrochemical components, the concept of efficiency is always tricky to grasp. This is particularly true for an electrolyzer, which needs at least two sources of energy: an electricity source and an external heat source. Without, for the moment, considering the necessary auxiliaries in an electrolyzer, two definitions of efficiency can conventionally be posited:

– the *energy efficiency*, defined in relation to the enthalpy of dissociation of water ΔH_d and enabling us to evaluate whether the energy injected into the electrolyzer system is actually used:

– in endothermic operation:

$$\eta_{energy} = \frac{\Delta H_d}{\Delta G_d + Q_{irreversible\_losses} + Q_{external\_source}} \times 100 \quad [2.9]$$

where $\Delta G_d + Q_{irreversible\_losses} + Q_{external\_source} \leq \Delta H_d$

– in exothermic operation:

$$\eta_{energy} = \frac{\Delta H_d}{\Delta G_d + Q_{irreversible\_losses}} \times 100 \quad [2.10]$$

where $\Delta G_d + Q_{irreversible\_losses} \geq \Delta H_d$

where $Q_{irreversible\_losses}$ (kJ/mol)[29] is the heat produced by the irreversible losses (activation, transport of species and charges) relating to the electrochemical reaction, and $Q_{external\_source}$ (kJ/mol) is the heat provided by the external source.

29 This implies the value per mole of hydrogen produced or per mole of water consumed. Remember that 1 mole of water gives us 1 mole of H_2 and half a mole of O_2.

– the *electrical efficiency*[30], defined in relation to the free enthalpy of dissociation of water ΔG_d, which enables us to evaluate, more specifically, how the electrical energy is used in the electrolyzer system:

$$\eta_{electrical} = \frac{\Delta G_d}{\Delta G_d + Q_{irreversible\_losses}} \times 100 \qquad [2.11]$$

Note that these two efficiencies assume values between 0 and 100%. These values will depend on the point of operation and the operating conditions.

The energy efficiency will only be 100% at the thermoneutral point, so we can see the advantage in seeking to find this point, if possible and pertinent[31], as for SO technology. Above or below this point, the energy efficiency will be less than 100%. From the point of view of the system, the energy efficiency is the only value that is important.

The electrical efficiency, which is far less easy to grasp[32], is specific to the electricity source. It will only ever be 100% with an ideal component, but this would necessarily involve the use of an external heat source. A 100% electrical efficiency means that all the electrical energy is used only to directly supply the free enthalpy of reaction ΔG_d and nothing more. In a real component, as long as the electrical efficiency is between $\Delta G_d/\Delta H_d$ (≈83% with liquid water, 25°C, 1 bar) and 100%, the excess electrical energy is not lost because it indirectly contributes, by way of the irreversible losses relating to the reaction of dissociation of water, to the provision of the entropic heat required by that reaction. Below the efficiency value equal to $\Delta G_d/\Delta H_d$, the operation changes to exothermic mode (cooling becomes necessary) and the electrical energy, exceeding ΔH_d, can no longer do any more than offset the irreversibilities of the reaction.

In practice, it is helpful to speak of everything in terms of voltages, which give values that are more easily manipulated and measured. In order to express the values as voltages, we need only divide the terms in equations [2.9–2.11] by 2F. We then get:

– for the energy efficiency:

- in endothermic operation:

30 This is sometimes called the "voltaic" efficiency.

31 We must not lose sight of the fact that with given operating conditions, it corresponds to a fixed current density.

32 The same is not true of a fuel cell functioning as an electrical generator with exothermic behavior.

$$\eta_{energetic} = \frac{E_{tn}}{E_{rev} + \left(\eta_{activation} + \eta_{transport} + \eta_{ohm}\right) + \frac{Q_{external\_source}}{2F}} \times 100$$
$$= \frac{E_{tn}}{U_{cell} + \frac{Q_{external\_source}}{2F}} \times 100 \qquad [2.12]$$

where $U_{cell} \leq E_{tn}$

- in exothermic operation:

$$\eta_{energy} = \frac{E_{tn}}{E_{rev} + \left(\eta_{activation} + \eta_{transport} + \eta_{ohm}\right)} \times 100 = \frac{E_{tn}}{U_{cell}} \times 100 \qquad [2.13]$$

where $U_{cell} \geq E_{tn}$

– for the *electrical efficiency*:

$$\eta_{electrical} = \frac{E_{rev}}{E_{rev} + \left(\eta_{activation} + \eta_{transport} + \eta_{ohm}\right)} \times 100 = \frac{E_{rev}}{U_{cell}} \times 100 \qquad [2.14]$$

The above definitions of efficiency are valid no matter what the technology used in the electrolyzer and no matter what the thermal mode of operation (endothermic or exothermic) of the electrolyzer.

As explained earlier, in practice, PEMWE and electrolyzers will exhibit exothermic function with their operational current densities. No external heat source will be used; far from it – in fact, a cooling system will need to be employed. Equations [2.13] and [2.14] will therefore be used. The optimum energy efficiency (100%) will actually be attained with operation at the thermoneutral point, corresponding to very low current densities for PEMWE and AWE technologies. If these hypotheses are true, the electrical efficiency will at best be equal to $E_{rev}/E_{tn} \approx 83\%$ (liquid water, 25°C, 1 bar).

With SOWE technology, equations [2.12] and [2.14] will be used most frequently, but exothermic operation, and therefore use of equation [2.13], is possible with high current densities.

With all these formulae defined, the question arises of the values to be used for the different thermodynamic values ΔH_d and ΔG_d, and there is no agreement between the authors in the bibliography on this issue. The question at the center of the debates hinges, more precisely, on the choice for the value of the enthalpy of reaction ΔH_d: HHV or LHV? In other words, in the energy balance equation, do we need to consider the enthalpy of vaporization of water, the difference between the HHV and the LHV?

If the electrolyzer is fed with liquid water (which is very common with PEMWE and AWE devices), it seems pertinent to consider the HHV because the enthalpy used to vaporize the water is usually not then recovered. If the electrolyzer is fed with a source of vapor (which may potentially be the case with a SOWE in real-world exploitation), it is relevant to consider the LHV in drawing the energy balance of the electrolyzer.

Table 2.11 summarizes the formulae and data for the various cases. The results will be dependent on the temperature and the pressure, and on the point of operation ($U_{cell} = f(I)$), which will be linked to the sensitivity of the irreversible phenomena (activation, transport of species and charges) to operating conditions.

	Exothermic operation $U_{cell} \geq E_{tn}$		Endothermic operation $U_{cell} \leq E_{tn}$		
Energy efficiency	$\frac{\Delta H_d}{\Delta G_d + Q_{irreversible\_losses}} \times 100 = \frac{E_{tn}}{U_{cell}} \times 100$		$\frac{\Delta H_d}{\Delta G_d + Q_{irreversible\_losses} + Q_{external\_source}} \times 100 = \frac{E_{tn}}{U_{cell} + \frac{Q_{external\_source}}{2F}} \times 100$		
Electrical efficiency	$\frac{\Delta G_d}{\Delta G_d + Q_{irreversible\_losses}} \times 100 = \frac{E_{rev}}{U_{cell}} \times 100$				
Data if the water injected into the electrolyzer is liquid	**1 bar pressure**	**ΔH_d [kJ/mol] (HHV)**	**E_{tn}[V]**	**ΔG_d [kJ/mol]**	**E_{rev} [V]**
	25°C	285.8	1.481	237.1	1.229
	100°C	283.5	1.469	225.2	1.167
	1000°C	289.9	1.502	179.9	0.932
Data if the water injected into the electrolyzer is vapor	**1 bar pressure**	**ΔH_d [kJ/mol] (LHV)**	**E_{tn}[V]**	**ΔG_d [kJ/mol]**	**E_{rev} [V]**
	25°C	241.8	1.253	228.6	1.185
	100°C	242.8	1.258	225.2	1.167
	1000°C	249.2	1.291	179.9	0.932

Table 2.11. *Formulae and data (at 1 bar) for calculating the energy efficiency of an electrolyzer*[33]

33 The formulae and data correspond to one cell of the electrolyzer. If the electrolyzer has more than one cell (N_s), we usually express values in terms of the equivalent average cell (EAC): $U_{EAC} = U_{electrolyzer}/N_s$. It is also possible to multiply everything by N_s.

REMARK 2.1.– in the existing body of literature, we can find examples of efficiencies greater than 100%. Thus, if we apply equation [2.13] to voltages below the thermoneutral point E_{tn}, the efficiency will artificially be made greater than 100% because we ignore the heat supplied from outside. Strictly speaking, there would be no reason for this to be true if the formulae were correctly applied.

Hitherto, we have not considered the necessary auxiliaries in the electrolyzer. There are many possible formulae, of varying degrees of sophistication, to take these auxiliary elements into consideration. We shall use the simple and most widely applicable approach, viewing them only in terms of the efficiencies, which may obey more or less precise laws. Naturally, it only makes sense to consider them at the level of the energy efficiency:

– in endothermic operation:

$$\eta_{energy} = \eta_{auxiliaries} \times \frac{E_{tn}}{U_{cell} + \frac{\eta_{external\_source} \times Q_{external\_source}}{2F}} \times 100 \qquad [2.15]$$

where $U_{cell} \leq E_{tn}$

– in exothermic operation:

$$\eta_{energy} = \eta_{auxiliaries} \times \frac{E_{tn}}{U_{cell}} \times 100 \qquad [2.16]$$

where $U_{cell} \geq E_{tn}$

with $\eta_{auxiliaries}$ representing the alteration of the energy efficiency by the auxiliaries[34] essentially consuming electrical energy and $\eta_{external\_source}$ the efficiency from the external heat source.

In the technical specifications of PEMWE- or AWE-type commercial products, the manufacturers very often express the performances of their electrolyzers in kWh/Nm^3 or kWh/kg of hydrogen produced, because the primary need of the clients is often a source of hydrogen. Unfortunately, it is not always very clear whether the drying of the hydrogen has been considered and whether the auxiliaries have been taken into account. At 25°C and 1 bar, the theoretical values are 39.7 kWh/kg and 3.54 kWh/Nm^3 when we start with liquid water. In practice, a typical order of magnitude is approximately 5 kWh/Nm^3 (i.e. 55 kWh/kg), giving us a typical energy efficiency of around 70%.

34 The literature speaks of "BoP", which stands for "Balance of Plant". For instance, in [STO 10b], reference is made to objectives set by the US Department of Energy (DoE) for the production of H_2 from wind energy, which considers a Balance of Plant as $\eta_{BoP} = 95\%$.

REMARK 2.2.– the literature also offers up other considerations for the performance balances of an electrolyzer – e.g. the *Faradaic efficiency*, the ratio between the current injected and the theoretical current. In general, it is considered very nearly equal to 1 on condition that the parasitic reactions are negligible [MIL 07]. Strictly speaking, we also need to consider the impact of the phenomenon of crossover of the gases through the membrane, which very slightly reduces the amount of gas produced, and therefore affects the *efficiency of matter produced*. The phenomenon of crossover will be all the more prevalent at higher operational pressure; it will also increase as the component ages. This efficiency is not usually taken into account in balances, because the phenomenon of crossover is very difficult to measure during operation.

2.5.2. *Electrical behavior in the quasi-static state*

Here, we wish to describe the relation between the voltage U of the electrolyzer and its current I. Very often, this relation $U(I)$ is called the *polarization curve* or indeed the *quasi-static curve*.

The theoretical voltage at the terminals of an electrolyzer is $E_{rev} = \Delta G_d / 2F$.

In practice, it will be higher than this, because of the physico-chemical phenomena linked to the occurrence of the reaction of dissociation of water: phenomena of activation, transport of species and charges.

On the scale of a cell, the polarization curve has the following general equation:

$$U_{cell}(I) = E_{rev} + |\eta_{activation}(I)| + |\eta_{transport}(I)| + |\eta_{ohm}(I)| \qquad [2.17]$$

where U_{cell} is the real voltage of the electrolysis cell, and $\eta_{activation}$, $\eta_{transport}$ and η_{ohm} are, respectively the overvoltages (defined in relation to the reversible voltage E_{rev}) of activation (chemical kinetics), transport of species and Ohmic transport (movements of the charge carriers). The absolute values applied to each phenomenon are there to prevent any ambiguity as regards the fact that we are in fact dealing with overvoltages.

Theoretically, it is possible to separate the contribution of each electrode. In practice, this is fairly tricky to do for a monocell, and very difficult on the scale of an entire stack. Hence, in our discussions, we shall quite deliberately adopt the policy of considering only the overall contribution, in terms of voltage at the terminals of the electrolyzer, made by each of the phenomena which take place locally at the level of each electrode.

In the case of an electrolyzer stack, the voltage at its terminals will be the sum of all the voltages of the N_s cells which make up that stack and which are electrically connected in a series:[35]

$$U_{stack}(I) = N_s E_{rev} + \left|\eta_{activation\_stack}(I)\right| + \left|\eta_{transport\_stack}(I)\right| + \left|\eta_{ohm\_stack}(I)\right| \quad [2.18]$$

In the case of a stack, it is usual to express things in terms of the equivalent average cell (EAC) in order to be able to manipulate values whose orders of magnitude are well known:

$$U_{EAC}(I) = \frac{U_{stack}(I)}{N_s} = E_{rev} + \left|\eta_{activation\_EAC}(I)\right| + \left|\eta_{transport\_EAC}(I)\right| + \left|\eta_{ohm\_EAC}(I)\right| \quad [2.19]$$

Similarly, it is fairly commonplace to use the current density i rather than the current I, again with the aim of being able to work with values whose orders of magnitude are well known, in the knowledge that $i = I/S$, with S being the surface area of the cell shared between all the cells in the stack. Obviously, this has no impact on the value of the overvoltages:

$$U_{EAC}(i) = E_{rev} + \left|\eta_{activation\_EAC}(i)\right| + \left|\eta_{transport\_EAC}(i)\right| + \left|\eta_{ohm\_EAC}(i)\right| = U_{EAC}(I) \quad [2.20]$$

We shall now describe each of the terms of the polarization curve.

2.5.2.1. *Reversible potential*

The reversible potential is dependent on the temperature and pressure, with the relation being expressed by the following formula:

$$E_{rev}(T,P) = E^0(T) + \frac{RT}{2F}\ln\left(\frac{P_{H_2} P_{O_2}^{\frac{1}{2}}}{a_{H_2O}}\right) \quad [2.21]$$

where E^0 is the standard voltage ("potential") defined for the pressure of 1 bar, P_{H2} and P_{O2} are the relative partial pressures (bar) of the gases and T is the temperature (K) of the component.

With regard to the water, if the vast majority of it is liquid (which is typically the case with PEMWE and AWE electrolyzers), we can consider that $a_{H_2O} = 1$. If the water is in gaseous form (which is typically the case with high-temperature SOWE electrolyzers), $a_{H_2O} = P_{H_2O}$, the partial pressure of the water.

35 Essentially, they are fluidically connected in parallel.

The law of temperature dependency of the standard potential $E^0(T)$ needs to be determined on the basis of thermodynamic tables. Figure 2.15 gives an illustration of this.

2.5.2.2. *Activation overvoltage*

At the overall level, the phenomena of activation, related to the kinetics of the reaction of dissociation of water, are governed by a *Butler–Volmer law*, presented here in the conventional notation used when speaking about generators[36] ($I < 0$ in electrolyzer operation):

$$I = I_0^{FC} e^{\frac{2\alpha_{FC}F}{RT}\eta_{activation}} - I_0^{ELYZ} e^{-\frac{2\alpha_{ELYZ}F}{RT}\eta_{activation}} \quad [2.22]$$

where:

– I_0^{FC} is the activation current (A) for the reaction relative to a positive current produced by the component (Fuel Cell operation);

– I_0^{ELYZ} is the activation current (A) for the reaction relative to a negative current received by the component (ELYZ operation);

– α_{FC} is the transfer coefficient for the reaction relative to a positive current produced by the component (Fuel Cell operation);

– α_{ELYZ} is the transfer coefficient for the reaction relative to a negative current received by the component (ELYZ operation).

– T is the operating temperature of the component (K).

– $n = 2$ corresponds to the quantity of electrons exchanged during the reaction.

This formulation supposes that there is no problem with the transport of the species. We shall question this hypothesis in section 2.5.2.3.

The Butler–Volmer law is defined for a null current: the activation losses are therefore null.

However, this formula is not formally invertible in the state to obtain $\eta_{activation}$ as a function of I, as required to model the polarization curve. In order to invert this formula, we need to make the hypothesis that the current I in the component is far greater (in terms of absolute value) to the activation current I_0. This hypothesis is known as the *Tafel hypothesis* and enables us to neglect one exponential term in favor of the other, depending on the sign of the current, and thus invert the formula.

36 This choice is more generic in terms of a potentially-reversible component.

In the present example of the electrolyzer ($I < 0$), we can use the Tafel hypothesis and write:

$$I = I_0^{FC} e^{\frac{2\alpha_{FC}F}{RT}\eta_{activation}} - I_0^{ELYZ} e^{-\frac{2\alpha_{ELYZ}F}{RT}\eta_{activation}} \approx -I_0^{ELYZ} e^{-\frac{2\alpha_{ELYZ}F}{RT}\eta_{activation}} \quad [2.23]$$

$$\text{if} \quad |I| >> I_0^{ELYZ}$$

Thus:

$$\eta_{activation} = -\frac{RT}{2\alpha_{ELYZ}F}\ln\left(\frac{-I}{I_0^{ELYZ}}\right) = -\frac{RT}{2\alpha_{ELYZ}F}\ln\left(\frac{|I|}{I_0^{ELYZ}}\right) \quad < 0 \quad [2.24]$$

$$\text{if} \quad |I| >> I_0^{ELYZ}$$

We obtain a negative value for the activation overvoltage which is simply due to the fact that the Butler–Volmer law intrinsically enables us to predict, on the basis of the sign of the current, if we will see a drop in voltage ($I > 0$; operation as a fuel cell; $\eta_{activation} > 0$) or an overvoltage ($I < 0$; operation as an electrolyzer; $\eta_{activation} < 0$) using a general expression for the variation in voltage $E_{rev} - \eta_{activation}$. It is for this reason that the absolute value is considered in equations [2.17–2.20].

Equation [2.24] is known as *Tafel's law*.

REMARK 2.3.– With a receiver convention ($I > 0$ in electrolyzer function), we would have obtained the form more commonly found in the literature for Tafel's law:

$$\eta_{activation} = \frac{RT}{2\alpha_{ELYZ}F}\ln\left(\frac{I}{I_0^{ELYZ}}\right) \quad > 0 \quad [2.25]$$

$$\text{if} \quad I >> I_0^{ELYZ}$$

Tafel's law presents the advantage of explicitly describing the activation losses as a function of the current, but the disadvantage of not defining them for $|I| \ll I_0^{ELYZ}$, and particularly for $I = 0$. We shall see in section 2.5.2.5 how this problem can be circumvented.

2.5.2.3. *Species transport overvoltage*

In the previous section, we supposed that the phenomena of species transport had no effect on the activation phenomena. In reality, this is not the case.

In support of the discussion below, we shall be forced to use certain geometric considerations. Figure 2.18 offers an overview of the internal make-up of an electrolyzer. Each electrode is taken to comprise a diffusive zone and a reaction zone (or active zone).

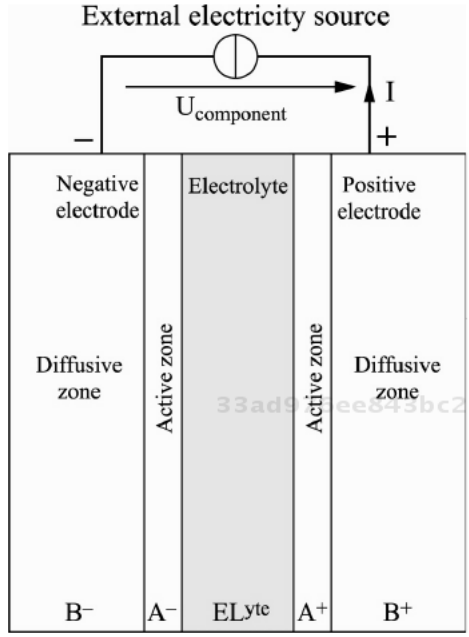

Figure 2.18. *Diagrammatic overview of the make-up of an electrolyzer (generator convention)*

If we look at the impact of the phenomena of species transport, the Butler–Volmer law [2.22] is expressed as follows in its "generalized" form:[37]

$$I = I_0^{FC}\left(\frac{C_{H_2}^{act-,FC}}{C_{H_2}^{eq-}}\right)^{\gamma_{H_2}}\left(\frac{C_{O_2}^{act+,FC}}{C_{O_2}^{eq+}}\right)^{\gamma_{O_2}}\left(\frac{C_{ion}^{act\ \psi,FC}}{C_{ion}^{elyte\ \psi,FC}}\right)^{\gamma_{ion,FC}} e^{\frac{2\alpha_{FC}F}{RT}\eta_{activation}} \quad [2.26]$$
$$-I_0^{ELYZ}\left(\frac{C_{H_2O}^{act\ \psi,ELYZ}}{C_{H_2O}^{eq\ \psi}}\right)^{\gamma_{H_2O}}\left(\frac{C_{ion}^{act\ -\psi,ELYZ}}{C_{ion}^{elyte\ -\psi,ELYZ}}\right)^{\gamma_{ion,ELYZ}} e^{-\frac{2\alpha_{ELYZ}F}{RT}\eta_{activation}}$$

37 Readers are invited to refer to [RAL 11] for the demonstration of this formula. In [RAL 11], the demonstration is performed for a PEM-type component. Here it has been extended to the other two technologies – alkaline and SO – discussed in this chapter. The underlying hypotheses are, firstly, that the activation losses at the negative electrode are negligible in comparison to those of the positive electrode and, secondly, that the connection between "pure" activation and species transport is nonlinear (which gives us the coefficients γ_X).

where the new elements of notation in comparison to equation [2.22] are:

– "ion" denotes H^+, OH^- and O^{2-} respectively for PEMWE, AWE and SOWE technology;

– "ψ" denotes the sign of the ion in question, and "-ψ" the opposite sign;

– $C_X^{act\,y,z}$ is the concentration of species X ($X = H_2$, O_2, H_2O or ions) in the active zone y (y = + denotes the active zone of the positive electrode; y = – that of the negative electrode) for z operation (z = FC or ELYZ, respectively for fuel cell or electrolyzer mode);

– $C_X^{eq\,y}$ is the concentration of the species X ($X = H_2$, O_2, H_2O) at the input/output of the electrode y (y = + denotes the positive electrode; y = - the negative electrode) whatever the mode of operation. This value is regulated and is assumed to be kept constant. $C_X^{act\,y,z} = C_X^{eq\,y,z}$ at rest ($I = 0$), so is given the name "equilibrium concentration" (eq).

– $C_{ion}^{elyte\,y,z}$ is the concentration of the ion involved at the interface of the electrolyte/y (y = + denotes the active zone of the positive electrode; y = - that of the negative electrode) for z operation (z = FC or ELYZ, respectively for fuel cell and electrolyzer mode). $C_{ion}^{elyte\,y,z} = C_{ion}^{eq}$ at rest ($I = 0$);

– γ_X is the coupling coefficient between the phenomena of activation and species transport. This coefficient is *a priori* different to 1, which implies nonlinear coupling.

Readers can refer to Figure 2.19 in order to gain a fuller understanding of the notations and, more generally, for a schematic visualization of the consequences of the phenomena of species transport on the profile of concentration of the different species for the different technologies.

In Figure 2.19, we can see how the concentration gradients are reversed for each species depending on whether the component is operating as an electrolyzer or a fuel cell. In this figure, a separate view of the different species is given in the interests of ease of visualization, but everything happens "simultaneously" – particularly the transport of water and oxygen to the positive electrode in the case of PEM technology, and transport of water and hydrogen to the negative electrode in the case of alkaline and SO technologies.

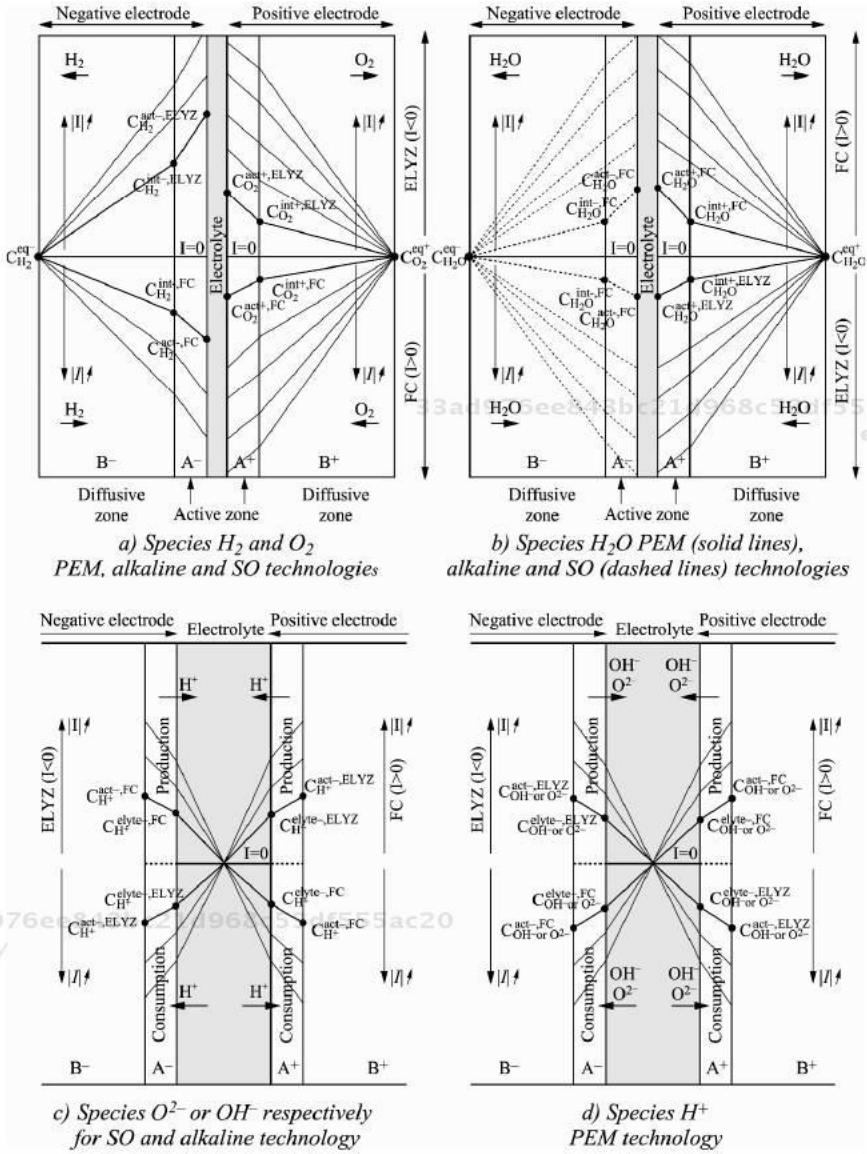

Figure 2.19. *Phenomena of species transport in a fuel cell or electrolyzer component (A and B respectively denote the active and diffusive zones; + and – represent location at the positive or negative electrode)*

The Butler–Volmer law [2.26] is said to be "globalized", because it is the result at the level of the component of the Butler–Volmer law which in reality applies to

each of the electrodes. Only the concentrations of the reactants (including the ion involved) play a part at the level of each exponential term.[38]

As the law [2.26] is not invertible, we again begin accept the Tafel hypothesis (electrolyzer operation: $I < 0$):

$$I \approx -I_0^{ELYZ} \left(\frac{C_{H_2O}^{act\ \psi,ELYZ}}{C_{H_2O}^{eq\ \psi}} \right)^{\gamma_{H_2O}} \left(\frac{C_{ion}^{act\ -\psi,ELYZ}}{C_{ion}^{elyte\ -\psi,ELYZ}} \right)^{\gamma_{ion,ELYZ}} e^{-\frac{2\alpha_{ELYZ}F}{RT}\eta_{activation}} \quad \text{if} \quad |I| >> I_0^{ELYZ} \qquad [2.27]$$

Hence:

$$\eta_{activation} = -\frac{RT}{2\alpha_{ELYZ}F}\ln\left(\frac{-I}{I_0^{ELYZ}}\right) + \frac{RT}{2\alpha_{ELYZ}\gamma_{H_2O}F}\ln\left(\frac{C_{H_2O}^{act\ \psi,ELYZ}}{C_{H_2O}^{eq\ \psi}}\right) + \frac{RT}{2\alpha_{ELYZ}\gamma_{ion,ELYZ}F}\ln\left(\frac{C_{ion}^{act\ -\psi,ELYZ}}{C_{ion}^{elyte\ -\psi,ELYZ}}\right) \quad \text{if} \quad |I| >> I_0^{ELYZ} \qquad [2.28]$$

We see the expression of the activation overvoltage [2.24] corrected by two terms relating to transport of water to the active zone where it is consumed and to transport of the involved ions between the electrolyte and the active zone where they are consumed (see Figure 2.19).

If we suppose the transport to be governed by Fick's law within the two zones A and B of the electrode in question (see Figure 2.9b), for water we shall have:

38 This does not mean that there is no influence from the products of the reaction which go in the opposite direction (toward the outside of the component). This influence will only be felt when solving the transport laws considered. The Stefan–Maxwell equation can be used to solve the simultaneous diffusion of different species within the same volume, taking account of the interactions. It is also possible to adopt a "simpler" approach, using Fick's law based on an "effective" coefficient of diffusion, with the qualifier "effective" meaning that it integrates the interactions between the species. In an electrolyzer, the effective coefficient relating to the water will integrate the effect of the evacuation of oxygen or hydrogen depending on which form of technology is being used. The difficulty is that these effective coefficients of diffusion are heavily dependent on the point of function and the operating conditions. For this reason, it is preferable to identify them (or their consequences) experimentally, as [RAL 11] proposes.

$$\frac{C_{H_2O}^{act\ \psi,ELYZ}}{C_{H_2O}^{eq\ \psi}} = \frac{C_{H_2O}^{act\ \psi,ELYZ}}{C_{H_2O}^{int\ \psi,ELYZ}} \frac{C_{H_2O}^{int\ \psi,ELYZ}}{C_{H_2O}^{eq\ \psi}} = \left(1 - \frac{|I|}{I_{\lim_{A\psi H_2O}}}\right)\left(1 - \frac{|I|}{I_{\lim_{B\psi H_2O}}}\right) \quad [2.29]$$

where:

$$I_{\lim_{A\psi H_2O}} = I_{\lim_{A\psi H_2O}}^{pur} \left(1 - \frac{|I|}{I_{\lim_{B\psi H_2O}}}\right) \quad [2.30]$$

$$I_{\lim_{A\psi H_2O}}^{pure} = \frac{2FSD_{A\psi\ H_2O}^{eff} C_{H_2O}^{eq\ \psi}}{\xi_{H_2O}\delta_{A\ \psi}} \quad [2.31]$$

$$I_{\lim_{B\psi H_2O}} = \frac{2FSD_{B\psi\ H_2O}^{eff} C_{H_2O}^{eq\ \psi}}{\xi_{H_2O}\delta_{B\ \psi}} \quad [2.32]$$

where the new notations used mean:

– $C_{H_2O}^{int\ \psi,ELYZ}$ is the concentration (mol/m^3) of the species H_2O at the interface between zone A and zone B of the electrode in question (given by the sign ψ of the ion involved).

– $I_{lim_{A\psi}}{}_{H_2O}$ and $I_{lim_{B\psi}}{}_{H_2O}$ are the *effective* limit currents of diffusion (A) respectively in zones A and B of the said electrode. Note that these two currents are logically connected by a coupling law that is a function of the point of operation;

– $I_{lim_{A\psi}}{}_{H_2O}^{pure}$ is the *effective* limit current of diffusion (A) in zone A of the said electrode if there were only one zone;

– $D_{A\psi}{}_{H_2O}^{eff}$ and $D_{B\psi}{}_{H_2O}^{eff}$ are the *effective* coefficients of diffusion (m^2/s) respectively for zones A and B of the said electrode;

– $\delta_{A\psi}$ *and* $\delta_{B\psi}$ are respectively the thicknesses (m) of zones A and B of the electrode;

– $\mathcal{S}$ is the surface area (m^2) of the component;

– ξ_{H_2O} is the stoichiometric coefficient of the water ($\xi_{H_2O} = 1$ with PEM and SO technologies, and $\xi_{H_2O} = 2$ for alkaline technology).

With a similar approach (see Figure 2.9c and d), we would have the following for the ion involved:

$$\frac{C_{ion}^{act-\psi,ELYZ}}{C_{ion}^{elyte-\psi,ELYZ}} = 1 - \frac{|I|}{I\lim_{A-\psi_{ion}}} \quad [2.33]$$

where:

$$I\lim_{A-\psi_{ion}} = \frac{2FSD_{A-\psi_{ion}}^{eff} C_{ion}^{elyte-\psi,ELYZ}}{\xi_{ion}\delta_{A-\psi}} \quad [2.34]$$

where the new notations used mean:

– $I_{lim_{A-\psi_{ion}}}$ is the *effective* limit current of diffusion (A) in zone A of the electrode in question (given by "-ψ", i.e. minus the sign ψ of the ion involved).

– $C_{H_2O}^{elyte\ \psi,ELYZ}$ is the concentration (mol/m^3) of the species H_2O at the interface between zone A and the electrolyte at the electrode in question (given by the sign ψ of the ion involved).

– $D_{A-\psi_{ion}}^{eff}$ is the *effective* coefficient of diffusion (m^2/s) for zone A of the electrode concerned.

– $\delta_{A-\psi}$ is the thickness (m) of zone A of the electrode.

– ξ_{ion} is the stoichiometric coefficient of the ion involved ($\xi_{H^+} = 2$, $\xi_{OH^-} = 2$ and $\xi_{O^{2-}} = 1$).

By substituting [2.29] and [2.33] in [2.28], we get:

$$\eta_{activation} = -\frac{RT}{2\alpha_{ELYZ}F}\ln\left(\frac{|I|}{I_0^{ELYZ}}\right) + \frac{RT}{2\alpha_{ELYZ}\gamma_{ion,ELYZ}F}\ln\left(1-\frac{|I|}{I\lim_{A-\psi_{ion}}}\right)$$
$$+\frac{RT}{2\alpha_{ELYZ}\gamma_{H_2O}F}\ln\left(1-\frac{|I|}{I\lim_{A\psi H_2O}}\right) + \frac{RT}{2\alpha_{ELYZ}\gamma_{H_2O}F}\ln\left(1-\frac{|I|}{I\lim_{B\psi H_2O}}\right) \quad [2.35]$$

if $|I| >> I_0^{ELYZ}$

Starting with a general expression for the variation in voltage E_{rev} - $\eta_{activation}$, we only have overvoltages because the terms in ln(1-I/I_{lim}) are negative.

It is usual to separate this term into two terms: an overvoltage of "pure" activation $\eta_{pure\_activation}$ and an overvoltage $\eta_{transport}$ due to the transport of the water and the ion involved. The label "pure" will not be retained from hereon in.

2.5.2.4. *Ohmic overvoltage (transport of charges)*

Ohmic phenomena in fact include all phenomena of conduction of charges (protons and electrons) including contact phenomena within the electrolyzer when the medium changes (diffusion layer/active layer, for instance).

They are defined by Ohm's law ($I < 0$ in generator convention):

$$\eta_{ohm} = R_{ohm} \cdot |I| \qquad [2.36]$$

where:

$$R_{ohm} = \mathrm{R}_{\text{electrolyte}} + \sum_i R_{i\ \text{electronic}} + \sum_i R_{i\ \text{contact}} \qquad [2.37]$$

Whilst it is very often possible to assimilate R_{ohm} to $R_{electrolyte}$ in the case of a fuel cell, this is generally no longer the case with an electrolyzer. For instance, in the case of a PEMWE electrolyzer, the necessary presence of porous media renders the electronic resistances non-negligible, and also possibly the contact resistances.

2.5.2.5. *Balance of the quasi-static behavior of an electrolyzer*

Here we shall only give an overview on the scale of a cell of an electrolyzer. The reader can refer to the introduction to section 2.5.2 for the case of an electrolyzer stack.

From sections 2.5.2.1, 2.5.2.2, 2.5.2.3 and 2.5.2.4, we can write that the voltage at the terminals of an electrolyzer cell is:

$$U_{cell}(I) = E_{rev} + |\eta_{activation}(I)| + |\eta_{transport}(I)| + |\eta_{ohm}(I)| \qquad [2.38]$$

with:

$$E_{rev}(T,P) = E^0(T) + \frac{RT}{2F} \ln\left(\frac{P_{H_2} P_{O_2}^{\frac{1}{2}}}{a_{H_2O}}\right) \qquad [2.39]$$

$$|\eta_{ohm}(I)| = R_{ohm} \cdot |I| \qquad [2.40]$$

$$\left|\eta_{activation}\ (I)\right| = \frac{RT}{2\alpha_{ELYZ}F}\ln\left(\frac{|I|+I_n}{I_0^{ELYZ}}\right) \qquad [2.41]$$

If we set $\beta_{ion,ELYZ} = \alpha_{ELYZ}\gamma_{ion,ELYZ}$, $\beta_{A\psi H_2O} = \alpha_{ELYZ}\gamma_{A\psi H_2O}$ and $\beta_{B\psi H_2O} = \alpha_{ELYZ}\gamma_{B\psi H_2O}$[39]:

$$\left|\eta_{transport}(I)\right| = -\frac{RT}{2\beta_{ion,ELYZ}F}\ln\left(1-\frac{|I|}{I_{\lim_{A-\psi ion}}}\right) - \frac{RT}{2\beta_{A\psi H2O}F}\ln\left(1-\frac{|I|}{I_{\lim_{A\psi H2O}}}\right) - \frac{RT}{2\beta_{B\psi H2O}F}\ln\left(1-\frac{|I|}{I_{\lim_{B\psi H2O}}}\right) \qquad [2.42]$$

It is noteworthy that equation [2.41] is not absolutely identical to equation [2.24]. A term I_n has been introduced, in accordance with what is usually done in the literature. Firstly, this term enables us to extend the mathematical validity of the Neperian logarithm to zero current values. Secondly, it also enables us to simulate the open-circuit voltage of an electrolyzer which is not equal to E_{rev} in practice:

$$U_{cell}(0) = E_{rev} + \frac{RT}{2\alpha_{ELYZ}F}\ln\left(\frac{I_n}{I_0^{ELYZ}}\right) \qquad [2.43]$$

This term I_n is often assimilated to the parasitic phenomenon of crossover of the gases through the electrolyte. However, this physical interpretation is open to debate in view of the introduction of this term I_n, essentially with a mathematical point of view.

If we now consider the current to be low in comparison to the limit currents of diffusion, it becomes possible to linearize the expression of the overvoltage relating to species transport. Thus, for the voltage at the terminals of an electrolyzer cell, we get:

$$U_{cell}(I) = E_{rev} + \frac{RT}{2\alpha_{ELYZ}F}\ln\left(\frac{|I|+I_n}{I_0^{ELYZ}}\right) + R_{ohm}\cdot|I| + \frac{RT}{2F}\left(\frac{1}{\beta_{ion,ELYZ}I_{\lim_{A-\psi ion}}} + \frac{1}{\beta_{A\psi H_2O}I_{\lim_{A\psi H_2O}}} + \frac{1}{\beta_{B\psi H_2O}I_{\lim_{B\psi H_2O}}}\right)\cdot|I| \qquad [2.44]$$

39 We use this opportunity to attribute a coefficient γ_{H_2O} to each zone A and B of the electrode in question, because there is no reason for the nonlinearity to be identical in general.

Separation of the different terms relating to species transport will require rather unwieldy measurements and methodologies [RAL 11]. With this in mind, equation [2.42] can also be simplified by globalizing the phenomena of transport which can also be linearized if need be:

$$U_{cell}(I) = E_{rev} + \frac{RT}{2\alpha_{ELYZ}F}\ln\left(\frac{|I|+I_n}{I_0^{ELYZ}}\right) + R_{ohm}\cdot|I| - \frac{RT}{2\beta F}\ln\left(1-\frac{|I|}{I_{\lim}}\right) \approx E_{rev} + \frac{RT}{2\alpha_{ELYZ}F}\ln\left(\frac{|I|+I_n}{I_0^{ELYZ}}\right) + R_{ohm}\cdot|I| + R_{diff0}\cdot|I| \quad [2.45]$$

with:

$$R_{diff0} = \frac{RT}{2F\beta I_{\lim}} \quad [2.46]$$

where β is the globalized diffusion coefficient and I_{lim} the globalized limit current of diffusion.

Assuming it is not possible either to separate the contribution of the phenomena of species transport from that of the Ohmic phenomena, the expression [2.45] can be simplified still further:

$$U_{cell}(I) = E_{rev} + \frac{RT}{2\alpha_{ELYZ}F}\ln\left(\frac{|I|+I_n}{I_0^{ELYZ}}\right) + R_{tot}\cdot|I| \quad [2.47]$$

with:

$$R_{tot} = R_{ohm} + R_{diff0} \quad [2.48]$$

Figure 2.20 shows an illustration of formula [2.45] in the case of a 25 cm² prototype PEM electrolyzer cell. The data for 40°C and 5 barg are supplied in Table 2.12.

E_{rev} [V]	α_{ELYZ}	I_0^{ELYZ} / i_0^{ELYZ}	I_n / i_n	β	I_{lim} / i_{lim}	R_{ohm} / r_{ohm}
1.258	0.63	8×10^{-7} A	0.028 A	0.1	43 A	0.0119 Ω
		3.2×10^{-8} A/cm²	1.12×10^{-3} A/cm²		1.6 A/cm²	0.2975 Ω.cm²

Table 2.12. *Data for a 25 cm² prototype PEM electrolyzer monocell (40°C, 5 barg) [RAL 11]*

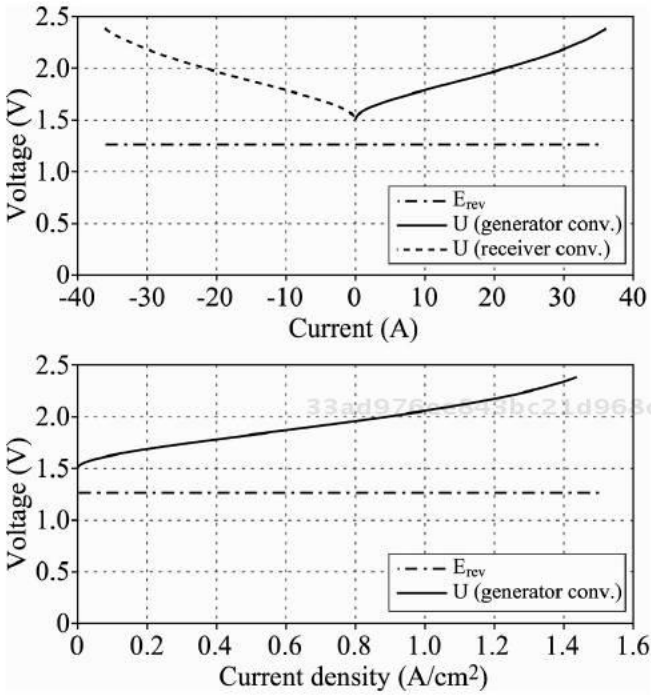

Figure 2.20. *Example of the polarization curve for a 25 cm² prototype PEM electrolyzer monocell as a function of the convention and the choice of current or current density for the plot [RAL 11]*

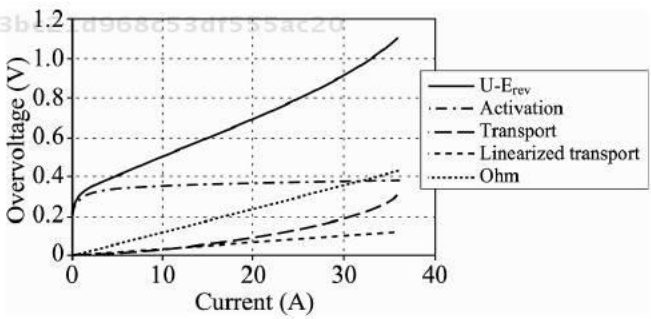

Figure 2.21. *Distribution of the overvoltages within the 25 cm² prototype PEM electrolyzer monocell receiver convention [RAL 11]*

Figure 2.21 shows the distribution of the overvoltages making up the polarization curve in Figure 2.20. The U-E_{rev} curve is the sum of all the overvoltages. Note that, in the case of low-temperature PEM electrolysis, the activation losses are the prevailing losses, except with high currents, when the Ohmic losses become very significant. The losses relating to species transport are the least of all the different forms of losses, but may become significant at high current values. Figure 2.21 also includes the linearized curve for the losses relating to species transport: logically, the behavior of the linearized curve is very satisfactory until medium currents are attained, and then becomes increasingly divergent with the non-linearized expression of these phenomena.

REMARK 2.4.– In the particular case of high temperature, the activation phenomena will generally behave in a linear fashion with normal operation. Their behavior will be identical to their tangent to the origin. It is possible to calculate this tangent to the origin using the Butler–Volmer law[40] and the properties relating to the derivative of the reciprocal function of a function:[41]

$$I = I_0 e^{\frac{2\alpha_{FC}F}{RT}\eta_{activation}} - I_0 e^{-\frac{2\alpha_{ELYZ}F}{RT}\eta_{activation}} \qquad [2.49]$$

For $\eta_{activation} = 0$, $I = 0$. The derivative with respect to current of $\eta_{activation}$ at this point is than calculated as follows:

$$\frac{\partial \eta_{activation}}{\partial I}(0) = \frac{1}{\frac{\partial I}{\partial \eta_{activation}}(0)} = \frac{1}{I_0\left(\frac{2\alpha_{FC}F}{RT}e^{\frac{2\alpha_{FC}F}{RT}\times 0} + \frac{2\alpha_{ELYZ}F}{RT}e^{-\frac{2\alpha_{ELYZ}F}{RT}\times 0}\right)} \qquad [2.50]$$

$$= \frac{RT}{2FI_0\left(\alpha_{FC}+\alpha_{ELYZ}\right)}$$

The voltage at the terminals of an SO electrolyzer cell is thus written:[42]

$$U_{cell}(I) = E_{rev} + \frac{RT}{2FI_0\left(\alpha_{FC}+\alpha_{ELYZ}\right)}|I| + R_{ohm}\cdot|I| + R_{diff0}\cdot|I| \qquad [2.51]$$
$$= E_{rev} + R_{total}\cdot|I|$$

40 We suppose that the activation currents are identical for both modes of operation.

41 If f is a continuous function in an interval I, bijective on I and derivable into x_0 and such that $f'(x_0) \neq 0$, then its reciprocal function f^{-1} is derivable into $y_0 = f(x_0)$ is $(f^{-1})'(y_0) = 1/f'(x_0) = 1/f'(f^{-1}(y0))$.

42 Here, we do not take account of the possible phenomenon of crossover.

where:

$$R_{total} = \frac{RT}{2FI_0\left(\alpha_{FC} + \alpha_{ELYZ}\right)} + R_{ohm} + R_{diff0} \qquad [2.52]$$

Each overvoltage value will behave in an "Ohmic" manner. Yet Figure 2.12, which uses the experimental readings taken by [LEF 11], proves that the value of the equivalent resistances will be able to vary to a greater or lesser extent with the current.

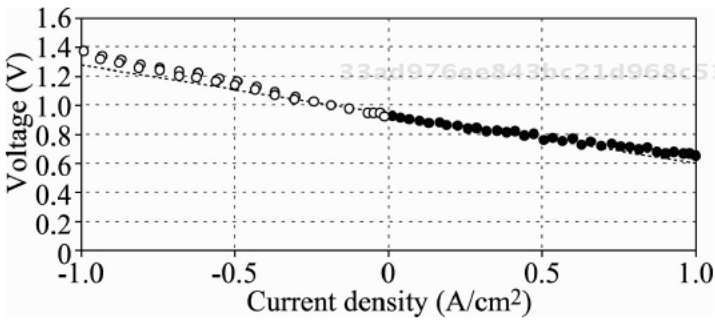

Figure 2.22. *Polarization curve for a 100 cm² SO monocell at 800°C with 50% vol. H_2O (data taken from [LEF 11])*

Thus, equation [2.51] must not be considered as set in stone for SO technology. Depending on the operating conditions, we also need to use the different formulations for species transport and possibly also for the activation phenomena.

2.5.3. *Electrical behavior in the dynamic state with a large signal*

In the extensive discussion above, we have focused on the quasi-static behavior of an electrolyzer. To deal with dynamic behavior, and particularly with a large signal, is a highly ambitious aim. For practicality's sake, we cannot go into detail here. Thus, we invite the reader to refer to [TUR 08] and [RAL 11] for all explanations.

The activation phenomena are coupled with the electrochemical double layer phenomena, which are comparable to a capacitor in the electrostatic sense of the term. The phenomena of species transport are, by their very nature, dynamic: in our approach, they will be assigned a dynamic via pseudo-capacitors. The Ohmic phenomena will be considered to have no perceptible dynamic.

2.5.3.1. *Coupling of the phenomena of activation and double electrochemical layer*

The electrochemical double layer phenomena manifest themselves at each interface between an electrode and the electrolyte. Around these two interfaces, there is spontaneous accumulation of charges of opposite signs on either side of the interface. It is these phenomena which are exploited and maximized in ultracapacitors.

These electrochemical double layer phenomena are equivalent to a genuine capacitor in the electrostatic sense of the term. We shall model them by way of a single equivalent capacitor (denoted as C_{dl}), because we shall not separate out the contribution made by each electrode.

As happens with fuel cells, these phenomena play a crucially important role in the interactions with the static converters (power electronics), as shown in [RAL 11]. They act as an internal filter against high-frequency current ripples. More generally, the electrochemical double layer phenomena constitute a true electrostatic inertial point at each electrode, preventing the potential from changing instantaneously.

The electrochemical double layer phenomena are directly coupled with the charge transfer phenomena, i.e. the activation phenomena, at each electrode/electrolyte interface. They constitute veritable charge reservoirs, which are emptied or filled depending on the variations of the point of operation of the component, thereby imposing the dynamics of variation of the activation phenomena.

This strong coupling can be modeled by a parallel electrical arrangement of the activation and electrochemical double layer phenomena, as shown in Figure 2.23. The activation phenomena are modeled by a source of current $I = f(\eta_{activation})$ governed by the Butler–Volmer law (equation [2.22]) which is guided by the voltage at its terminals.

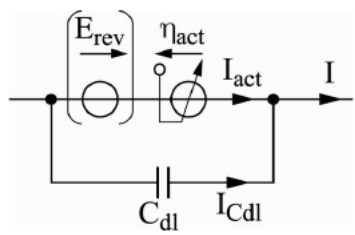

Figure 2.23. *Circuit model of the coupling between the phenomena of activation and double layer; $\eta_{act} < 0$ (equation [2.24]) for an electrolyzer in generator convention, which does indeed lead to an overvoltage*

2.5.3.2. *Dynamics of the species transport phenomena*

As discussed in [RAL 11], using electrochemical impedance spectroscopy (EIS) to analyze a PEM electrolyzer very clearly reveals slow diffusion dynamics (very low frequencies), and less clearly, fast diffusion dynamics (low/medium frequencies) and very fast diffusion dynamics (high/very high frequencies). As, for our purposes, the truth of this observation is very comprehensive, we shall consider it to be general hereafter.

In view of our discussion about the phenomena of species transport in section 2.5.2.3, our physical interpretation is logically to associate:

– the slow dynamics with transport of water into the diffusive zone (B) of the electrode in question;

– the fast dynamics with transport of water into the active zone (A) of the electrode in question;

– the very fast dynamics with transport of the ions involved between the electrolyte and the active zone where they will be consumed.

We know that, in terms of small variations, the electrical phenomena of species transport by diffusion can be closely modeled by the well-known "telegraph line", which is made up of an infinite number of RC circuits connected in parallel.[43] Suppose that we were already content with a single RC. Echoing the approach adopted in [RAL 11], the idea is then to "integrate" that "small-signal" electrical model in order to obtain a "large-signal" model. Thus, starting with a dipole R_{diff}-C_{diff}, we obtain a dipole I_{diff}-C_{diff} which represents a parallel association of a voltage-controlled current source I_{diff} with a pseudo-capacitor C_{diff}. Here we speak of a pseudo-capacitor because it is a fluidic/electrical analogy, unlike the double layer capacitor which is a true capacitor. This pseudo-capacitor in fact gives us an image, in the electrical domain, of the volumetric storage of the species concerned in the zone in question.

The formulation of I_{diff} (< 0 in generator convention) is obtained by inverting the formula for diffusion overvoltage, whose expression is of the type "$\ln(1-|I|/I_{lim})$":

$$I_{diff} = -I_{\lim}\left(1 - e^{+\frac{2\beta F}{RT}\eta_{diff}}\right) \qquad [2.53]$$

The model proposed for transport of water into the electrode in question is represented in Figure 2.24. The dipole I_{slow_diff}-C_{slow_diff} is imbricated in the dipole

43 [DIA 96] offers a demonstration, in terms of the electrochemical components.

I_{fast_diff}–C_{fast_diff}, which in fact enables us, on the dynamic level, to demonstrate the strong correlation between the diffusion in the two zones A and B of the electrode in question. The static coupling is expressed by relation [2.30], which links the limit currents.

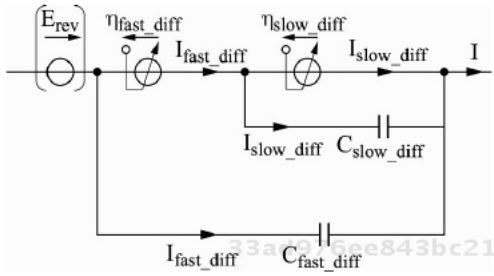

Figure 2.24. *Circuit model for the transport of water; $\eta_{diff} < 0$ (equation [2.53]) for an electrolyzer in generator convention, leading to an overvoltage*

For the transport of the ions involved between the electrolyte and the active zone where they will be consumed, it is possible to apply the same approach. The circuit model proposed is shown in Figure 2.25.

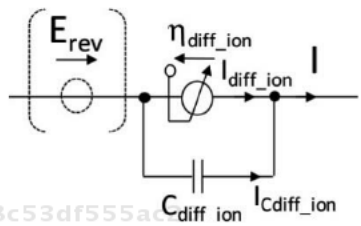

Figure 2.25. *Circuit model for the transport of the ions involved between the electrolyte and the active zone where they will be consumed; $\eta_{diff\_ion} < 0$ (equation [2.53]) for an electrolyzer in generator convention, leading to an overvoltage*

2.5.3.3. *Large-signal dynamic model of an electrolyzer*

The complete model is represented in Figure 2.26.

From the standpoint of the imbrication of the phenomena, the fast and slow phenomena of water transport have been imricated in the activation dipole, thus dynamically coupling these phenomena, as the "generalized" Butler–Volmer law (equation [2.36]) does in the static state: the dynamics of transport of reactants is, logically, coupled with the dynamics of charge transfer.

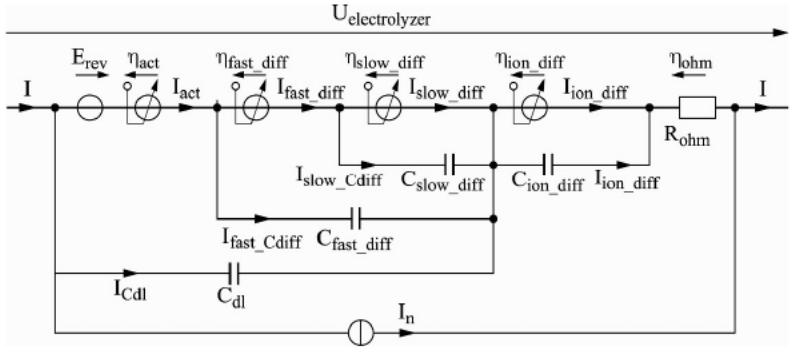

Figure 2.26. *Large-signal dynamic model of an electrolyzer in generator convention (all the η terms will be negative, leading to overvoltages)*

On the other hand, we have positioned the dipole related to ion transport outside of the activation dipole, considering that it takes place in the electrode/electrolyte interface, which we assume to be uncoupled from the other areas of the electrode concerned.

The Ohmic losses, which are *a priori* affected by none of the phenomena being modeled here, are outside of any dynamics. Only the current I_n affects them.

The current I_n, which is positive here, has been introduced mainly in order to model the open-circuit voltage of the component. We can see that this source of current I_n is connected in parallel to the whole circuit, so it is able to affect all the phenomena: this is a proposal that is open to debate.

In order to illustrate the potential strengths of this model, we offer a comparison of simulations with experiments carried out on a monocell prototype PEM electrolyzer. The experiments consisted of stimulating the component with large sinusoidal currents by various low frequencies and measuring its responses in terms of voltage. The model uses the parameters shown in Table 2.13. The results are illustrated in Figure 2.27. We can see that the behavior of the model is highly satisfactory.

R_{ohm} (Ω)	β	I_0(A)	I_n (A)	C_{dc} (F)	$\beta_{fastdiff}$	$\beta_{slowdiff}$	β_{H+diff}	$I_{lim\,fastdiff}$ (A)	$I_{lim\,slowdiff}$ (A)	$I_{lim\,H+}$ (A)
0.013	0.63	**3×10^{-7}***	0.02	**2**	0.16	0.1	0.1	110	32	140

Table 2.13. *Unique set of parameters identified for the simulation of the model of a 25 cm² monocell prototype PEM. * Except for 15 mH: $I_0 = 6\times10^{-7}$ A [RAL 11]*

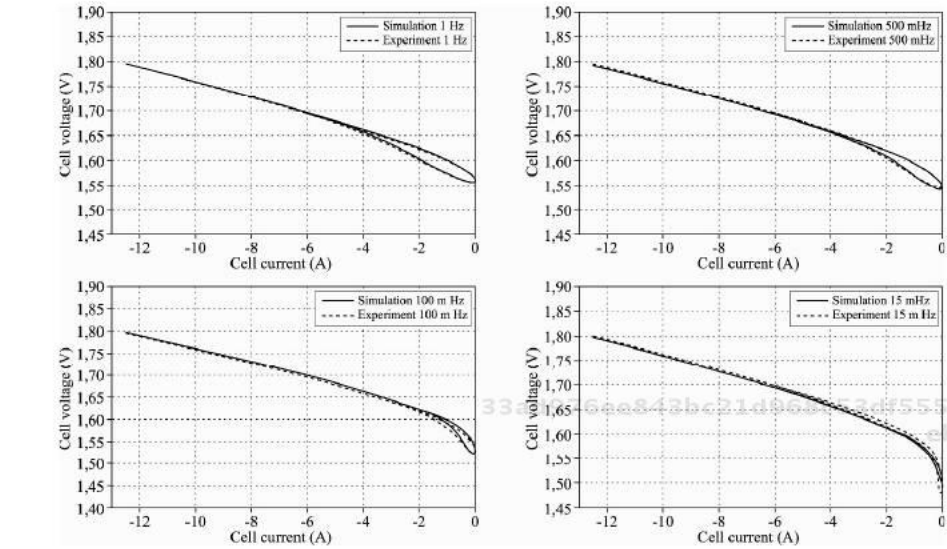

Figure 2.27. *Behavior of the large-signal dynamic model with the parameters from Table 2.13 for a 25 cm² prototype monocell PEM electrolyzer in the case of large sinusoidal sweeping currents for low frequencies. Experimental conditions: 40°C, 5 barg [RAL 11]*

2.5.4. *Electrical behavior in a dynamic state with a small signal (impedance)*

The large-signal dynamic model is rather complicated to work with. It is often easier to use the small-signal dynamic model, also called the impedance model. The approach, in fact, involves choosing a particular point of operation and studying the tangential behavior of the voltage, which is equivalent to "deriving the large-signal dynamic model with respect to current".

If we look around a certain point of operation, we can, by neglecting all the coupled and second-order terms in the process of derivation, obtain the circuit presented in Figure 2.28.

E_{rev}, as it is independent of the current, has disappeared. The case of I_n is less clear-cut: we shall not discuss it here.

All the voltage-controlled sources of current have become resistances, for which we are going to write the expressions. The dynamic imbrications remains unchanged, similarly as the capacitors and the Ohmic resistance.

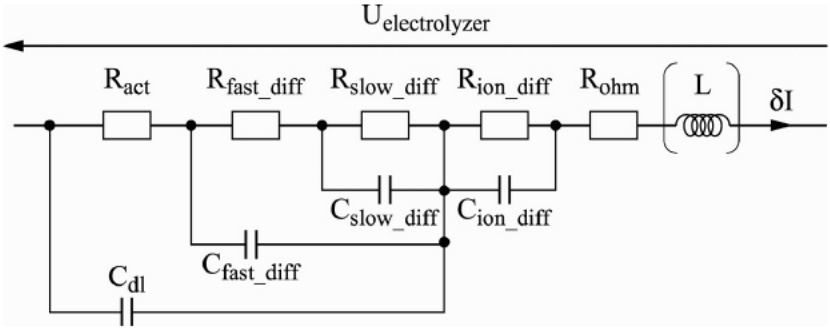

Figure 2.28. *Small-signal dynamic model of an electrolyzer derived directly from the large-signal dynamic model*

We can see, finally, that this procedure has resulted in the appearance of an inductance L which expresses the inductive behavior which is systematically found at high frequencies with experimental measures of impedance. Its origin is most often linked to the way in which the voltage at the terminals of the component is measured.

The different expressions of the resistances are as follows:

$$R_{act} = \left|\frac{\partial \eta_{act}}{\partial I}\right| = \frac{RT}{2\alpha_{ELYZ}F}\frac{1}{|I|} \quad [2.54]$$

$$R_{fast\_diff} = \left|\frac{\partial \eta_{fast\_diff}}{\partial I}\right| = \frac{RT}{2\beta_{fast\_diff}F}\frac{1}{I_{\lim fast\_diff} - |I|} \quad [2.55]$$

$$R_{slow\_diff} = \left|\frac{\partial \eta_{slow\_diff}}{\partial I}\right| = \frac{RT}{2\beta_{slow\_diff}F}\frac{1}{I_{\lim slow\_diff} - |I|} \quad [2.56]$$

$$R_{diff\_ion} = \left|\frac{\partial \eta_{diff\_ion}}{\partial I}\right| = \frac{RT}{2\beta_{diff\_ion}F}\frac{1}{I_{\lim diff\_ion} - |I|} \quad [2.57]$$

Remember that, in our approach and our interpretation, the phenomena of slow diffusion and fast diffusion relate to the transport of water into the electrode in question depending on the technology. The transport of ions, for its part, takes place between the electrolyte and the active zone of the electrode in question, where they are consumed.

While the approach – both small signal and large signal – developed hitherto is very satisfactory below medium/low frequencies, it is not particularly satisfactory with high frequencies from a dynamic point of view. Indeed, the case of porous

electrodes causes certain effects at high frequencies, particularly on the electrochemical double layer phenomena and the ion transport phenomena. Thus, these networks of pores will behave like an infinite number of parallel RC circuits, as illustrated in Figure 2.29, rather than as simple RC circuits as in the circuit shown in Figure 2.28.

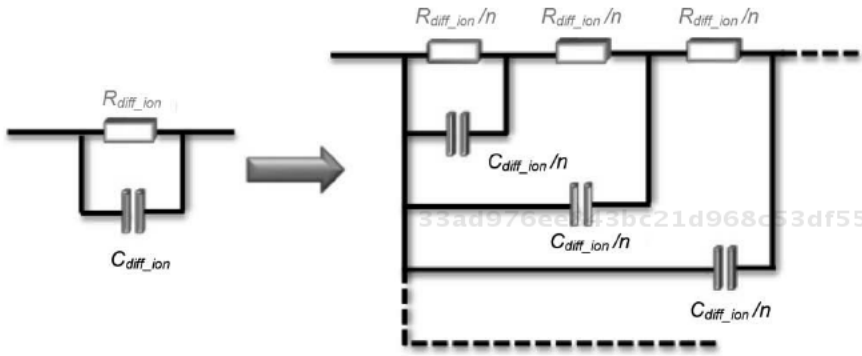

Figure 2.29. *Small-signal dynamic model with and without consideration of the porosity of the electrodes*

The approach with non-integer powers can be used to compactly formulate this infinite number of RC circuits [OUS 97]. This has been successfully applied to a PEM electrolyzer in [RAL 11].

If we introduce non-integer powers (nip), the impedance of an electrolyzer can be expressed in the following manner, preserving as much generality as possible:

$$Z = Z_{act} + Z_{diff\_ion} + Z_{ohm} \qquad [2.58]$$

with:

$$Z_{act} = \frac{R_{act} + Z_{diff}}{\left[1 + j\left(R_{act} + Z_{diff}\right)C_{dl}\,\omega\right]^{nip\_act}} \qquad [2.59]$$

$$Z_{diff} = \frac{R_{fast\_diff} + Z_{slow\_diff}}{\left[1 + j\left(R_{fast\_diff} + Z_{slow\_diff}\right)C_{fast\_diff}\,\omega\right]^{nip\_fast\_diff}} \qquad [2.60]$$

$$Z_{slow\_diff} = \frac{R_{slow\_diff}}{\left[1 + jR_{slow\_diff}C_{slow\_diff}\,\omega\right]^{nip\_slow\_diff}} \qquad [2.61]$$

$$Z_{diff\_ion} = \frac{R_{diff\_ion}}{\left[1 + jR_{diff\_ion}C_{diff\_ion}\omega\right]^{nip\_diff\_ion}} \quad [2.62]$$

$$Z_{ohm} = R_{ohm} + jL\omega \quad [2.63]$$

To clarify some orders of magnitude, [RAL 11] identified, for the case of a PEM electrolyzer, that:

– nip_diff_ion is typically 0.5;

– nip_act assumes values between 0.7 and 1;

– nip_fast_diff is typically 1;

– nip_slow_diff assumes rather varied values, ranging from 0.3 to 1.

This model is extremely potent in terms of analyzing the experimental impedance spectra. The issue then becomes one of transferring this to the large-signal model. We then need to "decompress" the non-integer power with a small number of embedded IC circuits: this very soon becomes a complex task, and is therefore done only rarely. In addition, the large-signal model is generally used for studies at the level of low/medium frequencies, and to make the approximation that the powers are all equal to 1 is not too far from the truth.

In order to illustrate the potential of this model, below we give a comparison of simulations with experiments performed on a prototype monocell PEM electrolyzer. The experiments consisted of carrying out impedance spectroscopy for a variety of current densities. The model uses the parameters from Tables 2.14 and 2.15. The results are exhibited in Figure 2.30. We note that the model's behavior appears to be highly satisfactory.

B	0.63
C_{dl} (F)	1.5
β_{fast_diff}	0.16
C_{fast_diff} (F)	5
β_{H+_diff}	0.1
C_{H+_diff} (F)	0.12
β_{slow_diff}	0.1
C_{slow_diff} (F)	1000
nip_slow_diff	0.3
nip_act	0.86
nip_fast_diff	1
nip_H+_diff	0.5
L (H)	6.70E-09

Table 2.14. *Unique set of parameters identified for the impedance model simulation of a 25 cm² prototype monocell PEM [RAL 11]*

J (A/cm²)	0.1	0.3	0.5	0.6	0.7	0.8	0.9	1	1.1
R_{ohm} (Ω)	0.0119	0.012	0.0121	0.0121	0.012	0.012	0.0119	0.0119	0.0118
$I_{lim\_H+\_diff}$ (A)	200	180	150	140	110	105	97	94	90
$I_{lim\_fast\_diff}$ (A)	150	150	150	150	150	150	150	150	150
$I_{lim\_slow\_diff}$ (A)	150	120	100	70	55	46	43	43	46

Table 2.15. *Continuation of the set of parameters dependent on the current identified for the impedance model simulation of a 25cm² prototype monocell PEM [RAL 11]*

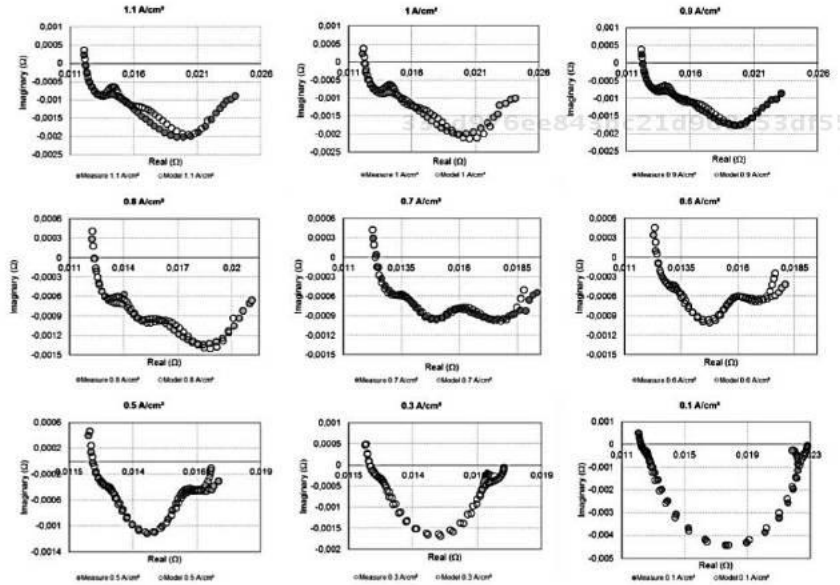

Figure 2.30. *Behavior of the impedance model with the parameters shown in Tables 2.14 and 2.15 for a 25 cm² prototype monocell PEM electrolyzer for different decreasing current densities. The frequency range is 0.3 Hz–16 kHz, except for 0.3 A/cm²: 0.022 Hz–16 kHz. Experimental conditions: 40°C, 5barg [RAL 11]*

2.6. Experimental characterization of the electrical behavior of an electrolyzer

All the techniques for characterizing the electrical behavior which are presented in this section can be applied using one of the two electrical setups presented in Figure 2.31.

The first setup (a) consists of connecting the terminals of the component to an adjustable active source which will supply the electrolyzer with electrical energy drawn from the grid. In general, this is a source of voltage whose current is limited: the dynamic performances will often be considerably reduced.

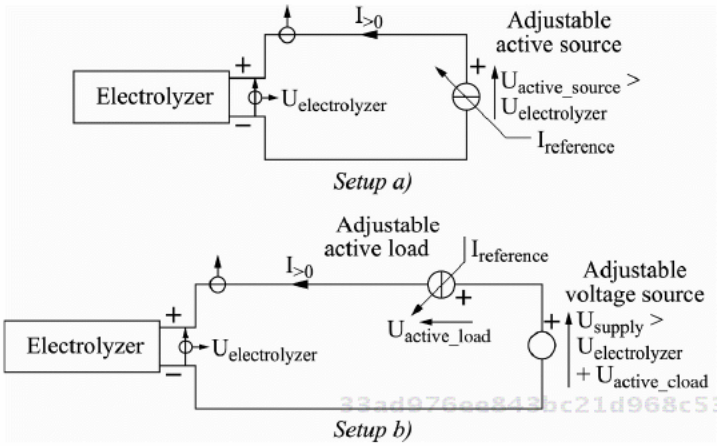

Figure 2.31. *Electrical setups for the electrical characterization of an electrolyzer (receiver convention)*

If the characterization sought requires good dynamic performances, the second setup (b) will be favored. It comprises a source of near-static voltage and an active load that is as dynamic as possible. The source of voltage will supply the electrolyzer's voltage, plus an additional voltage that enables the active load to function. Obviously, it is useful to limit the value of this additional voltage, and therefore the energy which will be dissipated as heat in the active load, to the absolute minimum in order to limit the energy needing to be supplied by the voltage source (which, for its part, will take all of its energy from the grid).

The reference current imposed on the adjustable active source/load corresponds to the excitation which we wish to lend to the electrolyzer. The voltage and the current of the component are measured and will constitute the data, which we shall then go on to exploit. It should be pointed out that the frequency bandwidths of the sensors need to be adapted to the level of excitation being applied.

The characterizations which we shall present below are the plot of the polarization curve, impedance spectroscopy response to current value steps and responses to large amplitude current sweepings. These are all non-intrusive characterizations on the scale of the component (or of each cell), and are intended to characterize its electrical behavior in the static and dynamic states in real operating conditions. These characterizations will enable us, on the one hand, to appreciate the performances of the electrolyzer, and on the other, if we cross them, to parameterize the different models presented above.

Other, more specific characterizations, such as cyclic or linear voltammetry [DIA 96], do exist, but they will not be discussed here. However, they may constitute interesting data, which would help to refine the simulation, but the interpretation of these methods is the business of specialists.

2.6.1. *Polarization curve (quasi-static characterization)*

The polarization curve, which links the voltage to the current, is the systematic characterization which is performed in order to quantify the performances of an electrolyzer. It is also sometimes called "static" or "quasi-static" characterization, but the term "polarization curve" appears to be more general. Indeed, we very often observe hysteresis with this curve; in other words, the curve plotted for increasing currents is not superimposed on that of the decreasing currents: hence, the static state in the strict sense of the term is never reached. Nevertheless, the curve is generally stabilized/"repeatable", meaning that we go along the same paths again if we cyclically repeat the characterization.

There are no official norms as to how this polarization curve should be plotted. Thus, caution must be exercised when interpreting published versions of polarization curves, because the authors do not always take sufficient care in terms of specifying the conditions in which the data were obtained, which have a very great impact on the result.

It is possible to plot this curve "by hand", i.e. by gradually varying the current, and reading off the voltage, value by value. Automation of the plotting of the polarization curve, where possible, is undoubtedly preferable, because it minimizes the impact of the tester on the results obtained, and offers good reproducibility of the characterization. Two solutions are discussed in the next section: one with current stairway-type steps and the second with very-low-frequency current sweepings.

2.6.1.1. *Current stairways*

Figure 2.32 shows the typical shape of stairway characterization imposed on the component. In a general approach, the length of the steps Δt may not be identical for each and every step; the same is true of their height $|\Delta I|$. The dots on the graph indicate the moment at which the reading of the voltage was taken. At present, there is no norm describing the value of these two parameters. The tester must choose them, ideally specifying them, at least on the basis of the response time of the regulations of the system in which the electrolyzer is being adjusted. For instance, a variation in current density can lead to a variation in temperature: in this case, we then need to wait at least until the thermal regulation mechanism has worked for the system to return to the characteristic temperature. In general, we need to take

account of the time necessary for adaptation of the operating conditions each time we change the point of operation.

This technique is in fact the direct automation of the "manual" plots described above, with the slight difference that the switch from one level of current to another is quicker (in extreme cases, there is a step; a ramp in current is often adopted). The same switch can be strictly applied for all the changes.

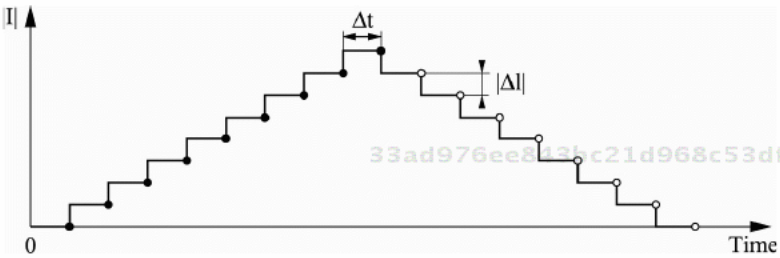

Figure 2.32. *Excitation current for the plot of a stairway polarization curve*

2.6.1.2. *Very-low-frequency current sweeping*

As Figure 2.33 illustrates, this technique involves subjecting the electrolyzer to a very-low-frequency sinusoidal current whose amplitude is equal to the range of current which we wish to characterize. Unlike the stairway plot, the plot for the current sweeping is a continuous curve.

Figure 2.33. *Excitation current for the plot of a polarization curve by very-low-frequency current sweeping*

The lower the sweeping frequency (a few mHz), the better the operating conditions will be able to adapt to the level of current. For low frequencies (a few 100 mHz), this needs to be examined on a case-by-case basis.

It is also possible to use a triangular current. There are few differences between a sinusoidal sweeping and a triangular sweeping, exception at the extremities of the

ranges of current, where the sinusoidal sweeping is *a priori* richer in information, because its rate decreases.

2.6.1.3. *Comparison of the two techniques*

Figure 2.34 offers an experimental comparison in the case of a monocell PEM electrolyzer.

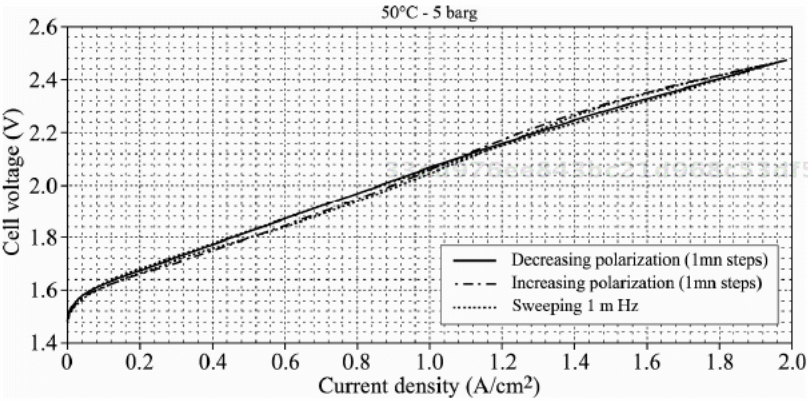

Figure 2.34. *Experimental comparison of the two approaches to plot a polarization curve for a 25 cm² prototype monocell PEM electrolyzer. Experimental conditions: 50°C, 5 barg. 1 mHz sinusoidal sweeping of current value; stairway plot largely equivalent to 0.33 mHz (25 pts there/25 pts back). Note: the stairway-type curves have been smoothed beyond 50 points [RAL 11]*

A sinusoidal sweeping of current at 1 mHz was imposed on the electrolyzer. A there-and-back stairway plot of the current was also made: it is equivalent to a frequency of 0.33mHz. All the results were projected onto the voltage/current plane. We note that the two techniques efficiency similar results for similar frequencies.

Finally, note that in both cases, there is hysteresis on the voltage between the increasing and decreasing currents, even at such very low frequencies.

2.6.2. *Impedance spectroscopy (dynamic small-signal characterization)*

Dynamic small-signal characterizations have the objective of characterizing the component around a fixed point of operation, supposing that if the amplitude of the excitation is small, then the component's behavior will be quasi-linear.

Impedance spectroscopy classically involves subjecting the component to currents of low amplitudes (<10%) with a progressive evolution[44] of the frequency as presented in Figure 2.35. The component exhibits a response in terms of voltage for each of the frequencies, and the V/I ratio for each of the frequencies can be used to obtain the impedance for each frequency. An impedance spectrum is finally obtained: it is generally plotted on the Nyquist plot.

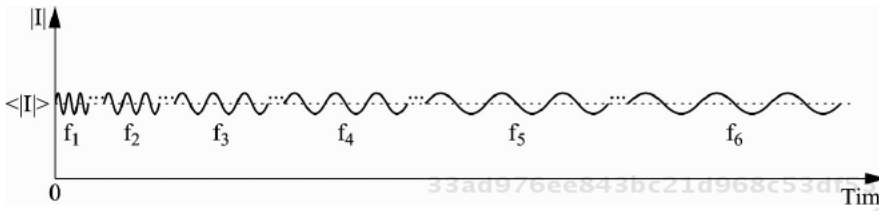

Figure 2.35. *Conventional excitation current for the plot of an impedance spectrum* ($f_1 > f_2 > f_3 > f_4 > f_5 > f_6 > \ldots$)

For each frequency, an settle time is always left (typically 5–10 periods) in order to allow the transitory currents to die away, and the measurement of impedance is then taken by averaging the measurements over several cycles (typically 5–10 as well).

The range of frequencies swept usually extends from very high frequencies (some 10 kHz) to low frequencies (some 100mHz), or even to very low frequencies (some mHz). It is preferable to go from higher frequencies to lower, because at low frequencies, slight instabilities may begin to manifest themselves.

The domain of frequency swept may also be reduced to a range of specific frequencies (in this case we speak of "targeted" impedance spectroscopies), or even in the extreme case, a single frequency. Targeted impedance spectroscopies are used, notably, when we are interested only in the value of the Ohmic resistance which is obtained at the intersection of the impedance spectrum with the axis of the real parts at high frequencies (see Figure 2.30).

Some examples of typical impedance spectra for a monocell PEM electrolyzer are shown in Figure 2.30.

44 There are variants in the organization of the frequencies which enable us better to appreciate the potential instabilities in measurement. The notion of "interleaved" spectroscopies was put forward in [PHL 09].

2.6.3. *Current steps*

The current step is a rather tricky characterization. It is generally used to estimate the Ohmic resistance via the $R_{ohm} \approx |\Delta V|/|\Delta I|$ ratio where ΔV is the jump in voltage when the step is applied.

The problem is that, in practice, it is difficult to apply an ideal step because of the non-infinite bandwidths of the sources used to impose the current.[45] Therefore, the voltage jump will not be due solely to the Ohmic phenomena (as the variation in current is never instantaneous), leading to potentially very grave errors in the calculation of the Ohmic resistance. In addition, this requires very high-performance measuring equipment in order to have enough points at the level of the step.

One example of how to circumvent these problems is given in [PHL 09], whereby we are able to cope with the imperfection of the step. Nevertheless, the current step method will always be tricky, because it necessarily leads to a change in the point of operation, and therefore potentially to a variation in R_{ohm}.

Figure 2.36 exhibits a type of current step which it may be interesting to use. The step is only a small one, and it is short in duration. If the duration of the step is short, then the estimated value of the Ohmic resistance will be apparently the same for the upward and downward fronts, because its characteristics (e.g. hydration of the membrane for PEM technology) will not have had time to change; we know that a small amplitude of the step *a priori* guarantees a slight variation in these characteristics.

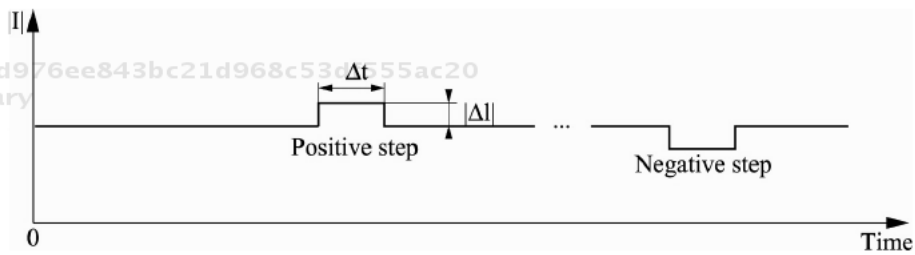

Figure 2.36. *Excitation currents for small current steps*

45 In the particular case where the current is interrupted, it is possible to use a static switch which can be switched in the space of a few tens of nanoseconds. However, the advantage to this specific test is fairly limited.

For all the above reasons, it is recommended that high-frequency targeted impedance spectroscopy is used to determine the value of the Ohmic resistance with no ambiguity.

The current step can also be used to characterize the dynamic behavior of an electrolyzer, whether in the case of a small or a large signal depending on the amplitude of the step. The difficulty in exploitation is that a current step will dynamically change the values of all the phenomena, and it will be tricky to separate out their contributions.

2.6.4. *Current sweeping (large-signal dynamic characterization)*

This type of excitation was introduced by the laboratory LAPLACE (*Laboratoire PLAsma et Conversion d'Energie* – Plasma and Energy Conversion Lab) in Toulouse [TUR 08]. The shape of the excitation current is exactly the same as that shown in Figure 2.33. The only change, in fact, is the frequency domain. Indeed, we shall see frequencies which dynamically excitate the various phenomena. This may lead to an increase in the frequency up to ten Hz.

We always need to be conscious of the impact on the operating conditions from the sweeping frequency; remember that the amplitude of the excitation is high (typically the value of the nominal current). This is all the more true when the frequency becomes low. With the highest frequencies, to a certain extent, we shall benefit from the effect on internal filtering of the double layer phenomena.

Illustrations are given in Figure 2.27 in the case of a monocell PEM for different frequencies (1 Hz, 500 mHz, 100 mHz and 15 mHz).

2.6.5. *Combining the approaches to characterization (advanced approach)*

By superposing the characterization methods, our aim is to obtain the maximum amount of information in the minimum amount of time.

As an initial example, consider the combination of the current stairway technique and impedance spectroscopy. The principle is illustrated in Figure 2.37. Here, for each polarization current, we want to obtain the voltage corresponding to that point and the small-signal dynamic behavior around that point of operation. The impedance spectroscopy aspect will generally not be extended to very low frequencies in the interests of reasonable duration of measuring campaigns.

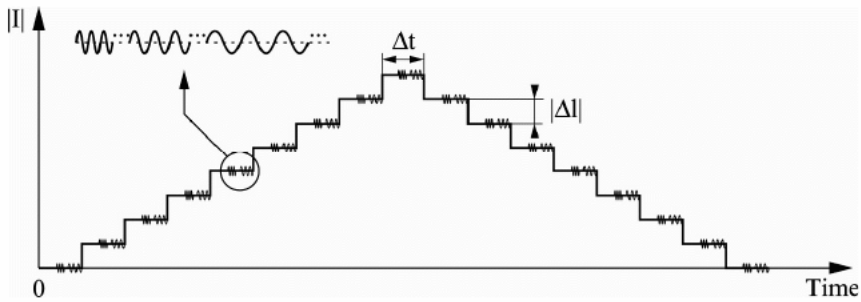

Figure 2.37. *Excitation current combining current stairways and impedance spectroscopy*

For our next example, let us look at the superposition of targeted impedance spectroscopy (high frequency) with low-frequency current sweeping, as illustrated in Figure 2.38. The aim here is to obtain the polarization curve and the dependency of the Ohmic resistance on the current. This superposition is not easy to implement: the sweeping frequency must not be too high.

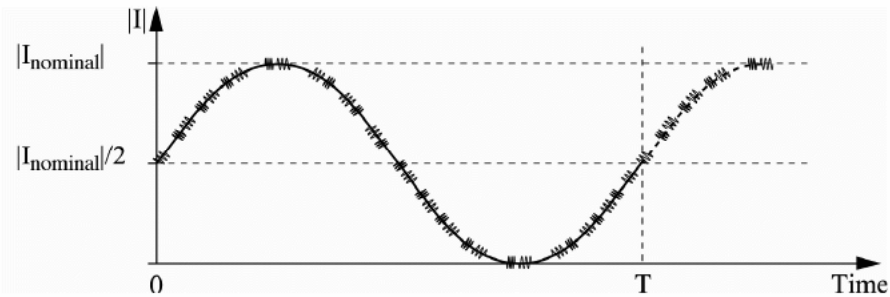

Figure 2.38. *Excitation current combining targeted impedance spectroscopies with current sweeping*

2.7. Procedures for parameterizing the models

The simulation put forward in section 2.5 uses a certain number of parameters. The approach we now advocate is not to set preconceived values for these parameters, but instead to identify them on the basis of systematic experimental characterizations. Thus, if the model is generic, the result of the parameterization will ultimately always be specific to the particular electrolyzer in question. The experimental characterizations upon which this section is based are those presented in section 2.6.

As seen in section 2.5.2.5, the model of the polarization curve will include at least four parameters:[46] a_{ELYZ}, I_n, I_0 and R_{tot}. If we undertake an optimization with the single experimental polarization curve, it is possible to find an infinite number of values for the parameters. If we have very good knowledge of the technology being tested, we will be able to restrict the domain of possible values, but the parameters will nevertheless be able to assume value intervals.

Depending on the objectives behind the use of the model, this may not be problematic if we are aware of it. For instance, if we wish to make a detailed comparison between different components or use the model to track the state of health of the component, this approach will not be helpful.

At the very least, we need to be able to parameterize the model of the polarization curve as unequivocally as possible. In order to dissociate the different phenomena from one another, we will in fact need to use dynamic characterizations. The different phenomena have more-or-less distinct dynamics, which can to a certain extent be used to tell them apart. Thus, if we try to parameterize the static model detailed, dynamic parameters will be determined during the course of the approach. Complete and detailed parameterization of the large-signal dynamic, model is the most ambitious goal, but elements of methodology will be put forward.

The elements in this section should be considered as avenues already tested successfully but not finalized, and by no means as truths set in stone.

2.7.1. *Minimal combinatorial approach to experimental characterizations*

As shown in section 2.5.2, the phenomena of species transport often exhibit linear behavior once the point of operation becomes sufficiently far from the diffusion limit current. Thus, from the standpoint of an optimizer, the Ohmic and "linearized" transport phenomena are totally indissociable from one another. This is to say nothing of SO electrolysis, where the activation phenomena also behave linearly.

By marrying polarization curves or low-frequency current sweeping with a measure of the Ohmic resistance R_{ohm} – e.g. using targeted impedance spectroscopies (high frequency) – we are able to appreciably reduce the domain of possibilities for the values of the other parameters. Hence, we advocate the minimal combinatorial approach.

---

46 With the exception of the particular case of HTE, where the number of parameters of the model can be reduced to one, in extreme cases.

2.7.2. *Multiple impedance spectra approach*

In a conventional scenario, the small-signal dynamic approach (impedance spectroscopy) is only able to characterize the impedance of the component around a particular point of operation. Working with only one impedance spectrum, or on a spectrum-by-spectrum basis, generally enables an infinite range of solutions for the parameters involved.

If we measure the impedance spectra all the way along the polarization curve, we may witness a certain dissociation of the different phenomena owing to their different dynamics, and to the fact that those spectra manifest themselves to a greater or lesser extent depending on the range of current values. Figure 2.30 illustrates these assertions in the case of a PEM electrolyzer. It is this which the approach set out here is intended to exploit.

Originally, the "multiple impedance spectra" approach consists of simultaneously modeling all the impedance spectra obtained along the polarization curve. This necessitates the use of an impedance model defined on the basis of the current and valid all along the polarization curve, such as that which we presented in section 2.5.4. Employing simultaneous optimization on all the spectra, this approach enables us to determine a single set of parameters that can be used to describe all the impedance spectra.

This approach has been successfully applied to the case of a PEM electrolyzer: the model parameters listed in Tables 2.14 and 2.15 (section 2.5.4) were obtained by way of this methodology. The excellent behavior of the model thus parameterized is illustrated in Figure 2.30.

This very promising approach enables us to determine all the parameters of the large-signal dynamic model, including the dynamic parameters (though of course within the limit of the frequencies explored for the impedance spectroscopies), with the exception of the parameters I_n and I_0, which disappear during the stage of derivation of the large-signal model, enabling us to obtain the small-signal model. Hence, the approach needs to be supplemented as we shall see in section 2.7.4 in order to have complete parameterization.

This method can be applied in a program such as Excel in view of the relative straightforwardness of the calculations: no dynamic simulation is necessary.

2.7.3. *Low-frequency multi-sweeping approach*

While the "multiple impedance spectra" approach represents a very big step toward dynamic characterization of the electrolyzer throughout the entire range of its

operation and therefore toward characterization of its large-signal dynamic behavior, the "low-frequency multi-sweeping" approach is a step toward impedance spectroscopy which, by its very principle, explores numerous frequencies.

Indeed, current-sweeping methods are – by nature – large-signal approaches, and they are also – by nature – single-frequency approaches. We can see that it would be difficult to separate of the different phenomena using only one frequency. One idea to combat this problem is to simultaneously model several sweepings obtained with different low frequencies (Figure 2.39). Naturally, we need to have a large-signal dynamic model such as that presented in section 2.5.3 (Figure 2.26). Once again, the aim is to determine a single set of parameters which can be used to model all the sweepings in question by performing a single optimization.

Figure 2.39. *Low-frequency multi-sweeping method*

This approach requires heavy-duty computational equipment, because it involves simulating the large-signal dynamic model at each iteration of the optimization. The resolution may take a long time. This is a fairly strong argument in favor of the "multiple impedance spectra" approach, which can be applied with software such as Excel, although the "low-frequency multi-sweeping" approach is capable, for its part, of determining all of the parameters.

This method has been tested on a PEM electrolyzer in [RAL 11], with encouraging results.

2.7.4. *Toward an optimal and systematic combinatorial exploitation of the experimental characterizations*

The idea here is ultimately to combine all the characterization methods in order to parameterize the model of the component with an increasingly high "confidence index", and increasingly rapidly. Figure 2.40 shows a diagrammatic representation of this original combinatorial approach.

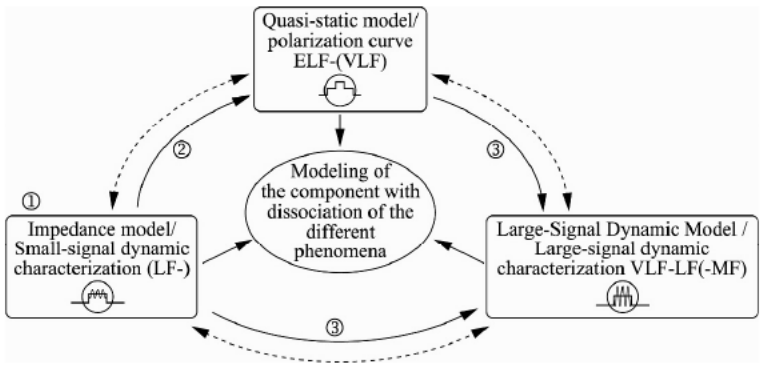

Figure 2.40. *Toward a combinatorial exploitation of the different characterization methods*

Many different combinations are possible. One of the most promising is as follows (illustrated with the numbers 1, 2 and 3 in Figure 2.40):

– Step 1: the "multi impedance spectra" approach is applied (see section 2.7.2).

– Step 2: the static parameters obtained are all fed into the polarization curve model. Optimization on the basis of the experimental polarization curve enables us to determine the two remaining parameters I_n and I_0.

– Step 3: all of these parameters are fed into the large-signal dynamic model. In order to verify the robustness of the model thus parameterized, we carry out simulations of the large-signal low-frequency sweepings which have been carried out experimentally. A few final parametric adjustments can then be carried out if need be.

It is precisely this approach which is successfully applied in [RAL 11] in the case of a PEM electrolyzer. Figure 2.27 illustrates the excellent behavior of the large-signal dynamic model parameterized in steps 1 and 2. If we compare Table 2.13 with Tables 2.14 and 2.15, we note that only three parameters have been readjusted. The readjustment is very slight, with the exception of I_0, which has been noticeably decreased.

2.8. Combination with a fuel cell. Concept of the "hydrogen battery"

Electrolyzers and fuel cells generally do not perform well in the reverse mode to that for which they have been optimized, with the probable exception of SO technology (Figure 2.22). Thus, to carry out a local function of storage and release of electrical energy, it will also generally be necessary to combine a fuel cell

with an electrolyzer: this is the concept of the "H_2/O_2 battery" or "H_2 battery"[47] if oxygen is not stored. This was notably conceptualized in [GAI 11].

2.8.1. *General considerations*

The design of the "H_2/O_2 battery" is based on a tandem comprising the two electrolyzer and fuel cell functions, performed by two distinct processes so as to maximize the number of degrees of freedom (Figure 2.41). Here, this tandem is accompanied by two gas tanks to store the hydrogen and oxygen, and a water tank. In order for the two processes to function correctly, the H_2/O_2 battery includes auxiliaries, which are necessary for the hydric, fluidic, thermic and electrical management of the two processes. Finally, the H_2/O_2 battery has an interface for power exchanges with the application, via two power converters in this case, again to maximize the number of degrees of freedom.

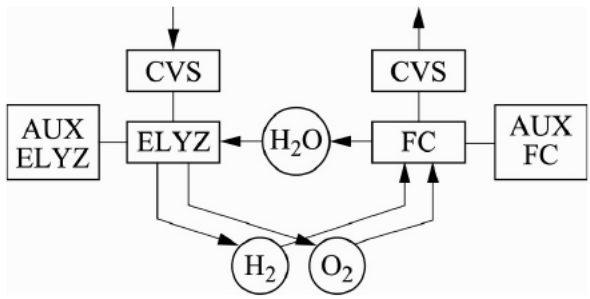

Figure 2.41. *Make-up of the "H_2/O_2 battery", with a maximum number of degrees of freedom considered*

In some cases, it is envisageable to deploy an H_2/O_2 battery built differently to that shown in Figure 2.41, taking account at least of the following questions: Number of cores?[48] Technology used in the core(s)? Shared power converter? Does oxygen need to be stored? What form of storage is to be used for the gases? Which auxiliaries should be used (e.g. air compressor or not)? Is the heat given off profitably exploited by the process(es)?

Unlike a "conventional" battery (lead acid, Li-ion, etc.), a hydrogen battery is able to dissociate energy and power from one another. The energy is set by the

47 This must not be confused with the "nickel-hydrogen battery" (NiH_2 battery) used in space applications – particularly in the International Space Station (ISS) [MIL; THA 03].
48 The literature uses the terminology "URFC" (Unitized Regenerative Fuel Cell) for a solution with a single core, and "RFC" (Regenerative/Reversible Fuel Cell) for a solution with two cores.

design of the gas storage, and the power by that of the electrochemical processes. This energy/power dissociation is also to be found in redox flow batteries – one of the main competitors for the hydrogen battery.

Having two cores (RFC) enables us to set the recharge power (and therefore recharge time), and the same for discharge, appropriately for the application. In the case of a single core (URFC), these designs will no longer be uncoupled and, as with a "conventional" battery, one mode will always be better optimized than the other, which necessitates oversizing of one of the two modes.

SO technology intrinsically appears to be the most appropriate in terms of reversibility, given that it can function at a high temperature. Indeed, the high temperature minimizes the problems of chemical kinetics and those relating to species transport, because everything takes place in the gaseous phase (Figure 2.22).

With the other two technologies, reversible prototypes have been developed – particularly for PEM technology [MIT 98; STR 08] – but overall the performances remain fairly limited, for reasons of compromise on the choice of materials. For instance, with PEM technology, the optimal catalysts are not the same for the positive electrode. In another example, the carbon electrodes of a PEM fuel cell have very poor resistance to the conditions highly favorable to the corrosion of carbon (and therefore to their destruction) imposed in electrolyzer mode. One as-yet-unexplored avenue for PEM technology would be to switch to using water vapor, which would facilitate reversible operation [MIT 11].

For alkaline and PEM technologies, the dual-core solution therefore remains, at present, that which offers the best performances in terms of energy and durability.

In a two-core solution, each of the two functions is able to draw on an advantage of one technology over another. The level of power or the dynamic, for instance, are elements which might sway a decision one way or another, as are the technological, industrial and commercial maturity of the solution. If we wish to share the maximum possible number of auxiliaries and thus minimize the mass, volume and cost of the system, it seems fairly logical that the two cores should use the same technology.

It may prove indispensable to have a power converter for each function if two degrees of freedom are necessary. This may help to optimize the energy efficiencies in view of the characteristics of the two electrochemical cores. In addition, it can offer an additional degree of freedom in the design of the electrical architecture for the application. On the other hand, saving on the second power converter by mutualizing a single power converter to serve both functions can facilitate a significant gain – particularly in terms of integration and cost. If there is only one core, then *a priori* there will only be one power converter.

The gas storage in itself can be done in different ways. For instance, we can use pressurized gas bottles, tanks of gas in liquid form at very low temperature, or, for hydrogen, storage in solid compounds such as metal or complex hydrides. For storage of hydrogen and oxygen, the pressurized storage seems the most credible solution, both technically and industrially. In the case of pressurized storage, the electrolyzer needs to be capable of functioning under pressure (at least several tens of bars) to obtain useful energy efficiencies from the system: mechanical compression is indeed very energy-hungry, and must be limited as far as possible.

The choice to store and use pure oxygen lends the H_2/O_2 battery certain advantages [VER 11]. In particular, the efficiency of the fuel cell increases and may be greater than 60%; the power density is also greater [MIT 11]. In addition, the use of pure oxygen limits the pollution of the battery core with foreign particles present in the air. The H_2/O_2 processes also exhibit better dynamics and shorter response times. In addition, there is no longer a need for specific conditioning of the oxidant as in the case of air (purification filter, compressor, humidifier, etc.). Conversely, the pure oxygen produced by the electrolyzer necessitates certain precautions for its storage, from the point of view of corrosion[49], possible mechanical compression of the gas, and more generally, safety. In particular, it is necessary to find a solution[50] to prevent the phenomenon of crossover of the hydrogen[51] through the electrolyte, in order to avoid a dangerous accumulation of hydrogen in the oxygen storage compartment.

In the case of "low-temperature" technologies, both modes of operation are exothermic, and it is therefore possible to wonder about how to make profitable use of the produced by electrical and/or thermal cogeneration, which noticeably complexifies the system. In the case of "high temperature" technologies, it can be envisaged to store the heat lost in fuel cell mode and exploit it in electrolyzer mode, which is generally endothermic.

2.8.2. *Static characteristics of an H_2/O_2 battery*

An H_2/O_2 battery includes a fuel cell function and an electrolyzer function. Whether it uses one or two cores, the static characteristics are similar in terms of their literal expression (generator convention):

$$U_{cell}(I) = E_{rev} \pm |\eta_{activation}(I)| \pm |\eta_{transport}(I)| \pm |\eta_{ohm}(I)| \quad [2.64]$$

49 A drying stage may be necessary in addition to a condensation stage.

50 For instance, catalytic combustion.

51 This is the prevailing phenomenon. However, we also see crossover of oxygen.

In electrolyzer operation ($I < 0$), the different phenomena (activation, species transport and charge transport) will lead to overvoltages (+), and in fuel cell mode ($I > 0$) they will cause voltage drops (–).

A graphic illustration is given in Figure 2.42. Whilst it is still fairly general, it is rather illustrative of alkaline and PEM technologies. Figure 2.22 is more representative of SO technology.

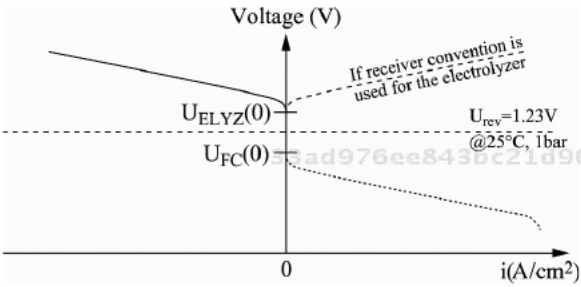

Figure 2.42. *Shape of the polarization curve of an electrolyzer cell and a fuel cell for an H_2/O_2 battery in generator convention*

2.8.3. *Deadband of an H_2/O_2 battery*

While an H_2/O_2 battery enables us to dissociate the recharge power, stored energy and discharge power thanks to its many degrees of freedom, and to avoid the auto-discharge problem encountered with a conventional battery[52], it does exhibit certain peculiarities in terms of operation which can, in certain cases, become rather restrictive drawbacks for the electrical energy storage application for which it is intended.

The best-known of these peculiarities are the startup and stop times (rise or fall in pressure and/or temperature[53], release of inerting gas, etc.), and the fairly limited response times (such is the case with the H_2/air fuel cell and its compressor; $dI/dt > 0$ is deliberately limited in the interests of a longer lifetime[54], etc.).

---

52 For instance, by evacuating the reactive gases on shutdown and using nitrogen to inert the processes. It is true that this means we need to manage a third gas, but is very helpful in terms of the lifetime of the processes.

53 Particularly in the case of SO technology, for which it is highly advisable to limit the number of on/off switches in order to prolong the lifetime.

54 Particularly in the case of fuel cells, for which the sudden and significant demands for additional power are harmful to the lifetime because of inevitable depletions of the gas, even if these fluctuations are only momentary. One solution, for example, is to use the power converter to limit the dI/dt.

For reasons of safety, it is also preferable to make an electrolyzer work beyond a minimum current density (typically greater than 0.1–0.2 A/cm² for PEM technology). This does indeed limit the phenomenon of crossover, which is characterized by a transfer of hydrogen toward the oxygen side, which can give rise to explosive conditions in the components for regulating pressure and/or oxygen storage.

As regards the fuel cell, its lifetime decreases with prolonged operation at low power where, for instance, the deterioration of carbon electrodes is favored with PEM technology. Therefore, it is generally recommended to have it work above a minimum threshold for the current density (typically greater than 0.1–0.15 A/cm² for PEM technology).

At present, therefore, the whole power range for an H_2/O_2 battery cannot be continuously swept from recharge to discharge and vice versa, because it involves two processes with certain delays for startup and minimum power thresholds in order to operate. We also need to take account of the impact of the consumption of the auxiliaries for the electrolyzer, which cannot function without a sufficient power supply to feed them (Figure 2.43). Therefore, we see the apparition of a range of power in which the H_2/O_2 battery cannot operate, and which represents a "deadband of power" (cross-hatched area in Figure 2.44).

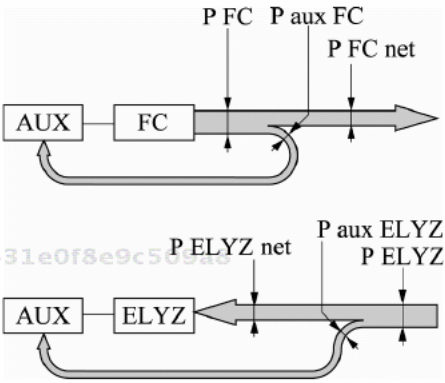

Figure 2.43. *Power balances for an electrolyzer and a fuel cell*

Depending on the intended application, this deadband will be more or less of a problem. If, for instance, the H_2/O_2 battery is connected to the grid, it will not really be of concern: the grid operator simply needs to be aware of these limitations. For example, if that H_2/O_2 battery were now to be used in an application wherein it had to operate autonomously and with no interruption (such is the case, for instance, with an isolated dwelling whose main source of power is a photovoltaic generator),

it will be necessary to couple it with another means of electricity storage in order to compensate for this power deadband [GAI 11; GAI 12].

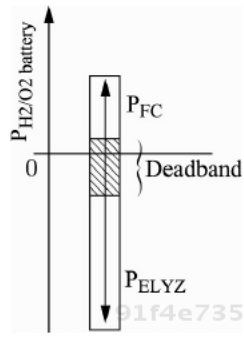

Figure 2.44. *Power deadband of an H_2/O_2 battery*

2.8.4. *Brief overview of situation with industrial developments*

The earliest work done in this field [KLE 69] and to date certainly the most successful (for onboard applications) were the developments performed by NASA for spatial applications – notably for spacecraft. It should be mentioned that the theoretical mass power of an H_2/O_2 battery is 3667 Wh/kg, which renders it potentially very advantageous by comparison to conventional batteries.[55] In practice, it seems to be higher than 400 Wh/kg and could reach up to 1000 Wh/kg [MIT 98]. These developments are being performed in collaboration, notably, with the American company GINER Inc. [MIT 11]. The potential applications are spacecraft, satellites, Martian and lunar bases, etc. The European Space Agency (ESA) is also performing research on a URFC in collaboration with the Norwegian company CMR Prototech in the context of applications in satellites [STR 08].

Aeronautical applications constitute another domain of application for the hydrogen battery: satellite planes, drones, etc. Once again, NASA has been highly successful in this domain. Of its many projects [WIK7], we can cite its famous "atmospheric" satellite plane prototype HELIOS, which bore a great deal of work surrounding URFCs [MIT 97]. Recently, the evaluation of the potentialities began for airplanes, as attested by the announcement made in October 2012 by the company IHI (Ishikawajima Harima Heavy Industries), explaining that they had successfully tested an RFC on board a BOEING 737.

55 For instance, that of a Li-ion battery is between 150 and 200 Wh/kg.

Another major potential outlet for hydrogen batteries is renewable energy storage (photovoltaic energy, wind power, etc.). Many projects have been carried out with RFCs over the past 25 years (see section 2.9.2.1). French industry is rather heavily involved with the projects PEPITE [GAI 11], MYRTE [MYR 13] and JANUS [JAN 12], for which the company AREVA Stockage d'Energie supplies H_2/O_2 batteries (see Figure 2.45).

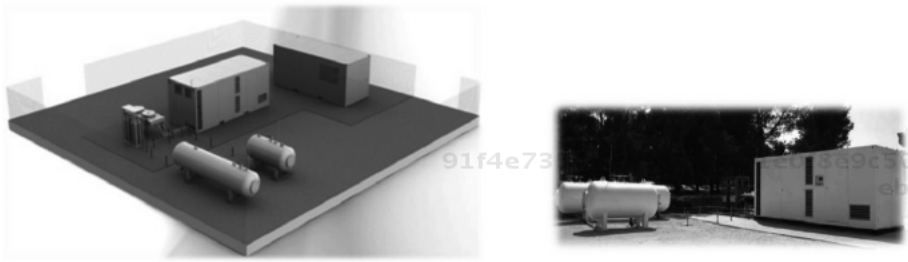

Figure 2.45. *Greenergy Box™ made by the French company AREVA Stockage d'Energie*

The major industrial players that we can distinguish for the hydrogen battery are:

– for aerospace applications: NASA, GINER Inc., CMR Prototech;

– for stationary applications: GINER Inc., PROTON on site, AREVA Stockage d'Energie.

We conclude with the point that the main competitive technologies for hydrogen batteries are redox flow batteries (VRB Power Systems) and sodium-sulfur (NaS) batteries (NGK Insulators).

2.9. A few examples of applications for electrolyzers

As it currently stands, hydrogen is essentially used by the chemical and oil industries (95% of the market). Figure 2.46 shows the distribution, as at 2007, of so-called "industrial" hydrogen use. The other uses (around 5% of the market) relate to the pharmaceutical industry, the semi-conductor industry, the food industry (hydrogenation of certain foodstuffs), the flatscreen industry, heat treatment, particularly for the metallurgy industry, cooling of certain electrical power plants, etc. This "industrial" hydrogen market is growing fast.

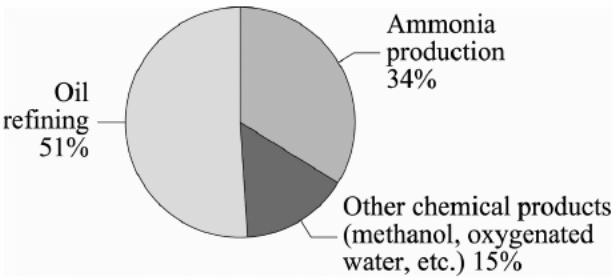

Figure 2.46. *Industrial hydrogen use in 2007. Distribution for the chemical and oil industries (around 95% of the total market)*

The market for energy production from hydrogen is scarcely perceptible at the present time. However, world hydrogen production is, at present, responsible for a little under 2% of world energy consumption. Hydrogen energy is a market which remains to be constructed.

According to [AND 12; HAM 11], in particular, in the short term, the most mature market for hydrogen energy appears to be that for specific electricity production (emergency, isolated sites, etc.): telecommunications, IT centers, portable electrogen groups (to a lesser extent), etc. In the medium term, the significant markets which are developing will be those of heat production (injection of hydrogen into the natural gas network), storage and release of electricity[56] (particularly renewable in origin) and cogeneration of heat and electricity. Finally, in the long term, the market for private transport by fuel-cell vehicles could take off. In the meantime, specific markets such as that of forklift trucks or that of public (buses) or private captive fleets could develop [SUT 12].

In this section, we propose first of all to outline the role already played and which could be played by electrolysis as regards industrial hydrogen, and then give a state of the art for applications coupling solar/photovoltaic and hydrogen, with a detailed examination of some recent projects in France as case studies.

2.9.1. *Points about industrial hydrogen production by electrolysis*

According to [AND 12; HAM 11], the markets that currently exist for industrial players in PEM electrolysis are essentially:

– "analytic" hydrogen for laboratories. The requirement is typically between one and a few grams of H_2 per hour. This market is fairly limited.

56 Services to the grid, such as participation in its stabilization, are obviously envisaged.

– "industrial" hydrogen for certain industrial processes such as the manufacture of semi-conductors. The requirement is typically between a few hundred grams and a few kilograms of H_2 per hour.

The common point between these applications is a need for very pure hydrogen, which PEM technology can serve more easily than can alkaline technology, although the ground truth is not quite as simple as this affirmation, particularly at an industrial level. The problem of the energy cost of electrolysis is of little importance in these applications; it is essentially the cost of the initial investment, and also that of maintenance, possibly, which is important.

Again according to [AND 12; HAM 11], the existing markets to be conquered or to continue to conquer are:

– the market for cooling of certain electricity production plants. According to [AND 12], over 18,000 electricity production installations the world over are cooled with hydrogen. This improves, *a priori*, the efficiency of these plants and therefore reduces greenhouse gas emissions. The considerable investment would very quickly show a return. This market seems a very significant one. The requirement is estimated at between 10 and 100 kg H_2/day per site [BOU 07]:

– the semi-conductor industry;

– the flatscreen industry (computers, tablets, televisions, etc.). The requirement is estimated at between 100 and 1000 kg H_2/day per site [BOU 07];

– thermal treatment, particularly for the metallurgy industry. The requirement is estimated at between 100 and 1000 kg H_2/day per site [BOU 07]; and

– analytical chemistry (carrier gases for the chemical engineering industry, etc.).

Once again, the common point between these applications is a need for very pure hydrogen, which PEM technology is capable of satisfying fairly easily. However, when production begins to reach above a few hundred kilograms of H_2 per day, alkaline technology may (again) become competitive, even with an advanced and therefore expensive hydrogen purification system.

Referring to the introduction to this section (2.9), all of the markets mentioned above, together, represent only 5% of the hydrogen energy market. Electrolysis could become capable of conquering some of the remaining 95% if the oil and chemical industries decided to reduce their environmental impact. Indeed, these industries consume vast quantities of hydrogen [BOU 07]: between 100 and 1000 tons of hydrogen per day for an ammonia production site; and between 10 and 100 tons of hydrogen per day for an oil refinery. Remember that this hydrogen is currently produced by the reforming of fossil hydrocarbons (natural gas or oil

depending on the case) on this type of site. Thus, the use of "green" hydrogen produced by water electrolysis, ideally fed by renewable energies, could come to contribute to decreasing the environmental footprint of this type of industrial site. We still need electrolysis to become able to compete, in an economically viable manner, with the reforming of fossil fuels. At this level of hydrogen production, only alkaline technology – and possibly one day SO technology if the heat lost during the processes can be profitably exploited – seems capable of attaining this objective [BOU 07] – all the more so given that the requirement in terms of purity is less high. Nevertheless, we need to be aware of the fact that the requirement in terms of power would be several hundred MW… The challenge is a major one, and the pertinence of the solution at all levels has yet to be demonstrated.

In conclusion to this section, it seems fairly clear that the markets for water electrolyzers are more immediate than those for fuel cells, because of this need for industrial hydrogen.

2.9.2. *State of the art on applications coupling solar photovoltaic and hydrogen; close examination of the French projects MYRTE, PEPITE and JANUS*

As we saw in the introduction to section 2.9, the market for storage/release of renewably-sourced electricity could, in the medium term, be a very significant market for hydrogen. As we shall see, the coupling of photovoltaic electricity and hydrogen power has been tested in many projects over the course of the past 25 years, providing us with initial feedback. We shall also see that France has become more powerful in this field in the past decade, with three significant projects. Indeed, in the second part of this discussion we shall look in detail at the French projects MYRTE, PEPITE and JANUS. It is clear that these developments need to be closely linked with section 2.8, above, about hydrogen batteries.

2.9.2.1. *State of the art on applications coupling solar photovoltaic and hydrogen [GAI 11]*

Large-scale projects financed by governments, universities or research institutes have been carried out, with the primary objective of demonstrating the feasibility of hydrogen as a means of storage of electrical energy. More specifically, the aim was also simply to advance the technology surrounding hydrogen, be it in terms of its implementation, operational safety or improvement of the processes.

Since 1985, worldwide, no fewer than twenty-five projects have been carried out with this aim. Here, we can cite the main ones: HYSOLAR (1985), SWB (1986), NEMO (1989), FIRST (1989), SCHATZ (1989), FHG – ISE (1992), SAPHYS (1994), HRI (2000), HARI (2001), UTSIRA (2004), HHC (2004), CEC (2007),

MYRTE (2007) and also PHOEBUS (1993), which we shall discuss in detail later on.

Figure 2.47 shows a map of all the projects of which we were able to find a record. It is notable that the majority of projects took place in Europe, and particularly in Germany. The last projects listed are French. Of course, we make no claim that this list is exhaustive. Details about all of these projects are given in Table 2.16.

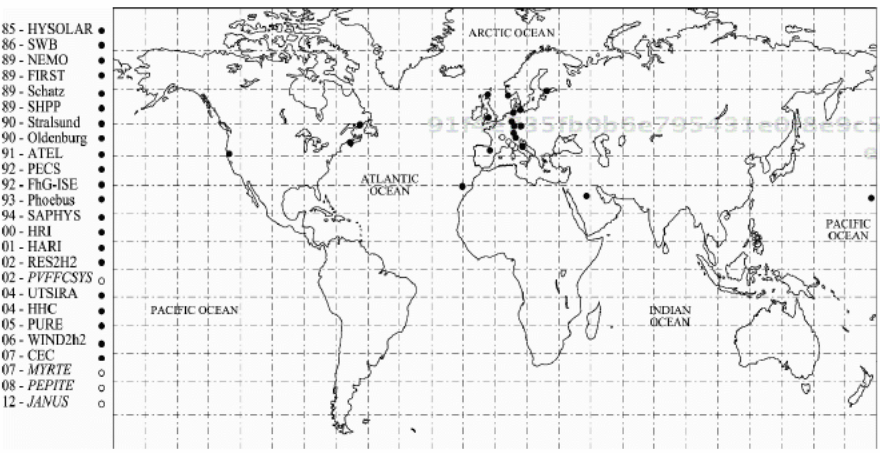

Figure 2.47. *Map of stationary applications combining photovoltaic energy and hydrogen over the past 25 years. The dates supplied correspond to the year in which each project was begun [GAI 11]*

The German project PHOEBUS was one of the most successful and one of the most emblematic. In addition, this project communicated a great deal of feedback on its results.

The PHOEBUS project demonstrated that an application (in this case a university library, requiring 15 kVA) can be entirely autonomous and independent of the public grid, functioning all year round on the basis of renewable resources and with no emission of pollution. The experiment was conducted on the central library of the Forschungszentrum Jülich in Germany for ten years between 1993 and 2003. The data issuing from the first years of its operation were used to feed a digital simulation of the system in order to optimize the initial system, in terms of energy, at as low a cost as possible. The final objective was to obtain a system which was simple, effective, entirely automated and above all, reliable.

Year project began	Location	ENR (PV, other specified)	Electrolyzer	Storage of gases	Fuel cell	Batteries
1985 HYSOLAR	Stuttgart (Germany) Riyadh (Saudi Arabia)	10 kWc, 350 kWc	10 kW ALK, 350 kW ALK	Undisclosed	Undisclosed	Undisclosed
1986 SWB (US$39M)	Neunburg worm Wald (Germany)	370 kWc	2×100 kW ALK 1 bar 100 kW ALK 32 bar	H_2: 5000 Nm^3 O_2: 500 Nm^3	6.5 kW ALK 10 kW PEM 73 kW PA	Connected to the grid
1989 NEMO	Finland	1 kWc	0.8 kW ALK 30 bar	H_2: 8 m^3 25 bar	0.5 kW PA	14 kWh
1989 FIRST	Spain	8.5 kWc	5.2 kW ALK 6 bar	8.8 m^3 200 bar 24 m^3 MH	10 kW PA 2.5 kW PEM 5 kW PEM	Undisclosed
1989 Schatz	California (United States)	9.2 kWc	5.7 kW ALK 7.9 bar	5.3 m^3 7.9 bar	1.5 kW PEM	24 V 220 Ah
1989 SHPP	Helsinki (Finland)	1.3 kWc	0.8 kW ALK 30 bar	200 Nm^3	0.5 kW PA	14 kWh
1990 Stralsund	Stralsund (Germany)	10 kWc 100 $kW_{wind\ p}$	20 kW ALK 25 bar	H_2: 8 m^3 25 bar	0.35 kW PEM	Undisclosed
1990 Oldenburg	Oldenburg (Germany)	6.2 kWc, 5 $kW_{wind\ p}$, 12 kW_{diesel}	0.8 kW ALK 1 bar	H_2: 0.25 m^3 120 bar	0.6 kW ALK	210 V 300 Ah
1991 ATEL	Switzerland	90 kWc	90 kW PEM	Undisclosed	2×3 kW PEM	Undisclosed
1992 PECS	United States	150 Wc	3×95 W PEM 7 bar	2×1.2 m^3 MH	Undisclosed	Undisclosed
1992 FhG – ISE	Freiburg (Germany)	4.2 kWc	2 kW PEM	H_2: 15 m^3 30 bar O_2: 7.5 m^3 30 bar	0.5 kW PEM	20 kWh
1993 PHOEBUS	Jülich (Germany)	42.3 kWc	26 kW ALK 7 bar	H_2: 26.8 m^3 120 bar O_2: 20 m^3 70 bar	6 kW PEM	220 V 300 kWh
1994 SAPHYS	Italy	5.6 kWc	5 kW ALK 20 bar	H_2: 15 m^3 20 bar	3 kW PEM	34 V 1500 Ah
2000 HRI	Trois-Rivières (Canada)	1 kWc, 10 $kW_{wind\ p}$, 10 $kW_{simulated}$	5 kW ALK 7 bar	H_2: 3.8 m^3 10 bar O_2: 1 m^3 8 bar	5 kW PEM	48 V 42.2 kWh
2001 HARI	West Beacon Farm (England)	13 kWc, 2×25 $kW_{wind\ p}$ 3 kW_{hydro}	36 kW ALK 25 bar	H_2: 2856 Nm^3 137 bar	2+5 kW PEM	20 kWh
2002 RES2H2	Canary Islands (Spain) Greece	500 $kW_{wind\ p}$	25 kW ALK 25 bar	40 Nm^3 MH + bottles 220 bar	Undisclosed	Connected to the grid
2002 PVFCSYS	Sophia-Antipolis (France) + [Agrate (Italy)]	3.6 kWc + [null]	3.6 kW ALK 10 bar + [2.4 kW ALK 30 bar]	H_2: 0.4 Nm^3 O_2: 0.2 Nm^3 + [H_2: 4 Nm^3]	4 kW PEM + [2 kW PEM]	2 4V 80Ah + [Undisclosed]
2004 UTSIRA	Utsira (Norway)	2×600 $kW_{wind\ p}$	48 kW	12 m^3 200 bar	10 kW	50 kWh
2004 HHC	Hawaii (United States)	4.9 kWc, 7.5 $kW_{wind\ p}$	2 kW PEM 12 bar	H_2: 5.4 Nm^3 12 bar	5 kW PEM 2 bar	48 V
2005 PURE	Shetland Isles (United Kingdom)	2×15 $kW_{wind\ p}$	18 kW 55 bar	H_2: 44 Nm^3	5 kW	Undisclosed
2006 WIND2H2	United States	2×5 kWc, 100 + 10 $kW_{wind\ p}$	40 kW ALK 10 bar 6 kW PEM 13.8 b	H_2: 6.3 Nm^3 241 bar	Ø	Connected to the grid
2007 CEC	Denizli (Turkey)	5 kWc	3.35 kW PEM	H_2: 5.4 Nm^3 14 bar MH	2×1.2 kW	150 Ah 28k Wh
2007 MYRTE (€21M)	Corsica (France)	550 kWc	200 kW PEM 35 bar	H_2: 2800 Nm^3 O_2: 1400 Nm^3 H_2 and O_2: 35 bar	200 kW PEM	Connected to the grid
2008 PEPITE	Aix-en-Provence (France)	13.4 $kWc_{simulated}$	22 kW PEM 35 bar	H_2: 200 Nm^3 O_2: 100 Nm^3 H_2 and O_2: 35 bar	13 kW PEM	48 V 450 Ah (Ac-Pb)
2010 JANUS	La Croix Valmer (France)	30 kWc	Undisclosed PEM 35 bar	(12 hours' autonomy at 20 kW) H_2 and O_2: 35 bar	50 kW PEM	Undisclosed

Table 2.16. *A few details about the listed projects of stationary applications coupling photovoltaic energy and hydrogen over the past 25 years. The dates supplied correspond to the year in which each project was begun [GAI 11]*[57]

57 PEM = Proton Exchange Membrane, ALK = Alkaline, PA = Phosphoric Acid, MH = Metal Hydrides.

To supply the library, four independent photovoltaic fields, each with a particular orientation due to the architecture of the building, were installed. The first significant level of storage in lead batteries ensured a few days of autonomy, and seasonal storage was done with an alkaline electrolyzer, pressurized gas tanks and an alkaline fuel cell. The characteristics of the devices can be seen in the principle diagram (Figure 2.48).

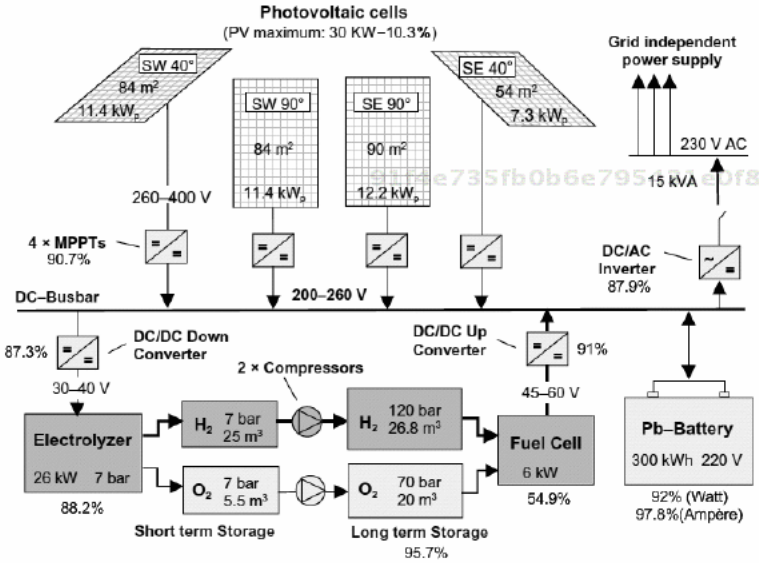

Figure 2.48. *Diagram of the principle behind the PHOEBUS project (Jülich) [GHO 03]*

After functioning for a few years, the alkaline fuel cell began to show weaknesses which were not acceptable in an automated autonomous system. It was therefore replaced with a membrane fuel cell (PEMFC) in late 1999. In the meantime, a fuel cell emulator connected to the public grid was installed to keep the system functioning. In addition, in 1997, the MPPT converters were removed, leaving a direct connection between the panels and the DC bus. The loss of solar production was compensated for by the energy gained by removing these intermediary elements.

The results of this project indicate that progress can be made fairly easily. Indeed, the photovoltaic panels were not ideally positioned, causing a 30% loss of illumination. The electrolyzer was designed for the peak power of the solar generator, whereas in reality, the library consumed several kilowatts above and beyond this. The stage of compression of the gases for storage was also very energy-hungry, and improvements can be made. As a best-case scenario, in the authors'

view, the compressors could even be removed if the output pressure of the electrolyzer were increased. In addition, the water produced by the fuel cell was not stored or reused. Finally, the study shows that the overall efficiency of the system (54%) could be increased to 65%; although this efficiency is not well defined in [GHO 03], it gives us an order of magnitude for the possible margin of improvement.

2.9.2.2. *Close-up examination of the French projects MYRTE, PEPITE and JANUS*

The first project run in France was, in fact, the PVFCSYS project (2002), which set out to compare a PV/battery combination with a PV/hydrogen combination [BUS 03]. Two sites were equipped – one at Sophia-Antipolis in France, and the other at Agrate in Italy. The details on the hardware being tested in given in Table 2.16.

Three other projects then saw the light of day: MYRTE (2007), PEPITE (2008) and JANUS (2010), all of which exploited an H_2/O_2 battery (see section 2.8). Below are some details and illustrations concerning these three projects.

2.9.2.2.1. MYRTE project (Corsica, France) [MYR 13]

The MYRTE project (*Mission hYdrogène Renouvelable pour l'inTégration au réseau Electrique* – Renewable Hydrogen for Integration to the Electrical Grid) is a €21M massive-scale project, financed with European funds and contributions from various local public institutions. Run by the University of Corsica, the other partners in the project are the company *AREVA Stockage d'Energie* (AREVA Energy Storage) and the CEA. The aim of the project is to use a 550 kWc photovoltaic farm, able to inject energy into Corsica's public grid to smooth supply at peak times (around 11:00 and 18:00) and thus take the strain off the existing grid: this is known as "peak shaving". With the particular goal of being able to assist the public grid at around 18:00 and – to a certain extent – to combat the intermittence of photovoltaic production, a 3.5 MWh[58] H_2/O_2 battery is combined with the photovoltaic generator.

The first phase of the project involved creating a system with a 100 kWe PEM fuel cell (Figure 2.50) and a 50 kW PEM electrolyzer (10 Nm^3/h) (Figure 2.51), supplied by a 550 kWc photovoltaic field (Figure 2.49). This system was installed on site at Vignola in Corsica.

58 With a supposed efficiency of 42% for the fuel cell, giving a conservative estimation and taking account of the aging.

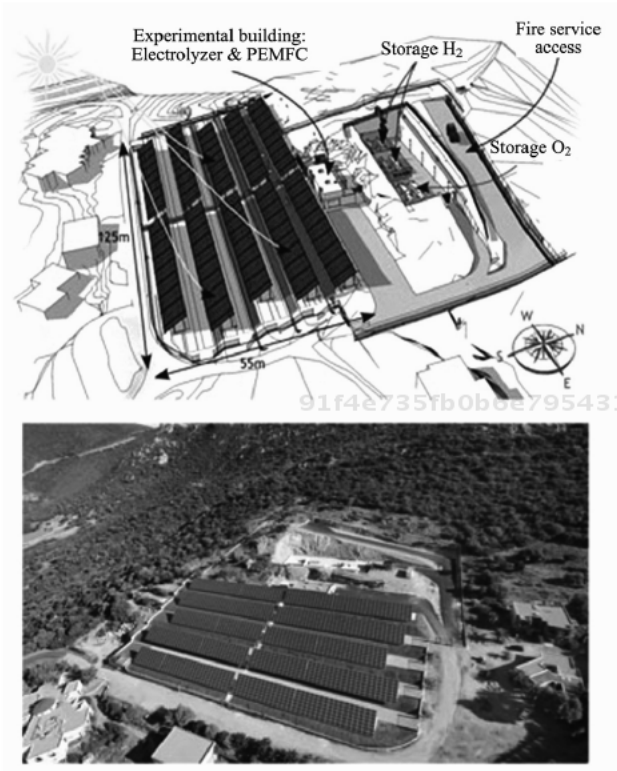

Figure 2.49. *From the project in 2007 to the platform in 2011 [MYR 13]*

Figure 2.50. *Left: 100 kWe PEM fuel cell; and right: 10 Nm^3/h 35 bar (50 kWe) PEM electrolyzer, first phase [GAI 11]*

Figure 2.51. *Installation of gas storage tanks on site [GAI 11]*

In terms of energy reserves, tanks are installed, holding 2800 Nm^3 for hydrogen (i.e. 250 kg of H_2) and 1400 Nm^3 for oxygen, storing 3.5 MWh at full capacity. The gases are stored at 35 bar with no additional mechanical compression between the electrolyzer and the tanks.

In the second phase, the power of the fuel cell will be doubled, to deliver 200 kWe, and the capacity of the electrolyzer will be quadrupled to 40 Nm^3/h (which is around 200 kWe).

The platform became operational on 9 January 2012.

2.9.2.2.2. *PEPITE project (Aix-en-Provence, France) [GAI 11]*

PEPITE (*Projet d'Etudes et d'expérimentation de Puissance pour la gestion des energies Intermittentes par les Technologies Electrochimiques* – Research and Power Experimentation Project for the Management of Intermittent Energies by Electrochemical Technologies) is a project run by the company AREVA Stockage d'Energie and bringing together the University of Corsica, the CEA, the LAPLACE Laboratory and ARMINES. It was financed in part by the *Agence Nationale de la Recherche* (National Research Agency) as part of the Pan-H research program running from 2008 to 2011.

In the same vein as the projects discussed previously, PEPITE intends to show that renewable energies coupled with hydrogen power are capable of rising to various challenges which are representative of potential future markets. For this reason, it has three parts. The first is a study of an autonomous system to provide uninterrupted power supply to an isolated technical site, using photovoltaic energy. The second part relates to power supply to an isolated village on the island of Réunion, and the third part is a

preliminary study to the MYRTE project, whose aim is the peak shaving of the insular grid to which it is connected, as presented just above.

Here, we shall look only at the part relating to uninterrupted power supply to an isolated technical site, using photovoltaic energy. The need for storage capability is explained at least by the necessity to be able to function during the night-time. For this project, an H_2/O_2 battery was chosen. As we saw in section 2.8.3, an H_2/O_2 battery has a deadband, which in this case proves problematic in view of the intended autonomy of the application. To compensate for this deadband, a small lead–acid battery (with autonomous operation of a few hours) was introduced into the system.

Many different electrical architectures were put forward as regards how to link the separate elements. The three arrangements shown in Figure 2.52 are those which were compared theoretically with a view to making a choice for the final demonstrative prototype.

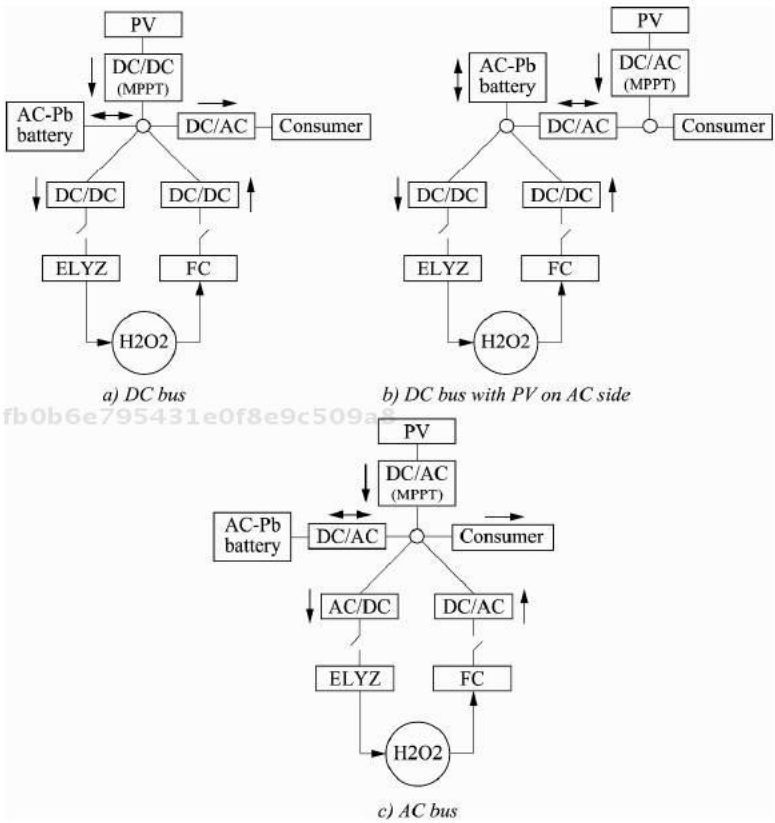

Figure 2.52. *Electrical architectures chosen for a theoretical evaluation*

With parameterization of the models based on the industrial hardware originally intended for the demonstrator, the AC bus architecture proved to be the most energy-efficient solution. However, this result is not universal, and examinations will need to be carried out in other similar case studies.

At an experimental level, the DC bus architecture was finally tested also at the LAPLACE laboratory, on a small scale with emulators, except for the lead–acid battery. The demonstrator for the project was built in Aix-en-Provence on a site owned by AREVA Stockage d'Energie. In fact, a photograph of this demonstrator is shown in Figure 2.45. The AC bus architecture and the characteristics of the different components are set out in Figure 2.53. The photovoltaic generator was emulated, notably, in the interests of greater flexibility for the tests. In terms of energy reserves, the tanks were 200 Nm^3 for hydrogen (18 kg of H_2) and 100 Nm^3 for oxygen, giving 300 kWh[59] at full capacity (compared to 21 kWh from the lead–acid battery). This represents a demonstration on a scale of 1/20 in relation to the dimensions necessary for 24-hour autonomy [DAR 10b]. The gases were stored at 35bar with no additional mechanical compression between the electrolyzer and the tanks. This demonstrator successfully operated over the course of many different experimentation campaigns, spread over several months.

2.9.2.2.3. JANUS project (La Croix Valmer, France) [JAN 12]

The JANUS project is, to our knowledge, the first experiment – at least in France – with a publicly-commercializable application based on an H_2/O_2 battery. This project began in 2010 in terms of the design phase and setting up of funding arrangements.

The first stage of the JANUS project related to a children's center in the city, inaugurated in September 2012. It consisted of the installation of a 30 kWc (200 m^2) photovoltaic plant, coupled with a Greenergy Box™ (as shown in Figure 2.45) delivering 50 kWe of power. The objective is to ensure partial autonomy (45–85%) of the building, and electricity backup in case of network failure (12 hours' autonomy at 20 kW of power). These buildings are among the first "Green Buildings" according to [JAN 12]. The heat produced by the processes is also exploited to serve all or part of the building's heating needs.

59 With a supposed 50% efficiency from the fuel cell.

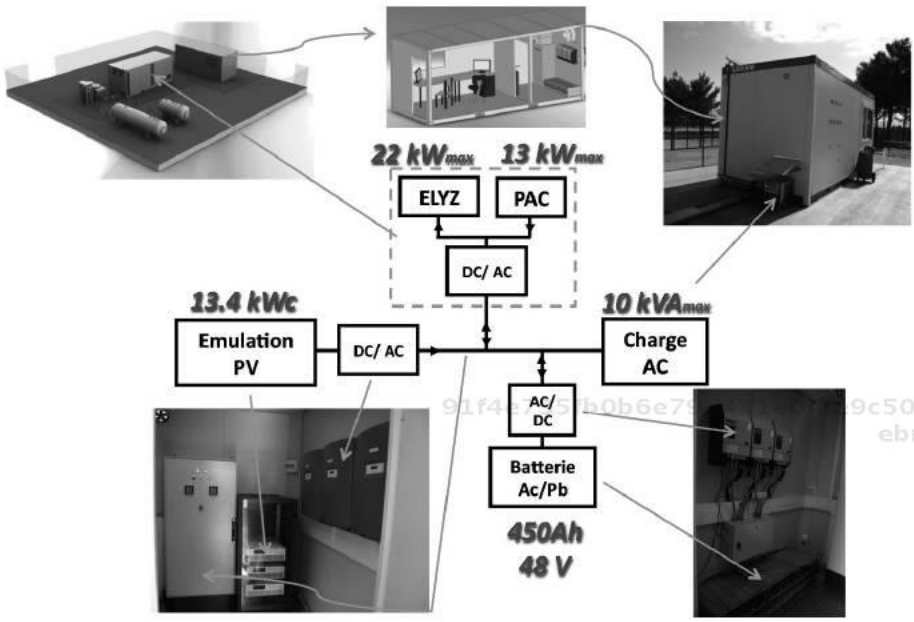

Figure 2.53. *AC bus electrical architecture of the demonstrator built for the PEPITE project [GAI 11]*

The second stage will consist of extending the concept to four other municipal buildings.

2.10. Some points about the storage of hydrogen

Hydrogen can be stored directly in three forms:

– pressurized gas (e.g. 200 bars, 350 bars, 700 bars);

– liquid at cryogenic temperature (20 K, so –253°C);

– in metal hydrides.

Figure 2.54 shows the different densities of mass- and volumetric energy for each of these solutions.

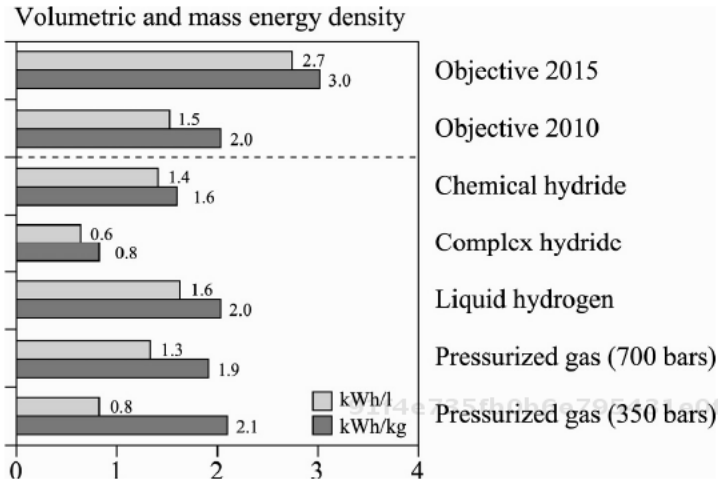

Figure 2.54. *Performances of the different forms of hydrogen storage in terms of volumetric and mass energy density [CLE 05]*

Remember that hydrogen alone has a mass energy of 33 kWh/kg. Gasoline, for its part, has a mass energy of around 12 kWh/kg and a volumetric energy of 8.8 kWh/l. We can see that even the target objectives are well below the quoted quantities for gasoline, once again illustrating the energy density offered by this hydrocarbon.

We see the reaffirmation of a known result, which is that storage at 700 bar pressure efficiencies have similar performances to those of cryogenic storage. The performances of the chemical hydride are not far behind either.

Let us now revisit the case of hydrogen production by water electrolysis.

The simplest form of storage is probably storage under pressure, especially if we also wish to store oxygen. There is, in fact, no equivalent to metal hydrides for oxygen storage. Certainly, oxygen could also be stored in liquid form at cryogenic temperature (90 K, which is –183°C). However, in view of the complexity of such a solution, storage under pressure appears far simpler to implement.

When pressurized storage is chosen for the gases produced, the ideal is for the operational pressure of the electrolyzer to be as close as possible to the desired storage pressure. This enables us to minimize the energy necessary for the mechanical compression required by the compressor.

If we do not wish to store oxygen, the metal-hydride solution is a competitive solution which offers better safety than pressurized storage, particularly in stationary applications where there is no problem of weight. However, this comes at the cost of increased complexity.

2.11. Conclusions and perspectives

This chapter has dealt with the fundamental aspects of water electrolysis. It has provided the reader with the theoretical and technological elements and, to a certain extent, practical elements.

Alkaline electrolysis has been being applied industrially for over a century, and can now be deemed to be mature. We have shown that it is still the subject of research aimed at enhancing its performance still further.

PEM electrolysis, first put forward 50 years ago, has not yet reached complete maturity. Commercial products do exist, but still need to be proven.

SO electrolysis, which is still at the development stage, has not yet taken off. There are no true commercial products in existence. The few products which are on sale are modeled on the prototype. Nevertheless, this technology is very promising because of its capacity to profitably exploit the heat lost – heat which must, however, be sufficiently high in energy.

In a rapidly and constantly changing energy landscape, water electrolysis undoubtedly has a very important part to play, because of its capacity to transform electricity from renewable energies (photovoltaic, wind power, etc.) into hydrogen – hydrogen which can be turned back into electricity at any time by a fuel cell. In order to perform this role, the electrolyzer in question should ideally be compatible with the variability of renewable production. It seems that PEM technology is better able to fulfill this purpose than alkaline technology. Nevertheless, we shall remain cautious, because this needs to be verified and validated. With regard to SO technology, it is, as yet, a little early to draw conclusions about its capabilities.

2.12. Exercises

Exercise no. 1:

Write the equations for the reactions relative to the three main water electrolyzer technologies.

Solution to exercise no. 1:

– Alkaline Water Electrolysis (AWE): equations [2.2] and [2.1].

– Proton Exchange Membrane Water Electrolysis (PEMWE): equations [2.3] and [2.1].

– Solid Oxide Water Electrolysis (SOWE): equations [2.4] and [2.1].

Exercise no. 2:

Of the following balance equations, which are valid for a water electrolyzer? Justify your answer.

$$H_2O + \text{electricity} + \text{heat} \rightarrow 2H_2 + O_2 \quad [2.65]$$

$$2H_2O + \text{electricity} + \text{heat} \rightarrow 2H_2 + O_2 \quad [2.66]$$

$$H_2O + \textbf{electricity} + \textbf{heat} \rightarrow H_2 + \frac{1}{2}O_2 \quad [2.67]$$

$$4H_2O + \text{electricity} + \text{heat} \rightarrow 4H_2 + 2O_2 \quad [2.68]$$

Solution to exercise no. 2:

With the exception of equation [2.65], all these equations are valid.

Equation [2.65] is not balanced: the quantities of hydrogen and oxygen are not the same on both sides of the equation; for example, a coefficient "2" is missing in front of the term "H_2O".

Equations [2.66] and [2.67] are those which are usually found in the literature: these expressions are the minimal formulations in terms of the stoichiometric coefficients, depending on whether or not we prefer to work with fractional values. Equation [2.68] is strictly identical to equations [2.66] and [2.67], but is not a minimal formulation, as the stoichiometric coefficients can still be divided by 2 or 4.

Exercise no. 3:

Assess the validity of the follow balance equations for a SOWE:

Cathode:	$2H_2O + 4e^- \rightarrow 2H_2 + O^{2-}$	[2.69]
Anode:	$O^{2-} \rightarrow \frac{1}{2}O_2 + e^-$	[2.70]
Balance equation:	$2H_2O \rightarrow 2H_2 + O_2$	[2.71]

Solution to exercise no. 3:

The balance equation [2.71] is correct and balanced. Equations [2.69] and [2.70], however, are wrong.

Equation [2.69] is not balanced in terms of the oxygen or the charges. To balance out the quantities of oxygen, we need to add a coefficient 2 in front of the oxygen ion on the right-hand side of the equation, because the left-hand side is adapted to obtain the balance equation. By doing that, we restore the electroneutrality of the two sides of the equation, because there are 4 negative charges on both sides.

Turning to equation [2.70], we see that it is not balanced from the point of view of the charges: it is necessary to place a coefficient 2 in front of the term e^- on the right-hand side of the equation. Hence, adding equations [2.69] and [2.70] will not give us the balance equation [2.71]. Therefore, we also need to multiply the whole of equation [2.70] by 2 so as to restore equilibrium of the species and charges.

In order to gain an overall view of the corrections and modifications made, let us rewrite all the equations:

Cathode:	$2H_2O + 4e^- \rightarrow 2H_2 + 2O^{2-}$	[2.72]
Anode:	$2O^{2-} \rightarrow O_2 + 4e^-$	[2.73]
Sum of the two equations:	$2H_2O + 4e^- + 2O^{2-} \rightarrow 2H_2 + 2O^{2-} + O_2 + 4e^-$	[2.74]
Thus, we get the balance equation:	$2H_2O \rightarrow 2H_2 + O_2$	[2.75]

Exercise no. 4:

1) When was water electrolysis first observed?

2) What was the first type of electrolyzer made commercially available? What is the situation of this device today?

3) When were the first PEM electrolyzers developed?

4) Give a few key elements on the history of high-temperature electrolysis.

Solution to exercise no. 4:

1) In parallel to the French Revolution, the earliest observation of water electrolysis was made by 1789 in Holland by A. Paets van Troostwijk and J.R. Deiman. Some authors attribute the discovery to two British scholars, W. Nicholson and A. Carlisle, in 1800.

2) The first electrolyzers to be deployed were alkaline. They were commercialized from the late 19th Century onwards. Today, alkaline technology is the ultra-dominant form of technology, accounting for 99% of the electrolyzer market.

3) The first PEM (Proton Exchange Membrane) electrolyzers were developed at the same time as the earliest PEM fuel cells (PEMFCs) as part of the US space program GEMINI, run in the 1960s by NASA.

4) Solid-oxide (SO) high-temperature electrolysis also began to be developed in the American space programs run by NASA during the 1960s. However, the electrolyte typically used (YSZ – Yttria-Stabilized Zirconia) was discovered at the beginning of the 20th Century by Nernst. During the 1970s and 1980s, it was in Germany (with the industrialists Dornier and Lurgi) and the United States (with Westinghouse) that the most significant developments took place. During the 1990s, developments continued mainly in Japan. Since the start of the 21st Century, this technology has birthed many more important works all over the world, especially with a view to creating systems for cogeneration of electricity and heat.

Exercise no. 5:

1) What is the value of the thermoneutral voltage in the case of a SOWE electrolyzer? What is the advantage to working at this particular point?

2) Supposing there are no irreversible losses, what would be the voltage at the terminals of a PEMWE electrolyzer fed with liquid water? How about one fed with water vapor?

3) What is the range of voltage for a SOWE electrolyzer fed with water vapor for endothermic operation? What is the advantage to such operation?

4) What is the thermal behavior of an AWE electrolyzer functioning below a temperature of 100°C?

5) Is it advantageous to work at the thermoneutral voltage for a PEMWE electrolyzer?

Solution to exercise no. 5:

1) The thermoneutral voltage is around 1.29 V between 800°C and 1000°C for a SOWE electrolyzer. It is advantageous to work at this particular point because, theoretically, there is no need for either an external heat source or a cooling system. The electrolyzer is in thermal equilibrium with the environment. The electricity source directly provides the free enthalpy of dissociation ΔG_d to the electrochemical reaction and indirectly the entropic heat $T\Delta S_d$ via the irreversible losses relating to the reaction (activation, species transport and charge transport). The electricity source also has to provide the energy for vaporization of the water, again by way if the irreversible losses of the reaction, if that water is injected in liquid form.

2) When there is no indication as to the operating conditions of a PEMWE electrolyzer, it is normal to give the values for 25°C and 1 bar when specifying these conditions. Thus, in the absence of irreversible losses, the voltage at the terminals of a PEMWE electrolyzer will be equal to the reversible voltage E_{rev} – i.e. at 25°C and 1 bar, of around 1.23 V for supply with liquid water, and around 1.19 V for supply with water vapor.

3) In endothermic operation, the range of voltage for a SOWE electrolyzer fed with water vapor will be between E_{rev} and E_{tn}, so at 1000°C and 1bar, between ≈0.93 V and 1.29 V. Such operation is particularly advantageous when we want to decrease electricity consumption for electrolysis by using an external heat source which is less expensive than electrical energy.

4) Below 100°C, the behavior of an alkaline water electrolyzer (AWE) will, for the vast majority, be exothermic. Indeed, the irreversible losses relating to the reaction (activation, species transport and charge transport) limit endothermic operation to very low current densities. From the point of view of the current density, the thermoneutral voltage will be surpassed very early on.

5) Operation at the thermoneutral voltage is not particularly advantageous for a PEMWE electrolyzer. Indeed, in the same vein as an AWE electrolyzer, because of the irreversible losses caused by the reaction (activation, species transport and

charge transport), the corresponding current density will be very low, leading to very low gas production, and therefore very likely economic non-viability.

Exercise no. 6:

1) What is the amount of energy, expressed in kWh, needed to produce 1 kg of hydrogen from liquid water? Justify your answer. From this, deduce the efficiency of a PEMWE electrolyzer consuming 4.5 kWh/Nm^3 of hydrogen produced.

2) What are the efficiencies of a SOWE electrolyzer cell, fed by a source of water vapor, for respective voltages of 1.2 V and 1.4 V? Assume an operating temperature of 1000°C and pressure of 1 bar.

3) What is the efficiency of an electrolyzer functioning at its thermoneutral point?

4) What is the quantity of water needed to produce 1 kg of hydrogen? How will this value be affected by the efficiency of the electrolyzer?

Solution to exercise no. 6:

1) When there is no indication as to the operating conditions, it is normal to give the values for 25°C and 1 bar when specifying these conditions.

The enthalpy of dissociation of water is ΔH_d= 285.8 kJ/mol when using liquid water.

As 1 Wh is equal to 3600 J, ΔH_d= 285.8 / 3600 ≈ 0.079 4 kWh/mol.

Given that 1 kg of H_2 contains 500 mol, ΔH_d= 0.0794 × 500 ≈ 39.69 kWh/kg.

In 1 Nm^3 of H_2, there are 44.62 mol. 1 kg of H_2 therefore represents 500 / 44.62 ≈ 11.21 Nm^3.

Thus, ΔH_d= 39.69 / 11.21 ≈ 3.54 kWh/Nm^3.

In summary, we have just demonstrated once again that ΔH_d = 285.8 kJ/mol ≈ 39.69 kWh/kg ≈ 3.54 kWh/Nm^3 at 25°C and 1 bar when using liquid water.

We can therefore calculate the efficiency of a PEMWE electrolyzer consuming 4.5 kWh/Nm^3 of hydrogen produced. It would be 3.54 / 4.5 × 100 ≈ 78.7%.

2) With this type of question, we first need to accurately locate the thermoneutral point. In the operating conditions specified, it is approximately E_{tn} = 1.291 V. This

means that the operation is endothermic for the point 1.2 V and exothermic for the point 1.4 V.

For the point 1.2 V, as the statement gives no information about the external heat injected, it is not possible to calculate the energy efficiency. Only the electrical efficiency can be calculated: $\eta_{electrical} = E_{rev} / U_{cell} \times 100 = 0.932 / 1.2 \times 100 \approx 77.7\%$. This efficiency is not easy to interpret. It is easier to say that the electricity source provides $U_{cell} / E_{tn} \times 100 = 1.2 / 1.291 \times 100 \approx 92.5\%$ of the requirement of the reaction in terms of energy. The remainder is provided by an external heat source.

For the point 1.4 V, it is possible to calculate the energy and electrical efficiencies:

$$\eta_{energy} = E_{tn} / U_{cell} \times 100 = 1.291 / 1.4 \times 100 \approx 92.2\%.$$

$\eta_{electrical} = E_{rev} / U_{cell} \times 100 = 0.932 / 1.4 \times 100 \approx 66.6\%$. Once again, this efficiency is difficult to interpret. It is easier to understand that the electricity source provides $U_{cell} / E_{tn} \times 100 = 1.4 / 1.291 \times 100 \approx 108.4\%$ of the energy requirement of the reaction, which confirms that the operation is indeed exothermic (the component needs to be cooled).

3) The energy efficiency of an electrolyzer functioning at its thermoneutral point is 100%.

Its electrical efficiency is $\eta_{electrical} = E_{rev} / U_{cell} \times 100 = 1.229 / 1.481 \times 100 \approx 83\%$ for 25°C and 1 bar, supposing that the water injected is liquid. This efficiency is tricky to interpret. It is more comprehensible to say that the electricity source provides 100% of the reaction's energy needs.

4) As 1 kg of H_2 contains 500 mol, we need to electrolyze 500 mol of water ($H_2O \rightarrow H_2 + ½\ O_2$), so $n_{H_2O} \times M_{H_2O} = 500 \times 18 = 9000$ g, so 9 kg.

At 25°C, the density of water is 0.997 L/kg. Therefore we need $9 \times 0.997 \approx 8.973$ L.

This value is not affected by the energy efficiency of the electrolyzer because the quantity of water consumed depends only on the quantity of hydrogen produced, which is proportional to the current injected rather than to the energy injected. However, the Faradaic efficiency, which is the ratio between the injected current and the theoretical current, could slightly affect this value: in general, it is considered to be very nearly equal to 1. Strictly speaking, we also need to consider the

phenomenon of crossover of the gases through the membrane, which very slightly reduces the quantity of gas produced.

Exercise no. 7:

1) The slope of the polarization curve at high current densities enables us to determine the Ohmic resistance: true or false? Comment.

2) For low-temperature technologies, the activation losses are very significant at low current densities and the other losses are at high current densities: true or false? Comment.

3) Assuming we can approximate the polarization curve for an electrolyzer $U = E + RI$, what is its maximum power?

4) Express equation [2.45] as a function of the current density and for a stack of N_s cells.

5) Consider an electrolyzer with 12 cells. In order to be able to carry out simple calculations, we shall approximate its behavior in terms of voltage in the static state by the law $U = E + RI$, where $E = 18.8$ V and $R = 58$ mΩ. If we inject 2 kW into this electrolyzer, how much hydrogen will be produced? What amount of water will be consumed if we continue to operate in this regime for 24 hours? Give an estimation of the efficiency of the electrolyzer for this regime of operation.

Solution to exercise no. 7:

1) False.

All the phenomena contribute to the slope at all points of the polarization curve, as attested by the derivative of its equation (here established on the basis of equation [2.45]):

$$\frac{\partial U_{cell}(I)}{\partial I} = \frac{RT}{2\alpha_{ELYZ}F}\frac{1}{|I|+I_n} + R_{ohm} + \frac{RT}{2\beta F I_{\lim}}\frac{1}{1-\frac{|I|}{I_{\lim}}} \qquad [2.76]$$

$$\approx \frac{RT}{2\alpha_{ELYZ}F}\frac{1}{|I|+I_n} + R_{ohm} + \frac{RT}{2\beta F I_{\lim}} \quad \text{if } |I| << I_{\lim}$$

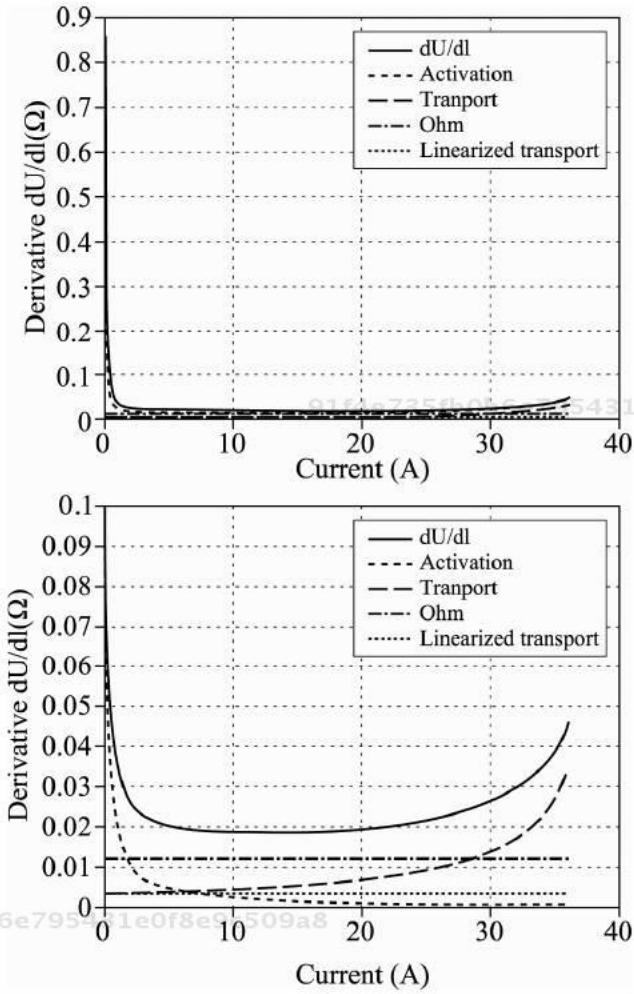

Figure 2.55. *Derivative in relation to the current on the polarization curve with the parametric values given in Table 2.12*

By numerical application using the parameters given in Table 2.12, we can see that it is not, in fact, possible to estimate the Ohmic resistance on the basis of the slope of the polarization curve. It could be possible if and only if the phenomena of species transport were negligible as illustrated in Figure 2.56.

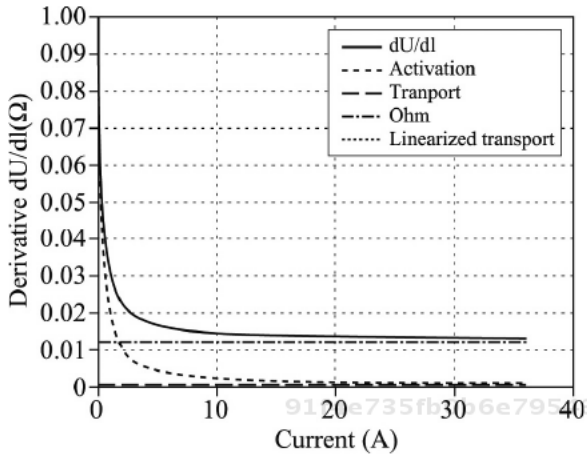

Figure 2.56. *Derivative with respect to the current on the polarization curve with the parametric values given in Table 2.12 with i_{lim} multiplied by 10 (16 A/cm²)*

2) False.

This is an error which is often made for low-temperature technologies, particularly PEM technology, for which the activation losses are generally greatest within the usual ranges of current densities.

In general, we must never lose sight of the fact that all the phenomena (activation, species transport and charge transport) coexist at every point on the polarization curve. In order to clarify our ideas and confirm them, we can refer to Figure 2.21. Affirmations as strong as conveyed by the statement could only be proven in very specific cases.

3) In theory, there is no limitation of power for an electrical receiver such as an electrolyzer.

The same is not true for a fuel cell which, like all impedant generators of the type $U = E - RI$, will have its power limited to $P_{max} = E^2/4R$.

In practice, there will naturally be a limit to the power for an electrolyzer, imposed at least by the capacity of its cooling system and, in the long term, by the resistance of the materials in strained conditions, particularly in terms of voltage.

4) Remember equation [2.45], showing the voltage-to-current relationship for an electrolyzer cell:

$$U_{cell}(I) = E_{rev} + \frac{RT}{2\alpha_{ELYZ}F}\ln\left(\frac{|I|+I_n}{I_0^{ELYZ}}\right) + R_{ohm}\cdot|I| - \frac{RT}{2\beta F}\ln\left(1-\frac{|I|}{I_{\lim}}\right)$$
$$\approx E_{rev} + \frac{RT}{2\alpha_{ELYZ}F}\ln\left(\frac{|I|+I_n}{I_0^{ELYZ}}\right) + R_{ohm}\cdot|I| + R_{diff0}\cdot|I| \qquad [2.77]$$

In order to obtain the voltage at the terminals of a serial stack of N_s cells, we need only multiply expression [2.77] by N_s, if we assume that the behavior of each cell is identical, or that that expression [2.77] is that of the equivalent average cell for the stack.

Finally, we need to know the surface area S of a cell and define multiple values to express the voltage as a function of the current density $i = I/S$:

$$U_{stack}(I) = N_s\left(E_{rev} + \frac{RT}{2\alpha_{ELYZ}F}\ln\left(\frac{|i|+i_n}{i_0^{ELYZ}}\right) + \gamma_{ohm}\cdot|i| - \frac{RT}{2\beta F}\ln\left(1-\frac{|i|}{i_{\lim}}\right)\right)$$
$$\approx N_s\left(E_{rev} + \frac{RT}{2\alpha_{ELYZ}F}\ln\left(\frac{|i|+i_n}{i_0^{ELYZ}}\right) + \gamma_{ohm}\cdot|i| + R_{diff0}\cdot|i|\right) \qquad [2.78]$$

where:

$$i_n = \frac{I_n}{S} \qquad i_0^{ELYZ} = \frac{I_0^{ELYZ}}{S} \qquad \gamma_{ohm} = R_{ohm}\cdot S \qquad i_{\lim} = \frac{I_{\lim}}{S} \qquad \gamma_{diff0} = R_{diff0}\cdot S \qquad [2.79]$$

5) The electrolyzer in question comprises 12 cells and is assumed to obey the law $U = E + RI$ where $E = 18.8$ V and $R = 58$ mΩ.

In order to work out the hydrogen production if we inject 2 kW into that electrolyzer, we first need to calculate the current corresponding to that power by solving the following equation:

$$(E + RI)I = P = 2000$$

which gives us the second-degree equation to solve:

$$I^2 + {}^{E}/_{R}\, I - {}^{P}/_{R} = 0.$$

Only the following solution works:

$$I = -{}^{E}/_{2R} + {}^{1}/_{2}\sqrt{{}^{E^2}/_{R^2} + {}^{4P}/_{R}} \approx 84.4A.$$

To obtain the hydrogen production of the stack, we now need to multiply the production of one cell by the number of cells that are electrically connected:

$$J_{H2} = N_s \, {}^{I}/_{2F} \approx 12 \times {}^{84.4}/_{2 \times 96485} \approx 5.25 \times 10^{-3} \; mol/s$$

Hence, $J_{H2} \approx 5.25 \times \frac{10^{-3} \; mol}{s} \times {}^{3600}/_{500} \approx 0.0378 \; kg/h$, because 1 kg of H_2 contains 500 mol.

If this power regime is pursued for 24 hours, as we know that the molar flowrate of water is the same as that of hydrogen, the amount of water consumed will be:

$$J_{H_2O} = J_{H_2} = {}^{dn_{H_2O}}/_{dt}$$

$$\rightarrow \; n_{H_2O} = \int_{O}^{tf} J_{H_2} \, dt \approx 5.25 \times 10^{-3} \times 24 \times 3600 \approx 453.6 \; mol$$

Thus, $m_{H_2O} = m_{H_2O} \times M_{H_2O} \approx 453.6 \times 0.018 \approx 8.2 \; kg$.

It is not easy to give an estimation of the efficiency of this electrolyzer, because we have no information about its technology and operating conditions. If we calculate the ratio $E/N_s = 18.8/12 = 1.56$ V, this leads us to think that it is probably a low-temperature technology. By making this hypothesis, and also supposing that the electrolyzer is supplied with liquid water, we can estimate the energy efficiency using the thermoneutral voltage E_{tn} at 25°C and 1 bar:

$$\eta_{energetic} = {}^{E_{tn}}/_{U/N_s} \times 100 = {}^{E_{tn}}/_{(E + RI)/N_s} \times 100$$

$$\approx {}^{1.481}/_{(18.8 + 0.058 \times 84.4)/12} \times 100 \approx {}^{1.481}/_{1.975} \times 100 \approx 75\%.$$

Exercise no. 8:

1) Consider a parallel R-C dipole. Demonstrate than we obtain a semi-circle on the Nyquist plot.

2) What is the frequency corresponding to the minimum of the imaginary part? What application could this formula be used for?

3) We now connect to this parallel R-C dipole a resistance R_{ohm} and an inductance L. Plot the overall impedance spectrum, specifying the individual points.

Solution to exercise no. 8:

1) The impedance of this dipole is easy to calculate:

$$1/Z = 1/R + jC\omega, \text{ so therefore } Z = R/(1 + jRC\omega)$$

$$Z = R(1 - jRC\omega)/(1 + jRC\omega)(1 - jRC\omega) = R(1 - jRC\omega)/(1 + R^2C^2\omega^2)$$

The Nyquist plot represents the imaginary part as a function of the real part of the impedance:

$$Re(\omega) = R/(1 + R^2C^2\omega^2) = x$$

$$Im(\omega) = -R^2C\omega/(1 + R^2C^2\omega^2) = y$$

We find ourselves with a curve parameterized in terms of ω. By combining the two equations, we get the following equation: $x^2 + y^2 - Rx = 0$, which can be expressed in a more explicit form: $(x - R/2)^2 + y^2 = R^2/4$.

We indeed obtain the equation of a circle with center (R/2; 0) and radius R/2.

As the pulsation ω can only vary between 0 and infinity, we would in fact have a semi-circle located in the quadrant Re(ω) > 0 and Im(ω) < 0.

2) Two methods are possible: either we use the derivative of Im(ω), or we solve the problem geometrically: we get the equation Im(ω) = –R/2.

The more generic approach is to use the derivative of Im(ω):

$$\frac{\partial Im(\omega)}{\partial \omega} = R^2C(-1 + R^2C^2\omega^2)/(1 + R^2C^2\omega^2)^2$$

The derivative of Im(ω) disappears if $-1 + R^2C^2\omega^2 = 0$, so $\omega_{min} = 1/RC$ so for the corresponding frequency: $f_{min} = 1/2\pi RC$.

We can easily show that $Im(\omega_{min}) = -R/2$.

This formula can, *a priori*, enable us to estimate the value of the capacitor or pseudo-capacitor of the phenomenon involved, using the experimental impedance diagram.

3) If we add in series a resistance and an inductance, the total impedance is given by $Z_{tot} = {}^{R}/_{1 + jRC\omega} + R_{ohm} + jL\omega$. The series resistance will move the semi-circle of the R-C dipole by R_{ohm} along the real axis. The inductance will lead us into the quadrant Re(ω) > 0 and Im(ω) > 0.

Figure 2.57 illustrates all the results of this exercise.

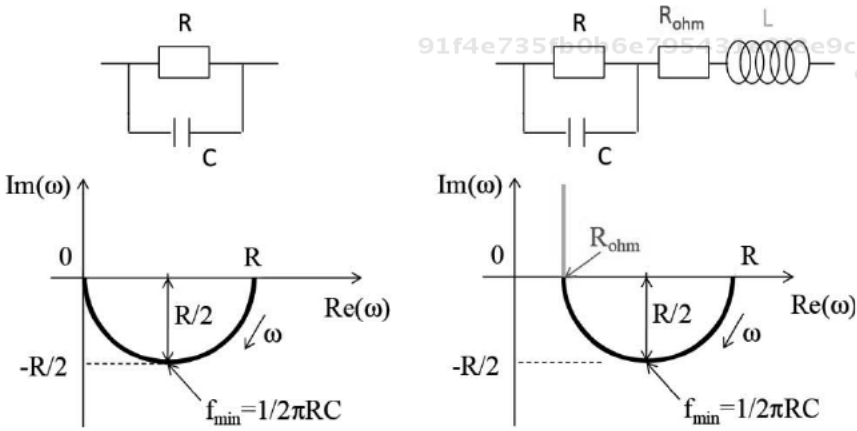

Figure 2.57. *Impedance diagrams of a parallel RC circuit, first alone and then combined with a resistance and an inductance*

Chapter 3

Fuel Cells

3.1. Introduction

A fuel cell is an electrochemical converter which continuously converts the chemical energy from a fuel and an oxidant into electrical energy, heat and other reaction products. The fuel and the oxidant are stored outside of the cell, and are transferred as the reactants are consumed. Thus, the sizing in terms of power depends only on the fuel cell itself, whereas the sizing in terms of energy, which notably determines the autonomy, depends on the capacity of the external fuel- and oxidant tanks. This characteristic is one of the fundamental differences with an accumulator battery.

The original idea behind fuel cells is traditionally attributed to two chemists: Welshman, William Grove and a Swiss, Christian Schönbein [WIK 8]. The former developed the first cells to produce electricity between 1839 and 1842. These works aroused the interest of many scientists, including Christian Schönbein, who was a specialist in the chemistry of oxygen. The pair exchanged a large amount of correspondence seeking to explain what they then referred to as the inverse phenomenon of water electrolysis, which had been known about since 1800.

The development of fuel cells gained momentum in the mid-20th Century under the leadership of Francis T. Bacon, who created the first powerful prototypes (1 kW in 1953 and 5 kW in 1959). This work enabled modules to be included on board the manned space flights in the Gemini program, followed by the Apollo program.

The rather slow emergence of this technology is due to competition from other, simpler processes to generate electricity. However, the twofold concern about the rarefaction of fossil energy sources, such as oil and natural gas, and the desire to reduce our carbon footprint has revived this technology which, combined with electrolysis, is able to achieve conversions between two energy vectors: hydrogen and electricity.

It is worth pointing out that commercial fuel cells, regardless of the technology used, are not reversible at present. Indeed, if a fuel cell works as an electrolyzer, it causes premature aging of the electrodes. Also, a hydrogen battery is envisaged by combining an electrolyzer with a fuel cell, rather than relying on the reversibility of the fuel-cell system [AGB 12; DAR 10b; MYR].

In addition, a fuel cell is a power converter. Hence, it is designed in terms of power; not of energy. Indeed, the system's energy depends on the dimensions of the reactant storage facilities (in most cases, it is the fuel tank which is the determining factor; as the oxidant used is oxygen from the air, it is not stored). For this reason, the inclusion of fuel cells on a Ragone plot (i.e. on the plane of mass energy vs. mass power) only makes sense if we specify which type of fuel storage is envisaged [CHR 00].

These two characteristics – the irreversibility and the power-oriented design of the fuel cells – clearly set them apart from accumulator batteries, making them a complementary, rather than directly competitive, resource in numerous applications.

The acronym for "fuel cell" (FC) is used in the terminology denoting the different technological approaches. This chapter deals exclusively with hydrogen fuel cells and focuses on two types of cells: Proton Exchange Membrane Fuel Cells (PEMFCs) and Solid Oxide Fuel Cells (SOFCs).

3.2. Classification of fuel cell technologies

Hydrogen fuel cells work by the oxidation of hydrogen and reduction of oxygen; these reactions require the introduction of a catalyst, the nature of which depends on the reactional medium.

There are various different types of fuel cell technologies, for which the acronyms are listed in Table 3.1 [STE 00; STO 10; LAR 00].

Acronym	Type of fuel cell
PEMFC	Proton Exchange Membrane Fuel Cell
AFC	Alkaline Fuel Cell
PAFC	Phosphoric Acid Fuel Cell
MCFC	Molten Carbonate Fuel Cell
SOFC	Solid Oxide Fuel Cell

Table 3.1. *Acronyms for fuel cells*

Various types of classifications can be established, based on the operation of the electrolyte.

3.2.1. *Classification on the basic of the acid/basic medium*

We can differentiate cells on the basis of the acidic or basic nature of the electrolyte. Fuel cells functioning in a basic medium are known as "Alkaline Fuel Cells" (AFCs). Thus, the electrolyte is a solution of potassium hydroxide (KOH). The ions moving in the electrolyte are hydroxide ions OH^-. The reactions that occur respectively at the anode and cathode are:

$$H_2 + 2OH^- \rightarrow 2H_2O + 2e^-$$
$$\frac{1}{2}O_2 + 2e^- + H_2O \rightarrow 2OH^- \qquad [3.1]$$

The advantage of AFCs is that the catalysis of the reactions at the electrodes does not require the use of noble metals at low temperature. For instance, materials such as nickel (Ni) can be used. They may, in some cases, be doped with a noble metal (platinum, palladium, gold) at a low level of charge. These cells function throughout a broad range of temperatures (typically 65–200°C) and present good performances – in particular, low activation overvoltages, owing to the basic medium. They exhibit two drawbacks which limit their applications. First of all, the electrolyte is liquid, so there is a danger of leakage. The major disadvantage to them, however, is their high sensitivity to carbon dioxide (CO_2), which causes the carbonation of the electrolyte. This necessitates the use of very pure gases, both at the anode and the cathode. Yet carbon dioxide is generally present in the hydrogen made by reforming hydrocarbons, and in the oxygen drawn from the air, which is a widely-used source in aerobic applications. Thus, this type of fuel cell tends to be

reserved for anaerobic applications, such as applications in space-flight (e.g. the Apollo missions) or in submarines.

Proton exchange membrane fuel cells (PEMFCs) and phosphoric acid fuel cells (PAFCs) have acid electrolytes, which are conductive of protons.

3.2.2. *Classification on the basis of the operating temperature*

One very commonly used classification is based on the operating temperature. Three classes of fuel cells can be defined, operating at low, medium and high temperatures (Table 3.2). The temperature values listed in this table are merely orders of magnitude, given that the specifications for the same type of fuel cells can vary from one manufacturer to another.

Temperature class	Type of cell	Nominal operating temperatures
Low	PEMFC	[50°C–80°C]
	AFC	[65°C–200°C]
Medium	PAFC	[180°C–250°C]
High	MCFC	[600°C–700°C]
	SOFC	[750°C–1000°C]

Table 3.2. *Classification of fuel cells on the basis of temperature*

This criterion is interesting because it has a significant impact on the structure of the cell, the balance of plant to operate it and its domain of application. The operating temperature conditions the quality of the heat produced which accompanies electricity production. The higher the temperature at which the heat flux is produced, the better it can be exploited so as to enhance the overall yield of the system. Also, the higher the operating temperature, the less sensitive the system is to the presence of carbon monoxide in the reactants, which simplifies the processes of conditioning of the gases. Finally, medium and high temperatures enable us to forego the use of noble metals to catalyze the redox reactions, thereby greatly reducing the cost of the electrodes.

3.2.3. *Classification on the basis of the type of electrolyte*

A more detailed classification can be given – on the basis of the type of electrolyte present in the cell (Table 3.3).

Type of cell	Electrolyte	Type of ions exchanged
PEMFC	Polymer membrane	H^+
AFC	KOH	OH^-
PAFC	H_3PO_4	H^+
MCFC	Carbonate ion salt CO_3^-	CO_3^-
SOFC	Oxide-based ceramic	O^{2-}

Table 3.3. *Classification of fuel cells on the basis of the electrolyte*

AFCs (described above), PAFCs and MCFCs have a liquid electrolyte, whereas PEMFCs and SOFCs have a solid electrolyte, which eliminates the risk of leakage. It is on these latter types that most R&D efforts since the turn of the millennium have been focused. In addition, we shall give a brief description of PAFCs and MCFCs in this section, whereas the rest of this chapter will be devoted to SOFCs and PEMFCs.

3.2.3.1. *PAFCs (Phosphoric Acid Fuel Cells)*

The reactions that occur at the electrodes of a PAFC are:

$$H_2 \rightarrow 2H^+ + 2e^-$$
$$\frac{1}{2}O_2 + 2e^- + 2H^+ \rightarrow H_2O \qquad [3.2]$$

The electrolyte is concentrated liquid phosphoric acid (H_3PO_4), immobilized in a porous silicon carbide matrix. It exhibits good proton conductivity at medium temperature (180°C–250°C). However, it solidifies at around 42°C, so this type of fuel cell cannot begin operating at ambient temperature, so it is necessary to maintain the temperature of the cell, even when it is not operating. Platinum is needed to catalyze the reactions.

In view of their operating temperature, these fuel cells can cope with the presence of carbon monoxide (CO) of up to around 1% in the reactant gases. Thus, the anode can be fed with hydrogen gained from the reforming of a hydrocarbon, typically natural gas, which is mainly methane (CH_4), without the oxidation of the CO becoming overly complex. It should be noted that the natural gas first needs

to be desulfurized, because sulfur poisons the catalysts in fuel cells, regardless of which form of technology is being used.

These characteristics make PAFC technology well adapted for stationary applications – electricity supply to buildings, either autonomously or in addition to the electrical grid. Furthermore, its operating temperature also enables the heat produced to be recovered and used to feed the heating circuit and the hot water circuit of the building.

3.2.3.2. *MCFCs (Molten Carbonate Fuel Cells)*

The reactions that occur at the electrodes of a molten carbonate fuel cell (MCFC) are:

$$2H_2 + 2CO_3^- \rightarrow 2H_2O + 2CO_2 + 4e^-$$
$$O_2 + 2CO_2 + 4e^- \rightarrow 2CO_3^- \qquad [3.3]$$

The electrolyte is a salt of carbonate ions (CO_3^- – usually $Li_2CO_3K_2CO_3$). The carbonate ions produced at the cathode move from the cathode toward the anode, where they react with hydrogen, thus maintaining the composition of the electrolyte constant. Note that the cathode is supplied with a mixture of air (70%) and carbon dioxide (30%). This carbon dioxide is in fact produced at the anode, where it needs to be captured and recycled for use at the cathode. This renders the management of the system more complex, because we need to deal with the movement not only of the fuel and oxidant, but also of the CO_2.

The melting point of the electrolyte and the obtaining of good ion conductivity necessitate operation above 600°C, and mean the system cannot be started up at ambient temperature. On the other hand, this means we can use nickel, which is a non-noble metal, to catalyze the reactions.

At this temperature, the carbon monoxide at the anode no longer poses problems, and takes part in the oxidation reaction. It is therefore possible to directly use the gas created by hydrocarbon reforming – particularly methane – so long as it has been desulfurized.

The fact of being able to feed MCFCs easily with natural gas, and their high operating temperature, naturally orient their use toward stationary applications. Co-generation may consist of exploiting the heat produced either to heat buildings or indeed to drive a thermo-electrical generator.

3.3. Proton Exchange Membrane Fuel Cells (PEMFCs)

3.3.1. *Constitution*

The reactions that occur at the electrodes of a PEMFC are:

$$H_2 \rightarrow 2H^+ + 2\ e^-$$
$$\frac{1}{2}O_2 + 2\ e^- + 2H^+ \rightarrow H_2O \qquad [3.4]$$

A PEMFC is made up of a succession of layers: the electrolyte, the electrodes, bipolar plates and sealings (Figure 3.1).

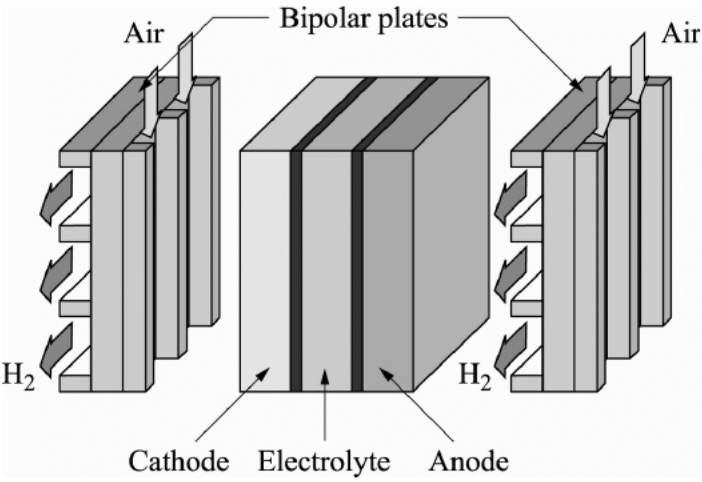

Figure 3.1. *Diagram of the principle of a PEMFC*

The electrolyte comprises a polymer membrane whose thickness ranges from 50 to 200 μm. Like any electrolyte, it needs to have all the following properties: good conductivity of ions (in this case, protons), electron insulation, chemical stability, mechanical solidity, and impermeability to the reactant gases. The reference product is a perfluorosulfonic polymer, the commercial name for which is Nafion®, marketed by DuPont™. The membrane is composed of long polymer chains oriented in parallel to the thickness, where fluorine atoms are substituted for hydrogen atoms (this substance is polytetrafluorethylene – PTFE or Teflon®). On this long chain, there are hanging chains which have an SO_3H group (Figure 3.2). Proton conduction takes place because of these groups, but the membrane needs to be hydrated for this to happen. It can absorb up to 50% of its own mass in water.

The conductivity of the membrane depends on the degree of its hydration. However, this is altered by a great many phenomena in the fuel cell. The need to preserve the water content of the electrolyte membrane limits the operating temperature of the PEMFC to below 80°C. Beyond this temperature, the membrane becomes dehydrated, the ionic resistance increases very rapidly and the performances suffer drastically. The thickness of the membrane results from a compromise between low ionic resistance – which requires as thin a membrane as possible – and sufficient mechanical strength. Indeed, it has to be able to withstand pressure variations on both sides of its surface during the operation of the cell.

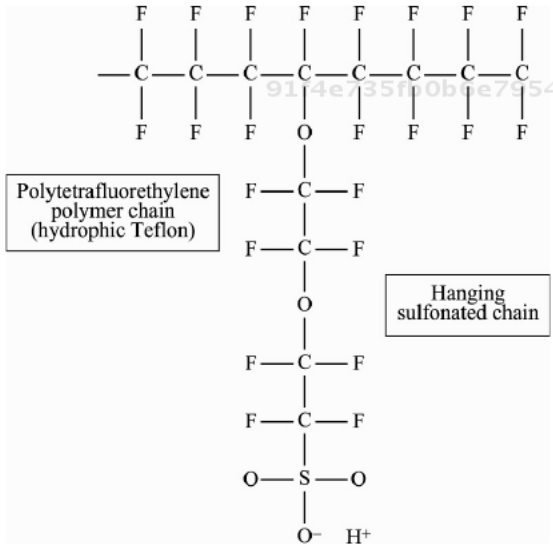

Figure 3.2. *Structure of hydrophobic Nafion®*

The electrodes are the site of the redox reactions. They are also the site of numerous linked phenomena: electrical, chemical, thermal and mass transfer phenomena (see Chapter 1). They are made up of two zones: the active zone and the diffusion zone.

The active zone is at the interface between the electrolyte and the electrode. It comprises a carbon felt, hosting nanometric particles of platinum or a platinum alloy and impregnated with electrolyte. Thus, we get a reaction zone which is conductive of both protons and electrons. The reaction takes place at the surface of the grains of catalyst at the "triple point", so called because the gaseous species, the ionic species and the electrons are all present at this point. The charge in the catalyst is expressed per unit surface of the electrode and varies from one cell to another, between 0.1 and 1 mg/cm^2.

The gas diffusion layer (GDL) is a porous layer which takes care of the transport of the gases to the active zone, the evacuation of water and electron conduction.

The assembly of the electrolyte and electrodes is called the "Membrane Electrodes Assembly" (MEA). We can distinguish two types of procedures. Either the active layer is deposited on top of the GDL, and the electrodes thus constituted are assembled on both sides of the membrane; or the GDLs are deposited on both sides of the membrane, and the diffusion layers are then assembled.

A planar structure is thus obtained. Gas leakages have to be avoided. Because of the low operating temperature, we can use silicone joints on a metal casing.

Figure 3.3. *20-cell stack made by the company UBZM*

Bipolar plates are placed between two cells of a stack. These plates are said to be "bipolar" because they are in contact, on one side, with the anode of one cell, and on the other, with the cathode of the adjacent cell. They not only form the electrical link between the cells, but also supply the gases, provide mechanical strength and ensure separation of the reactants of two neighboring cells. They are involved in the evacuation of water, unconsumed reactants and the heat produced in the cell. They may be made of graphite, into which are machined channels for the flow of the gases. This solution offers excellent performances from the point of view of the lifetime, but is expensive from the standpoint of industrialization. Solutions using embossed metal plates help to lower production costs, but offer less of a guarantee regarding the lifetime (for instance, there is the risk of corrosion). Their thickness varies depending on the technology and the manufacturer, ranging from 1 to 10 mm. The bipolar plates may also contain channels for a water- or air cooling circuit.

The cells are assembled to form the stack and are pressed together with drawstrings to ensure good electrical contact between the different elements and good airtightness, and collar terminal plates are often used to contribute to heat dissipation.

3.3.2. *Characteristics*

3.3.2.1. *Electrical performances*

The static characteristic curve of an electrical generator is a curve expressing the voltage as a function of the current, also known as the polarization curve. It can be plotted for a cell or a stack. In order to be able to compare cells or stacks of different dimensions, this characteristic curve is often adjusted to reflect a cell with unitary electrode surface. The usual unit of cell surface is cm^2. Thus, the current density is defined as:

$$j = \frac{I}{S} \qquad \left[A/m^2 \right] \text{ or } \left[A/cm^2 \right] \qquad [3.5]$$

j is the current density expressed in A/m^2 or A/cm^2, I is the current of the cell or stack, and S is the surface area of the electrode expressed in m^2 or cm^2 (which is indeed appropriate for the orders of magnitude encountered).

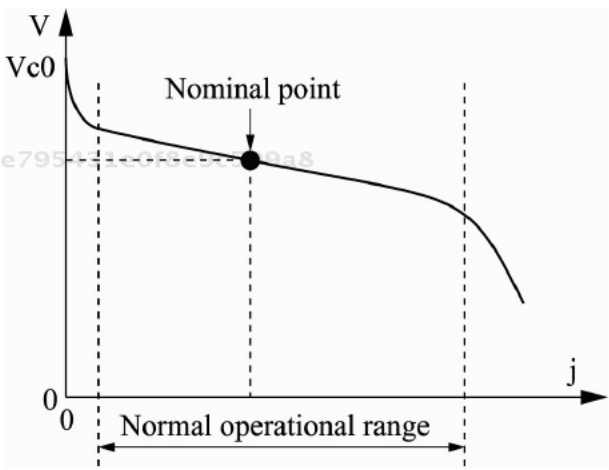

Figure 3.4. *Shape of the polarization curve for a cell or stack of a PEMFC – V is the cell voltage or average voltage of a cell in a stack, as a function of the current density*

In the case of a stack, the voltage is often divided by the number of cells, giving us an average voltage per cell.

$$V_{cell} = \frac{V_{stack}}{N} \quad [V] \qquad [3.6]$$

N is the number of cells in the stack.

The shape of the polarization curve for a stack is similar to that of a cell, described in Chapter 1 for given operating conditions.

The in-depth study of the polarization curve is developed in Chapter 1 for an electrochemical cell. Here we recall a semi-empirical expression of the voltage as a function of the current density, which can be interpreted as the reversible potential less the activation-, concentration- and Ohmic overvoltages:

$$V = E_{rev} - \frac{RT}{\alpha nF}\ln\left(\frac{j_f + j_n}{j_0}\right) + \frac{RT}{\alpha nF}\ln\left(1 - \frac{j_f}{j_{\lim}}\right) - r_{cell} j_f \qquad [3.7]$$

$$E_{rev} = E^0 + \frac{RT}{nF}\ln\frac{\prod_j a_{iproducts}^{vj}}{\prod_i a_{ireagents}^{vi}} \qquad [3.8]$$

where E_{rev} is the reversible potential of the cell; E^0 is the reversible potential of the cell at temperature T, at atmospheric pressure; a_i is the activity of the species i; v_i the stoichiometric coefficients; j_f is the Faradaic current density, equal to the current density in the stabilized regime; T is the temperature of the cell; R is the ideal gas constant; α is the transfer coefficient; n is the number of electrons exchanged ($n = 2$ in the case of a hydrogen battery); j_0 is the exchange current density; j_n is the internal current density; $j_{\lim}$ is the limit current density; and r_{cell} is the surface Ohmic resistance of a cell ($\Omega\, cm^2$ if the current density is expressed in Acm^{-2}). The phases of the reactants and products (and therefore their activities), the limit and exchange current densities, and the resistance of the cell depend on the operating conditions. In addition, the activation term is not defined for a zero current density.

Also, for a simpler approach, we can adopt other models which depend not on the activities of the species at the electrode/electrolyte interface, but rather on measurable values outside the cell. Thus, we can use the following model, in which we "combine" the influence of the partial pressures of the reactants on entering the

cell [BOU 08]. This model is a very macroscopic approach to the phenomena internal to the cell as described in Chapter 1. Its domain of validity around specific operating conditions is reduced, and it cannot be used to describe operating conditions which stray too far from these prerequisites. The parameters A, B, C, D, j_0, j_n, j_{lim} and r_{cell} can be identified on the experimental results, with a limited domain of validity and for a given operating temperature.

$$V = E_0 + A\ln\left(\frac{P_{O2}}{P_0}\right) + B\ln\left(\frac{P_{H2}}{P_0}\right) - C\ln\left(\frac{j_f}{j_0}\right) + D\ln\left(1-\frac{j_f}{j_{\lim}}\right) - r_{cell}\, j_f \quad [3.9]$$

The open circuit voltage of a cell is approximately 1 V. The voltage falls fairly sharply in the low current density zone, because of the activation overvoltages (see Chapter 1). For higher current densities, the voltage also drops more sharply, due to the significant influence of the diffusion term.

We can plot the surface power curve ($\mathrm{Wcm^{-2}}$) as a function of the current density. This curve passes through a maximum point.

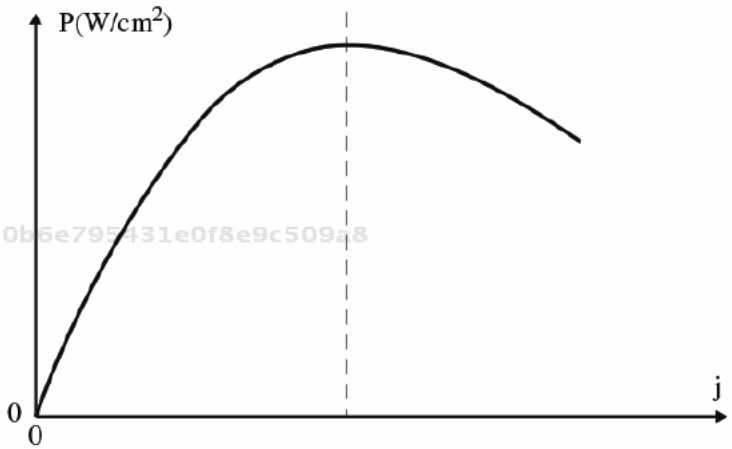

Figure 3.5. *Shape of the curve of power for a PEMFC cell or stack as a function of the current density*

The current produced by a cell or stack of fuel cells depends on the average current density and on the surface area of the cell. In a power generator, the nominal current density varies in the interval 0.5 A/cm^2–0.8 A/cm^2 with maximum current

densities of around 1 A/cm^2. In a laboratory environment, on cells of a few cm^2, it is possible to reach significantly higher and achieve current densities of several A/cm^2.

At the nominal current density, the cell voltage varies between 0.7 and 0.5 V depending on the performances of the cell.

The range of operation of a cell covers a fairly broad spread of current density. However, there are two ranges in which we should avoid working:

– Firstly, low current densities lend the cell a high potential which favors parasitic reactions, notably leading to the corrosion of the carbon in the electrodes. This greatly degrades the electrodes and reduces the lifetime of the cell.

– Secondly, high current densities cause the cell to work in a regime where the diffusion of the reactant gases in the GDLs becomes prohibitive.

In order to increase the power produced by a stack, it seems natural to increase the surface area of the cells so as to increase the current delivered. The cell surface area is indeed a parameter of the sizing of a stack. Yet the larger the cell, the more difficult it is to maintain homogeneous operating conditions across the entire surface. Temperature gradients and differences in the concentration of reactants may arise; certain areas of the cell are then subject to high current density whereas other areas exhibit far lower current densities. The average current density obtained is therefore mediocre, and the cell is poorly exploited. The surface of the cells is far from standardized between the different manufacturers, but the size of the cells tends to level out below 300 cm^2.[1]

The other parameter that can be used to increase the power of a stack is the number of cells. Increasing the number of cells increases the voltage of the stack. If the cells all function in exactly the same way, the voltage of the stack is proportional to the number of cells. However, the longer the stack, the more difficult it is to maintain operating conditions that are identical for all the cells. Thus, the cells at the end opposite the reactant input may be under-supplied, and their voltage may fall dramatically. In addition, as the cells are serially connected, the performances of the whole are limited by the weakest cell in the stack, and if one cell has failed, the entire stack is out of service. Also, the number of cells found in a single stack in power applications is usually less than 200.

In order to increase the power of a fuel-cell system beyond the apparent limits currently attained with a single stack, it is preferable to combine a number of stacks, in a series and/or in parallel. Thereby we obtain a benefit: in terms of modularity,

1 For instance, some characteristics of stacks can be consulted at: http://www.ballard.com/fuel-cell-products/.

because we can standardize a power module, and in terms of reliability because if one stack is lost, we do not lose all of the power, so reduced-mode operation is still possible.

Two important characteristics are the mass power, particularly for onboard applications, and the volumetric power, which is important for all types of application. At present, the mass power of the stack is around 1 kW/kg and the volumetric power between 1 and 1.5 kW/l.[2]

The notion of the efficiency of a stack η_{stack} may be relatively ambiguous – there are various definitions which could be given. We propose the following definition: the efficiency is the ratio between the output electrical power P_{stack} and the energy flux contained in the reactants $P_{chemical}$:

$$P_{stack} = V_{stack} I_{stack} \quad [3.10]$$

$$P_{chemical} = -\dot{n}_{H2} \Delta h_f \quad [3.11]$$

$$\eta_{stack} = \frac{P_{stack}}{P_{chemical}} = \frac{V_{stack} I_{stack}}{-\dot{n}_{H2} \Delta h_f} \quad [3.12]$$

where Δh_f is the enthalpy of formation of a mole of water, which also corresponds to the heat released by complete combustion of a mole of hydrogen; $\dot{n}_{H2}$ is the molar flowrate of hydrogen consumed by the cell to supply the power P_{elec}. The efficiency of a PEMFC stack is approximately 50% for an extensive range around the nominal point.

3.3.2.2. *Dynamic behavior*

In Chapter 1, we calculated the electrochemical impedance of an electrode. It comprises three terms for each electrode: two terms of impedance of diffusion and convection – one for the change in concentration of the reduced form $Z_{red,i}$ and the other for the change in concentration of the oxidized form $Z_{ox,i}$, and a term of transfer resistance, $R_{t,i}$. The terms of diffusion and convection are greatly nonlinear.

The impedance of the whole cell comprises an electrochemical impedance for each electrode, the resistance of the membrane and the connectors R_m, to which we

2 Idem.

need to add the capacities of the double layer $C_{dl,i}$ relating to the distribution of charge at the electrode/electrolyte interface. Thus, we can put forward an equivalent electrical diagram of the impedance of a cell or, in the case of a stack, an average cell (Figure 3.6).

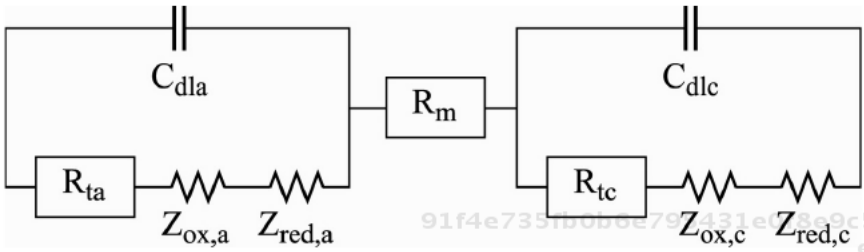

Figure 3.6. *Equivalent electrical diagram of a fuel cell*

This equivalent diagram can be partly simplified by discounting $Z_{ox,a}$ and $Z_{red,c}$, which respectively represent the influence of the variation of the concentration of H^+ at the anode and of H_2O at the cathode. We can go a little further and discount $Z_{red,a}$, the diffusion/convection impedance, relating to the diffusion of hydrogen, which has a high diffusion constant [LAF 08].

Yet even if we use these simplistic hypotheses, the nonlinear nature of the terms relating to diffusion means the calculations become very complex. There again, if we wish to construct a simpler model of the behavior of the electrodes, we can construct it on the basis of a single (R-C) cell (Figure 3.7).

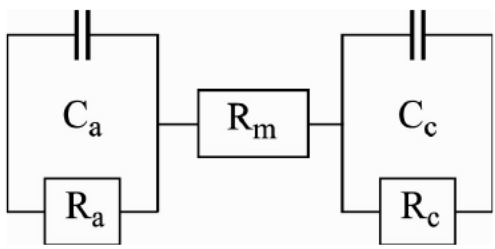

Figure 3.7. *Simplified equivalent electrical diagram for a fuel cell with differentiated electrodes*

It is not easy to distinguish between the contributions of each electrode. Therefore, we can obtain a cell impedance which is even more approximate where the two electrodes are not dissociated (Figure 3.8) [LAR 00].

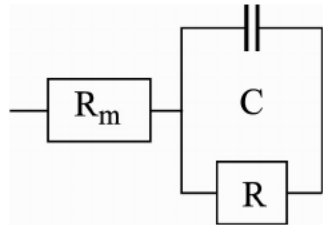

Figure 3.8. *Simplified equivalent electrical diagram for a fuel cell with non-differentiated electrodes [LAR 00]*

3.3.2.3. *Water management*

The management of the water in the cell is a key element to its correct functioning, but is no easy task. Indeed, it is crucial to maintain the degree of hydration of the membrane so as to limit Ohmic drops. Conversely, an excess of water leads to the condensation of the water vapor in the GDLs, the drops of liquid water then block the pores and prevent the gases from reaching the active layers. This is referred to as the "drowning" of the electrode. Drowning tends more to occur at the cathode, where the water is produced. The phenomenon of condensation may also happen in the channels in the bipolar plates.

Both lack of water (leading to the dehydration of the membrane) and excess of water (leading to flooding) cause a drop in the cell voltage, which makes it tricky to detect and diagnose the problem.

Water management is difficult because the movements of water within the cell are numerous and complex. There are two phenomena which govern these movements of the water. The first is diffusion because of concentration gradients – water moves from the most concentrated area to the least concentrated area, tending toward equilibrium of the concentrations. The second is proton migration within the electrolyte, which is accompanied by a flow of water molecules in the wake of the protons: this is electro-osmosis. This second phenomenon creates a movement of water which is always oriented from the anode toward the cathode. *A contrario*, water diffusion can take place in both directions. Water is produced by the reaction at the cathode, but this does not mean that the concentration of water is always greater on this side. Indeed, the water produced is generally not sufficient to maintain the hydration of the membrane. Also, the gases entering the cell are

hydrated, i.e. rich in water vapor, either at the anode, the cathode or on both sides. Finally, the flows of effluents, i.e. gases exiting the cell, also evacuate water. Thus, diffusion can create a movement of water in either direction (Figure 3.9).

The ensemble of these phenomena is very tricky to understand and model, and it is not easy to predict the state of hydration.

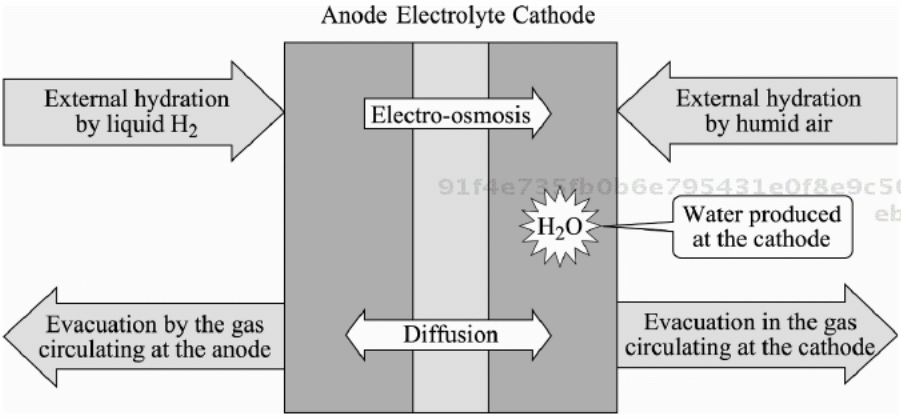

Figure 3.9. *Movements of water within a cell*

3.3.2.4. *Sensitivity to contaminants*

Pure hydrogen is the best fuel for PEMFCs from the point of view of the electrochemical performances. However, they can be fed with gases reformed from hydrocarbons, which are rich in hydrogen. This gas has to be completely desulfurized to prevent irreversible poisoning of the electrodes by sulfur.

Carbon monoxide (CO) is present on output from the reformer and needs to be oxidized into carbon dioxide (CO_2). Indeed, CO poisons the catalyst of the PEMFC by adsorbing to its surface, thereby preventing reaction with the hydrogen. The effect is noticeable with levels of only a few tens of ppm (parts per million); it is cumulative, meaning that the performances fall ever further as an increasing proportion of the surface of the catalyst becomes covered. This effect is reversible, and the CO can be desorbed by sweeping the anode with a high flowrate of air. Of course, this means interrupting the power supply during the regeneration of the catalyst. Sensitivity to carbon monoxide can be slightly reduced by an appropriate formulation of the catalyst – particularly by using an alloy of platinum and ruthenium (Ru). Sensitivity to CO also decreases with an increase in temperature, but this solution is limited because of the danger of dehydration.

3.4. Solid Oxide Fuel Cells (SOFCs)

As the name suggests, the electrolyte of a solid-oxide fuel cell is solid: it is a ceramic which is conductive of the oxide anion O^{2-} at high temperature (typically beyond 700°C for standard materials). When the cell is supplied with hydrogen at the anode, the reactions taking place at the electrodes are as follows:

$$\begin{aligned} H_2 + O^{2-} &\rightarrow H_2O + 2e^- \\ \frac{1}{2}O_2 + 2e^- &\rightarrow O^{2-} \end{aligned} \qquad [3.13]$$

Water is produced at the anode, in gaseous form in view of the operating temperature.

The high operating temperature of SOFCs facilitates the oxidation of carbon monoxide, present in the gases from reforming of hydrocarbons, which thus participates in electricity production as a fuel:

$$\begin{aligned} CO + O^{2-} &\rightarrow CO_2 + 2e^- \\ \frac{1}{2}O_2 + 2e^- &\rightarrow O^{2-} \end{aligned} \qquad [3.14]$$

The high operating temperature also means we can avoid using a noble catalyst. However, it does limit the number of materials that can be used for the electrodes and the electrolyte. Indeed, these materials not only need to have sufficient properties of ion and electron conduction, but also need to be able to withstand the high temperatures, and the mechanical stresses linked to expansion with a rise in temperature. In addition, the cellular structure implies that the coefficients of thermal expansion of the three layers must be similar so as not to give rise to excessive mechanical stresses when the temperature changes.

The standard materials used to construct the cell (see Figure 3.9) are described below:

– for the electrolyte: a zirconia (ZrO_2, zirconium dioxide) stabilized with yttrium (Y_2O_3), or yttria-stabilized zirconia (YSZ). The material for the electrolyte needs to be dense so as to be impermeable to the gases. The thickness of the electrolyte is 25–50 μm;

– for the anode: a cermet (material comprising a ceramic, "cer-", and a metal binder "-met") formed by nickel (Ni) onto a zirconia skeleton. The electrode is porous so as to allow the mass transport of the fuel and product gases;

– for the cathode: a strontium-doped lanthanum manganite. As with the anode, the cathode needs to be porous to facilitate the transport of the gases.

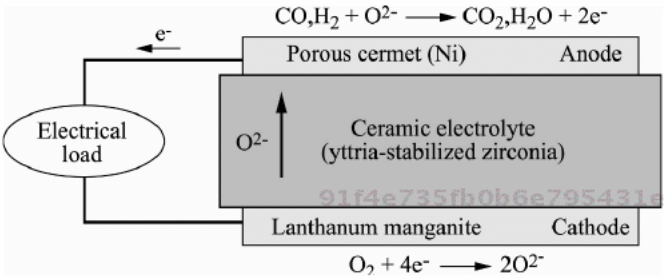

Figure 3.10. *Diagram of the principle of operation of an SOFC with standard materials for the electrolyte and the electrodes*

The bipolar plates or interconnections form the serial connections between SOFCs. The material used needs to have good electron conductivity, good chemical stability and offer airtightness: they can be ceramics, metals or cermets.

One of the problems for the realization of an SOFC, and *a fortiori* of a stack, is that of sealing. Indeed, the expansion is very significant when the stack goes from ambient temperature to the operating temperature. Thus, two technologies exist: the tubular structure and the planar structure. The tubular structure is illustrated in Figure 3.11. The cell shown is a cathode-supported SOFC – the cathode forms the innermost layer, which forms a cylinder with air circulating inside it, on top of which the electrolyte and then the anode are deposited. The whole ensemble is placed in an enclosed tube, which is then injected with hydrogen. The tubes are serialized to form the stack. This technology limits the problem of sealing, which arises only at the interconnection between two cells, connecting the outer anode of one cell to the inner cathode of the neighboring cell. However, this procedure entails a high manufacturing cost, and has poor compactness.

The planar structure consists of piling up flat layers, in the same way as the case of a PEMFC. The gases are then injected through bipolar plates made of a connecting material, into which channels have been scored. This solution necessitates the use of seals around the cell to keep the gases inside the cell. The quality of these joints has a powerful bearing on the lifetime of the cell and of the stacks. However, the manufacturing cost is less high, and the electrical performances are better than with the tubular structure.

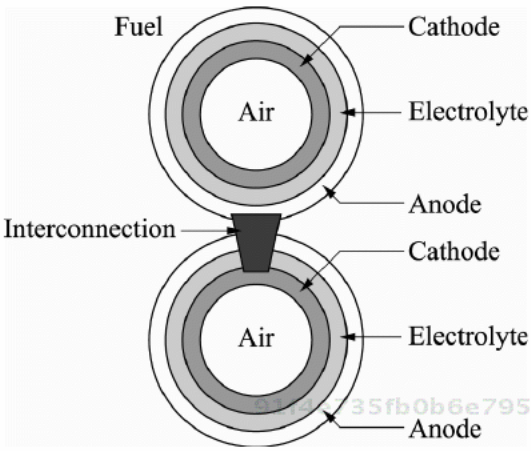

Figure 3.11. *Diagram of the principle of a tubular structure SOFC*

Like all cells functioning at high temperature, SOFCs can be envisaged with co-generation because they produce heat at high temperature. They do not need noble catalysts, but the powders necessary for the elaboration of the cells are expensive. The kinetics of the electrochemical reactions is very fast because of the high temperature; the activation overvoltages are very low (see Chapter 1) and the Faradaic efficiency is high. They are particularly sensitive to heat cycling, i.e. to the successive switches between ambient temperature and the operating temperature. Ideally, the cell should be kept at a constant temperature, whether or not it is providing power. The sealing, linked to the tenacity of the joints, is also a highly important issue from the point of view of the lifetime.

Research is actively being carried out on electrolyte materials with a view to finding a good ion conductor at a temperature lowered to around 600°C, in order to reduce the thermal and mechanical stress on the cells, reduce the costs and increase the lifetime, thus creating ITSOFCs (Intermediate Temperature Solid Oxide Fuel Cells).

The macroscopic modeling described for the PEMFCs can also be applied to the case of an SOFC fed with hydrogen if we have tests which enable us to identify the different parameters. The activation overvoltage term is far smaller in the case of an SOFC. In fact, the open circuit voltage of a cell is nearest to the reversible potential of the cell. Because of the high temperature, all the species are in gaseous form, and their activity is equal to their partial pressure. The Ohmic resistance of the MEA (the electrodes and the membrane) is highly dependent on the temperature.

The polarization curve for an SOFC fed with pure hydrogen can thus be expressed in the following semi-empirical form:

$$V = E_{rev} - A\ln\left(\frac{j_f + j_n}{j_0}\right) + B\ln\left(1 - \frac{j_f}{j_{\lim}}\right) - r_{cell}\, j_f \qquad [3.15]$$

$$E_{rev} = -\frac{\Delta g_f^0(T)}{2F} + \frac{RT}{2F}\ln\left(\frac{P_{H2}P_{O2}^{\frac{1}{2}}}{P_{H2O}}\right) \qquad [3.16]$$

$$r_{cell} = Ce^{(-DT)} \qquad [3.17]$$

with A, B, C, D, j_0, j_n and j_{lim} being parameters which need to be identified experimentally.

An electrochemical impedance model similar to that of the PEMFC can be adopted for SOFCs.

3.5. Fuel-cell systems

3.5.1. *General points*

A fuel cell stack has to be surrounded with actuators and devices which are necessary for its operation. The ensemble is called a fuel-cell system. It is not easy to generically define a fuel-cell system and its limitations. Indeed, on the one hand, the elements contained in the system depend on the fuel-cell technology being used, the application in question and the technical specifications pursued. On the other hand, a fuel-cell system is a multi-physical system because it involves chemical, electrical, fluidic and thermal phenomena whose effects are closely interrelated. Thus, the interactions between the different elements of the system and the environment are significant. Figure 3.12 offers a generic description of the elements of the system and sets the general outlines of the system [CAN 07; PER 07; HIS 09]. Besides the stack, which is the heart of the system, we can identify various different circuits:

– the fuel supply circuit includes the storage and conditioning of the fuel until it enters the stack;

– the oxidant supply circuit. The most common oxidant used is oxygen from the air; in this case there is no storage. There are anaerobic applications with which there is oxygen storage;

– the exhaust treatment circuit. Depending on the type of fuel, and the choice of architectures for the anodic and cathodic circuits, the gases ejected from the cell can be partially valorized: the water can be recovered, the residual fuel burnt or recycled, and the gases fed into a turbine or used in a thermal machine;

– the thermal management of the stack to maintain the nominal temperature, and possibly valorization of the heat produced;

– the conditioning of the stack electrical power to feed the load and the auxiliaries of the system;

– the energy storage components, present to support the cell or to recover the energy, given that a fuel cell, no matter what the form of technology being used, is not reversible;

– the control and supervision module to manage the auxiliaries of the system and the exchanges of thermal and electrical energy between the cell, the storage devices and the charge.

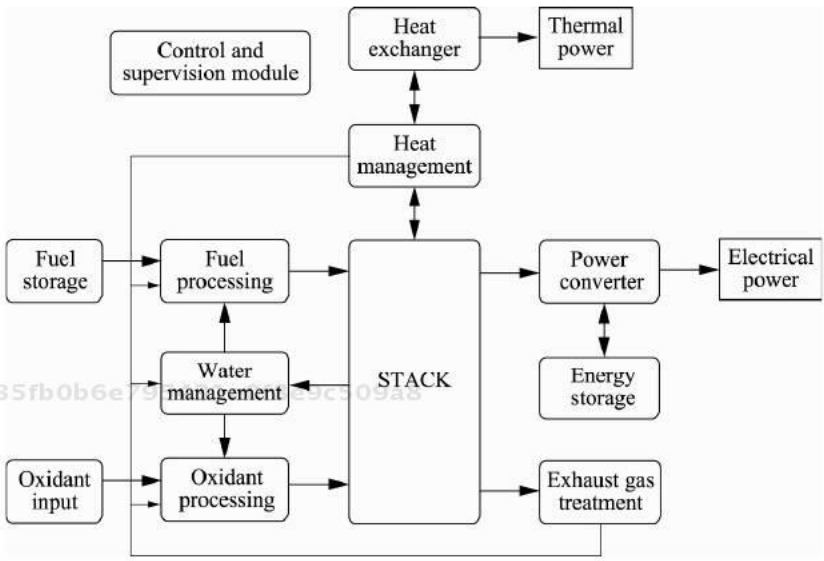

Figure 3.12. *Fuel cell system*

Fuel cell technologies have experienced major advances since the 1990s in terms of their electrical performances, their specific powers, the reliability of the components and the lifetime of the stacks. However, demonstrator programs have clearly established that it is the performances on the scale of the whole system which need to be evaluated. Indeed, the stack supplies its own auxiliaries. Thus, we define the gross power output from the stack, the net power output of the system and the

net efficiency of the system, with P_{aux} denoting the power dissipated in the auxiliaries:

$$P_{gross} = P_{stack} = V_{stack} I_{stack} \quad [3.18]$$

$$P_{net} = P_{stack} - P_{aux} \quad [3.19]$$

$$\eta_{net} = \frac{P_{stack} - P_{aux}}{P_{chemical}} = \frac{V_{stack} I_{stack} - P_{aux}}{-\dot{n}_{H_2} \Delta h_f} \quad [3.20]$$

3.5.2. *PEMFC systems*

Even if we restrict the definition of a system to a specific technology, numerous variants of architectures can be envisaged, as well as numerous control solutions. However, it is possible to give a few points which are more specific to PEMFCs [CAN 07; PER 08].

PEMFCs, in most applications, work at "atmospheric" pressure. This means that the fuel and oxidant are injected at a pressure that is slightly higher than atmospheric pressure, so as to compensate for the pressure drop of the cell, which is no more than a few bars (typically 0.5–2 bar). The polymer membrane can withstand a moderate difference in pressure between the anode and the cathode – typically less than 1 bar. Beyond this, there is a danger of mechanical fatigue, leading to the breakdown of the membrane. Also, it is useful to balance the pressure of the fuel and the oxidant at input to the cell, whilst it is operational.

3.5.2.1. *The fuel circuit*

PEMFCs are sensitive to contaminants – particularly carbon monoxide and sulfur. The most commonly used fuel is pure hydrogen, which is stored in liquid form, at high pressure or low pressure. In view of the low operating pressure of PEMFCs, the hydrogen is expanded to the working pressure. The expansion of the hydrogen causes the gas to cool. However, if the gas is injected into the cell at too low a temperature, this can cause the condensation of the water vapor, which is likely to create a water blockage. As the calorific capacity of hydrogen is very slight, the heat exchange that takes place during the journey through the conduits between the tank and the cell input may be sufficient to raise the gas to an acceptable temperature. If not, a heat exchanger is necessary.

We can distinguish three types of architecture for the fuel circuit (Figure 3.13): open mode, closed mode and recycle mode. In open mode, the exhaust from the anodic compartment is at atmospheric pressure. The flowrate of hydrogen supplied to the cell therefore needs to be greater than that which is strictly necessary to

provide the required current, in accordance with Faraday's law. Indeed, this enables us to properly drain the gas diffusion layers and the channels in the bipolar plates from the anodic compartment. Therefore, we define the anodic factor of overstoichiometry, F_{SA}, which is the ratio between the amount of hydrogen flowing into the cell to the amount of hydrogen consumed. We can then envisage a pressure control where we regulate the pressure, or a flowrate control where we regulate the flowrate of hydrogen input.

$$\dot{n}_{H2} = F_{SA} \frac{NI_{stack}}{2F} \qquad [3.21]$$

This mode of operation is the most favorable for the performances of the stack. However, too high a F_{SA} decreases the net efficiency of the system, because some of the fuel is ejected back into the atmosphere.

In dead-end mode, the output from the anodic compartment is blocked. The hydrogen input pressure is regulated, and the input flowrate depends on the current required, with the cell consuming exactly the amount of hydrogen needed to supply that current ($F_{SA}=1$). In this mode of operation, the water and nitrogen which permeate through the electrolyte membrane accumulate at the bottom of the anodic compartment; this is the phenomenon of stratification. The amount of hydrogen entering the cell is decreased, causing a regular decrease in the voltage of the stack. Therefore, regular purging of the anodic compartment is necessary. This is done by opening the output valve from the anode, which causes a pressure drop and an increase in the amount of incoming hydrogen sweeping the anode. The purge restores the voltage of the stack. The disadvantage to this mode of operation is that the stack never functions in optimum conditions.

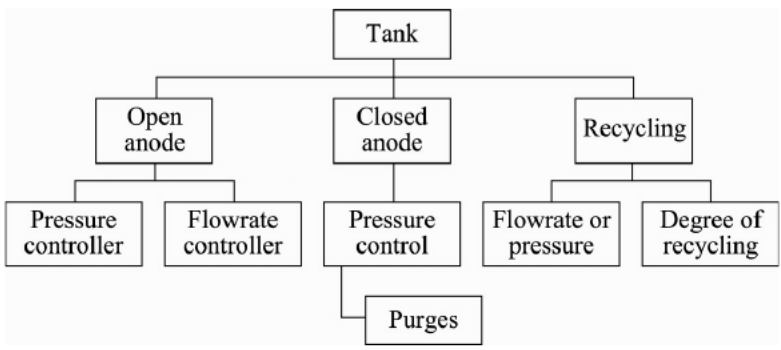

Figure 3.13. *Mode of operation of the fuel circuit in a PEMFC*

In recycle mode, the hydrogen flowrate is regulated with a F_{SA} greater than 1, but instead of releasing the surplus hydrogen back into the atmosphere, some of it is fed back to the input of the cell, with a given recycle rate. This operation enables us to stir the anode, which prevents stratification. We can envisage regulating the pressure or the flowrate.

3.5.2.2. *The oxidant circuit*

In the case of an anaerobic application where the oxidant is pure oxygen, we can envisage the same solutions as for the fuel circuit. When the oxidant is oxygen from the air, dead-end mode is not envisageable, because a large proportion of air is nitrogen (≈79% N_2, ≈21% O_2). As the nitrogen does not react, large quantities of it would accumulate, too quickly. Recycle mode presents little interest, because a large proportion of the recycled gases would be nitrogen. Thus, the only mode possible is open mode. The cathodic factor of overstoichiometry F_{SC} is often greater than that at the anode so as to improve the diffusion of the oxygen by increasing the drainage of the cathode, thereby preventing stratification.

To supply the cathode, the air is compressed. The air fed into the cell must be free of grease. The compression head therefore must be an oil-free technology or the air must be perfectly degreased. Increasing the operating pressure improves the gross efficiency of the cell, because it helps reduce the activation overvoltages. However, this involves increasing the consumption of the compressor, which decreases the net yield of the system. Hence, a compromise needs to be found, depending on the technical specifications of the application. The compression of the air heats the gas entering the cell. If the gas is too hot as it enters the cell, this can create a temperature gradient, or dehydration at the gas input. It is therefore helpful to include a heat exchanger in the circuit to regulate the air temperature.

The system can be controlled by regulating the flowrate, which is fairly simple to do using a compressor, because it involves controlling the speed of rotation of the compressor's drive motor. The system may also be controlled by regulating the input pressure. The most effective means of control is to regulate both the flowrate and the pressure, adjusting the flowrate by the speed of rotation of the compressor and the pressure by adding a counter-pressure valve at the output of the air circuit and adjusting the valve's aperture. The smaller the aperture, the higher the pressure in the compartment. This system for precisely regulating the oxidant circuit is, of course, the most costly.

For low-power systems, there are so-called "breathable" stacks. The cathodes are placed in contact with the surrounding air through channels running from the bipolar plates (Figure 3.18). The stack takes the oxygen it needs to function from the atmosphere. This completely passive system avoids having to use an auxiliary

component which would consume energy, but it does not enable us to precisely manage the water in the cell [ZEI 11].

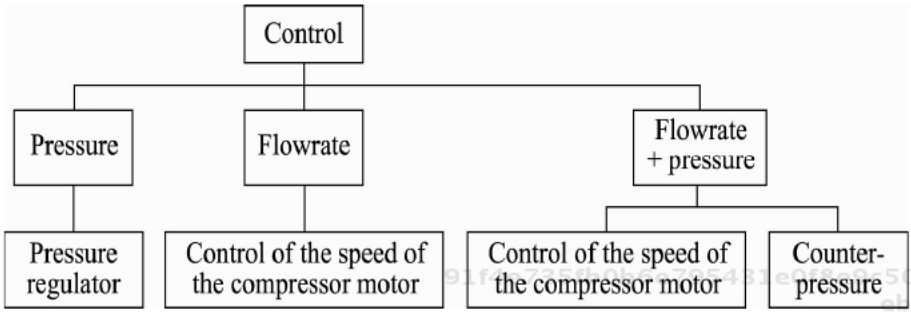

Figure 3.14. *Mode of control of the oxidant circuit in a PEMFC*

3.5.2.3. *The humidification circuit*

The fuel cell stack produces water at the cathode. The simplest system is to let diffusion balance the gradient of water concentration. However, this solution may lead to cases of severe dehydration when the flowrate at the cathode is high enough and drains out too much water as it passes the cathode.

To prevent this phenomenon, we can include a water-permeable membrane exchanger at the cathode output. The principle is this: on one side of the membrane is the flow of dry air entering the cell. On the other side, we route the output from the cell, which is low in oxygen but high in water. Thus, the dry air collects water before entering into the cell. By using an enthalpy wheel, we can improve the exchange of water between these two flows. This system is not able to very finely regulate the amount of water supplied to the cell.

In order to control the amount of water entering the cell, we can inject water into the flow of gases into the cell. This injection may be done at the cathode (which is most common), the anode or possibly on both sides. Many solutions are possible:

– a steam generator can be used to mix a flow of water vapor with the flow of reactant gas;

– a boiler, through which the reactant gas is passed to accumulate water; or

– a washer which injects liquid water in the form of fine droplets, which are then vaporized by heating the mixture.

In all cases, it is important to insulate the circuit in order to avoid condensation after the regulation of the humidification. Indeed, the liquid water drops need to be evacuated so as not to create a water blockage. The amount of water fed back into the cell is then no longer controlled.

In order to characterize the water vapor content of a gas, we can use various concepts. To begin with, it is helpful to recap the notion of saturating vapor. The partial pressure of water in a humid gas cannot be greater than the saturating vapor pressure P_{sat}. Indeed, above this pressure, the water condenses. The value of the saturating vapor pressure increases with temperature. Thus, the amount of water vapor that a mixture can contain is greater when the temperature is higher. We can therefore define the relative humidity RH:

$$RH(\%) = \frac{P_{H_2O}}{P_{sat}} \times 100 \quad [3.22]$$

We can also define the dew point of a gas: this is the temperature at which the mixture is saturated with water, i.e. the partial pressure of the water is equal to the saturating vapor pressure.

3.5.2.4. *The heat management circuit*

As it operates, a fuel cell generates a flow of heat which is likely to raise the temperature of the stack. The thermal management of the system may present different levels of complexity depending on the power and objectives sought.

The stack is cooled by channels with cooling fluid circulating in the bipolar plates. The heat transfer fluid may be:

– air: a booster pump provides a flow of air to cool the cells. In this case, the objective is simply to keep the temperature of the stack below the nominal operating temperature. Air cooling is simple, but it means a poorer volumic specific power because of the bulk of the cooling channels needed. Air cooling is generally not used for stacks of over 1 kW [CHR 08];

– deionized water: the water circuit runs through the whole of the stack. It is therefore useful to monitor the conductivity of the coolant water so as to avoid short-circuits between the cells. A pump can be used to regulate the flow of water;

– glycolated water: if the stack needs to start up at a negative temperature [BEG 08].

The nominal temperature of a stack is ranges between approximately 55 and 80°C, depending on the suppliers. A high temperature reduces the activation

overvoltages but can increase the Ohmic losses if the membrane becomes dehydrated and its ion resistivity increases. One of the strong points of this technology is that although the electrical performances are diminished if operating below the nominal temperature, it is always possible to start up at reduced power with positive or slightly negative ambient temperatures (> –5°C). However, a small accumulator battery is needed at startup of the system to supply the control chips and the compressor. Once a sufficient level of power is attained, the system becomes autonomous. With lower temperatures, freezing in the heart of the cell can cause a problem, with the different layers delaminating – particularly at the interface between the electrodes and the electrolyte. However, it is still possible to start the system up without damaging the cells, provided certain precautions are taken when stopping and restarting the stack. Once startup has been achieved, the losses caused by the cell's operation cause its temperature to rise. The temperature of the stack and the increase in temperature then depend on the electrical point of operation imposed by the load, because the cell heats up under the influence of its own losses [BEG 08].

If we wish to avoid loss of performance because of temperature during the startup phase, then we need to have a heat source, heat the temperature-exchange fluid and regulate the cell's temperature independently of its point of operation.

3.5.2.5. *Power balance in a PEMFC system*

The consumption by the auxiliaries in the system damages the net output yield of the stack. As Figure 3.15 demonstrates, the air circuit is the largest parasitic consumer, taking up around 25% of the stack's gross power, followed by the humidification circuit, with 5%.

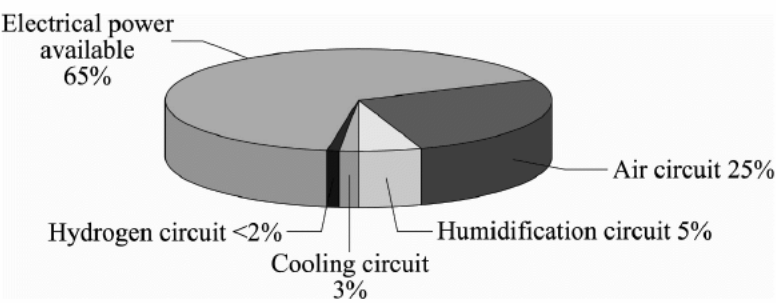

Figure 3.15. *Distribution of the gross power of a stack for a medium-power application (around 20 kW)*

3.5.3. *SOFC systems*

SOFCs cannot function at temperatures lower than around 700°C, beyond which the standard materials used as electrolytes become conductive of O^{2-} ions. Also, the stack needs to be placed in an adiabatic enclosure which is raised to the stack's nominal temperature before it can produce electrical power. Thus, the system cannot be started up at ambient temperature. The nominal operating temperature is between 750 and 850°C approximately, depending on the manufacturers of the stacks.

SOFC stacks respond badly to rapid and significant changes in the operating conditions. Also, any modification of the reference points, the fuel flowrate, oxidant flowrate, current or temperature of the chamber needs to be made in stages, followed by a period of thermal stabilization so as to preserve the lifetime of the stack.

3.5.3.1. *The fuel circuit*

SOFC systems can be supplied with hydrogen or with a gas from the reforming of a hydrocarbon with a high carbon monoxide content, because the high operating temperature means the CO can be oxidized into CO_2 in the anodic compartment. Supply with a reformed hydrocarbon is the most usual at present, because hydrogen distribution infrastructures are not yet in place in most cases.

The anode is made of a nickel-based cermet, which needs to be reduced the first time the temperature of the stack is raised. This is done by washing the anode with a reducing gas (e.g. a mixture of nitrogen and hydrogen) the first time the stack's temperature is raised.

Throughout the lifetime of the stack, it is crucially important to prevent the re-oxidation of the cermet, because the transition from metallic form to the nickel oxide form causes mechanical stresses that are likely to destroy the cells. Such re-oxidation is possible from 400°C onwards if the oxygen gets back into the cell. Thus, the stack needs to be constantly washed with a reducing gas throughout its operation, until it returns to ambient temperature with complete thermal cycling. Thus, SOFC systems are particularly vulnerable to a breakdown on the fuel circuit or a sudden increase in current, which would risk placing the anode in a sub-stoichiometric condition. In case of lack of fuel, irreversible damage or complete destruction of the stack may occur in the space of a few seconds [WAN 11].

The only possible mode of operation for the anode, therefore, is an open anode with a high factor of overstoichiometry. At the anode's output, the effluent is therefore a mixture which is still very rich in fuel. This gas is then recycled into the system, and different forms can be envisaged:

– it is burnt and the heat released is used to heat part of the system – particularly to heat the air entering the cathode or the reformer if there is one;

– it is burnt and the heat is recovered by an exchanger and used in a co-generation application. As this is high temperature energy, the recovery of the heat is facilitated; or

– it is sent to a thermal machine connected to the SOFC system (e.g. a microturbine, a Stirling engine, etc.) [GAY 12].

3.5.3.2. *The oxidant circuit and heat management*

The air circuit is fed by a compressor. The air is heated by being passed through an exchanger. As with the anode, excess air is fed to the cell. This not only serves to supply the cathode but also to regulate the temperature of the chamber, with air acting as the heat exchange fluid. The reference flowrate is set in relation to this second criterion, except for low-power applications where the losses from the cell are insufficient to maintain the temperature of the chamber. In this case, the chamber is an oven, supported by an external heat source such as glow rods.

When the system is supplied by a reformer, the "cell + reformer" ensemble needs to be heated in order to be able to start up. The fuel is then burnt directly to give the necessary heat until the temperature is reached which enables reforming to start, fuel to be supplied and air to be heated so as to raise the temperature of the stack. Given that the complete thermal cycle (from 800°C to ambient temperature) causes accelerated aging of the stack, it is preferable to keep it at a constant temperature, in a reducing gas for the anode and a stream of air for the cathode, even when in is not running. Maintaining this temperature requires that a little fuel be burnt in the reformer's burner, but if the chamber is properly insulated, this consumption may be very slight. However, this constraint restricts the use of SOFC systems to applications which do not require frequent stoppages.

3.6. Applications for fuel cells

The potential applications for fuel cells are very broad. They cover a range of power from a µW (e.g. for hearing aids) to a MW, for grid-connected electricity production.

These applications may be described in three categories: mobile applications, stationary applications and transport applications (Figure 3.16). Certain applications do, of course, overlap the boundaries between these categories.

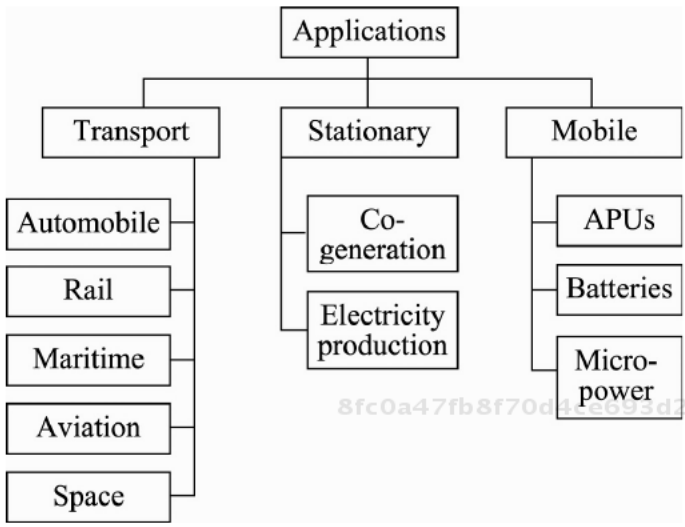

Figure 3.16. *Applications for fuel cells*

As yet, none of these applications has experienced mass commercial success, although some of them occupy niche markets, such as APUs (Auxiliary Power Units), which are able to replace diesel electrogen groups, for instance.

3.6.1. *Mobile applications*

The domain of portable applications covers the range from a kW to a μW. At powers of around a kW, we find all the applications of diesel electrogen groups – that is, *autonomous power units*. PEMFC systems are able to replace them, with a competitive advantage related to the absence of noise (on condition that the acoustics of the air compressor is controlled), the absence of pollutant emissions, the absence of hydrocarbon odors; and easier maintenance. Thus, for example, they could be used to power emergency medical units; temporary sites for attractions and events without having to draw power from the grid through cables; an open-air movie set with direct sound pick-up with no interference; electricity supply to a campsite. One might, for instance, cite Mobixane™, commercialized by the company Axane, which is a subsidiary of the *Air Liquide* group [AXA 13].

In a lower power range, *power supply to nomadic devices* (laptops, smartphones, cellphones, etc.) currently served by Li-ion accumulator batteries, is a very competitive mass market. The advantage of PEMFCs is how quickly they can be

replenished, because all we need to do is replace the empty fuel can with a full one. However, the constraint of the specific power is very potent, as are the constraints of reliability and cost. The technology described in this chapter is unable to satisfy these constraints. Also, the manufacture of these cells exploits technologies in microelectronics to create these microcells. In the same domain without the same issues of integration, and where more conventional techniques can be used, we find the application of *battery chargers*. The fuel-cell system does not directly supply power to the device, but is able to recharge its battery when the power grid is unavailable or non-existent (Figure 3.17). Figure 3.18 shows the flat, breathable cells developed for this application.

Figure 3.17. *Universal USB fuel-cell charger from PaxiTech, fed with a "Hycan" hydrogen can*

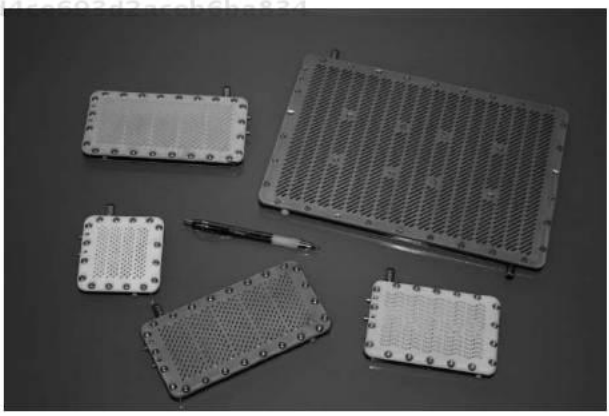

Figure 3.18. *Universal USB fuel-cell charger from PaxiTech, fed with a Hycan*

Certain *biomedical applications* such as hearing aids, heart valves, etc. use micropower, and in this case autonomy is a crucial point of argument. Could this domain represent a long-term field of application for fuel cells?

3.6.2. *Stationary applications*

The range of power in stationary applications extends from a few kW to a MW.

The supply of technical pylons, such as mobile network antennas, parabolas, etc. in isolated locations (not connected to the grid) and/or difficult to access, poses a problem of autonomy and maintainability. Fuel cells, either PEMFCs or SOFCs, could provide more satisfactory solutions than accumulator batteries. In this context, the project PEPITE, financed by the ANR, examined a prototype combining photovoltaic panels, an electrolyzer, hydrogen and oxygen tanks and a fuel cell [DAR 10a; DAR 10b; MYR].

Up to a few dozen kW, or a few hundred kW, *the supply of dwellings or installations isolated from the electrical grid* represents a significant potential application. Diesel electrogen groups cover some of these needs, with the drawbacks mentioned for portable applications (noise, pollution, hydrocarbon odors, and maintenance). *Power supply to small islands* which have no capacity for electricity production *in situ* requires the installation and maintenance of very costly undersea cables, so the use of gas pipelines (hydrogen or natural gas) combined with fuel cells is an interesting alternative. This activity is particularly well developed in Japan, where 30% of the territory is made up of archipelagos.

In order to progressively introduce renewable energies into electrical grids structured around high-power production plants, we need to review the way in which these grids are managed, to ensure their stability and reliability. Indeed, as it is difficult to store electricity, we need to be able, at all times, to balance production and consumption. However, renewable energies (primarily solar and wind power) are intermittent and are difficult to predict. It then becomes crucial to find energy storage solutions capable of dealing with consumption peaks and absorbing production peaks. The hydrogen energy vector could come to play an important part in the evolution of the grids, by way of the two converters – fuel cells and electrolyzers – coupled with hydrogen tanks and possibly oxygen tanks, which we can qualify as H_2/air batteries. The high- and low-temperature channels can be combined and play this role. The deployment of H_2/air batteries on the electrical grid would help balance these new grids, with centralized production to provide the bulk of the power, and *decentralized production* to balance out the fluctuations.

The applications listed hitherto focus on electricity production. Yet fuel cells also produce another type of energy: heat. Work is under way to develop *boilers* using high- and low-temperature cells. Heat production is the intended product; the electricity production associated with it is therefore a by-product, consumed on site or fed into the grid. The activity is guided by the requirement for heat, because this need experiences more significant seasonal variations than electricity, and it is easier to deport the electrical energy produced onto the mainstream grid than it is to recover the excess heat. The simultaneous valorization of the two forms of energy (heat + electricity) could offer very high overall yields – greater than 80%, particularly for the high-temperature technology.

Co-generation applications can also be envisaged from the point of view of electricity production alone if we combine high-temperature batteries with thermal machines, such as microturbines, Stirling engines, etc. The heat is then valorized and turned into electricity [GAY 12].

3.6.3. *Applications in transport*

All types of transport – land, sea, air, etc. – may constitute applications for fuel cells, of two types: energy production for motor function, or electricity production to feed the grid onboard the vehicle, whose power requirement is growing in all means of transport.

3.6.3.1. *Air travel applications*

Aerospace applications, which are anaerobic, were mentioned previously in the introduction.

The propulsion of aircraft by fuel cells can be envisaged for *lightweight unmanned surveillance drones*. The advantage in comparison to thermal motorization is the acoustic and thermal discretion, as the low temperature of PEMFCs renders heat tracking more difficult.

Regarding freight or passenger aircraft, the use of fuel cells is to be envisaged more to *supply the onboard power grid*. This grid needs to be available not only in flight but also during phases of maintenance on the ground. As it currently stands, electricity is produced by a turbine using kerosene. This generator has a very high efficiency and specific power. The two major drawbacks are the emission of pollutants into the atmosphere and the noise pollution, which becomes very problematic for companies, essentially when the airplane is on the ground. Replacing this turbine with a fuel-cell system would contribute to a significant reduction in both these forms of nuisance. In addition, the production of water by the system during the flight would reduce the amount of water that needs to be taken on

before takeoff, providing the water necessary for the crew and the passengers (humidification of the cabin air, the toilet facilities, etc.). This is a not-insignificant collateral advantage, given that every kilogram gained is crucial either in terms of fuel economy or of passenger seating.

The third possible application in air travel could be to replace the *RAT* (Ram Air Turbine) currently used. When all sources of energy on board are out of service, the plane can glide, which may help it to reach an appropriate area for an emergency landing. A wind turbine, the RAT, is then deployed underneath the plane, driven by the wind generated by the aircraft's own velocity. It supplies an electrical generator for the crucial auxiliary equipment. A fuel-cell based solution, supplied directly with hydrogen and oxygen for immediate availability has been studied as a replacement for the wind-driven system in order to see if it could increase its reliability, but has not as yet been shown to be satisfactory, because it is a long way from fulfilling the constraints in terms of specific power.

The implementation of a fuel cell in an airplane is a significant challenge:

– The installed power on a large carrier may be very significant – around 800 kW for an A380, and more than 1 MW for the B787 Dreamliner. This trend should only be reaffirmed with the development of airplanes using more electrical power [KOL 09]. However, there are not many prototype generator cells at this level of power, particularly in solid-electrolyte technologies – PEMFCs and SOFCs.

– From the point of view of fuel, two choices are possible: either onboard hydrogen, which poses a problem in terms of volume of storage, or kerosene reforming, which is very difficult.

– In addition, the approval and certification of a new technology is a highly complex process in the aerospace industry, particularly from the point of view of reliability and safety. As regards safety, the presence of hydrogen on board is an additional risk factor which needs to be dealt with – particularly if it is stored.

– The oxidant conventionally used is oxygen from the air; however, the air pressure decreases with altitude, so the partial pressure of oxygen falls, although the proportion of oxygen remains the same. Therefore, we need to increase the compression force. The other solution is to store compressed oxygen on board, which poses problems in terms of safety, particularly when coupled with that posed by the hydrogen.

– Finally, the specifications in terms of volumetric and particularly specific power are very demanding. Fuel cell generators are not yet capable of satisfying these specifications, particularly when competing with the tried-and-tested technology of gas turbines, even if we choose to reform kerosene.

3.6.3.2. *Maritime applications*

Similarly as for mobile applications, chargers for Pb batteries aboard sailboats have been developed.

As with isolated sites on land, we can envisage supplying electricity to beacons and lights.

Fuel-cell-propelled *submarines* have been developed by HDW for the German navy. Diesel propulsion is used for normal movement, whereas fuel cell mode is reserved for stealthy movement, at depth for at most 3 weeks. The technology used is PEMFCs, for their low temperature, fed with hydrogen and oxygen. This choice was guided by the anaerobic context of the application, as it improves the efficiency of the FC system.

Electrical propulsion of boats using a fuel-cell system is envisageable for small craft. Particularly on board sailboats, an engine is needed for maneuvers in port, where sailing is prohibited. The advantages to motorization of this type, the absence of acoustic and atmospheric pollution, are of course very much in phase with wind propulsion once at sea.

However, as with air travel applications, the medium-term outlet for this technology relates more to the supply of the onboard electricity for the vessels. Currently, this energy is sourced from marine diesel oil (MDO), burned in the combustion engine. This engine is, of course, designed for propulsion at sea. However, when the boat is docked, the diesel engines still operate in a very low regime, with a poor efficiency, simply to drive the alternator. The implementation of a fuel-cell system would separate the needs for propulsion from the needs for electricity generation, with the diesel engines being reserved for propulsion.

The use of a fuel-cell system for marine applications poses problems, some of which were mentioned above in the context of air travel applications:

– in terms of fuel, in this case we can also store either hydrogen or MDO on board, but MDO is not much easier to reform than kerosene;

– the specific power, which is also critical, cannot be delivered by modern systems for commercial craft;

– the certification of a new technology is almost as complex as in the aeronautics;

– the salty air poses a problem for the supply of cells (be they PEMFCs or SOFCs). The air flowing into the cell needs to be carefully filtered to remove the salt, otherwise there is a danger of blocking the porous layers of the electrodes.

3.6.3.3. *Terrestrial applications*

In terms of long-distance passenger rail transport, there is nothing that can compete with cabled electrical supply, and fuel-cell technology offers no added value.

However, for *end-of-line applications*, railway yards, locomotives and hybrid diesel/electric booster engines are being investigated, and in this context, fuel cells could find a part to play.

For *light rail* travel, such as streetcars on rails or tires, it may be advantageous to combine a fuel-cell system with cabled supply, for bimodal operation: because cables are not appropriate in certain town centers, or on the other hand for suburban travel for non-equipped journeys.

The major concern, and the subject of most economic and commercial conjectures, remains the application in automobile vehicles, whether heavy such as buses and trucks, or light such as utility vehicles or private cars. Indeed, this is a mass market, which is expanding on a global scale and which represents the majority of CO_2 emissions attributable to transport.

As with the other modes of transport, we can distinguish two types of applications: *APUs for the supply of the onboard electricity grid* and *propulsion*.

Regarding the supply of the onboard grid by a generator separate from the combustion engine, the argument is similar to that put forward for maritime applications. The electrical needs on board vehicles are growing, stimulated by increasingly numerous comfort and safety devices. Up until now, this increase has been catered for by the increasing optimization of the onboard alternators.

The auxiliary functions which consume most energy are the air-conditioning of the cabin for private vehicles and trucks, and the cold groups for refrigerated trucks. Given that the battery does not have the capacity to supply them on its own, the power to these functions is cut off when the combustion engine is shut down. In the case of prolonged stoppage, e.g. during a night spent at a rest stop, the combustion engine operates in a low regime, producing a great deal of pollution and a poor yield because it is a long way from its optimal point of design. Certain countries, including Switzerland, have now prohibited the use of an idling engine when stopped. It is therefore becoming advantageous to devise an onboard generator which is unconnected to the propulsion mechanism.

The company DELPHI has developed an APU, comprising a reformer and an SOFC. This choice is attributable to the fact that the reforming of a hydrocarbon, which must be desulfurized, is simpler for SOFCs. Two versions have been put

forward: first a gasoline version and later a diesel version, given that the reforming of diesel is a more complex task. Startup in around ten minutes has been achieved. The performances of the stack are satisfactory, and significant gains in terms of the net yield can still be made by optimizing the system. Progress is expected in terms of durability, thermal cycling and cost [MUL 08].

As regards propulsion, the technical feasibility of the fuel cell solution was demonstrated in the 1990s by the pioneers in the domain: Ballard for the PEMFC system and Daimler Chrysler for its integration into a vehicle. They developed numerous versions, becoming ever more compact and high-performing, giving rise to the NECAR (No Emission CAR) series, which birthed a Class A fuel cell vehicle. Various solutions for fuel storage were tested: liquid hydrogen, methanol, and compressed hydrogen. The liquid fuels, liquefied hydrogen and methanol, deliver greater autonomy, but for the former the cost of liquefaction is prohibitive, whereas for the latter, whilst it is simple to reform, its toxicity is a considerable obstacle. All the major automobile manufacturers have also demonstrated their expertise in the domain, and to describe all such projects is beyond the mandate of this book. However, certain invariant factors between the different prototypes can be picked up on:

– use of gaseous hydrogen as a fuel; and

– hybridization with a reversible electricity storage device, supercapacitors or accumulator batteries. This helps reduce the dynamic constraints on the fuel-cell system and to recover energy from braking. The respective sizing of these elements may be extremely variable: from a low-power cell, of a few kW, considered to be a range extender for a high-capacity battery, to a high-power cell, of several dozen kW, assisted by a battery and/or supercapacitors for rapid transitions.

With regard to fuel cell buses, a real-scale experiment was carried out between 2003 and 2006, thanks to support from the European Union, by the Clean Urban Transport (CUTE) project Thirty Mercedes buses, equipped with Ballard fuel cells, were deployed in 10 European cities on commercial routes. These buses were “all FC” buses, with no hybridization and therefore no energy recovery when braking. This choice was debatable for an application on urban routes, but it is explicable by the fact that the objective was more to demonstrate the viability of the concept in a real context than to optimize the buses.

Technological barriers still have to be overcome for this highly constrained mass market, with significant economic stakes.

The *integration of the fuel-cell system* on board a vehicle is a point that has been extensively studied, thanks to numerous demonstrators made by the various

manufacturers. However, in the interests of a vehicle which is quiet, economical and clean, a number of points are critical. Good integration includes the *optimization of the whole system*, because the auxiliaries may occupy up to 70% of the total volume and consume up to 35% of the gross power of the stack. The operation of the stack is entirely silent, but the same is not true of the air compressor, whose *level of noise emissions* needs to be monitored. As hybridization with a storage device is crucial, the *management of the energy flows* within the vehicle is a point of fundamental importance for the economical behavior of the vehicle. The *management of heat* in the vehicle is markedly different from that of a conventional vehicle, because all the components operate at low temperature (below 80°C) and need to be properly cooled (the fuel cell, the electrical engine, the electronics) despite the slight gap between the component operating temperature and the ambient air temperature. The hydrogen fuel-cell vehicle emits no pollutants into the atmosphere locally, but it is more difficult to draw a *well-to-wheel balance*, because it depends on the primary source of energy used for the production of the hydrogen.

Cold start performance needs to be carefully managed, because the customer expects the same service from the vehicle regardless of the weather conditions. The technical specifications for automobiles for such an application prescribe the capacity to start up in less than 30 seconds at –30°C. The simplest solution, which is totally accepted in Canada, for instance, for conventional vehicles, is to use a "block heater", which includes electrical coverings or heating resistances that are plugged into the electrical grid. More transparent solutions from the customers' point of view are under investigation to overcome this difficulty.

The *cost* is a massive obstacle to the introduction of commercial vehicles using such systems. As a simple illustration, we can place the cost of installing 1 kW of power for a FC system between €500 and €1000 (this range is very approximate, as the product is not fully commercially mature). Taking an average, for a vehicle carrying a 40 kW fuel cell, the cost of the FC system alone stretches to €30 k, which is the price of a family-size sedan. Thus, the cost needs to be reduced practically tenfold so as to attain a competitive objective of around €60/kW. In the cost of the system, the auxiliary components represent a significant proportion – this certainly varies on the basis of the number of actuators and the complexity of the control mechanism adopted, but it can be estimated at around 50%. To reduce the cost of the stack, significant gains are to be expected from the effect of mass production, industrialization of bipolar plates (the technology for embossed metal plates is very promising from this perspective), and the decreasing cost of the materials for the MEA. The cost of the platinum used, which is only a marginal part of the current cost, represents a major part of the target cost (see exercise 3.7.1). Similarly for the auxiliary components, as there are few dedicated components in FC applications for air compression (within the proper range of flowrate and pressure, in a grease-free technology) and for humidification, the rare elements that are available are costly,

and are not always particularly well optimized in relation to the technical specifications. There again, significant gains are to be expected. However, it is impossible to affirm that a reduction by a factor of 10 will be able to be attained in the short term.

The *reliability* and the *lifetime* are also crucial points. For a lightweight vehicle, the expected lifetime is around 5000 hours of use. This is largely achieved with a small cell at constant current, but the results may drop drastically to between 2000 and 3000 hours on the scale of a stack in a dynamic current regime [WAH 07; GER 10; GER 11] and is reduced still further for the whole system. The results of experiments on stationary applications show that most breakdowns occur because of failure of the auxiliary components, but such failures may have repercussions for the stack itself.

Prototypes lean toward the use of stored hydrogen as a fuel, because the reforming of hydrocarbons is complicated when dealing with PEMFC technology. At present, the storage solutions available are unable to deliver sufficient mass yields (that is, the mass of hydrogen in comparison to the mass of the tank) – around 3%, which is prohibitive in terms of autonomy. In addition, the *hydrogen distribution infrastructure* is practically non-existent, and to create such an infrastructure would entail enormous investment costs.

Finally, the *acceptance* of a new technology by the public is obviously a condition *sine qua non* for its commercial success. Hydrogen is not widely known as a fuel, and its explosiveness and flammability cause concern, although solutions are in existence to deal with these risks, as is the case with fuels for combustion engines. However, these misgivings are always somewhat irrational. Thus the driver of a combustion vehicle, who is sat directly on top of a tank of highly flammable fuel but does not consider himself to be in danger, might mistrust the hydrogen canisters on board his fuel-cell vehicle. Thus, a public information campaign is a crucial first step. The continuation of the development of standards adapted for this technology is also necessary to facilitate the homologation of this type of vehicle.

3.7. Corrected exercises

3.7.1. *Calculation of the cost of platinum for an electrode*

The price of Pt experiences significant variations, and depends on its degree of purity. Assuming a price of €30/g, calculate the cost of Pt in €/kW for a PEMFC electrode charged at 0.2 mg/cm^2, whose nominal point is (0.6 A/cm^2; 0.7 V), and then for a cell, assuming the same charge of the two electrodes.

Solution

Calculate the total electrode surface needed to provide 1 kW at the point of operation in question:

$$P = V \times j \times S \text{, so } S = \frac{P}{V \times j} = \frac{1000}{0.7 \times 0.6} = 2381\, cm^2$$

$$Cost = S \times m_{Pt} = 2381 \times 0.2 \times 10^{-3} \times 30 = €14.30$$

This gives us a cost of platinum for an electrode as €14.30, and for a cell, €28.60.

3.7.2. *Dimensions of a "standard" fuel cell module*

To attain the levels of power required by an application, it is preferable to combine identical modules, whose production can be standardized. In view of the current technological limitations on the size of PEMFC stacks and considering a nominal point of operation of (0.6 A/cm^2; 0.7 V), propose the dimensions and calculate the power of a standard module for high-power applications.

Solution

The current state of the art shows that we can serially combine around 200 cells, with a surface area of 250 cm^2, without adversely affecting the point of operation. Considering a point of operation of (0.6 A/cm^2; 0.7 V), the power of the module is:

$$P = N \times V \times j \times S = 200 \times 0.7 \times 0.6 \times 250 = 21\, kW$$

The standard module proposed has a stack of 200 cells, with surface area 250 cm^2, and 21 kW of power.

3.7.3. *Calculation of the flowrate of reactant gases entering the cell*

Consider a PEMFC stack with nominal power of 5 kW, comprising 100×200 cm^2 cells, with nominal current density of 0.5 A/cm^2. We impose a factor of overstoichiometry of 2 at the cathode and assume closed-mode operation at the anode (we shall ignore the flow of hydrogen during purges). We take M_H as the atomic molar mass of hydrogen (1 g), M_O as the atomic molar mass of oxygen (16 g), M_N as the atomic molar mass of nitrogen (14 g) and F Faraday's constant (96485 C).

– calculate the average voltage of a cell;

– calculate the mass flowrate of hydrogen entering the cell;

– calculate the mass flowrate of air entering the cell.

Solution

Calculation of the average voltage of a cell

$$V_{cell} = \frac{P}{N \times j \times S} = \frac{5000}{200 \times 0.5 \times 100} = 0.5\,V$$

Calculation of the mass flowrate of hydrogen: we apply Faraday's law to calculate the molar flowrate, and then calculate the molar mass of the hydrogen to get the mass flowrate of hydrogen.

$$\dot{n}_{H_2} = \frac{N \times j \times S}{2F} = \frac{200 \times 0.5 \times 100}{2 \times 96485} = 0.0518\ mols^{-1}$$

$$M_{H_2} = 2 \times M_H = 2g/mol^{-1}$$

$$\dot{m}_{H_2} = \dot{n}_{H_2} \times M_{H_2} = 103.6\ mgs^{-1}$$

Calculation of the mass flowrate of air: we apply Faraday's law, taking account of the factor of overstoichiometry to calculate the molar flowrate of oxygen, and then we calculate the molar flowrate of nitrogen, the molar masses of oxygen and nitrogen and finally the mass flowrate of air.

$$\dot{n}_{O_2} = F_{sc} \frac{N \times j \times S}{4F} = 2 \times \frac{200 \times 0.5 \times 100}{4 \times 96485} = 0.0518\ mols^{-1}$$

Air contains 21% oxygen and 79% nitrogen, so the calculated flowrate of oxygen is accompanied by a molar flowrate of nitrogen:

$$\dot{n}_{N_2} = \frac{0.79}{0.21} \dot{n}_{O_2} = 0.1949\ mols^{-1}$$

The molar masses of oxygen and nitrogen are:

$$M_{O_2} = 2 \times M_O = 32\ g/mol^{-1} \text{ and } M_{N_2} = 2 \times M_N = 28\ g/mol^{-1}.$$

The mass flowrate of air is therefore:

$$\dot{m}_{air} = \dot{n}_{O2} \times M_{O2} + \dot{n}_{N2} \times M_{N2} = 7gs^{-1}.$$

3.7.4. *Calculation of the water content of the air upon input and output of the cell. Calculation of the dew point at the cell output*

The saturating vapor pressure at temperature $T(K)$ can be approximated by the Clapeyron equation:

$$\ln \frac{P_{sat}}{P_0} \approx \frac{ML_v}{R}\left(\frac{1}{T_0} - \frac{1}{T}\right)$$

where M is the molar mass of water in kg/mol, L_v the latent heat of vaporization of water, which is 2.26×10^6 J/kg, T_0 the boiling temperature expressed in K at pressure P_0, R the ideal gas constant: 8.314. We give M_H the atomic molar mass of the hydrogen (1 g), M_O the atomic molar mass of oxygen (16 g), and M_N the atomic molar mass of nitrogen (14 g).

Consider a stack of 100 cells, supplied by a mass flowrate of dry air of 7 gs^{-1}, when providing a 100 A current. The temperature of the cell, which is supposed to be isothermic, is 65°C. To obtain 80% humidity at the cell input, we inject water into the flow of air. The pressure is 1.5 bar on entering the stack, and is equal to atmospheric pressure on exiting (free exhaust output):

– calculate the partial pressures of water, oxygen and nitrogen at cell input;

– calculate the molar flowrates of oxygen and nitrogen at cell input;

– calculate the mass flowrate of water to be injected to obtain 80% at cell input;

– give the dew point of the water at cell input;

– calculate the mass flowrate of water produced in the cell;

– if we make the hypothesis that the flow of water through the membrane is zero and that hydrogen does not permeate, calculate the composition of the fluid at cell output;

– calculate the partial pressure of water at cell output. Does condensation take place?

Solution

Calculation of the partial pressure of water

$$\ln \frac{P_{sat}}{P_0} = \frac{ML_v}{R}\left(\frac{1}{T_0} - \frac{1}{T}\right)$$

The boiling point of water at atmospheric pressure is 100°C, which is 373 K, so the saturating vapor pressure at 65°C, 338 K, is:

$$P_{sat} = \exp\left(\frac{ML_v}{R}\left(\frac{1}{T_0} - \frac{1}{T}\right)\right) = \exp\left(\frac{18\times10^{-3}\times2.26\times10^{6}}{8,314}\left(\frac{1}{373} - \frac{1}{338}\right)\right)$$

$$P_{sat} = 0.257\ bar$$

The humidity is 80%, so the partial pressure of water is:

$$P_{H_2O} = 0.8\times P_{sat} = 0.205\ bar$$

Calculation of the partial pressures of oxygen and nitrogen at cell input

The total pressure of the gas is 1.5 bar. If we consider all the gases to be ideal, and therefore the mixture to be ideal, we can write:

$$P_{total} = P_{H_2O} + P_{O_2} + P_{N_2}$$

Therefore we can calculate the pressure of dry air:

$$P_{dry\ air} = P_{O_2} + P_{N_2} = P_{total} - P_{H_2O} = 1.5 - 0.205 = 1.295\ bar$$

As the gases are ideal, we can write, according to the ideal gas law and the proportions of nitrogen and oxygen in the dry air:

$$P_{O_2} = 0.21\times P_{dry\ air} = 0.272\ bar$$

$$P_{N_2} = 0.79\times P_{dry\ air} = 1.023\ bar$$

Calculation of the molar flowrates of oxygen and nitrogen at cell input

The flowrate of dry air is 7 g/s. This mass flowrate comprises 21% oxygen, with molar mass 32 g, and 79% nitrogen, with molar mass 28 g:

$$\dot{m}_{dry\ air\ in} = \dot{n}_{O2in} \times M_{O_2} + \dot{n}_{N2in} \times M_{N_2}$$

$$\dot{m}_{dry\ air\ in} = \dot{n}_{O2in} \times \left(M_{O_2} + \frac{0.79}{0.21} M_{N_2} \right)$$

$$\dot{n}_{O_2\,in} = \frac{\dot{m}_{dry\ air\ in}}{M_{O_2} + \frac{0.79}{0.21} M_{N_2}}$$

$$\dot{n}_{O_2\,in} = \frac{7}{32 + \frac{0.79}{0.21} \times 28} = 0.05097\ mols^{-1}$$

$$\dot{n}_{N_2\,in} = \frac{\dot{m}_{dry\ air}}{\frac{0.21}{0.79} M_{N_2} + M_{N_2}} = 0.19174\ mols^{-1}$$

Calculation of the molar and then mass flowrate of water at cell input

As the gases are ideal and the mixture of gases is ideal, we can write:

$$\frac{P_{H_2O}}{P_{total}} = \frac{\dot{n}_{H_2O\,in}}{\dot{n}_{total\ in}}; \quad \frac{P_{O_2}}{P_{total}} = \frac{\dot{n}_{O_2\,in}}{\dot{n}_{total\ in}}; \quad \frac{P_{N_2}}{P_{total}} = \frac{\dot{n}_{N_2\,in}}{\dot{n}_{total\ in}}$$

$$\dot{n}_{total\ in} = \dot{n}_{O_2\,in} \times \frac{P_{total}}{P_{O_2}} = \dot{n}_{N_2\,in} \times \frac{P_{total}}{P_{N_2}} = 0.2811\ mols^{-1}$$

$$\dot{n}_{H_2O\,in} = \frac{P_{H_2O}}{P_{total}} \times \dot{n}_{total\ in} = 0.0384\ mols^{-1}$$

$$\dot{m}_{H_2O\,in} = \dot{n}_{H_2O\,in} \times M_{H_2O} = 0.0384 \times 18 = 0.6915\ gs^{-1}$$

Calculation of the dew point at cell input

The dew point is the temperature at which humid air is saturated, i.e. has 100% humidity. In this case the partial pressure of the water is equal to the saturating vapor pressure. Thus, we can write:

$$\ln \frac{P_{sat}}{P_0} = \ln \frac{P_{H_2O}}{P_0} = \frac{ML_v}{R} \left(\frac{1}{T_0} - \frac{1}{T_{dew}} \right)$$

$$T_{dew} = \frac{1}{\frac{1}{T_0} - \frac{R}{ML_v} \ln \left(\frac{P_{sat}}{P_0} \right)} = 332.8\ K$$

The dew point is therefore 332.8 K, which is 59.8°C.

Calculation of the molar and then mass flowrate of water produced in the cell

According to Faraday's law, the rate of water production in the cell is:

$$\dot{n}_{H_2Oprod} = \frac{N \times I}{2F} = \frac{100 \times 100}{2 \times 96485} = 0.0518\ mols^{-1}$$

$$\dot{m}_{H_2Oprod} = 0.933 gs^{-1}$$

Calculation of the composition of the fluid at cell output

The nitrogen does not react and does not permeate, so all of it flows out of the cell:

$$\dot{n}_{N_2\,out} = 0.19174\ mols^{-1}$$

Some of the oxygen has reacted, so we calculate the amount that comes out:

$$\dot{n}_{O_2\,cons} = \frac{N \times I}{4F} = 0.0259\ mols^{-1}$$

$$\dot{n}_{O_2\,out} = \dot{n}_{O_2\,out} - \dot{n}_{O_2\,cons} = 0.0251\ mols^{-1}$$

The flowrate of water out of the cell is equal to the sum of the flowrate of water in and the flowrate of water produced, because we neglect the transversal flow of water through the membrane:

$$\dot{n}_{H_2O\,out} = \dot{n}_{H_2O\,in} + \dot{n}_{H_2O\,prod} = 0.0902\ mols^{-1}$$

The flowrate out is therefore made up of:

$$\dot{n}_{total\,out} = \dot{n}_{H_2O\,out} + \dot{n}_{O_2\,out} + \dot{n}_{N_2\,out} = 0.307\ mols^{-1}$$

This includes 62.4% nitrogen, 8.2% oxygen and 29.4% water.

Calculation of the partial pressure of water at cell output

We calculate the partial pressure of the water as though it were all in vaporous form:

$$P_{H_2O} = \frac{\dot{n}_{H_2O\,out}}{\dot{n}_{total\,out}} P_{atm} = \frac{0.0902}{0.307} P_{atm} = 0.294\ bar$$

Note that we obtain a value $P_{H_2O} > P_{sat}$, which means that the water condenses and finally the partial pressure of water at cell output is:

$$P_{H_2O} = P_{sat} = 0.257\ bar$$

3.7.5. *Calculation of the yield of a PEMFC*

Consider a stack of 20 cells of 250 cm^2 surface area, at 80°C. The nominal point of operation is (0.65 V; 0.6 A/cm^2) when the stack is functioning in open mode at the anode, with an anodic factor of overstoichiometry of 1.5. When the stack is in dead-end mode at the anode, the average cell voltage between two purges falls in obeisance to an exponential law between 0.65 V just after the purge and 0.40 V just before the purge, with the current density being maintained at 0.6 A/cm^2. We ignore the flowrate of hydrogen during the purge. Remember that the enthalpy of formation of water at atmospheric pressure, in liquid form at 80°C, is –285.84 kJ/mol^{-1}.

– calculate the molar flowrate of hydrogen entering the stack in both modes of function;

– calculate the yield of the stack in open mode;

– calculate the yield of the stack in dead-end mode, assimilating the voltage of the stack between two purges to its logarithmic mean.

Calculation of the flowrate of hydrogen in closed mode and then in open mode

We apply Faraday's law to calculate the flowrate of hydrogen in closed mode, considered equal to the flowrate of hydrogen consumed in the cell (we discount the purge flowrate):

$$\dot{n}_{H_2} = \frac{N \times j \times S}{2F} = \frac{20 \times 0.6 \times 250}{2 \times 96485} = 0.0155\ mols^{-1}$$

We take account of the anodic factor of overstoichiometry in open mode:

$$\dot{n}_{H_2} = F_{sa} \frac{N \times j \times S}{2F} = 1.5 \frac{20 \times 0.6 \times 250}{2 \times 96485} = 0.0233\ mols^{-1}$$

Calculation of the yield in open mode

Consider the following definition for the yield of the stack:

$$\eta_{stack} = \frac{V_{stack} I_{stack}}{-\dot{n}_{H_2} \Delta h_f} = \frac{20 \times 0.65 \times 0.6 \times 250}{0.0233 \times 285.84 \times 10^3} = 29.3\%$$

Calculation of the yield in closed mode

We calculate the logarithmic mean of the voltage of the stack between two purges:

$$V_{stack} = \frac{V_{\max} - V_{\min}}{\ln\left(\frac{V_{\max}}{V_{\min}}\right)} = 0,515 \ V$$

We calculate the yield in closed mode:

$$\eta_{stack} = \frac{V_{stack} I_{stack}}{-\dot{n}_{H_2} \Delta h_f} = \frac{20 \times 0.515 \times 0.6 \times 250}{0.0155 \times 285.84 \times 10^3} = 34.9\%$$

3.7.6. *Autonomy of an exploration submarine*

A stack of fuel cells feeds the onboard power grid for a small exploration submarine, with electric propulsion. The nominal power of the cell is 5 kW, and the active surface is 250 cm². The voltage at the terminals of a cell is 0.745V for a nominal current density of 0.3 A/cm². It is supplied with pure hydrogen and oxygen with stoichiometric coefficients of 1 and 1.2 respectively. We give M_H, the atomic molar mass of hydrogen (1 g), M_O, the atomic molar mass of oxygen (16 g) and F, Faraday's constant (96485 C).

– calculate the number of cells in the stack;

– calculate the mass of hydrogen and the mass of oxygen needing to be taken on board for a 3-hour dive if the stack has to deliver its nominal power throughout the duration of the dive.

Solution

Calculation of the number of cells in the stack

$$N = \frac{P}{V \times j \times S} = \frac{5000}{0.745 \times 0.3 \times 250} = 89.5$$

The stack has 90 cells.

Calculation of the flowrate of hydrogen entering the cell (molar, then mass)

$$\dot{n}_{H_2} = \frac{N \times j \times S}{2F} = \frac{90 \times 0,3 \times 250}{2 \times 96485} = 0.035\ mols^{-1}$$

$$\dot{m}_{H_2} = M_{H_2} \frac{N \times j \times S}{2F} = 2 \frac{90 \times 0.3 \times 250}{2 \times 96485} = 0.070\ gs^{-1}$$

Calculation of the mass of hydrogen to be stored aboard the submarine

$$m_{H_2} = \dot{m}_{H_2} \times \Delta t = 0.07 \times 3 \times 3600 = 756\ g$$

Calculation of the flowrate of oxygen entering the cell (molar, then mass)

$$\dot{n}_{O_2} = F_{SC} \frac{N \times j \times S}{4F} = 1.2 \frac{90 \times 0.3 \times 250}{4 \times 96485} = 0.021\ mols^{-1}$$

$$\dot{m}_{O_2} = M_{O_2} \times \dot{n}_{O_2} = 32 \times 0.021 = 0.672\ gs^{-1}$$

Calculation of the mass of oxygen to be stored aboard the submarine

$$m_{O_2} = \dot{m}_{O_2} \times \Delta t = 0.672 \times 3 \times 3600 = 7.26\ kg$$

3.7.7. *Power supply to an isolated farm site*

A 10 kW fuel cell generator supplies electricity to an isolated farm site. It is provided with 100%-humidified air via a compressor and a humidifier, with a factor of overstoichiometry of 2. The gas pressures on input to the generator are regulated at 1.2 bar. At the anode, the generator is fed with hydrogen and functions in recycle mode equivalent to a coefficient of overstoichiometry of 1.1. The cell's cooling circuit keeps the generator at 80°C.

The electrochemical converter is composed of 100 cm² cells whose I-V polarization curve can be modeled by the following equation:

$$E = E^0 + \alpha T \ln\left(\frac{P_{O2}}{P_0}\right) + \beta T \ln\left(\frac{P_{H2}}{P_0}\right) - AT \ln\left(\frac{j + j_n}{j_0}\right) - BT \ln\left(1 - \frac{j}{j_l}\right) - Rj$$

α(V/K)	β(V/K)	A(V/K)	B(V/K)	R(Ωcm²)	j_n(A/cm²)	j_0(A/cm²)	j_l(A/cm²)
3×10^{-4}	57×10^{-5}	6×10^{-5}	-1.5×10^{-4}	0.3	300×10^{-5}	3×10^{-5}	1

E^0 is the reversible potential of the cell at T; P_{O_2} and P_{H_2} denote the partial pressures of oxygen and hydrogen at cell input, and P_0 the atmospheric pressure; T is the temperature of the cell in (K). The nominal current density is 0.6 A/cm². The minimum voltage of the cell is 400 mV – below this value the generator is considered to be faulty and is shut down. The saturating vapor pressure at temperature $T(K)$ can be approximated by the Clapeyron equation:

$$\ln \frac{P_{sat}}{P_0} \approx \frac{ML_v}{R}\left(\frac{1}{T_0} - \frac{1}{T}\right) \qquad [3.23]$$

where M is the molar mass of water in kg/mol, L_v the latent heat of vaporization of water, which is 2.26×10^6 J/kg, T_0 the boiling temperature expressed in K at pressure P_0, and R the ideal gas constant: 8.314. We give M_H the atomic molar mass of the hydrogen (1 g), M_O the atomic molar mass of oxygen (16 g), and M_N the atomic molar mass of nitrogen (14 g). F, Faraday's constant, is 96485 C. The variation in Gibbs free energy at 80°C and atmospheric pressure during the formation of one mole of water is equal to –228.3 kJ/mol. Here we want you to work out the following:

– calculate the partial pressure of oxygen entering a cell;

– calculate the reversible potential of a cell at atmospheric pressure and at its operating temperature;

– calculate the open-circuit voltage of a cell;

– plot the polarization curve for a cell. Give the cell voltage at the nominal current density;

– calculate the number of cells necessary to provide 10 kW in nominal operation;

– to improve generator reliability and power availability, it is decided to combine two stacks in parallel in the FC generator. Give the nominal point of operation for the FC generator (current and voltage);

– assuming that all the cells behave in the same way, give the point of operation and the power provided by the fuel-cell generator when the 400 mV threshold is reached for the cell voltages;

– calculate the percentage variation of the voltage output by the generator; and

– what is the mass flowrate of hydrogen needed for the generator to operate at 10 kW?

– consider the following profile of daily consumption: 8 kW at 06:00–8:00, 12:00–14:00 and 18:00–21:00; 4 kW at 08:00–12:00 and 14:00–18:00, and 2 kW between 21:00 and 06:00. Calculate the mass of hydrogen necessary to supply electricity for 24 hours;

– a B50 gas canister contains 8.5 Nm^3 of hydrogen at 20°C, at a pressure of 200 bar. How many such canisters are needed per day?

– calculate the volume of liquid water produced in a day, supposing that the water vapor is able to be condensed entirely on exiting the cell. Is this production sufficient for sanitary usage, if we know that on average, a toilet flush consumes 10–12*l* and a shower 30–80*l*?

Solution

Calculation of the partial pressure of water equal to the a saturating vapor pressure at 80°C

$$\frac{P_{sat}}{P_0} = \exp\left(\frac{ML_v}{R}\left(\frac{1}{T_0}-\frac{1}{T}\right)\right) = \exp\left(\frac{18\times10^{-3}\times2.26\times10^{6}}{8.314}\left(\frac{1}{373}-\frac{1}{353}\right)\right)$$

$$P_{sat} = 0.475\ bar$$

Calculation of the partial pressure of oxygen

$$P_{dry\ air} = P_{total} - P_{H_2O} = 1.2 - 0.475 = 0.725\ bar$$

$$P_{O_2} = 0.21\times P_{dry\ air} = 0.152\ bar$$

Calculation of the reversible potential

$$E^0 = \frac{-\Delta g_f^0}{2F} = \frac{228.3\times10^3}{2\times96485} = 1.18\ V$$

Calculation of the open circuit voltage – i.e. the voltage for j = 0

$$E = E^0 + \alpha T \ln\left(\frac{P_{O2}}{P_0}\right) + \beta T \ln\left(\frac{P_{H2}}{P_0}\right) - AT \ln\left(\frac{j_n}{j_0}\right) = 0,92\ V$$

The polarization curve can be traced point by point from the equation $E(j)$

Calculation of the voltage at the nominal current density, i.e. for $j = 0.6\ A/cm^2$

$$E = E^0 + \alpha T \ln\left(\frac{P_{O2}}{P_0}\right) + \beta T \ln\left(\frac{P_{H2}}{P_0}\right) - AT \ln\left(\frac{j + j_n}{j_0}\right) - BT \ln\left(1 - \frac{j}{j_l}\right) - Rj$$

$$E = 0.579\ V$$

Calculation of the voltage at the nominal current density, i.e. for $j = 0.6\ A/cm^2$

$$N = \frac{P}{E \times j \times S} = \frac{10000}{0.579 \times 0.6 \times 100} = 287.85$$

The generator has to contain 288 cells.

Point of operation of the generator for two parallel stacks

The generator contains two parallel stacks of 144 cells. Therefore the nominal voltage of the generator is $V = N \times E = 83.4\ V$, and the current is $I = 2 \times j \times S = 120\ A$.

Calculation of the current and the power when the voltage per cell reaches 400 mV

The relation linking the cell voltage to the current density is not invertible. In order to find the current density for which E is 400 mV, we proceed by successive approximations, or find the point on the graph giving E as a function of j. We find the point (0.91 A/cm^2; 0.4 V).

Percentage variation of the voltage of the generator

$$\Delta V = \frac{0.579 - 0.4}{0.579} = 31\%$$

Mass flowrate of hydrogen entering the cell at 10 kW

$$\dot{m}_{H_2} = M_{H_2} \dot{n}_{H_2} = 2 F_{SA} \frac{N \times j \times S}{2 \times F} = 2 \times 1.1 \times \frac{288 \times 60}{2 \times F} = 0.197\ gs^{-1}$$

Hydrogen consumption over 24 hours

We can plot the power curve for a cell. For each level of power of the generator, we can calculate the power for each cell, by dividing by 288. For each value, we

look for the corresponding current density. We calculate the mass flowrate and then the quantity of hydrogen consumed during each time interval. From this, we deduce the total amount of hydrogen consumed throughout the day. We can also attempt to find the current density points by successive approximation.

P (kW)	8	4	2
P_{cell} (W)	27.8	13.9	6.9
j (A/cm²)	0.42	0.18	0.09
$\dot{m}_{H_2}$ (mg/s)	138	59	29.5
Δt (h)	7	8	9
m_{H_2} (kg)	3.477	1.7	0.956

The total mass of hydrogen consumed is 6.13 kg.

Calculation of the mass of hydrogen contained in a B50 canister

The Nm^3 means that this is the volume of gas which would 8.5 m^3 were it stored at atmospheric pressure and 15°C. By applying the ideal gas law:

$$m_{H_2} = M_{H_2} n_{H_2} = M_{H_2} \frac{P \times V}{R \times T} = 2 \times \frac{10^5 \times 8.5}{8{,}314 \times (273+15)} = 710\ g$$

To store the 6.13 kg consumed over the course of the day, we need 8.6 canisters.

Calculation of the mass of water produced in a day

$$n_{H_2 cons} = \frac{m_{H_2}}{M_{H_2} \times F_{SA}} = n_{H_2 Oprod} = 2786.4\ mols$$

$$m_{H_2O} = n_{H_2 Oprod} \times M_{H_2O} = 50.15\ kg$$

The fuel-cell generator produces 50.15 l, which is approximately the amount of water used by a shower, so the provision is poor in relation to the water needed for sanitation.

3.7.8. *Fuel-cell generator for a private vehicle*

We measure the polarization curve of a cell at 80°C, in different pressure conditions, and approximate this characteristic curve with the following equation (ignoring the effect of the concentration overvoltage term):

$$V = E^0 + A\ln\frac{P_{H2}}{P_0} + B\ln\frac{P_{O2}}{P_0} + C\ln\frac{j + j_n}{j_0} - rj$$

V is the cell voltage (V); E^0 is the reversible potential at ambient temperature and atmospheric pressure, j is the surface density of current (A/cm^2); j_0 is the surface density of exchange current (A/cm^2) equal to 0.01 A/cm^2; j_n represents the internal current density, equal to 1 mA/cm^2, A is a constant linked to the influence of the partial pressure of hydrogen, equal to 0.05 V; B is a constant linked to the influence of the partial pressure of oxygen equal to 0.026 V; C is the slope of the Tafel plot equal to –0.06 V; r is the surface resistance to polarization, equal to 0.3 Ωcm^2.

The MEA technology used enables us to industrially make maximum surfaces of 250cm^2, for a nominal current density of 0.6 A/cm^2. We wish to make a 50 kW fuel-cell generator to drive a small vehicle, hybridized with a battery. The anode is fed with pure hydrogen with an equivalent coefficient of overstoichiometry of 1.05. The cathode is fed with 100% humidified air, with a factor of overstoichiometry of 2. The gases enter into the cell at 80°C, at a pressure of 1.3 bar. The cells are considered to be isothermal at 80°C.

The saturating vapor pressure at temperature $T(K)$ can be approximated by the Clapeyron equation:

$$\ln\frac{P_{sat}}{P_0} \approx \frac{ML_v}{R}\left(\frac{1}{T_0} - \frac{1}{T}\right) \qquad [3.24]$$

where M is the molar mass of water in kg/mol, L_v the latent heat of vaporization of water, which is 2.26×10^6 J/kg, T_0 the boiling temperature expressed in K at pressure P_0, R the ideal gas constant: 8.314. We give M_H the atomic molar mass of the hydrogen (1 g), M_O the atomic molar mass of oxygen (16 g), and M_N the atomic molar mass of nitrogen (14 g). F, Faraday's constant, is 96485 C. The change in Gibbs free energy at 80°C and atmospheric pressure during the formation of one mole of water is –228.3 kJ/mol.

– Calculate the partial pressure of oxygen;

– calculate the reversible potential of a cell at atmospheric pressure and at its operating temperature;

– calculate the nominal point of operation of a 250 cm^2 cell (i.e. voltage and current), its nominal surface power and its nominal power;

– to achieve the necessary power, we build a generator comprising 4 identical stacks. The electrical coupling is as follows: two parallel branches, each comprising two serially-connected stacks. Propose the dimensions for the unitary stacks;

– give the nominal point of operation of the generator thus built;

– give the mass flowrates of hydrogen and air when the generator is providing its nominal power;

– the vehicle consumes 20 kW, generated by the fuel cell, at the speed of 50 km/h. A hydrogen cylinder at 300 bar pressure is able to hold 3.1 kg of hydrogen. Calculate the point of operation of the fuel cell generator (voltage and current at output). Calculate the range of the vehicle in these conditions.

Solution

Calculation of the partial pressure of water equal to the saturating vapor pressure at 80°C

$$\frac{P_{sat}}{P_0} = \exp\left(\frac{ML_v}{R}\left(\frac{1}{T_0}-\frac{1}{T}\right)\right) = \exp\left(\frac{18\times10^{-3}\times2.26\times10^{6}}{8.314}\left(\frac{1}{373}-\frac{1}{353}\right)\right)$$

$$P_{sat} = 0.475\ bar$$

Calculation of the partial pressure of oxygen

$$P_{dry\ air} = P_{total} - P_{H_2O} = 1.3 - 0.475 = 0.825\ bar$$

$$P_{O_2} = 0.21\times P_{dry\ air} = 0.173\ bar$$

Calculation of the reversible potential

$$E^0 = \frac{-\Delta g_f^0}{2F} = \frac{228.3\times10^3}{2\times96485} = 1.18\ V$$

Calculation of the cell voltage, the surface power and the power

$$V = E_0 + A\ln\frac{P_{H_2}}{P_0} + B\ln\frac{P_{O_2}}{P_0} + C\ln\frac{j + j_n}{j_0} - rj$$

$$V = 1.18 + 0.05\times\ln(1.3) + 0.026\times\ln(0.173) - 0.06\times\ln\left(\frac{0.6 + 10^{-3}}{0.01}\right) - 0.3\times 0.6$$

$$V = 0.72\,V$$

$$P_{surf} = 0.72\times 0.6 = 432\ mWcm^{-2}$$

$$P_{cell} = 108\,W$$

Calculation of the number of cells in the generator and the number of cells per stack

The generator contains $N = \frac{P}{P_{cell}} = \frac{50000}{108} \approx 463$ cells. If there are 4 identical stacks, there must be 116 cells per stack, giving us 464 cells in total.

Calculation of the point of operation of the generator

There are two serial stacks, so $V_{gene} = N_{stack}\times 2\times V_{cell} = 167\,V$.

There are two parallel stacks, so $I_{gene} = 2\times j\times S = 300\,A$.

Calculation of the flowrate of hydrogen

$$\dot{m}_{H_2} = M_{H_2}\dot{n}_{H_2} = 2F_{SA}\frac{N\times j\times S}{2\times F} = 2\times 1.05\times\frac{464\times 150}{2\times 96485} = 0.757\ gs^{-1}$$

Calculation of the flowrate of oxygen

$$\dot{m}_{O_2} = M_{O_2}\times\dot{n}_{O_2} = M_{O_2}F_{SC}\frac{N\times j\times S}{4\times F} = 32\times 2\times\frac{464\times 150}{4\times 96485} = 11.54\ gs^{-1}$$

$$\dot{m}_{N_2} = \frac{0.79}{0.21}\times M_{N_2}\times\dot{n}_{N_2} = \frac{0.79}{0.21}M_{N_2}\times\dot{n}_{O_2} = \frac{0.79}{0.21}\times 28\times 2\times\frac{464\times 150}{4\times 96485} = 38\ gs^{-1}$$

$$\dot{m}_{air} = \dot{m}_{O_2} + \dot{m}_{N_2} = 49.5\ gs^{-1}$$

Calculation of the current density corresponding to 20 kW

20 kW corresponds to a power of $P_{cell} = \frac{P}{464} = 43.1\,W$. We need to find the zero value for the function $f(j) = V(j)\,jS - 43.1$. We can program the function and find the zero numerically or proceed by successive approximations. A correct approximation is:

$$j = 0.18 Acm^{-2}; V_{cell} = 0.92V; P_{cell} = 41,4W; P = 20133\,W$$
$$I_{gene} = 90A; V_{gene} = 213.4\,V$$

Calculation of the range

We calculate the consumption of hydrogen at 20 kW:

$$\dot{m}_{H2} = M_{H2}\dot{n}_{H2} = 2F_{SA}\frac{N \times j \times S}{2 \times F} = 2 \times 1.05 \times \frac{464 \times 0.18 \times 250}{2 \times 96485} = 0.227\ gs^{-1}$$

The tank contains 3.1 kg of hydrogen. The vehicle can therefore run for $\Delta t = \frac{m_{H2}}{\dot{n}_{H2}} = 13656\ s$, which is 3.8 hours. At 50 km/h, the vehicle covers 190 km.

Chapter 4

Electrical Energy Storage by Supercapacitors

4.1. Introduction

Supercapacitors, or Electric Double Layer Capacitors (EDLCs), are devices for buffer storage of electrical energy. Their power density is higher than that of batteries, and they have a high energy density compared with that of electrolytic capacitors. Their lifetime is longer than that of batteries (around 10 years for vehicle applications). The Ragone plot (Figure 4.1) represents electrical energy storage systems in the area of specific power/specific energy. This graph shows that electrolytic capacitors have a very high power density but a very low specific energy. They are generally used with time constants less than a few hundred milliseconds. Batteries have a relatively low power density and a high specific energy. They can be used with a time constant longer than a minute. Between batteries and electrolytic capacitors (Figure 4.1) are supercapacitors. These devices are generally used with a time constant of a few tens of seconds [BEL 01; KOT 00; BUR 00].

Table 4.1 gives an overview of the performances of the storage devices presented above.

The data presented above depend on the operating conditions – especially the power levels (maximum current) and the temperature. From the data in Table 4.1, it is clear that the supercapacitor is the best device for electrical energy storage in the transient state. It can be used for peak power demands for periods between a few seconds and several tens of seconds. It should be noted that the maximum number of charge/discharge cycles for a supercapacitor is around 500 times greater than the same statistic for a battery. Furthermore, the supercapacitor can supply or absorb a

very high current [MAX 12]. Supercapacitors have a very low series resistance (< mΩ), the operating voltage for a cell of the order of 2.7 V and a capacitance which can attain 5000 F. At present, research is being done into 10000 F cells. The charge/discharge efficiency of a supercapacitor is over 90%, whereas for a battery it is between 70 and 85%.

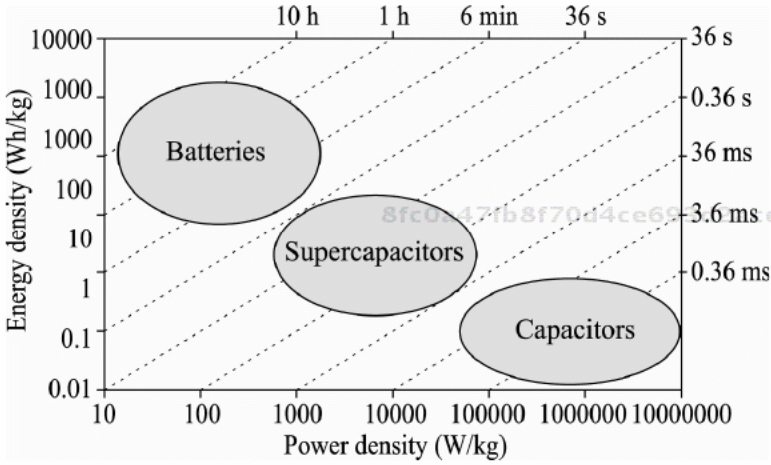

Figure 4.1. *Ragone plot*

	Electrolytic capacitor	Supercapacitor	Lead battery
Charge time t	µs < t <ms	1 s< t <30 s	1 h < t < 5 h
Discharge time	µs< t <ms	1 s< t <30 s	0.3h < t <3h
Charge/discharge yield	> 90%	between 85% and 98%	between 70% and 85%
Power density (W/kg)	> 10^6	10^4	< 10^3
Energy density (Wh/kg)		between 1 and 10	between 10 and 100
Lifetime (number of cycles)	10^{10}	5. 10^5	10^3

Table 4.1. *Comparison between some energy storage devices*

Currently, the most commonly used supercapacitor technology is based on activated carbon for the electrodes and organic electrolyte.

Supercapacitors are used in many domains: vehicles, trains, wind power, telecommunication, etc. In the military domain, supercapacitors are used in submarines (to control water levels in the ballast tanks), and to aid ignition in military vehicles, particularly when the weather conditions are severe (cold).

Supercapacitors are also used to provide power to open the doors on an Airbus A380 in case of emergency.

4.2. Operation and energy characteristics of EDLCs

There are various technologies for supercapacitors [LAR 09].

Activated-carbon-based supercapacitors are composed of two casings, on which a fine layer of powdered carbon is deposited. This layer of carbon is then activated, making its surface extremely porous. The activated carbon therefore has a very high specific surface area. Two types of electrolyte are used: aqueous electrolytes and organic electrolytes.

Aqueous electrolytes are characterized by high ion conductivity and consequently have a very low equivalent series resistance. The major drawback to these electrolytes is their voltage, which is limited to around 1.2 V. Organic electrolytes have low ion conductivity and therefore a relatively high equivalent series resistance in comparison with aqueous electrolytes. Conversely, their voltage capacitance is relatively high, at around 3 V. Activated-carbon supercapacitors are the most fully developed industrially.

Metal-oxide-based supercapacitors are characterized by a chemical reaction at the surface of the electrodes. This causes a charge transfer (pseudo-capacitance). The most widely-used metal oxide is ruthenium dioxide (RuO_2). This technology uses H_2SO_4 as the electrolyte and presents a very low internal resistance. However, the very high cost of metal oxides restricts their use to military or space applications.

Conductive-polymer-based supercapacitors store energy by polymer-doping processes. They have capacitances ranging from 200 to 300 F/g. Once again, this is pseudo-capacitance. These supercapacitor systems are not yet at an industrial development level.

In this chapter, only supercapacitors with activated carbon and organic electrolyte are presented.

4.2.1. *Structure and operation of supercapacitors*

The structure of the supercapacitor cell, studied in this chapter, consists of two activated carbon electrodes and a separator rolled together and impregnated with an organic electrolyte. The electrodes are made up of an aluminum metallic collector, coated on both sides with an active carbon powder material, which has a high surface area. The two electrodes are separated by a porous membrane (separator),

which prevents electronic conduction by physical contact between the electrodes but allows ionic conduction between them. Figure 4.2 represents the supercapacitor structure. The thermocouples are inserted only for heat modeling, and it may be advantageous to have an internal temperature measurement in a prototype intended for R&D. In commercialized supercapacitors there are, of course, no thermocouples.

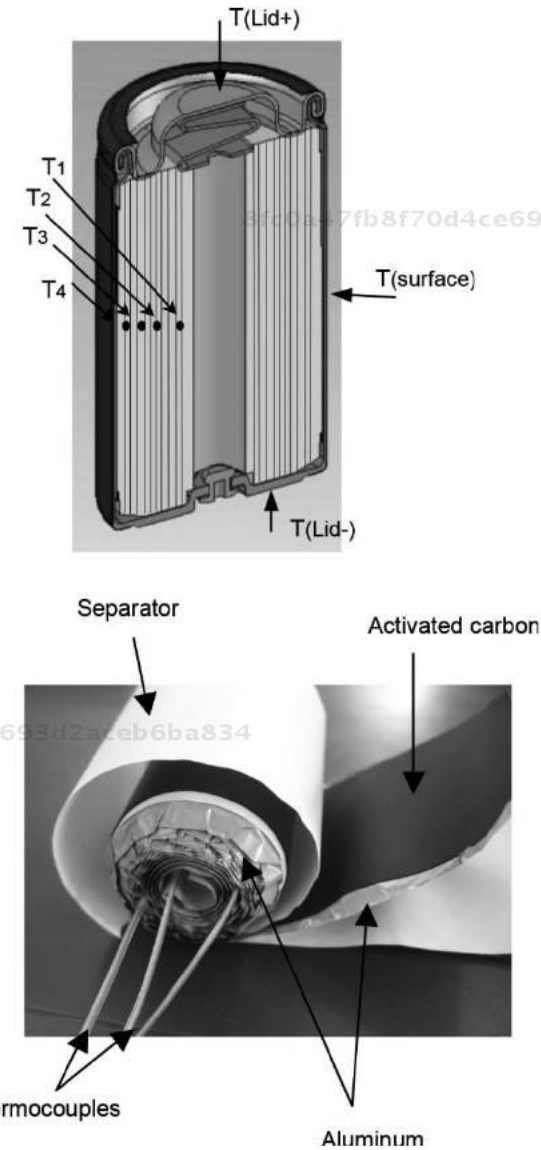

Figure 4.2. *Structure of a supercapacitor*

In the case of a dielectric capacitor, the capacitance is given by equation [4.1].

$$C = \frac{\varepsilon_0 \varepsilon_r S}{e} \qquad [4.1]$$

where C is the capacitance in F; ε_0 the vacuum permittivity in F.m^{-1}; ε_r the relative permittivity of the dielectric; S the surface area of the electrodes in m^2 and e the distance between the two electrodes in m.

In order to increase the capacitance, we can increase the surface area and decrease the thickness. A supercapacitor has an activated-carbon-based anode/cathode structure, which means its specific surface area is able to be considerably larger than conventional capacitors. This specific surface area may be as large as 2000 m^2/g. However, there is a part of this specific surface area which is not accessible, as we shall see later on. Therefore, in practice, the specific surface area which plays a part in the component's capacitance is often far smaller, but nevertheless it is able to deliver very high capacitance values, ranging from 1 to 5000 F. At present, research is under way in order to achieve capacitances of 10000 F.

The principle of operation of a supercapacitor is based on energy storage by adsorption of the ions from the electrolyte to the interfaces between the activated carbon and the electrolyte [LAR 09]. This is electrostatic storage, which does not involve a redox reaction, as in batteries for example. Consequently, the process is quick, reversible and offers very high mass power densities and lifetime. In practice, the lifetime of a supercapacitor is over 500,000 charge/discharge cycles. It should be noted that the lifetime depends primarily on the operating temperature and the polarization voltage. The lifetime decreases when these two parameters increase.

The specific surface area of the activated carbon is high because of its porosity. In particular, we can find micropores and mesopores, which differ in terms of their size. Micropores have a diameter smaller than 2 nm; mesopores have a diameter of between 2 and 50 nm; and we have mesopores; and beyond 50 nm they are macropores [LAR 09; CEZ 02; HAH 04; HAH 05]. The electrolyte is a salt dissolved in an organic solvent, which is often acetonitrile $(CH_3CH_2)_4NBF_4$. When a voltage is applied to the supercapacitor, a space of charge is formed at the two electrode/electrolyte interfaces (see Figure 4.3). At these two interfaces, there is an accumulation of electronic charge on the electrode side, and ionic charge on the electrolyte side. It is for this reason that supercapacitors are also known as electric double layer capacitors. The anions are negative ions drawn from the electrolyte under the influence of electrical polarization; they are 0.33 nm in size. As regards cations (positive ions) their size is 0.68 nm. Research has shown that at low frequencies, the capacitance depends on the activated carbon micropores.

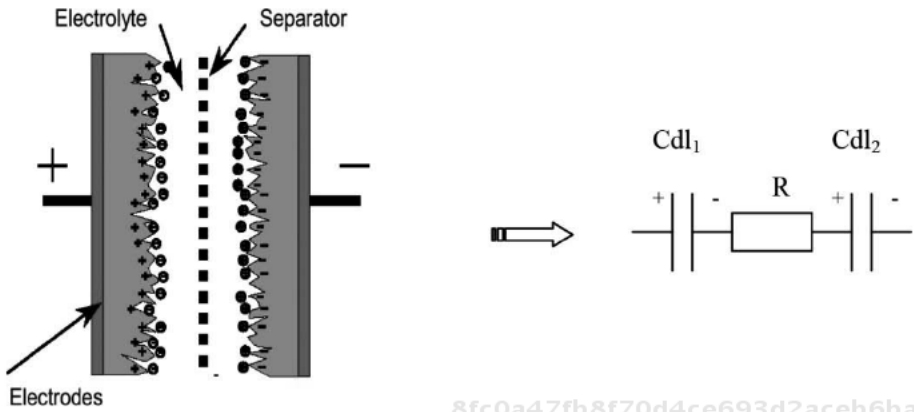

Figure 4.3. *Cross-sectional view of the structure of a supercapacitor*

Thus, we can consider the elementary structure of a supercapacitor as being two capacitors in series, separated by an equivalent resistance (see Figure 4.3).

4.2.2. *Electrical and energetic characterization of supercapacitors*

The supercapacitor can be characterized by a capacitance in series with a resistance. The capacitance represents its ability to store electrical energy. The series resistance represents the Joule losses. These losses cause the component's temperature to rise. The increase in temperature of the supercapacitor can degrade its energy performances and accelerate its aging.

The equivalent capacitance of a supercapacitor is calculated using the charge and discharge with a constant current (DC characterization) or by impedance spectroscopy (AC characterization). To determine the equivalent capacitance C and the equivalent series resistance R_1 during discharge in a DC regime, we use the IEC_62391 standard. This involves charging the supercapacitor at constant current and then at constant voltage (CC/CV). Once the supercapacitor has been charged to its maximum voltage, it remains polarized with an external voltage of 2.7 V for 30 minutes (see Figure 4.4).

When the supercapacitor is discharged at constant current, the equivalent series resistance causes a voltage drop at the beginning of discharge. Then, the voltage decreases due to the capacitive effect. Regarding the measurement of R_1, it is determined by the following expression: $R_1 = \frac{\Delta U_3}{I}$.

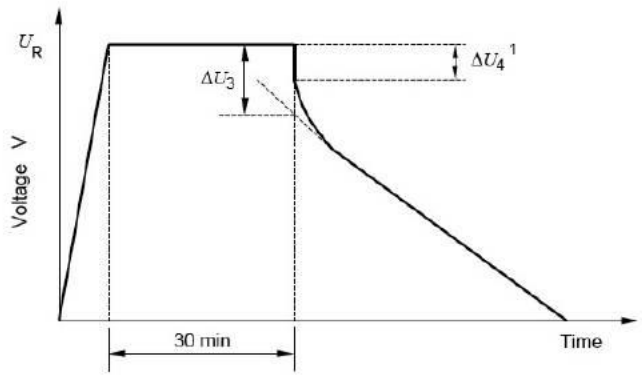

Figure 4.4. *Procedure for measuring the equivalent series resistance according to the IEC_62391 standard*

ΔU_3 is determined by the intersection between the tangent of the discharge curve at constant current and the vertical line originating at the start of the discharge (see Figure 4.4).

The equivalent capacitance is calculated using the following expression:

$C = \frac{I\Delta t}{\Delta U}$, where I is the discharge current; $\Delta t = t_2 - t_1$; $\Delta U = U_1 - U_2$; $U_1 = 80\% \times U_{max}$ and $U_2 = 40\% \times U_{max}$. U_{max} is the maximum voltage of the supercapacitor (2.7V). These parameters are represented in Figure 4.5.

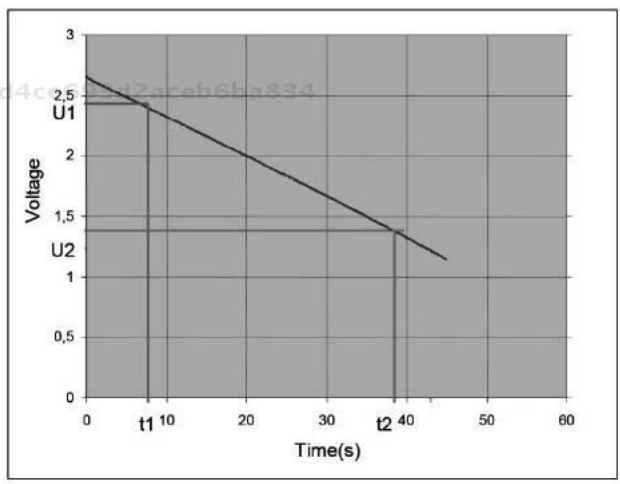

Figure 4.5. *Procedure for measuring the equivalent capacitance for discharge in accordance with the IEC_62391 standard*

Under alternating current (AC), the equivalent capacitance C and the equivalent series resistance R_1 depend on the frequency. Generally, these two parameters are determined by impedance spectroscopy. This technique enables us to measure the real part and the imaginary part of the supercapacitor's impedance. An initial approximation is to consider that R_1 is the real part of the impedance, and the equivalent capacitance C is calculated using the following expression [RAF 07; GUA 07]:

$$C = \frac{-1}{2\pi f \, \mathrm{Im}(Z)}$$

where $Im(Z)$ is the imaginary part of the impedance of the supercapacitor and f is the frequency.

In general, the frequency spectra are measured between 0.01 Hz and 1 kHz. Using a frequency spectrum, we can determine the physical origin of the impedances obtained.

The capacitance spectrum (see Figure 4.6) depends mainly on the properties of the activated carbon. The equivalent capacitance reaches its maximum value at very low frequency when there is time for the ions to reach the entire available surface on the carbon. If a large surface area is at the bottom of deep, narrow pores (micropores), the equivalent capacitance drops rapidly as the frequency increases.

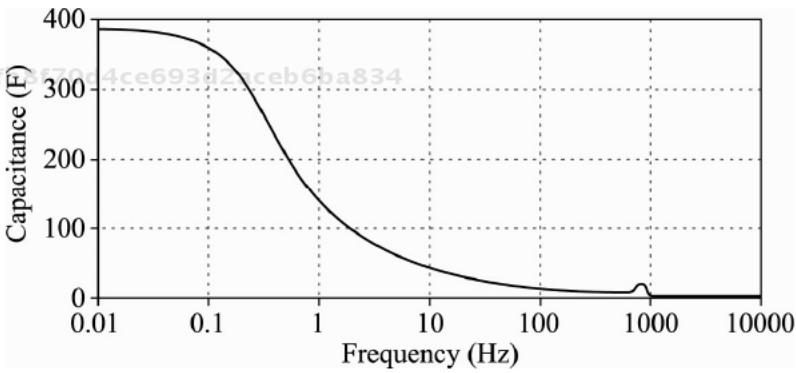

Figure 4.6. *Evolution of the capacitance of a 350 F cell as a function of the frequency*

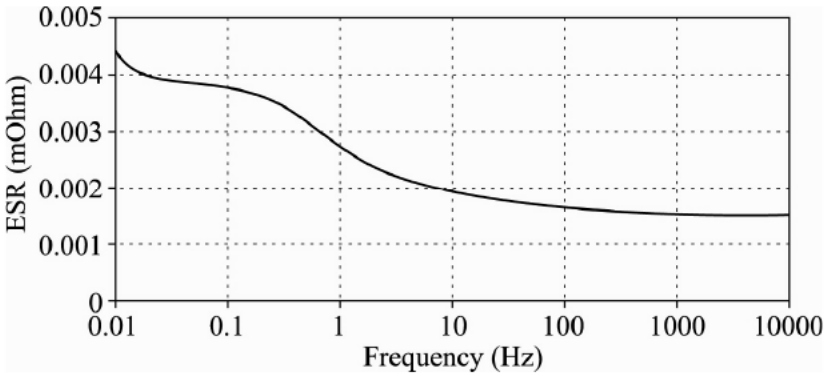

Figure 4.7. *Variation of the equivalent series resistance of a 350 F cell as a function of the frequency*

The equivalent series resistance of the supercapacitor (see Figure 4.7) can be decomposed into a number of components:

– the electronic resistance of the conductors and the collector;

– the contact resistance at the collector/carbon interface;

– the electronic resistance in the carbon;

– the ionic resistance in the electrolyte.

The Ohmic resistance in the activated carbon and the ionic resistance in the electrolyte form a parallel system which is in series with the other two sources of resistance. The data regarding the electrolyte are visible only at low frequency, in the domain of the millihertz. At higher frequency, the ions do not have the dynamic necessary to imitate the oscillations of the electrical field. As the ions are immobile, they do not dissipate energy, and therefore the ionic resistance is zero. At very high frequency, only the electronic part of the resistance can be seen. In the high-frequency domain, the measurement is skewed by the inductance of the measuring circuit. The series resistance due to the conductors is determined at high frequency – typically 1 kHz.

Figure 4.8 shows a significant variation of the capacitance on the basis of the voltage applied, at low frequency. In the case of a BCAP0350, the capacitance without a polarization component is 230 F. The K factor of variation of the nominal capacitance is 32 F/V.

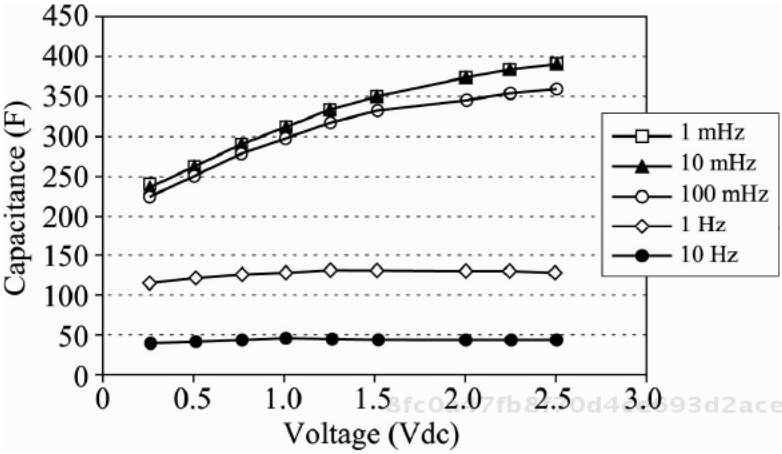

Figure 4.8. *Variation of the capacitance of a 350 F cell as a function of the voltage*

As regards the series resistance, its variation as a function of the voltage is slight.

In the case of a conventional capacitor, the capacitance is constant throughout the range of voltage, and is defined by the relation:

$$C = \frac{Q}{U} \qquad [4.2]$$

Q is the charge accumulated when the voltage applied to the capacitor is U.

For a supercapacitor, it is generally charged and discharged between its nominal voltage U_n and half of that voltage $U_n/2$. In this range of operation, we can assimilate the variation in capacitance with voltage to a linear variation. The equivalent capacitance C_1 is given by the following relation:

$$C_1(U) = C_0 + K \cdot U \qquad [4.3]$$

where C_0 is the value of the capacitance when the voltage is zero. The current of the capacitor is always given by the following relation:

$$i = \frac{dQ}{dt}$$

In view of the capacitance's dependence on the voltage, the relation between the current and the voltage becomes:

$$i(t) = (C_o + 2 \cdot K \cdot |U|) \frac{dU}{dt} \quad [4.4]$$

Similarly to the case of the capacitor, a differential capacitance C_{di} can be defined to calculate the relation between the current and the voltage, for a given polarization voltage:

$$C_{di} = C_o + 2 \cdot K \cdot |U| \quad [4.5]$$

Manufacturers define a capacitance C_n, which corresponds to the average value of the differential capacitance C_{di} in the range of voltage between the nominal voltage U_n and half of that value $U_n/2$:

$$C_n = C_o + \frac{3}{2} \cdot K \cdot |U_n| \quad [4.6]$$

This relation shows that the value of the "nominal" capacitance is higher when the nominal voltage is greater too. Thus, for a supercapacitor, two capacitances can be distinguished: a charge capacitance, and a differential capacitance linking the current to the charge voltage.

The energy E stored in a supercapacitor is given by the following expression:

$$E = \int (C_0 + 2 \cdot K \cdot U) U dU = \int (C_0 U + 2 \cdot K \cdot U^2) dU$$
$$= \frac{1}{2} C_0 U^2 + \frac{2}{3} \cdot K \cdot U^3 = \frac{1}{2} (C_0 + \frac{4}{3} \cdot K \cdot U) U^2$$

If we compare this expression with that of the energy of a capacitor (1/2 CU^2), we can define an energy capacitance for the supercapacitor by:

$$C_E = C_o + \frac{4}{3} \cdot K \cdot U \quad [4.7]$$

4.3. Supercapacitor module sizing

The sizing of a supercapacitor module consists of determining the number of elementary cells needing to be connected in a series and/or in parallel to satisfy the

technical specifications. The design needs to take account of the maximum power and the energy needed to serve the requirements of the intended application.

Generally, a supercapacitor module is designed to provide a large amount of power for a very limited period of time (typically less than ten seconds). We can study the problem in two different, but closely linked, ways. The first is based on the power and the second uses the stored energy.

4.3.1. *Power-based design*

A supercapacitor module is sized according to a set of specifications established on the basis of the power required and the duration for which the module provides the power. The design method is illustrated in Figure 4.9. This method consists of:

– setting the levels of the nominal voltages and currents;

– determining the total capacitance of the supercapacitor module to be used;

– determining the number of elements needing to be connected in a series and/or in parallel.

We define the following parameters:

– P the power prescribed by the technical specifications;

– Δt the time for which the supercapacitor module provides the required power (discharge time);

– $U_{M\max}$: maximum voltage of the supercapacitor module;

– $U_{M\min}$: minimum voltage of the supercapacitor module. In general, $U_{M\min} = U_{M\max}/2$, because the supercapacitor module discharges between $U_{M\max}$ and $U_{M\max}/2$. 75% of the stored electrical power is consumed;

– I: average discharge current of the supercapacitors;

– C_t: total capacitance of the supercapacitor module;

– R_1: total equivalent series resistance of the supercapacitors.

The total capacitance and the internal resistance R of the supercapacitor module are calculated on the basis of the number of cells connected in a series or in parallel. These two parameters are given by:

$$C_t = C\,(N_{\text{parallel}}/N_{\text{series}}) \text{ and } R = R_1\,(\mathrm{N}_{\text{series}}/\mathrm{N}_{\text{parallel}}),$$

where C and R_1 are respectively the capacitance and the series resistance of the supercapacitor cells used in the module, N_{series} the number of elements connected in series, and $N_{parallel}$ the number of elements in parallel.

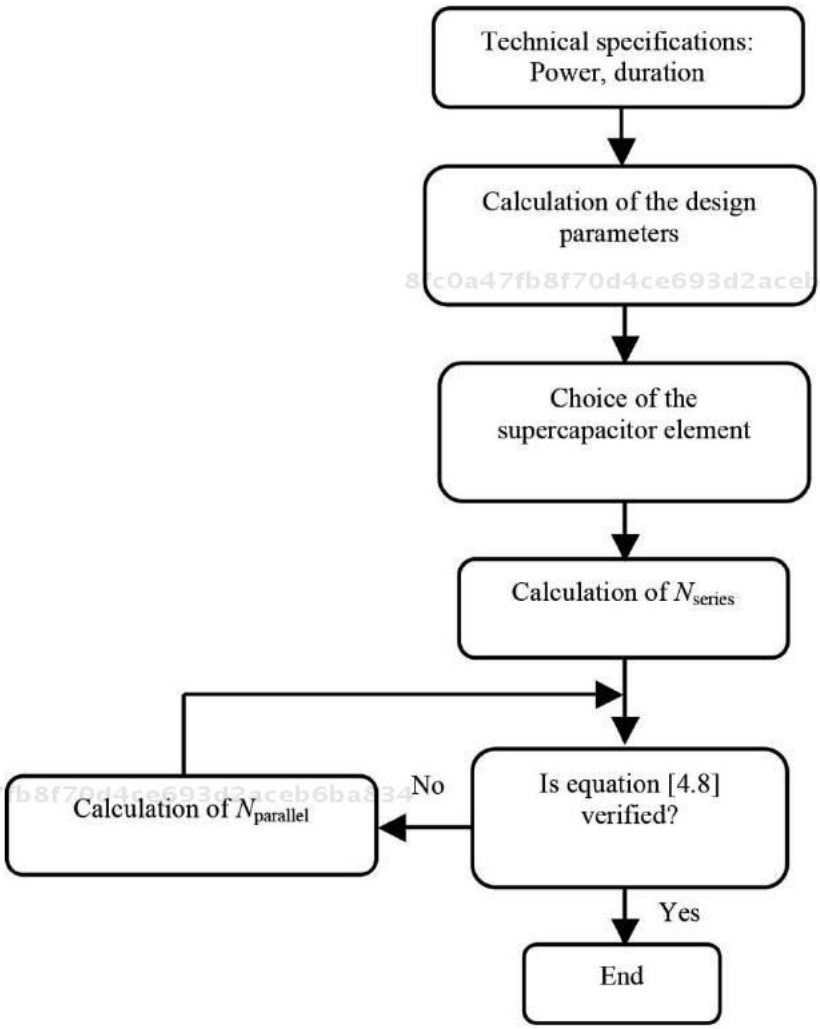

Figure 4.9. *Algorithm describing the sizing of a supercapacitor module on the basis of the power requirement*

In order to determine N_{series}, we need only divide the voltage U_{Mmax} needing to be achieved by the maximum voltage of which a supercapacitor element is capable, for given temperature profiles and a given duration of use.

The equation governing the change in voltage of the supercapacitor module is given by:

$$U_{M\max} - U_{M\min} = I\frac{\Delta t}{C_t} + RI \qquad [4.8]$$

To determine the average current I, we use the following expressions:

$I_{\max} = P/U_{M\min}$ and $I_{\min} = P/U_{M\max}$; $I = (I_{\max} + I_{\min})/2$.

4.3.2. *Dimension design based on the energy stored by the supercapacitor*

The number of supercapacitors needing to be connected in a series and/or in parallel is determined by the amount of energy, calculated on the basis of the technical specifications. The maximum voltage of a supercapacitor module is given by: $U_{M\max} = N_{series}U_{\max}$, and for activated carbon/organic electrolyte technology, $U_{\max} = 2.7$ V. This sizing method requires us to define the depth d of discharge (DOD) of the supercapacitors [SAI 04]. This value is given by the ratio of the minimum voltage of the supercapacitor module to the maximum voltage: $d = \frac{U_{M\min}}{U_{M\max}}$. In general, the supercapacitor module used is between U_{Mmax} and $U_{\mathrm{Mmin}} = U_{\mathrm{Mmax}}/2$. In this case, $d = 0.5$. The state of charge (SOC) is defined in the same way for a supercapacitor cell or a supercapacitor module. It is given by the amount of energy stored in the module. Thus, SOC = 1 (or 100%) if the module is completely charged, and SOC = 0 when it is charged at its minimum level.

Consider a supercapacitor module represented by its equivalent capacitance C_t. In this study, we shall limit ourselves to the expression of the stored energy $E = \frac{1}{2}C_tU^2$. Thus, the stored energy when the supercapacitor module is fully charged is given by the following expression: $E_{\max} = \frac{1}{2}C_tU_{M\max}^2$.

If the module is charged to any voltage U, the SOC of the supercapacitor module is given by $SOC = \frac{E}{E_{\max}} = \frac{U^2}{U_{M\max}^2}$. Obviously, this expression supposes that SOC = 0 when the supercapacitor module is fully discharged. This mode of operation is not realistic if the module is combined with a DC/DC converter, as is the case in numerous applications.

Above, we defined SOC = 0 when the module is charged to its minimum level. This minimum level is associated with a discharge depth denoted d [SAI 04].

$$SOC = \frac{1}{1-d^2}\left(\frac{E}{E_{\max}} - d^2\right) = \frac{1}{1-d^2}\left(\frac{U^2}{U_{M\max}^2} - d^2\right)$$

If $d = 0$, we see the same situation as before. If $d = 0.5$, then the SOC becomes $SOC = \frac{4}{3}\left(\frac{U^2}{U_{M\max}^2} - \frac{1}{4}\right)$.

Thus, we can conclude that the SOC of a supercapacitor module depends only on the voltage. It can therefore be determined simply by measuring U.

In order to design a supercapacitor module, we need to calculate the energy necessary for the application. Then, we have to set the depth of discharge d (generally $d = 0.5$). The next step is to determine the number of supercapacitors in a series and/or in parallel.

In a given application, the energy used is given by the following expression:

$$E_u = E_{\max} - E_{\min} = \frac{1}{2} C_t U_{M\max}^2 (1 - d^2).$$

If $d = 0.5$, the expression becomes:

$$E_u = \frac{3}{4}\left(\frac{1}{2} C_t U_{M\max}^2\right) = \frac{3}{4} E_{\max}.$$

The maximum power that the supercapacitor module can provide is calculated by using the impedance adaptation theorem. Its expression is given by the following relation:

$$P_{M\max} = \frac{U_{M\max}^2}{4R}, \text{ where } R = \frac{N_{series}}{N_{parallel}} R_1.$$

In a powerful electronic application, we generally use a voltage-boosting DC/DC converter between the supercapacitor module and a DC bus whose voltage is constant. Thus, the voltage $U_{M\min}$ (and consequently $U_{M\max}$) can be determined on

the basis of the boost ratio of the DC/DC converter. Let us consider the following example.

The voltage of the DC bus is set at 400 V (this is approximately the voltage used for the DC bus in an electric or hybrid vehicle). We consider a conventional or interlinked DC/DC voltage booster, with a maximum boost ratio of around 4. $U_{M\min}$ is given by:

$$U_{M\min} = (400/4) = 100 \text{ V}.$$

When $U_{\max} = 2.7$ V, we get $N_{series} = 100/2.7 = 37$ elementary cells in series. The number connected in parallel is determined by the energy E_u and the maximum power P_{max}.

$$E_u = \frac{1}{2} C_t U_{M\max}^2 (1 - d^2) \Rightarrow C_t = \frac{N_{parallel}}{N_{series}} C = \frac{2E_u}{(1 - d^2) U_{M\max}^2}$$

If we know N_{series} and $U_{M\max}$, and set values for d and C, we can calculate $N_{parallel}$.

NOTE 4.1.– The dimension design is done by choosing values such as d, $U_{M\max}$ and C. It is necessary to verify after this design stage whether or not the technical specifications are fulfilled. If not, we need to alter the choice of the aforementioned parameters. C and ESR are taken from the catalogs of the supercapacitor manufacturers. As yet, no standardized values have been published.

The analysis and research done on the behavior of supercapacitors when they are combined show the need for a balancing circuit so as to evenly distribute the voltage to each cell. For this reason, the various manufacturers offer two types of balancing circuits: passive and active.

4.3.3. *Balancing the supercapacitors*

The passive balancing circuit is the simplest to implement. It comprises a parallel resistance on each supercapacitor cell in a module. The value of the balancing resistance is determined by the ratio of the nominal voltage of the supercapacitor to the current we wish to divert by that resistance. The ideal is to divert the charge current of the supercapacitor module, which is usually strong (> 100 A) for transport applications. This poses a problem for the dimension design of the resistance. In addition, the parallel connection of the balancing resistance with a supercapacitor cell increases the current leaked from it. If we adopt this balancing solution, we need to make a compromise between the dimensions of the resistance, its cost and the

diverted current. In general, we choose a diverted current of a few amperes in strength.

The active balance circuit is more complex than the passive circuit. It generally comprises an electronic power circuit, placed in parallel with the supercapacitor. It is able to divert the current when the voltage of the supercapacitor is in the vicinity of the maximum acceptable voltage. The main drawback to this circuit is its very high cost (practically as much as the supercapacitor itself).

There is another weak-current active balancing circuit to compensate losses due to the leakage current. The cost of this circuit is very small in comparison to those discussed above. The circuit is placed between two supercapacitors. If there are N supercapacitor cells, we need N-1 balancing circuits. A diagrammatic representation of it is given in Figure 4.8. The principle of operation of this circuit is based on the comparison of the voltage of the two supercapacitor cells; the output signal from the comparison engine controls the auxiliary transistors, Q_1 and Q_2, thereby enabling us to divert the current from one cell to another. However, total diversion of the charge current is very costly, given its relatively high value (a few dozen to a hundred amperes). In general, the current diverted is no greater than a few amperes so as to reduce the cost of the balancing circuit.

The principle of use of this circuit is given in Figure 4.10. We consider a module of 5 supercapacitors in a series, for instance, respectively labeled A, B, C, D and E. Each group of two consecutive cells is balanced by a circuit. The advantage to this circuit is mainly its low cost, because it is made of weak-current electronics [GUA 07].

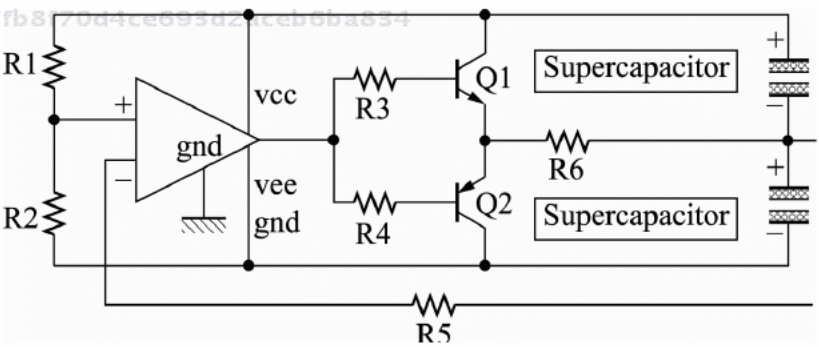

Figure 4.10. *Diagram of the principle behind an active balancing circuit*

In conclusion, balancing is absolutely crucial in a supercapacitor module. It may be passive or active. The first device is simple and less expensive, but it increases the current leakage by the supercapacitor. The second solution is more appropriate, and its effectiveness is linked to the current which is diverted. The greater this current, the better the performance of the balancing circuit will be.

4.4. Supercapacitor modeling

Supercapacitor modeling enables us to predict their behavior in different applications, on the basis of a representation of the main physical phenomena occurring in the component. There are many different models for supercapacitors (two-branch model, model based on a transmission line, single-pore model, multi-pore model, etc.) [BEL 01; HAM 06]. These models are in the form of equivalent electrical circuits. Using them, we can describe the supercapacitor's behavior quite accurately.

The impedance of a porous electrode has been studied by de Levie [DEL 67]. Frequency dependency is primarily caused by the dynamics of the ions in the electrolyte. At high frequency, the ions do not have the time to reach the difficult-to-access surfaces, located deep in the pores. This results in a decrease of the capacitance and the series resistance with increasing frequency.

The equivalent model used to describe this dependency is the transmission line shown in Figure 4.11. All the pores with depth (height) h and radius r are uniformly distributed along a transmission cable with lineic resistance R and lineic capacitance C. The impedance of the transmission line is given by:

$$Z(\omega) = R_W \frac{\coth\sqrt{j\omega R_W C}}{\sqrt{j\omega R_W C}}$$

where $R_W = \dfrac{h}{3\pi r^2 n\kappa}$

κ is the conductivity of the electrolyte, C the low-frequency capacitance of a pore, n the number of pores, h their height and r their radius. This model does not take account of the variation of the capacitance with the voltage.

Experience shows us that a simplified model [BON 07; BON 08; MAR 04a] is able to describe fairly accurately the electrical behavior of a supercapacitor. This model is made up of two branches (see Figure 4.12):

– the first branch, R_1C_1, called the main branch, represents the evolution of the energy during the charge or discharge of the supercapacitor (rapidly stored energy).

The capacitance C_1 is made up of a constant capacitance and a capacitance which is proportional to the voltage;

– the second branch, R_2C_2, called the slow branch, describes the internal redistribution of the charges and the leakage current.

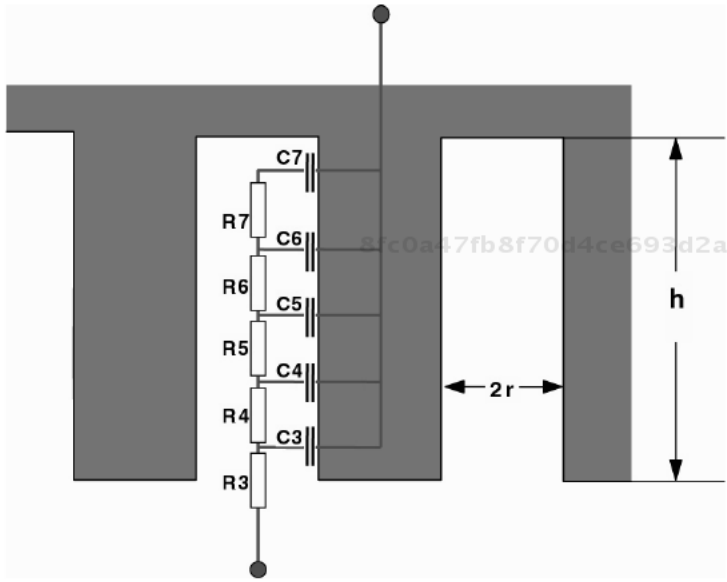

Figure 4.11. *Diagram of the principle behind a supercapacitor*

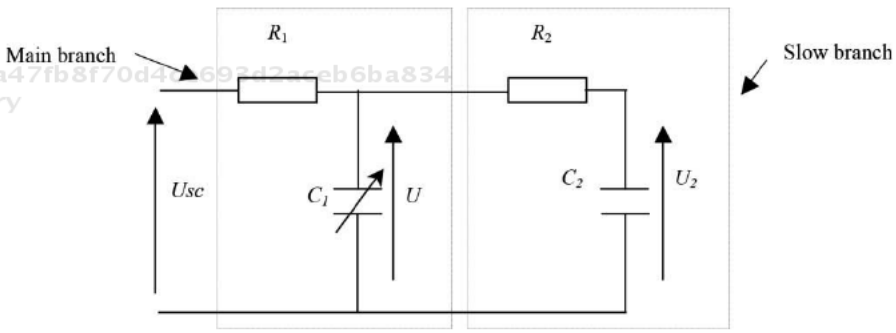

Figure 4.12. *Equivalent electrical circuit of a supercapacitor*

The two-branch model of the supercapacitor may be presented with a third branch, made up of an inductance and a parallel resistance which represents the leakage current.

The variation of the capacitance as a function of the voltage has its origin in the physical structure of the supercapacitor. Indeed, it comprises two capacitances connected in a series (hence the name "double layer"). Each capacitance, located at the interface between each of the electrodes and the electrolyte, is itself composed of two elements connected in a series:

– In the electrolyte near to the surface of the interface, the capacitance of the Helmholtz layer is due to the Coulomb interaction between the ions from the electrolyte and the electronic charges from the electrode. Conventionally, the increase in capacitance with increasing voltage is interpreted as being due to the increase in the dielectric constant of the electrolyte, or alternatively, to the decrease in the distance separating the charges.

– Within the electrode, the space charge is created by the movement of charges in the conductor. This charge movement is responsible for an electronic capacitance, which increases with the density of the electronic states. This latter increases with the energy of the electrons in the conductor, or in other words, it increases with the voltage.

The parameters for the slow branch are linked to the internal redistribution of the stored charge between the main branch and the slow branch. During this phase, the equivalent diagram of the supercapacitor is presented as shown in Figure 4.13.

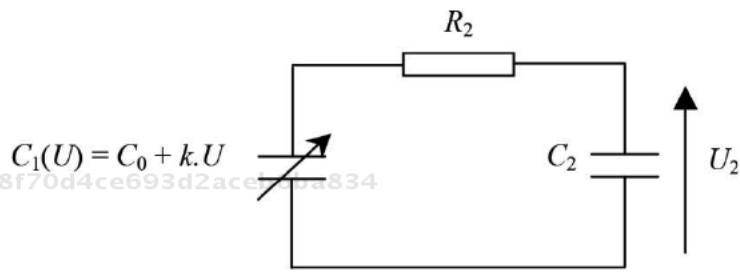

Figure 4.13. *Electric equivalent circuit of the supercapacitor during the phase of redistribution of the internal charges*

During this phase, the voltage of C_1 is equal to the voltage of the supercapacitor; hence, it is measurable. In this case, the initial conditions are written thus:

– for the capacitance C_1: $U(0) = U_f$, with U_f being the final voltage of the supercapacitor at the end of the charge period;

– for the capacitance C_2: $U_2(0) = 0$; this is the consequence of a slow branch that is supposed to be inactive during the charging phase.

The procedure for identifying the parameters of the two-branch model of a supercapacitor is based on the analysis of the variation of the voltage of the supercapacitor. During the phase of charge, it is the parameters of the main branch that are identified. When charging is completed, the internal redistribution of the energy of the component enables us to determine the parameters of the slow branch. This procedure is viable if we hypothesize that the time constants are far apart ($R_2.C_2 >> R_1.C_1$), to prevent the slow branch from influencing the charge cycle.

These parameters are determined experimentally on the basis of the charge and discharge of the supercapacitors at constant current. Generally we use a testing array based on a current-regulated buck converter (see Figure 4.14) [MAR 04a].

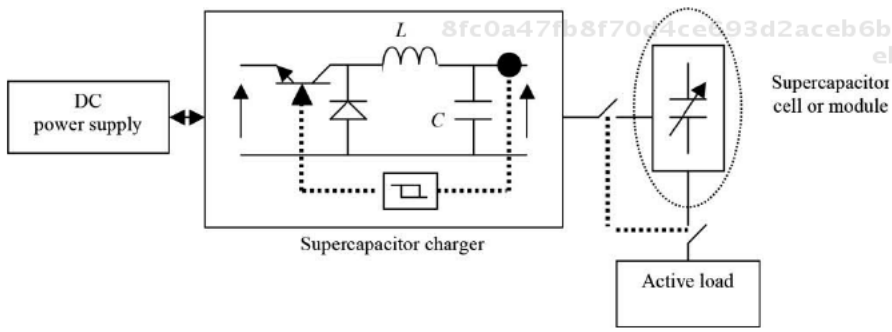

Figure 4.14. *Diagram of the principle behind a constant current charge/discharge of supercapacitor*

– Main branch parameters

The parameters of the main branch are identified from the component's voltage response during the charge/discharge phase at constant current. The slow branch is assumed to be inactive ($R_2C_2 >> R_1C_1$).

The resistance R_1 is determined on the basis of the initial variation in voltage, and C_0 and KU respectively on the basis of the initial slope of the voltage response and the stored charge.

Identification of R_1:

The start of the charge cycle at constant current results in a voltage step due to the series resistance of the supercapacitor (see Figure 4.15):

$$\Delta U = R_1.I$$

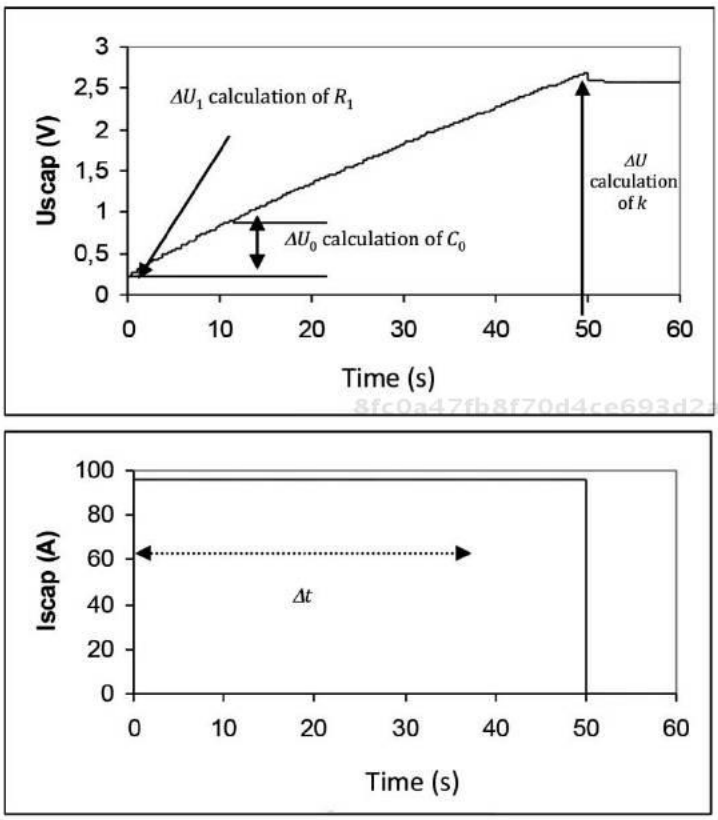

Figure 4.15. *Diagram of the principle used to identify the parameters of the main branch*

Identification of C_0:

This relation enables us to deduce the value of C_0 from the slope at the start of the charge cycle (Figure 4.15).

This gives us:

$$C0 = \frac{I}{\frac{dU}{dt}(0)}$$

In practice, we approximate the initial slope of U with a slope $\frac{\Delta U0}{\Delta t0}$, which we choose as being in the immediate vicinity of the starting instant (see Figure 4.15).

Identification of K:

The expression $dQ_t = I.dt$ and its integration over the whole of the duration of the charge cycle Δt, enable us to establish the expressions of the total stored charge Q_t.

$$Q_t = I.\Delta t \text{ and } Q_t = \int_0^{\Delta U} C_1 dU$$

Using these expressions and noting that ΔU is the total voltage rise of the supercapacitor, we obtain the following expression for total stored charge Q_t:

$$Qt = C_0.\Delta U + \frac{1}{2}.K.\Delta U^2$$

From these equations, we can deduce the expression of K:

$$K = \frac{2}{\Delta U^2}\left(I.\Delta t - C_0.\Delta U\right)$$

– Slow branch parameters

Once the charge cycle is complete, an internal redistribution of the stored charge between the main branch and the slow branch occurs. During this phase, the electric equivalent circuit of the supercapacitor is given by Figure 4.13.

Identification of R_2:

The initial current $i(0)$ is given by:

$$i(0) = \frac{U_f}{R_2}$$

$$i(0) = -C_1.\frac{dU_1}{dt}(0)$$

For the calculation of R_2 (Figure 4.16), we approximate the initial slope observed on U_{scap} by a quantity $\frac{\Delta U_2}{\Delta t_2}$, and adjust the terms $i(0)$ and C_1 for the median level of voltage, i.e. $U_f - \frac{\Delta U_2}{2}$. Then, R_2 can be expressed as:

$$R_2 = \frac{U_f - \frac{\Delta U_2}{2}}{C_1} \cdot \frac{\Delta t_2}{\Delta U_2}$$

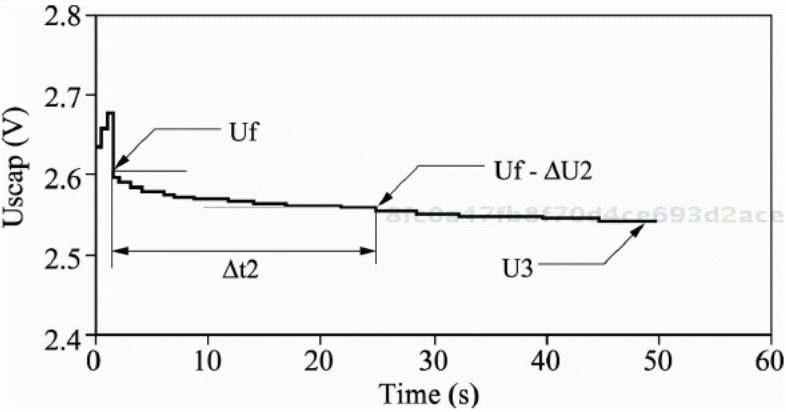

Figure 4.16. *Equivalent model during the redistribution phase*

Identification of C_2:

The capacitance C_2 is calculated at the end of the charge redistribution phase, or to be more precise, when the voltage at the edges of the component is no longer changing except for gradually – that is, just before the discharge cycle. The voltages U and U_2 at the edges of the capacitances C_1 and C_2 are therefore supposed to be equal to a voltage denoted as U_3. The stored-charge conservation equation means that we can establish the expression of C_2 as a function of Q_t and U_3. C_2 is determined by the following relation:

$$C_2 = \frac{Qt}{U_3} - \left(C_O + \frac{1}{2}.k.U_3 \right)$$

This identification procedure, based on the experimental analysis of the variation in voltage at the edges of supercapacitor, can be applied to identify the parameters of one or more cells. We can also use this method to identify the parameters of a module of supercapacitors connected in a series and/or in parallel. Thus, a supercapacitor module (irrespective of the number of cells used) can be modeled by a simple RC circuit.

4.5. DC/DC converter associated with a supercapacitor module

In numerous applications, DC/DC converters must be inserted between the supercapacitor and the load [CAM 07]. The dimension design of a DC/DC converter requires knowledge of the values of current in the coil and the input and output voltages. Generally, the switching transistor and its dissipater are designed on the basis of the voltage current and the frequency of the control signal. With a very high voltage, greater than 100 V, it is advisable to use IGBTs (Insulated Gate Bipolar Transistors); in the opposite case, MOSFETs (Metal-Oxide-Semiconductor Field-Effect Transistors) are better adapted.

Figure 4.17 illustrates the structure of a buck/boost DC/DC converter whose parameters are:

– U_{scap} – the voltage of the supercapacitor module;

– K_1 and K_2 – the IGBT switching transistors;

– PWM_1 and PWM_2 – the control signals for the two transistors;

– L – the current-smoothing coil;

– U_{bus} – the voltage of the DC bus (DC bus);

– C – the capacitance of filtering of the voltage of the DC bus.

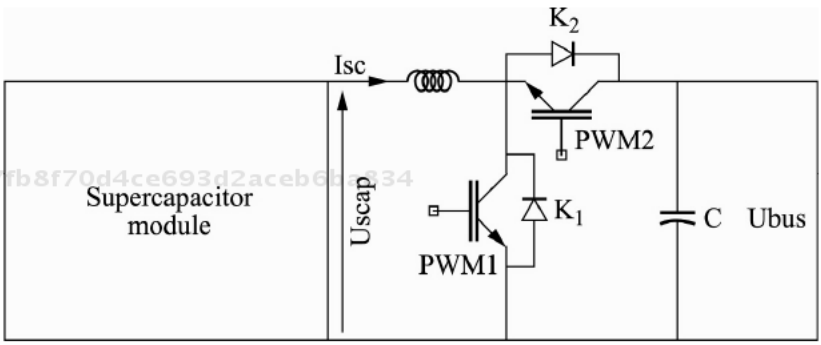

Figure 4.17. *Structure of the reversible buck/boost converter*

The capacitance C is used to filter the fluctuations in voltage due to the splitting of the converter. Similarly, the role of the inductor is to limit the fluctuations in current.

When the supercapacitors are supplying power, the converter operates in voltage booster mode. Consider a control signal with cyclical ratio α and period T. The

frequency of the control signal (PWM) is limited essentially by the type of switching transistor used.

4.6. Thermal behavior of supercapacitors

Temperature causes the aging, deterioration and destruction of most electronic and electrotechnical devices. Indeed, the operation of high-power components or electronic systems causes the heat production that is often linked to the Joule effect. The lower the possibility of evacuating this heat from the site where it is produced to the external environment, the higher the temperatures will be. This leads to the device's premature aging or the decrease in its performances. Therefore, it is important to know the way in which heat exchanges take place across interfaces which are more or less conductive of heat. The objective is to be better able to dissipate this unwanted heat.

In the case of supercapacitors, heat production is linked mainly to the Joule losses relating to the equivalent series resistance. Indeed, supercapacitor currents may be of the order of 400 A or more depending on the type and technology used, even if the series resistance is very low (less than 1 mΩ). This leads to a drastic increase in the temperature of the supercapacitor with repeated charge/discharge cycles. This heating may lead to the following consequences:

– a deterioration of the supercapacitor's properties, which affects its reliability and its electrical performances;

– premature aging of the metallic contacts – indeed, repeated heating to excessive temperatures can soon damage the supercapacitor's connecting engineering;

– reversible alternation of the supercapacitor's characteristics;

– evaporation of the electrolyte and therefore breakdown of the supercapacitor if the temperature goes beyond a certain critical value (around 70–80°C in operation), etc.

It is therefore necessary to study and model the thermal behavior of supercapacitors. The aims are:

– to gain a better knowledge of the temperature distribution inside and at the surface of a cell (hot points, etc.);

– quantification of the average temperature rise as a function of the power dissipated;

– thermal management of the supercapacitor modules;

– cooling of the supercapacitor modules.

It is therefore important to be familiar with and to understand the thermal behavior of supercapacitors, for a cell and for a module. This involves estimating the maximum temperature rise in time and space.

4.6.1. *Thermal modeling of supercapacitors*

From a physical point of view, heat transfer has its origins in temperature differences. Thus, a transfer of energy in the form of heat occurs any time that a temperature gradient exists within a system, or when two systems at different temperatures come into contact. There are three modes of heat transfer for a supercapacitor: heat conduction, heat convection and radiation. Inside the supercapacitor, conduction is the dominant mode of heat transfer; therefore, to begin with, we can discount the other two modes of heat transfer. However, it is helpful to take account of convective heat transfer between the ambient air and the outer surface of the supercapacitor.

For optimal design of the supercapacitor and its cooling system, when dealing with an assembly of many cells, it is important to know the change in temperature over time and space. For this purpose, we need to solve the heat balance equation. In the case of a cylindrical supercapacitor, we use the cylindrical coordinates. This equation is given by the following expression:

$$\lambda\frac{\partial^2 T(r,\varphi,z,t)}{\partial r^2}+\frac{\lambda}{r}\frac{\partial T(r,\varphi,z,t)}{\partial r}+\lambda\frac{\partial^2 T(r,\varphi,z,t)}{\partial \varphi^2} + \lambda\frac{\partial^2 T(r,\varphi,z,t)}{\partial z^2}+\rho c_p\frac{\partial T(r,\varphi,z,t)}{\partial t}=P(t) \quad [4.9]$$

where λ is the heat conductivity expressed in W.m^{-1}.K^{-1}; T is the temperature; r, φ and z are the radius, angle and height of the cylinder; ρ and C_p respectively are the volumetric density and the calorific capacitance; and $P(t)$ is the total power dissipated in the supercapacitor. $P(t) = \text{ESR}.I^2(t)$, $\text{ESR} = R_1$ is the equivalent series resistance of the supercapacitor and $I(t)$ is the current running through it.

The temperature following the angle φ is assumed to be constant, and in view of the difficulty of solving the equation in the transitory regime, we consider only the operation in the permanent regime. This means there is zero variation in the temperature over time and P is constant. In these conditions, the heat equation is given by:

$$\lambda\frac{\partial^2 T(r,z)}{\partial r^2}+\frac{\lambda}{r}\frac{\partial T(r,z)}{\partial r}+\lambda\frac{\partial^2 T(r,z)}{\partial z^2}=P \quad [4.10]$$

To begin with, we can make the following hypothesis: the supercapacitor is made of a single material with thermal properties (heat conductivity, calorific capacitance, etc.) which are equivalent with account taken of the respective thicknesses of the materials. The solution to the system can be found numerically in the permanent regime. In these conditions, the calculation of the thermal resistance and thermal capacitance of supercapacitor is the same as that for a tube whose internal and external radii are respectively r_i and r_{i+1}, and whose length is L. The expression of these two values is given by [GUA 11]:

$$R_i = \frac{\ln\left(r_{i+1}/r_i\right)}{2\pi\lambda_i L}$$

$$C_i = \rho_i C_{p_i} \pi L\left(r_{i+1}^2 - r_i^2\right)$$

$\rho_i C_{p_i}$ represent the volumetric density and calorific capacitance, and r_i is the radius of the interface i.

We also need to determine the heat resistance (R_a) due to convective heat exchange between the outer surface and the ambient air.

Convection obeys Newton's law [GUA 11]: $P = h\,S\,\Delta T = \Delta T/R_a$, when $R_a = \frac{1}{hS}$.

Here, h is the coefficient of convective heat exchange with the air and S the surface area of the heat exchange.

It is extremely difficult to accurately know the thermal parameters of the layers of supercapacitors in order to be able to simulate their thermal behavior. Indeed, if we consider the activated carbon, for instance, of which the electrodes are made, its properties depend on the process of its manufacture and the quality of the materials. The values that are to be found in the existing body of literature vary sometimes across a broad range of values. This variation makes this study more complicated. For our purposes, we can make estimations based on the different existing values. In order to facilitate thermal examination, we generally model the thermal behavior of a supercapacitor by an equivalent electrical circuit comprising a branch R_{th} C_{th}. This modeling is relatively simple and can be implemented in electrical simulation software.

R_{th} and C_{th} are respectively the equivalent thermal resistance and the thermal capacitance of the supercapacitor. This supposes that the temperature of a supercapacitor is uniform. This hypothesis is valid in the permanent regime and if the resistance of the connection is very low. Indeed, if this resistance is high (in

comparison with the internal resistance of the supercapacitor), we can have a hot point at the electrical connection, In order to take account of this effect, it is advisable to represent the connecting elements with an equivalent thermal resistance.

4.6.2. *Modeling by thermal/electrical analogy*

Heat conduction in solids is similar to electricity conduction in electrical conductors. The passage of a current is linked to the difference in electrical potential. With thermal exchange, the presence of a heat flux is linked to a difference in temperature. Table 4.2 gives the analogy between electrical and thermal parameters, which enables us to represent the thermal model with an equivalent electric circuit. The advantage to this method lies in the reduction of the computation time compared to other modeling techniques [SAK 10].

Thermal parameters	Electrical parameters
Heat conductivity λ ($W.m^{-1}.K^{-1}$)	Electrical conductivity σ ($\Omega^{-1}.m^{-1}$)
Temperature T (K)	Electrical voltage (V)
Electrical current (A)	Power of thermal flux P (W)
Electrical resistance (Ω)	Thermal resistance ($K.W^{-1}$)
Electrical capacitance (F)	Thermal capacitance ($J.\ W^{-1}$)
Electrical charge (C)	Quantity of heat (J)

Table 4.2. *Electrical/thermal analogy*

Thus, the thermal model of a supercapacitor can be represented by a first-order electric circuit (Figure 4.18). The thermal resistance represents the resistance linked to heat conduction in the supercapacitor.

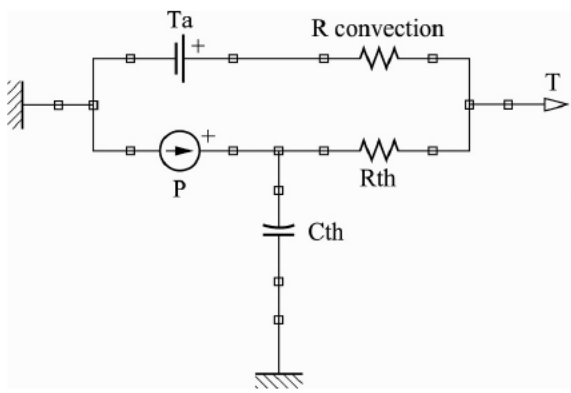

Figure 4.18. *Thermal model of a supercapacitor [SAK 10]*

$$P = C_{th}\frac{d\Delta T}{dt} + \frac{\Delta T}{R_{th}} \qquad [4.11]$$

The elements of the model are determined by experimental testing.

When the supercapacitor is heated with a constant level of power, its temperature increases until it reaches an equilibrium value T_∞. This value is defined when the power that it is receiving is equal to the power that it is giving off to the external environment. Thus we get the permanent regime.

In practice, the supercapacitor is charged/discharged at constant current and the temperature is measured at the surface of the supercapacitor. In the permanent regime, there are no temperature variations $\left(\frac{d\Delta T}{dt} = 0\right)$, and the temperature reaches T_∞. Equation [4.11] becomes $P = \frac{\Delta T}{R_{th}}$. If we know ΔT and P, we can calculate R_{th}. Below we outline the method to determine the time constant:

– plot the curve for the temperature at the surface of the supercapacitor over time when it is heated;

– plot a horizontal line whose ordinate is the final value of the temperature T_∞ of the supercapacitor;

– plot a straight line, beginning at the origin of the curve and tangent to the curve at that point;

– these two lines intersect at the abscissa value of time ($\tau = R_{\text{th}}\, C_{\text{th}}$), and at that abscissa, the value of the ordinate of the curve is:

$(1\text{-}e^{-1})\, T_\infty \approx 63\%\ T_\infty$.

Using the experimental results shown in Figure 4.19, we determine $\Delta T = T_\infty - T_a = 26.5 - 17.5 = 9°\text{C}$ (or 9 K because it is a difference or variation in temperature), the dissipated power is $P = \text{ESR}\ I^2$. To determine the thermal time constant $R_{\text{th}}\, C_{\text{th}}$, we use the transitory regime, as we do for an electrical RC circuit. When ESR = 0.39 mΩ and I = 75 A, we find R_{th} 4.2°C/W and C_{th} = 268 J/°C [SAK 10].

4.7. Hybrid electricity storage device: the LIC (Lithium Ion Capacitor)

R&D is currently under way to develop hybrid components for electrical energy storage. These hybrid devices need to combine a high energy density, a high power density and a long lifetime. The most advanced components at present are Lithium Ion Capacitors (LICs). The elementary structure of an LIC is composed of

an activated-carbon positive electrode, as is the case for supercapacitors, and a negative electrode of lithium-doped carbon, similar to that used in lithium batteries. Figure 4.20 gives an elementary representation of the LIC.

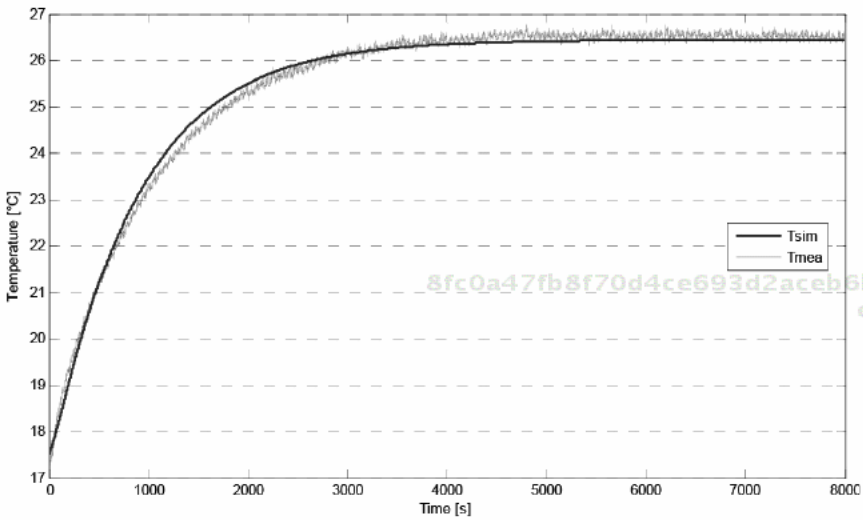

Figure 4.19. *Evolution of the temperature at the surface of a supercapacitor with capacitance of 1500 F*

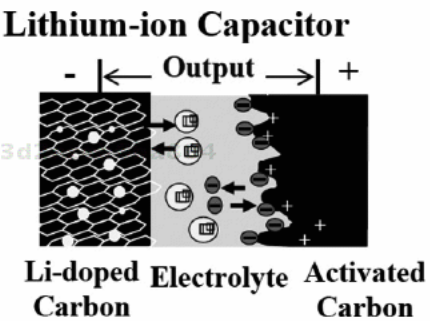

Figure 4.20. *Elementary diagram of an LIC*

The aim of this association (or hybridization) between a supercapacitor electrode and a lithium battery electrode is to obtain the performances of supercapacitors in terms of power density and lifetime, and those of a lithium battery in terms of energy density in a lone component. Experimentation shows that this association is complex, and generally when the power density increases, the energy density decreases. Therefore, we need to find a compromise or use different chemistry.

Figure 4.20 shows that the elementary structure of an LIC exhibits an equivalent capacitance made up of two capacitances in a series. The first is associated with the positive electrode, and is notated as C_{dl}. The second represents the capacitance of the negative electrode, denoted C_{li}. These two capacitances are connected in series, so the equivalent capacitance is given by the expression $\frac{1}{C_{eq}} = \frac{1}{C_{dl}} + \frac{1}{C_{li}}$.

The capacitance $C_{li} >> C_{dl} \Rightarrow C_{eq} \approx C_{dl}$.

This means that the charge and discharge of the LIC are primarily linked to the capacitance of the positive electrode. The LIC component operates between 3.8 and 2.2 V.

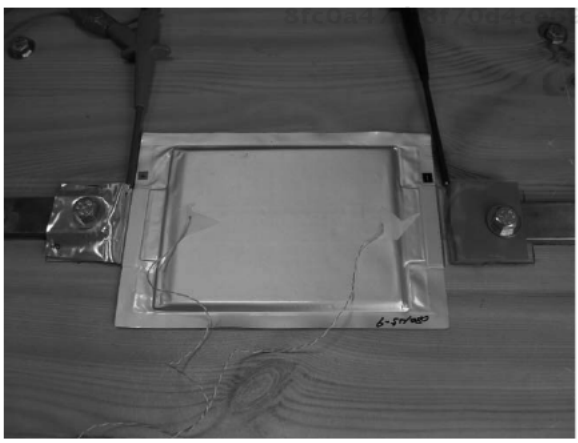

Figure 4.21. *Photograph of a 2000 F LIC*

4.8. Exercises – statements

Exercise 1:

Consider a supercapacitor with average capacitance $C = 3000$ F and series resistance $R_1 = 0.3$ mΩ.

1) Determine the energy that can be stored in that component in Joules and then in Watt hours;

2) This component is charged at constant current ($I_{ch} = 100$ A); determine the evolution of the voltage of the supercapacitor over time. Calculate the charge time when the voltage changes from 0 to 2.7 V, and when the component is charged between 1.35 and 2.7 V;

3) In the knowledge that the weight of this supercapacitor is 510 g, give its energy density.

Solution to Exercise 1:

1) To begin with, we consider that the capacitance is constant, and does not depend on the voltage. The energy in Joules that we can store is given by the following expression:

$$E = 1/2\ C\ U^2$$

Mathematical application:

$C = 3000$ F and $U = 2.7$ V;

we get $E = 0.5 \times 3000 \times 2.7 \times 2.7 = 10935$ J.

Given that 1 Wh = 3600 J, $E = 10935/3600 = 3.04$ Wh.

2) If the supercapacitor is equivalent to an ideal capacitor in a series with the equivalent series resistance, we can deduce that: the drop in voltage at the edges of the resistance $RI = 0.0003 \times 100 = 0.030$ V = 30 mV. With regard to the ideal capacitor, we have the following relation:

$$I = C\frac{dV}{dt} \Rightarrow \int_{Vi}^{Vf} dV = \int_{ti}^{tf} \frac{I}{C} dt;$$

however, the supercapacitor is charged at constant current, so we can deduce that:

$$V_f - V_i = \frac{I}{C}(t_f - t_i) \Rightarrow (t_f - t_i) = \Delta t = \frac{C(V_f - V_i)}{I}.$$

If we consider that $V_i = RI = 0.03$ V and $V_f = 2.7$ V, we obtain $(t_f - t_i) = \Delta t = 80.1$ s.

For $V_i = 1.35$ V and $V_f = 2.7$ V, we get $(t_f - t_i) = \Delta t = 40.5$ s.

3) The energy density is given: 3.03/0.510 = 5.96 Wh/kg.

Exercise 2:

Consider a supercapacitor module made up of 10 cells in a series. The capacitance of one cell is 3000 F, the series resistance is 0.3 mW and the maximum voltage is 2.7 V. Calculate:

1) the module's total capacitance;

2) its equivalent series resistance;

3) the total energy stored in the module between 0 V and its maximum voltage;

4) the energy stored when the module is charged between its maximum voltage and half that voltage.

Solution to Exercise 2:

1) The cells are connected in a series, so the total capacitance is $C_t = 3000/10 = 300$ F.

2) The equivalent series resistance of the module is ESR $= 10 \times 0.3 = 3$ mΩ.

3) The total energy stored in the module is $E = ½ \times C_t \times U^2$, when $U = 10 \times 2.7 = 27$ V. We find $E = 0.5 \times 300 \times 27 \times 27 = 109350$ J $= 30.375$ Wh.

4) If the module is charged between U and $U/2$, we get:

$\Delta E = ½ \times C_t \times U^2 - ½ \times C_t \times (U/2)^2 = 109350 - 27337.5 = 82012.5$ J $= 22.78$ Wh.

It may be remarked upon that when the module is operating between U and $U/2$, 75% of the maximum energy is used.

Exercise 3:

For a supercapacitor of average capacitance $C = 2000$ F, with equivalent series resistance $R_1 = 0.35$ mΩ, its thermal resistance is $R_{th} = 3.8$°C/W, and its thermal capacitance is $C_{th} = 410$ J/°C. The operating temperature is given by the manufacturer: $T_{max} = 65$°C and $T_{min} = -40$°C.

We know that the temperature of a supercapacitor is considered to be uniform, and the ambient temperature is around 25°C.

Calculate the variation in the supercapacitor's temperature in the permanent regime when it is charged and discharged at constant current (50 A, 100 A, 150 A).

Solution to Exercise 3:

1) The charge/discharge at constant current I causes a change in the supercapacitor's temperature $\Delta T = R_{th} P$ (see section 4.5.2).

$I = 50$ A; $P = 0.35\ 10^{-3} \times 50 \times 50 = 0.875$ W; $\Delta T = 3.8 \times 0.875 = 3.5$°C.
$I = 100$ A; $P = 0.35\ 10^{-3} \times 100 \times 100 = 3.5$ W; $\Delta T = 3.8 \times 3.5 = 13.3$°C.
$I = 150$ A; $P = 0.35 \times 10^{-3} \times 150 \times 150 = 5.25$ W; $\Delta T = 3.8 \times 5.25 = 19.95$°C.

Exercise 4:

The diagram (Figure 4.22) below represents a supercapacitor module. An elementary cell is a supercapacitor with capacitance $C = 1500$ F and series resistance $R_1 = 0.47$ mΩ. The maximum voltage of the supercapacitor is 2.7 V.

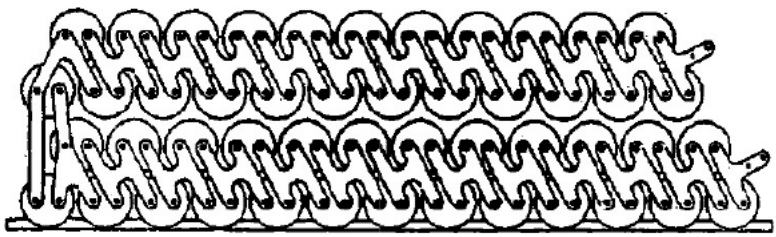

Figure 4.22. *Layout of a supercapacitor module*

1) Calculate the total capacitance and the equivalent resistance of the module; we neglect the resistance of the cables connecting the different supercapacitors;

2) Calculate the voltage at the edges of the module when the supercapacitors are fully charged.

Solution to Exercise 4:

1) The diagram of the setup shows that we can distinguish 48 supercapacitors, 24 of which are connected in a series in two parallel elements. By applying the course, we get $N_{\text{series}} = 24$ and $N_{\text{parallel}} = 2$.

The equivalent capacitance of this module is:

$$Ct = 1500 \times N_{parallel} / N_{series} = 1500 \times 2/24 = 125 \text{ F}.$$

The equivalent resistance of the module

$$R = R_1(N_{series}/N_{parallel}) = 0.47 \times (24/2) = 5.64 \text{ m}\Omega.$$

2) When the module is fully charged:

$$U_{module} = N_{series} \times U = 24 \times 2.7 = 64.8 \text{ V}.$$

Exercise 5:

We wish to fire up a vehicle with a combustion engine using a supercapacitor module. The characteristics of the engine are:

– Startup resistance torque of around 200 N.m, minimum startup speed 150 rpm, maximum startup voltage 13.5 V, and startup time < 2 s.

With a mechanical reduction of around 3 between the starter motor and the combustion engine, calculate:

1) the torque of the starter motor;

2) the speed at the beginning of startup.

Using the relation $P_u = C_{start}.\omega$, where P_u is the useable electric power which we need to start the combustion engine and ω is the angular velocity of the electric motor, calculate ω and P_u.

3) Give the dimensions for the supercapacitor module needed to fire the combustion engine with a voltage between 13.5 and 12 V.

4) Give the weight of the supercapacitor module.

Solution to Exercise 5:

1) The torque of the starter motor is: $C_{start} = 200/3 = 66.67$ N.m.

2) The speed of the starter motor is: $150 \times 3 = 450$ rpmn.

3) Using the relation $P_u = C_{start}.\omega$, where $\omega = 450 \times 2\pi/60 = 47$ rad/s, we get $P_u = 66.67 \times 47 = 3133$ W. If we take account of the losses in the device, the power of the supercapacitor module feeding the starter motor needs to be greater than 3133 W.

4) With a voltage of 13.5 V, we get a current $I_{min} = P_u/U = 3133/13.5 = 232.07$ A, and for a voltage of 12 V, $I_{max} = Pu/U = 3133/12 = 261.08$ A. The average current required is therefore $I = (I_{max} + I_{min})/2 = 246.58$ A. Using these data and the dimension design methodology presented in this chapter, we obtain a supercapacitor module with the following characteristics:

If we have 13.5 V $\Rightarrow N_{series} = 13.5/2.7 = 5$;
If we have 12 V $\Rightarrow N_{series} = 12/2.7 = 4.4$;

In both cases, we have 5 supercapacitor cells with voltage 2.7 V, each in a series.

In the knowledge that the startup current is 246.58 A, we need to choose cells whose electrical series resistance (ESR) is as low as possible. We set $\Delta U = 13.5 - 12 = 1.5$ V, meaning that the combustion engine can start up with a voltage between 13.5 and 12 V.

The dimension design relation is:

$$C_t = (I \times \Delta t)/(\Delta U - N_{series} \times I \times R_1).$$

If we choose cells of 3000 F with $R_1 = 0.3$ mΩ. We get:

$$C_t = (246.58 \times 2)/(1.5 - 0.0003 \times 5 \times 246.58) = 436 \text{ F}.$$

The choice of 5 serially-connected cells with 3000 F gives us a total capacitance of 3000/5 = 600F. We can therefore conclude that the module designed satisfies the technical specifications, because $C_t = 436$ F < 600 F.

If we choose 2000 F cells with $R_1 = 0.35$ mW, we get:

$$C_t = (246.58 \times 2)/(1.5 - 0.00035 \times 5 \times 246.58) = 461 \text{ F}.$$

The choice of 5 serially-connected cells with 2000 F gives us a total capacitance of 2000/5 = 400 F. We can therefore conclude that the module is insufficient, because $C_t = 461 > 400$ F.

5) The weight of the module chosen is: 5 × 510 g = 2.55 kg. The fact of firing the combustion engine with a supercapacitor module enables us to use considerably less power and hence a less cumbersome battery.

Exercise 6:

Consider an electric vehicle using a fuel cell and supercapacitors. These supply power in the transitory regime. The supercapacitor module has to provide 50 kW for a duration of 15 s. The power of the cell is around 40 kW. The supercapacitor module is connected to a DC/DC boost converter, whose boost ratio is 4 at most; the voltage of the DC bus on output from the converter is fixed at 400 V (see Figure 4.17). The supercapacitor module is used between its maximum voltage and half of that voltage.

1) Give the dimensions for the supercapacitor module.

2) Give the dimensions for the DC/DC converter with the following parameters: the current fluctuation is 5% maximum, the fluctuation of the voltage of the DC bus is around 1%, and the switching frequency is 20 kHz.

Solution to Exercise 6:

1) The supercapacitor module provides 50 kW for 15 s. There is no mathematical method for setting the voltage of the supercapacitor module. Therefore, we need to make a choice which takes account of the constraints imposed by the technical specifications. The voltage of the bus is 400 V, so with a boost ratio of 4, the minimum voltage for the supercapacitor module is 400/4 = 100 V. In order to deal with the drops in voltage at the edges of the switches, the minimum voltage needs to be > 100 V. We choose a minimum voltage of 135 V. The module operates between $U_{\min} = 135$ V and $U_{\max} = 2 \times U_{\min} = 270$ V. The number of serially-connected supercapacitors is $N_{\text{series}} = 270/2.7 = 100$. We need to determine N_{parallel} and the value of the module's capacitance.

With a voltage of 270 V, we obtain $I_{\min} = 50000/270 = 185.18$ A. For a voltage of 135 V, $I_{\max} = 370.37$. The average value of the current $I = (185.18 + 370.37)/2 = 277.77$ A.

The total capacitance is calculated on the basis of the expression (equation [4.8]):

$$U_{M\max} - U_{M\min} = I\frac{\Delta t}{C_t} + RI \Rightarrow C_t = \frac{I\Delta t}{((U_{M\max} - U_{M\min}) - RI)}.$$

Mathematical application:

$U_{M\max} = 270$ V, $U_{M\min} = 135$ V, $I = 277.77$ A.

To begin with, RI is neglible in comparison to (U_{Mmax} - U_{Mmin}), so:

$$C_t = (277.77 \times 15)/(270–135) = 30.86 \text{ F}.$$

The average current is relatively strong, so we need to choose a supercapacitor with the lowest possible resistance in order to minimize losses, and it also needs to have a relatively high capacitance. If we choose $C = 3000$ F and $R_1 = 0.3$ mΩ and if we consider $N_{series} = 100$ as determined above, then $C_t = 3000/100 = 30$ F. This value is less than the calculated value (30.86 F). Also, if we take the series resistance into account in our calculations, we find:

$$C_t = (277.77 \times 15)/(135–100 \times 0.3 \times 10^{-3} \times 277.77) = 32.89 \text{ F}.$$

Using the relation $C_t = C \times (N_{parallel}/N_{series}) \Rightarrow N_{parallel} = C_t \times N_{series}/C = 32.89 \times 100/3000 = 1.09$, and because $N_{parallel}$ is an integer, we get $N_{parallel} = 2$. Thus, we have a module of 200 supercapacitors comprising two parallel branches, and each branch contains 100 serially-connected supercapacitors. This being the case, $C_t = 3000\ (N_{parallel}/N_{series}) = 60$ F. The module is overdimensioned, because we only need 32.89 F. Therefore, we need to modify the choice of the elementary supercapacitor. If we choose a 2000 F supercapacitor, we get $C_t = 2000\ (N_{parallel}/N_{series}) = 40$ F.

For 1500 F, $C_t = 1500\ (N_{parallel}/N_{series}) = 30$ F.

In conclusion, the module which is capable of satisfying the technical specifications comprises two branches of 100 supercapacitors, each of 2000 F, connected in a series. The two branches are arranged in parallel.

2) With regard to the converter, a representation of it is given below: the switches K_1 and K_2 are chosen as a function of the maximum current and maximum voltage. For the coil and the capacitor, using the conventional expressions in high-power electronics:

$C = \dfrac{I_{bus} \cdot \alpha \cdot T}{\Delta U_{bus}} = \dfrac{(1-\alpha) \cdot \alpha \cdot I_{scap}}{\Delta U_{bus} \cdot f}$ and $L = \dfrac{\alpha \cdot (1-\alpha) U_{bus}}{f \Delta I_{scap}}$. In both cases, the maximum is obtained for $\alpha = 0.5$.

Mathematical application:

$\Delta I/I = 5\% \Rightarrow \Delta I = 0.05 \times 277.77 = 13.88$ A;

$U_{bus} = 400$ V; $\Delta U = 0.01 \times 400 = 4$ V;

$I_{scap} = 277.77$ A; $a = 0.5$, $f = 20$ kHz.

Using these data, we obtain:

$C = 0.8$ mF and $L = 0.36$ mH.

The diagram for the DC/DC converter connected to the supercapacitor module is given in Figure 4.15. Its function is to charge and discharge the supercapacitor module.

Exercise 7: Calculation of a supercapacitor module for a tramway application

In this exercise we are going to design a supercapacitor module to supply the engines of a tram.

Consider that the tram has the mass $m = 100{,}000$ kg. Its maximum velocity is $V = 50$ kmph = 13.89 m/s. The tram accelerates from 0 to 50 kmph every 3 minutes for 18 hours a day, 365 days a year. The vehicle has to reach its nominal velocity in $t = 10$ s at constant power. The operating voltage of the module is 560 V.

We wish to provide power to this tram with supercapacitors whose characteristics are:

– capacitance of a cell $C = 3000$ F;

– max cell voltage: $U = 2.7$ V;

– series resistance: $R_1 = 0.3$ mΩ.

1) Calculation of the amount of CO_2 produced

First we propose to calculate the amount of carbon dioxide (CO_2) produced per kWh when using gasoil as a fuel. The chemical formula for gasoil is $C_{21}H_{44}$. Consider the following data:

Molar mass of carbon $M_C = 12$ g/mole. Molar mass of nitrogen $M_N = 14$ g/mole. Molar mass of oxygen $M_O = 16$ g/mole. Molar mass of hydrogen $M_H = 1$ g/mole.

a) Calculate the molar mass of gasoil M_{gasoil}.

b) Calculate the molar mass of carbon dioxide M_{CO_2}.

c) Calculate of water (H_2O).

In 1 kg of gasoil, there are 3.37 moles. With oxygen from the atmosphere, the combustion of 1 kg of gasoil produces 3.1 kg of CO_2 ($21 \times 3.37 \times M_{CO_2}$) and 1.3 kg of water ($44/2 \times 3.37 \times M_{H_2O}$). The energy density of gasoil is 12 kWh/kg.

d) Calculate the amount of CO_2 produced per kWh of gasoil.

2) Yearly energy requirements

a) Calculate the vehicle's kinetic energy when in translational motion.

b) Calculate the total energy used each year to accelerate the vehicle.

3) Potential annual saving

The manufacturer claims that a 30% energy saving can be made with the supercapacitor module. This being the case, what is the saving in terms of energy and CO_2 per year?

4) Capacitance of the module

The maximum usage voltage is $U = 560$ V.

a) Show that when the supercapacitor module is used between U_{max} and $U_{max}/2$, 75% of the energy is available.

b) Calculate the capacitance of the module.

c) Calculate the number of supercapacitors in a series N_{series}, in parallel $N_{parallel}$ and the total resistance of the module.

5) Vehicle power

Calculate the power needed to accelerate the vehicle at constant power over time. Show that for a voltage U_1 at the edges of a supercapacitor, the maximum power that the supercapacitor can produce is $P_{max} = \frac{U^2}{4R_1}$. Calculate the maximum power that can be produced by the supercapacitor module described in question 4, above.

Solution to Exercise 7:

1) Calculation of the amount of CO_2 produced

a) The chemical formula for gasoil is $C_{21}H_{44} \Rightarrow$ Molar mass of gasoil $M_{gasoil} = 21 \times 12 + 44 \times 1 = 296$ g/mol.

b) The molar mass of carbon dioxide $M_{CO_2} = 12 + 2 \times 16 = 44$ g/mole.

c) The molar mass of water $H_2O = 2 \times 1 + 16 = 18$ g/mole.

d) The quantity of CO_2 produced per kWh of gasoil is: energy content of gasoil: 12 kWh/kg $\Rightarrow$ in order to produce 1 kWh, we need 1/12 = 0.0833 kg of gasoil. Given that 1kg of gasoil produces 3.1 kg of CO_2, using the rule of three we obtain a production of $0.0833 \times 3.1 = 0.258$ kg of CO_2 per kWh of gasoil.

2) Yearly energy requirements

a) The kinetic energy of the vehicle in translational motion is:

$E_{kin} = 1/2\ m \times V2 = 0.5 \times 100000 \times 13.892 = 9646605$ Joules ≈ 9.6 MJoules $= 2/7$ kWh.

b) At 50 km/h, therefore, the tram has a kinetic energy of 2.7 kWh. The total energy used per year to accelerate the vehicle is:

$$E_a = E_{kin} \times 365 \times 18 \times 60/3 = 354{,}780 \text{ kWh}.$$

3) Potential annual saving

The manufacturer announces a 30% energy saving with the supercapacitor module, which represents a saving of $0.30 \times 354{,}780 = 106{,}434$ kW, which is a saving of $106{,}434 \times 0.258 = 27{,}460$ tons of CO_2 per year.

4) Capacitance of the module

The maximum usage voltage is $U = 560$ V,

a) Show that when the supercapacitor module is used between U_{max} and $U_{max}/2$, 75% of the energy is available.

b) Calculate the capacitance of the module.

c) Calculate the number of supercapacitors in a series N_{series}, in parallel $N_{parallel}$ and the total resistance of the module.

a) When the supercapacitor module is used between U_{max} and $U_{max}/2$, the stored energy is:

$$\Delta E = \tfrac{1}{2} \times C \times U_{max}^2 - \tfrac{1}{2} \times C \times (U_{max}/2)^2 = \tfrac{3}{4}(\tfrac{1}{2} \times C \times U_{max}^2)$$
$$= 75\% \times \tfrac{1}{2} \times C \times U_{max}^2 = 75\% \text{ of energy available.}$$

b) On the basis of the maximum usage voltage given as $U_{max} = 560$ V, the expression of the maximum energy of one capacitor and the fact that only ¾ of the

energy is available between $U_{max}/2$ and U_{max} used, we obtain a capacitance such that: ΔE = 9646605 Joules= ¾(1/2 × C_t × U_{max}^2) ⇒ $C_t = (2 \times 4 \times \Delta E)/(3 \times U_{max}^2) = (2 \times 4 \times 9646605)/(3 \times 560 \times 560) = 82$ F.

c) $N_{series} = 560/2.7 = 207.4$, so there are 208 serially-connected supercapacitors. Using 3000 F supercapacitors, the number of parallel elements is $N_{parallel} = (C_t \times N_{series})/3000 = 5.68$, and because $N_{parallel}$ is an integer we take $N_{parallel} = 6$. In total there are $208 \times 6 = 1248$ supercapacitors.

Verification: $C_t = (3000 \times 6)/208 = 86$ F > 82 F necessary.

The total resistance is: $R = (N_{series}/N_{parallel}) \times R_1 = (208/6) \times 0.3$ mΩ = 10.4 mΩ.

5) Vehicle power

The power necessary to accelerate the vehicle at constant power in the desired time must be $P = E_{kin}/t = (9.6/10)$ MJoules/s = 960 kW. Using the expression $P_{max} = \frac{U^2}{4R_1}$, for a single supercapacitor we determine the power $P_{max} = (2.7 \times 2.7)/(4 \times 0.0003) = 6075$ W. For the module, we obtain a power of: $6075 \times 1248 = 7581.6$ kW.

Chapter 5

Electrochemical Accumulators

5.1. Introduction

The aim of this chapter is to give a brief overview of the main technologies used for electrochemical accumulators. A more in-depth study is presented in [GLA 12; GLA 13].

5.2. Lead accumulators

5.2.1. *Operational principle*

The lead-acid accumulator was invented by Gaston Planté in 1859 [WIK 9]. The negative electrode is made up lead (Pb) and the positive electrode of lead oxide (PbO_2). The electrolyte is an aqueous solution of sulfuric acid (H_2SO_4). The reactions that occur at the negative and positive electrodes respectively are as follows (in discharge mode, the equations are read from left to right – see Figure 1.1):

$$\begin{aligned} &\textit{electrode}\ (-) \quad Pb + HSO_4^- \leftrightarrow PbSO_4 + 2e^- + H^+ \\ &\textit{electrode}\ (+) \quad PbO_2 + HSO_4^- + 3H^+ + 2e^- \leftrightarrow PbSO_4 + 2H_2O \end{aligned} \qquad [5.1]$$

During discharge, lead sulfate accumulates on the electrodes and is consumed during recharging – this is sulfation. However, in certain conditions – particularly with a prolonged or excessively complete discharge, at too high a temperature – stable deposits of lead sulfate begin to form, which are no longer dissolved during

charging. The lead sulfate thus generated harms the cell's capacity by preventing the reactions on the electrode, and because of its poor electrical conductivity. This degradation is irreversible.

We can distinguish between different technologies on the basis of the geometry of the electrodes (flat plates or tubular plates) and the type of electrolyte (liquid or jellified). In the liquid version, which is also known as an open battery, the accumulator has a good lifetime, but requires regular and frequent maintenance – particularly a check on the level of the electrolyte. In its jellified version, with flat plates, the battery is closed or airtight; it is equipped with a safety valve (it is known as a valve-regulated lead-acid battery, VRLA battery), to prevent explosion in case of overloading for instance.

Table 5.1 shows a number of characteristics for a lead-acid accumulator element.

Open-circuit voltage	2–2.1 V
Practical specific capacity	7–20 Ah/kg
Specific energy	15–40 Wh/kg
Volumetric energy	40–100 Wh/l
Lifetime (number of cycles)	200–400 in the closed version 600–1000 in the open version
Operating temperature	–20°C to +60°C
Overall Faradaic efficiency	85–90%
Self-discharge	Around 15% per month

Table 5.1. *Characteristics of a lead-acid accumulator element [DEV 12; CAI 01; MON 09; ROB 04; VAN 06]*

5.2.2. *Advantages and disadvantages to this technology*

The main advantage to a lead accumulator is its cost: less than 1 €/kWh of power supplied. It is the least expensive technology for accumulators, which is the reason why the lead accumulator is one of the most widely employed technologies in industry (particularly in the automobile sector for combustion engine vehicles) [FUS 09].

Its disadvantages are as follows:

– its low mass energy density;

– the use of a corrosive liquid as the electrolyte, which is harmful if leaks occur, for instance;

– its toxicity due to the lead, which is a heavy metal dealt with by Directive 2006/66/EC of the European Parliament on batteries and accumulators and waste batteries and accumulators. This directive limits the commercialization of batteries or accumulators containing dangerous substances (e.g. lead, cadmium, etc.). Therefore, these batteries need a recycling circuit.

The main manufacturers are: Johnson Controls/Varta (USA), Panasonic (Japan), Power Sonic (USA), Huanyu Power Sources (China), Moll-Battieren (Germany), Exide Technologies (USA), Leclanché (Switzerland) and Steco (France) [DEV 12].

5.3. Nickel accumulators

5.3.1. *Nickel-Cadmium (Ni-Cd) accumulator*

This is one of the oldest technologies, as it was developed in 1900 by Waldemar Jungner.

The Ni-Cd accumulator uses a cadmium negative electrode and a nickel-hydroxide (NiOOH) positive electrode, which is reduced into nickel hydroxide ($Ni(OH)_2$) during the discharge of the battery. The electrolyte is an aqueous alkaline solution – potassium hydroxide (KOH) or caustic soda (sodium hydroxide, NaOH), and may or may not contain additional lithium hydroxide (LiOH, also known as lithine).

The electrochemical reactions that occur at the electrodes (from left to right during discharge):

$$\begin{aligned} &\textit{electrode}\,(-) \quad Cd + 2OH^- \leftrightarrow Cd(OH)_2 + 2e^- \\ &\textit{electrode}\,(+) \quad NiOOH + e^- + H_2O \leftrightarrow Ni(OH)_2 + OH^- \end{aligned} \qquad [5.2]$$

Table 5.2 lists some of the characteristics for a Ni-Cd accumulator element.

A Ni-Cd accumulator subjected to slight cycling (charge/discharge) tends to adapt to the characteristics of that treatment. If it is then subjected to a drastic discharge, the voltage at its terminals drops sharply when the discharge capacity attains the value involved in the previous cycling. The loss of capacity is not irreversible. A recharge wipes out this memory effect and facilitates later deep discharges. A Ni-Cd accumulator needs to be completely discharged in order to remain in the major cycle. Therefore, we can completely exploit the stored energy,

going down to low voltage levels (i.e. a deep discharge), unlike other accumulators where a minimum voltage is imposed for reasons of cyclability. However, if the accumulator is connected to the electrical grid via a converter, the need to take it down to a low voltage places stress on the converter. The accumulator, in this case, exhibits good thermal behavior, as it is able to function within a broad temperature range [DEV 12].

Open-circuit voltage	≈1.3 V
Practical specific capacity	30–50 Ah/kg
Specific energy	30–60 Wh/kg
Volumetric energy	80–160 Wh/l
Lifetime (number of cycles)	500–1000 if the depth of discharge is 100% at each cycle 5000–10000 if it is 25%
Operating temperature	Storage: –30°C to +50°C Charge: 0°C to +45°C Discharge: –20°C to +60°C
Overall Faradaic efficiency	75–80%
Self-discharge	Approximately 2% per day

Table 5.2. *Characteristics of a Ni-Cd accumulator element [DEV 12; CAI 01; MON 09; ROB 04; VAN 06; ROB 05]*

On the other hand, Ni-Cd accumulators cost around five times as much as Pb accumulators. They also have far poorer Faradaic efficiencies and a higher rate of discharge [FUS 09].

They are used in portable tools, in safety lighting and in applications which require high power or the ability to function at a relatively high temperature. They are also used for electric vehicles, but their applications are limited by directive 2006/66/EC, which prohibits the sale of batteries and accumulators containing more than 0.002% mass cadmium.

The manufacturers for Ni-Cd accumulators are Saft (France) and Varta/Johnson Controls (USA) [DEV 12].

5.3.2. *Nickel Metal Hydride (Ni-MH) accumulator*

The Nickel Metal Hydride (Ni-MH) accumulator was developed in the 1970s to deal with the problem posed by the use of Cadmium in the Ni-Cd accumulator, and

since the 1990s has largely come to replace it, with fairly comparable levels of performance and similar operation.

The negative electrode is a metal alloy capable of adsorbing and desorbing hydrogen. As with Ni-Cd accumulators, the positive electrode uses a nickel oxyhydroxide (NiOOH), which is reduced into nickel hydroxide ($Ni(OH)_2$) during the course of the discharge. The electrolyte is also of the same type, i.e. an aqueous alkaline solution, comprising potassium hydroxide (KOH) or caustic soda (NaOH), with the possible addition of lithine (LiOH).

The electrochemical reactions that occur at the electrodes are as follows:

$$\begin{aligned} &\text{electrode } (-) \quad MH + OH^- \leftrightarrow M + e^- + H_2O \\ &\text{electrode } (+) \quad NiOOH + e^- + H_2O \leftrightarrow Ni(OH)_2 + OH^- \end{aligned} \qquad [5.3]$$

Table 5.3 summarizes a few of the characteristics of a Ni-MH accumulator.

Open-circuit voltage	≈1.3 V
Practical specific capacity	45–60 Ah/kg
Mass energy density	60–90 Wh/kg
Volumetric energy density	200–350 Wh/l
Lifetime (number of cycles)	400–700 if the depth of discharge is 100% in each cycle
Operating temperature	Storage: –30°C to +40°C Charge: 0°C to +40°C Discharge: –20°C to +50°C
Overall Faradaic efficiency	90–95%
Self-discharge	2–4% per day

Table 5.3. *Characteristics of a Ni-MH accumulator [DEV 12; CAI 01; MON 09; ROB 04]*

The advantages to the Ni-MH accumulator are:

– a specific energy around two times greater than that of the Ni-Cd accumulator;

– the use of a metal alloy at the negative electrode, as an alternative to the use of Cadmium;

– an end of charge which is characterized by a slightly negative variation in voltage, which makes it easy to detect this point and automatically cut off the charge cycle [FUS 09].

Its disadvantages are:

– its high cost;

– the fact that at the end of discharge, a voltage of around 1 V must be preserved as an absolute minimum, because otherwise there is a risk of damage to the accumulator.

The manufacturers of Ni-MH accumulators are: Saft (France), Energizer (USA) for portable electronics, Panasonic (Japan) for the automobile industry and Varta/Johnson Controls (USA) [DEV 12].

They are used in "high-energy" applications (portable electronics, camcorders, office automation, toys, medical or scientific instruments), "high-power" applications (machine tools, modeling) and road transport (electrical and hybrid vehicles).

5.3.3. *Nickel-Zinc accumulator*

The Nickel-Zinc (Ni-Zn) accumulator was developed in the 1930s to replace the Silver-Zinc (Ag-Zn) accumulator.

Its negative electrode is made of zinc and its positive electrode of nickel oxyhydroxide (NiOOH), which is reduced to Nickel hydroxide ($Ni(OH)_2$) during the course of discharge. The electrolyte is an aqueous alkaline solution of KOH.

The overall electrochemical reaction (read from left to right during discharge) is:

$$2NiOOH + Zn + H_2O + KOH \leftrightarrow 2Ni(OH)_2 + K_2Zn(OH)_4 \qquad [5.4]$$

Table 5.4 summarizes a few of the characteristics of a Ni-Zn accumulator.

Open-circuit voltage	≈1.7 V
Practical specific capacity	45 Ah/kg
Specific energy	60–70 Wh/kg
Volumetric energy	120 Wh/l
Lifetime (number of cycles)	600–1000
Operating temperature	–20°C to +60°C

Table 5.4. *Characteristics of a Ni-Zn accumulator [DEV 12; POW 10]*

The Ni-Zn accumulator exhibits the advantage of having a lower cost than Ni-Cd and not being affected by directive 2006/66/EC. Its operational voltage is also 25% higher. It is robust, reliable, safe, maintenance-free and easily recyclable.

The main drawback to this technology is its lifetime. It presents poor cycling resistance due to the solubility of the zinc in the alkaline electrolyte, which creates dendrites of zinc that may cause short-circuits between the two electrodes. If the zinc comes into contact with a particle of nickel, hydrogen is released and the zinc is corroded [VAN 06].

The manufacturers of Ni-Zn accumulators are: Powergenix (USA), Evercell (USA) and Xellerion (USA). They are used primarily in the military and automobile sectors [DEV 12].

5.4. Lithium accumulators

5.4.1. *Why lithium?*

The advantage to using lithium in accumulators is twofold: it is both the lightest and the most reductive metal. In fact, lithium accumulators have begun to be widely used since the very beginning of the 2000s, and reveal themselves to be particularly promising. They are capable of delivering high densities both in terms of power and energy, in comparison to more "conventional" accumulator technologies (particularly for lead accumulators). To clarify, this enables us to attain values of around 1.5 kW/kg and 200 Wh/kg.

5.4.2. *Principle of their function*

In the category of lithium accumulators, we include all accumulators whose electrochemical reaction is based on lithium. These accumulators can be divided into two broad categories:

– *accumulators in which one of the electrodes is made of lithium in metallic form*: it will be the anode which is made of metallic lithium. Such was the case, in historical terms, with the earliest lithium accumulators (made in the 1980s);

– *accumulators in which the lithium is still in ionic form*: in this case, the anode is made of carbon-based material. We then speak of a lithium-ion accumulator.

Overall, though, the principle of operation of these accumulators remains the same (see Figure 5.1, for instance, showing the lithium-ion accumulator). Thus, during use (i.e. during the discharge of the accumulator), lithium is released by the

negative electrode in ion form (Li^+) and crosses through the electrolyte (which therefore must necessarily be an ion conductor) and joins with the crystalline mesh of the material making up the positive electrode. The passage of each Li^+ ion into the electrolyte is exactly compensated by the passage of an electron via the external circuit, thus causing an electrical current. The reverse phenomenon occurs when the accumulator is being charged.

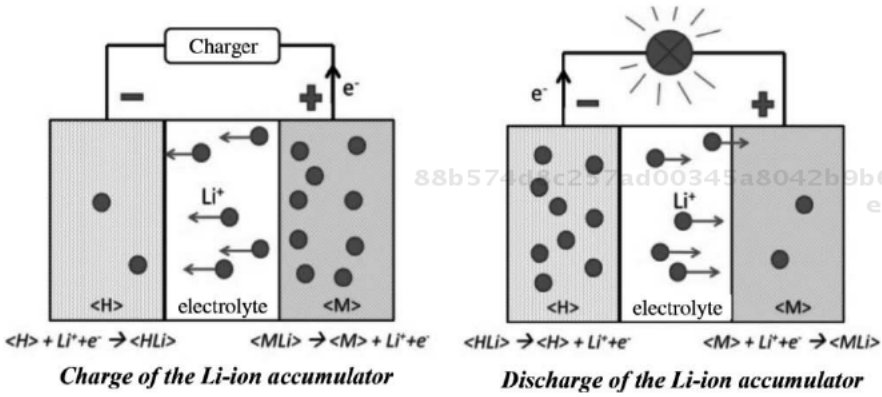

Figure 5.1. *Principle of operation of a Li-ion accumulator*

5.4.3. *Advantages and disadvantages to these technologies*

Historically, the use of metal-lithium-based accumulators soon raised a certain number of practical difficulties. Indeed, when the accumulator is charging, various problems come to light:

– *the lithium ions released tend to form a passivation film on the surface of the positive electrode* as they react with the electrolyte;

– *on the other hand, the lithium tends to be deposited in a dendritic, rather than uniform, manner on the negative electrode*. In certain cases, these dendrites may even pass through the electrolyte and reach the positive electrode, leading to a short circuit and potential destruction of the cell. Although this extreme scenario may not necessarily be realized, these aggregates can also sometimes break off and "wander" in the electrolyte, thereby reducing the capacity of the electrochemical cell.

The cumulative effect of these phenomena over the course of multiple charge/discharge cycles means it becomes necessary to provide an initial quantity of lithium which is 4–5 times greater than that which is theoretically needed.

In order to mitigate these problems originating from the technology, R&D has been carried out with two main foci:

– *new materials to be used for the negative electrodes have been developed:* this is the lithium-ion technology;

– *new solid polymer electrolytes have been developed:* this has offered new outlets for lithium-metal technology – lithium-metal-polymer technology.

5.4.4. *Lithium-ion technology*

This technology owes its name to the fact that the negative electrode is a compound, able to integrate the lithium ions which have migrated through the electrolyte. Thus, in principle, any material which is able to host lithium ions within it can be used as the basis for a lithium ion accumulator. This is the reason for the profusion of existing solutions. In practice, various different insertion compounds are considered. Notably, one might cite graphite or titanium oxide. Depending on the insertion compound used, the functionalities obtained may vary slightly.

Thus, if we consider titanium oxide as an insertion compound, we obtain a Li-ion accumulator which is better adapted to quick recharging (and quick restitution of that energy). In this case, we have a *Li-ion power* accumulator. On the other hand, if we consider graphite as an insertion compound, we obtain a Li-ion accumulator which is better adapted to "slow" recharges (of the order of a Coulomb) but with a greater capacity. In this case, we would have a *Li-ion energy* accumulator.

It is noteworthy (see Figure 5.1) that in line with the charge/discharge cycles, the lithium ions (Li^+) are in constant back-and-forth motion between the sites of the insertion compounds of the two electrodes in the accumulator: we speak of the *rocking-chair* effect.

The open-circuit voltage of a component using this technology will be approximately 3.7 V, which is relatively high for an electrochemical cell. The electrolyte is liquid, but not aqueous (because lithium is particularly reactive with water).

The advantages to the Li-ion accumulator are many:

– a mass energy density 2–5 times greater than that of Ni-MH accumulators;

– low bulk;

– a good lifetime for high-power industrial accumulators;

– low self-discharge;

– the absence of memory effect.

However, these accumulators do exhibit certain disadvantages:

– to begin with, their safety is an issue. Temperature increases occur, which can lead to the explosion of the accumulator. Hence, it is helpful to put preventative electronic devices in place;

– their cost, which is primarily linked to the cost of certain insertion compounds.

5.4.5. *Lithium-metal-polymer technology*

This name is based on the fact that the negative electrode is made of lithium in metal form and the electrolyte is a polymer. This technology is used in France by the company Batscap in particular, and in South Korea by KOKAM. One of the positive points for this technology lies in the fact that if the specific capacity of lithiated carbon (resulting from the insertion of lithium into a carbon-based insertion compound) is 372 Ah/kg, while that of lithiated aluminum is 800 Ah/kg, these values are considerably lower than those of the theoretical specific capacity of lithium in the metal state, which is 3862 Ah/kg (note, though, that by way of comparison, the specific capacity of cadmium is 477 Ah/kg). We can therefore envisage reaching better energy densities with this type of technology.

The operational principle is illustrated by Figure 5.2.

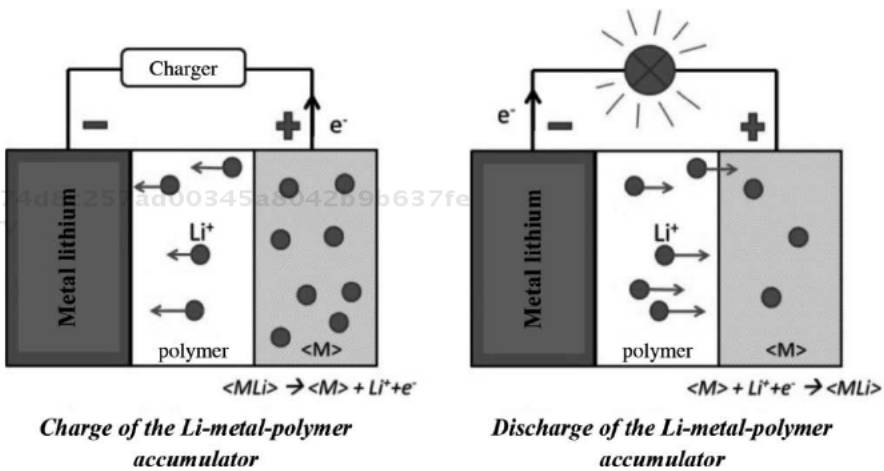

Figure 5.2. *Operational principle behind a Li-metal-polymer accumulator*

The use of a polymer electrolyte is crucial for this type of accumulator. Indeed, as well as preventing (or at least limiting) dendrite growth, this polymer also needs to ensure electrical separation between the two electrodes, ion conduction and must

not alter the physico-chemical properties of the electrodes. However, this electrolyte needs to be maintained at a temperature between 80 and 100°C so as to ensure good ionic conductivity of the polymer.

The advantages to the lithium-metal-polymer accumulator are as follows:

– it is very flexible, so can be given an appropriate shape, dictated by the intended application;

– it is lightweight;

– it has no memory effect;

– it exhibits a relatively long lifetime;

– the polymer electrolyte prevents the problems of safety which may be found with liquid-electrolyte Li-ion accumulators.

There again, there are certain drawbacks – particularly the need to function within a restricted temperature range in order to obtain optimal performances from the electrolyte.

5.4.6. *Other technologies*

There are other lithium accumulator technologies on the market. We shall discuss some of these in this section. Usually, they represent a particular case of one or other of the technologies mentioned above (Li-ion or Li-metal).

5.4.6.1. *Lithium-phosphate accumulator*

This is a particular case of lithium-ion technology, in which the positive electrode is based on a metal phosphate (e.g. iron phosphate: $LiFePO_4$). The open-circuit voltage obtained per cell is approximately 3.3 V. The interest in this technology lies mainly in:

– its cost: it is less expensive than lithium-ion or lithium-metal-polymer technology because the materials used for the positive electrode are themselves less expensive;

– its safety: there is no release of oxygen at the positive electrode (unlike what can happen with Li-ion accumulators). Hence, there is a decreased risk of fire or explosion of the accumulator.

Today, studies are still under way with a view to improving the durability of this technology. Indeed, increasing the temperature favors the dissolution of the iron, which further reduces the lifetime.

5.4.6.2. *Lithium-ion-polymer accumulator*

This accumulator is a particular case of lithium-ion technology. It still uses two electrodes based on insertion compounds. The difference here is that the electrolyte is a solid polymer matrix in which the conductive liquid is captive. Therefore, it is possible to make batteries of all sorts of geometric shapes.

The advantages to this technology are as follows:

– improved safety (owing to the use of a polymer matrix);

– low mass;

– a high number of cycles;

– no memory effect;

– low self-discharge of the accumulator.

Its main disadvantage (relating to the polymer electrolyte) is still the necessity of operating within a reduced temperature range (80–100°C) in order to obtain a maximum efficiency.

5.5. Characteristics of an accumulator or battery

An electrochemical accumulator (or a battery when we consider a group of accumulator cells) is often characterized by a number of values or indicators. These values depend on the technology (or the chemistry) of the battery, but also on the environment and the usage conditions. One might cite, for instance, the operating temperature, the discharge current, etc. The values which define a battery are: its capacity, its open-circuit voltage, its end-of-discharge voltage, the state of charge (SOC), the depth of discharge, etc.

5.5.1. *Capacity*

Charles-Augustin de Coulomb estimated that an accumulator receiving a charger current of 1 A receives 1 Coulomb of charge per second. In 10 seconds, a 10 Coulomb charge is passed into the accumulator, and so on. During output, the process is reversed. Thus, the storage capacity of an accumulator is defined by the amount of charge that can be obtained during a discharge. This capacity depends on the temperature, the state of aging of the accumulator, the discharge regime, etc. Generally, the capacity of an accumulator is given by the following equation:

$$Q = \int_{ti}^{tf} I_d \, dt \qquad [5.5]$$

where I_d represents the discharge current; ti and tf are respectively the initial time and the final time of the discharge.

Capacity is usually expressed in ampere-hours (Ah). 1 Ah = 3600 Coulomb. Generally, we can define the capacity C_n such that n is the length of time, in hours, for which the accumulator is being discharged. For example, if the capacity C_{10} = 100Ah, this accumulator can provide a current of 100/10 = 10 A for 10 hours. In theory, we can deduce that the product of the current by the duration of discharge is equal to the capacity of the accumulator (current × duration = capacity in Ah). It should be noted that the capacity depends on the temperature and the discharge current. Indeed, the variation in capacity as a function of the current is known as Peukert's effect, and is linked to the internal resistance of the accumulator: the more strongly the component is discharged, the greater is the drop in voltage. This effect stipulates that the capacity increases when the discharge current is weak. In order to take account of Peukert's effect, the capacity is defined by equation [5.6]:

$$C_p = I^k t_d \qquad [5.6]$$

where C_p is the Peukert capacity, k is the Peukert coefficient and t_d is the discharge time; k is greater than or equal to 1. Figure 5.3 shows the nominal capacity as a function of the Peukert capacity. We can see that for an ideal battery (meaning that $k = 1$), $C_n = C_p$. However, if k is greater than 1, the normalized capacity is less than the Peukert capacity.

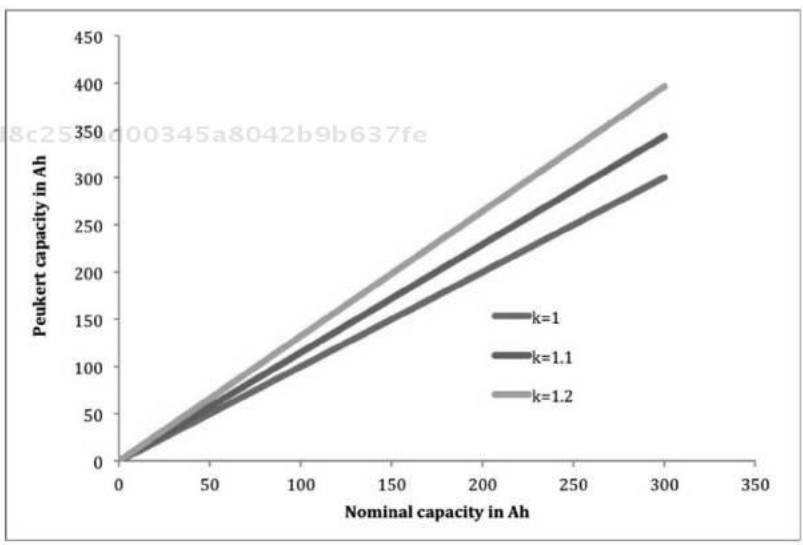

Figure 5.3. *Peukert capacity as a function of the nominal capacity of a battery*

The capacity depends on the regime in which the discharge takes place. The shorter the discharge time, the lesser the capacity.

To illustrate the influence of the Peukert coefficient on the performances of a battery, we have shown in Figure 5.4 the change in duration of discharge from a battery with capacity $C_{10} = 150$ Ah with changing discharge current. The graph shows the curves for three Peukert coefficients: 1, 1.1 and 1.2. These results demonstrate that, for instance, with a 15 A discharge current, the times are respectively 10 hours, 7.6 hours and 5.8 hours for $k = 1$, 1.1 and 1.2 (Figure 5.4). To help the reader understand this effect, we shall give a small example: suppose we have a 12-volt battery and a capacity of 150 Ah at a discharge rate of $C/15$. The battery is discharged with a 15 A current; in this case the duration of discharge is 150/15 = 10 hours. If the same battery is discharged with a current of 5 A, the discharge time would in this case correspond to 150/5 = 30 hours. However, in practice, this battery would supply a 5 A current for a length of time greater than 20 hours. All manufacturers seek to obtain batteries with a Peukert coefficient of 1.

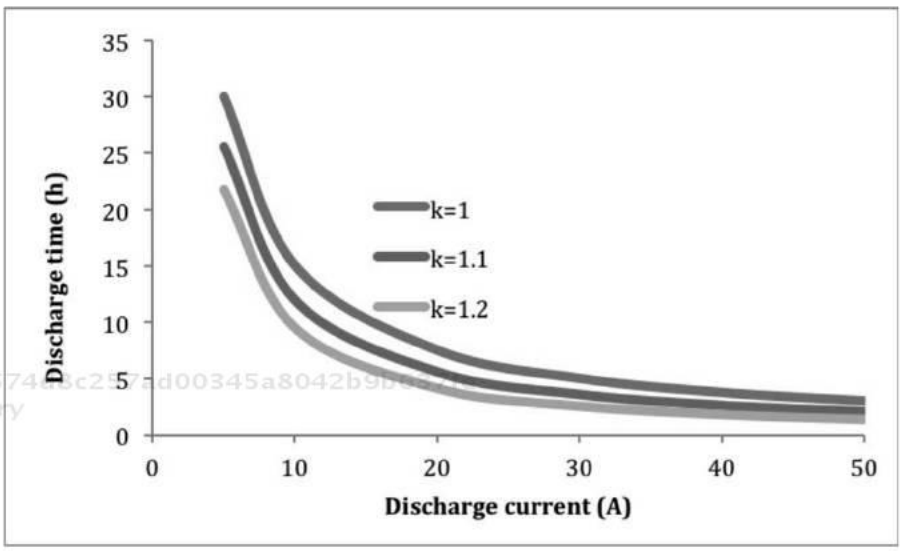

Figure 5.4. *Discharge time as a function of the current for different Peukert coefficients*

5.5.2. *Internal resistance*

The internal resistance of an accumulator generally represents losses by the Joule effect (irreversible losses) and the dip in the accumulator's output voltage. It is linked to the resistance of the electrolyte, the resistance of the two electrodes and the

electrical contact resistance. Therefore, during the charging or discharging of the accumulator, the internal resistance changes. Also, the internal resistance during charging and the resistance during discharging are different.

5.5.3. *Voltages*

An accumulator is characterized by two voltage values. The first is the nominal voltage, which is determined by the potential for chemical reaction of each element in the redox couple used. For instance, in the case of a lead accumulator, the nominal voltage (operational voltage) per cell is 2.1 volts. In the case of a lithium battery, it is around 3.8 V, depending on the chemistry used.

With regard to the open-circuit voltage, which is often notated as OCV, it is determined in the absence of electrical load, and is almost equal to the theoretical voltage when the accumulator is fully charged. The open-circuit voltage is the equilibrium voltage of the accumulator. It depends on the capacity and the SOC, and also on the temperature. Figure 5.5 represents the OCV as a function of the SOC of a lithium battery [BAD 12]. This curve is purely experimental and cannot be determined theoretically. It is specific to each battery. It is noteworthy that the relation between the OCV and the SOC of the battery is nonlinear. We shall discuss the SOC of a battery in greater depth later on.

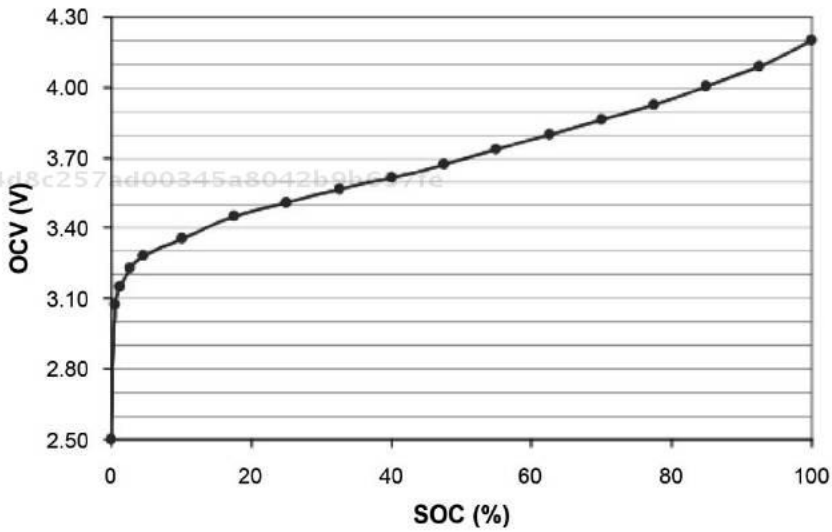

Figure 5.5. *Variation of the open-circuit voltage of a battery (Panasonic 18650) as a function of its state of charge [BAD 12]*

5.5.4. *Energy*

The battery stores the energy in chemical form, and releases it in the form of electricity. This energy depends on the voltage of the battery and the current. It can be defined as the amount of energy that the battery is capable of providing during a complete discharge. The energy of a battery depends on the temperature. It is expressed in Wh (1 Wh = 3600 Joules), and defined by equation [5.7]:

$$E = \int_{ti}^{tf} I_d(t)v(t)dt \qquad [5.7]$$

E is the energy, $I_d(t)$ is the discharge current (generally at constant current) and $v(t)$ is the voltage of the battery.

In order to compare the performances of the accumulators, we often speak of a the mass energy density (Wh/kg) and volumetric energy density (Wh/l). These two values are very important when choosing a technology for embedded applications such as an electric or hybrid vehicle, for example.

5.5.5. *State of charge of a battery*

The SOC of a battery can be compared to a tank of gasoline, for instance. When the tank is full, SOC = 100%, and when it is empty, SOC = 0%. In most applications using batteries, it is of crucial importance to know the SOC of these batteries. For electric vehicle applications, for example, the autonomy is directly dependent upon the state of charge of the batteries. This parameter is also used in managing the discharge of the battery. In addition, it is an indispensable input value for the electronic Battery Management System (BMS). This system prevents deep discharge of the battery. If we consider that $E_{\max}$ is the energy in the battery when it is fully charged and $E(t)$ the energy at a time t, SOC is defined by equation [5.8]:

$$SOC(t) = \frac{E(t)}{E_{\max}} \qquad [5.8]$$

SOC can also be defined by equation [5.9]:

$$SOC(t) = SOC_0 - \frac{\int_{to}^{t} I_d(\tau)d\tau}{C_n} \qquad [5.9]$$

where SOC_0 is the initial state of charge, $I_d(t)$ the discharge current, $\int_{to}^{t} I_d(\tau)d\tau$ the charge delivered by the battery at time t and C_n the nominal capacity of the battery.

In almost all cases, the SOC of a battery cannot be directly determined from the measurement of a parameter, it is necessary to take account of numerous electrical and electrochemical parameters of the battery (OCV, I_d, $V(t)$, etc.) as well as the temperature in order to estimate the SOC of a battery. With regard to lithium batteries, we can use automated methods, such as Kalman filters [DO 10], to estimate the SOC. The SOC of batteries also gives us valuable information about the internal state of the battery, and can inform the user about the remaining lifetime [DEL 97].

In order to optimize the usage and lifetime of the battery, it is advisable to vary the state of charge between 30 and 90%.

Similarly, we can define the depth of discharge (DOD) as an indicator about the discharge of the battery. Thus, if a battery is completely discharged, the DOD is equal to 100%, and it is 0% if the battery is charged.

5.6. Modeling of a battery

The modeling of an accumulator or battery of accumulators is a highly complex task. There are many different approaches, which will be more or less appropriate depending on the objectives required of the model. In order to replicate electrical behavior similar to that of a battery, we use a model in the form of an equivalent electrical circuit. Many different circuits are put forward in the existing body of literature: Thévenin equivalent circuit, improved Thévenin equivalent circuit, FreedomCar, etc. In all cases, the parameters used for these models are determined experimentally.

In this section, we propose two equivalent electrical circuits used to model the electrical behavior of lithium batteries: the model developed by FreedomCar and the Thévenin model.

5.6.1. *Thévenin model*

The Thévenin model is a relatively simple equivalent diagram for describing the electrical behavior of a battery. This model, represented by Figure 5.6, is frequently used because of its simplicity. It comprises an ideal voltage source V_0, an internal

resistance R_i, a capacitor C which models the polarization of the battery, also called the double-layer capacity, and a resistance R_0 which represents the charge transfer resistance at the electrode/electrolyte interface in the battery.

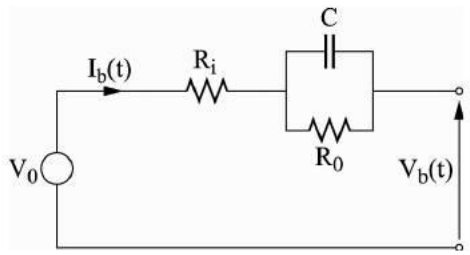

Figure 5.6. *Thévenin model of a battery*

In this model, all the elements of the equivalent circuit are supposed to be constant, and they are identical during the charging or discharging of the battery. This is a model which enables us to describe the behavior of a battery around a given point of operation with a great deal of approximation. Indeed, the parameters of this model vary depending on the state of charge of the battery.

5.6.2. *Improved Thévenin model*

The improved Thévenin model, presented in Figure 5.7, enables us to take account of the nonlinearities of the battery parameters. This model comprises one branch to describe the behavior during charging and another for discharging. Two opposite-facing diodes are used to distinguish the charge cycle from the discharge cycle.

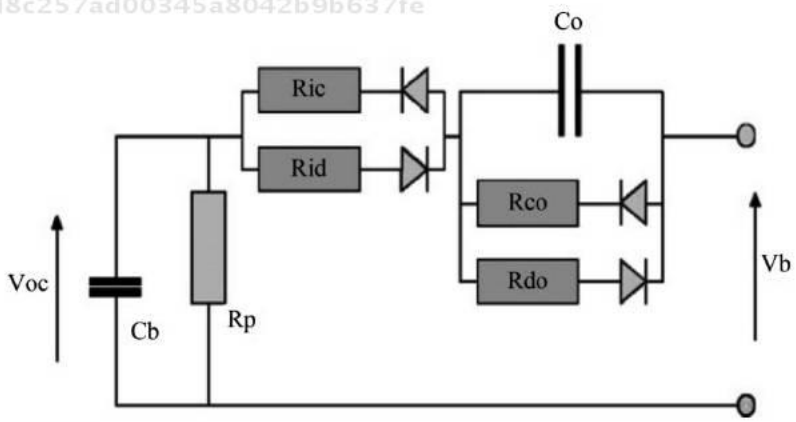

Figure 5.7. *Improved Thévenin model of a battery*

The improved Thévenin model comprises a self-discharge resistance R_p, two resistances R_{ic} and R_{id} for ohmic losses in voltage during charging and discharging respectively, two resistances R_{co} and R_{do} to model the electrochemical voltage losses, a battery capacitor C_b, and a double-layer capacitor C_o.

The parameters of this model are variable: they depend on the state of charge or the battery, or on its OCV. Therefore, they are difficult to identify.

5.6.3. *FreedomCar model*

The FreedomCar model enables us to model the electrical behavior of lithium batteries. It is a second-order model. It is represented by Figure 5.8.

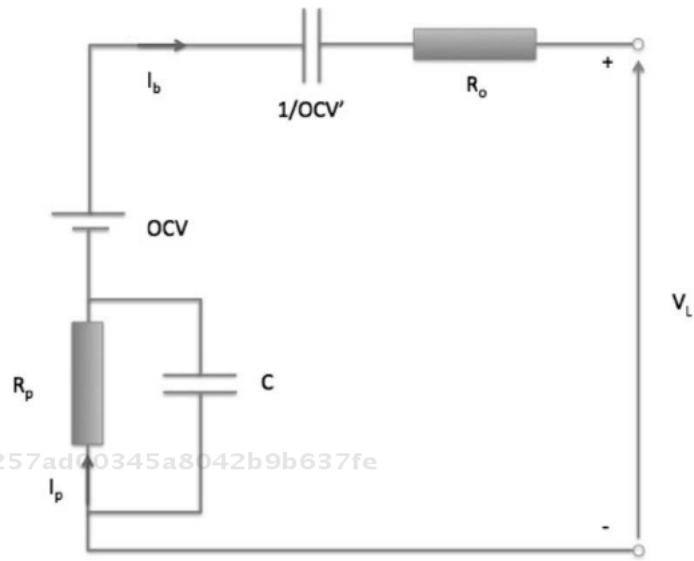

Figure 5.8. *Model of a lithium battery [NOS 12]*

In this figure:

– R_0: the internal resistance of the battery;

– OCV: the open-circuit voltage (the battery does not provide current);

– 1/OCV': a fictive capacitor which represents the variation in voltage over time. This parameter can be used to model the variation in OCV as a function of the SOC of the battery;

– R_p: the polarization resistance of the battery;

– C: Capacitor which, with R_p, gives us a time-constant related to the polarization;

– I_p: the polarization current.

The voltage output from the battery V_L can be expressed by equation [5.10]:

$$V_L = OCV - OCV' \int I_L dt - R_0 I_L - R_p I_p \qquad [5.10]$$

5.7. Aging of batteries

The lifetime of a battery is strongly linked to the usage conditions. It depends on the number of cycles, the temperature, the state of charge, the charge/discharge current, etc.

In general, the aging of a battery result in a deterioration in its energetic performances (decreased capacity, increased internal resistance, etc.). For vehicular applications, a battery is considered to be aged or no longer capable of fulfilling its function if its capacity drops by 20% or the resistance increases by a factor 2.

Figure 5.9 shows the increase in the internal resistance of a lithium battery as a function of the cycle number and for different temperatures. These results show that the temperature is a factor which accelerates the ageing of the batteries. We note that negative temperatures and temperatures greater than 40°C considerably accelerate the aging of lithium batteries.

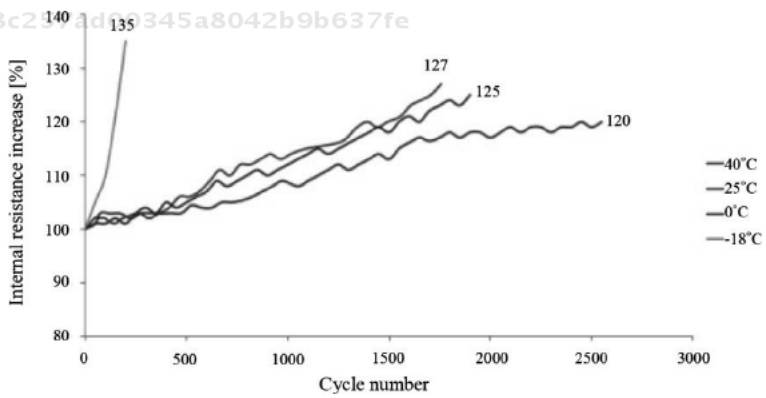

Figure 5.9. *Change in the internal resistance with the cycling of the lithium battery [NOS 12]*

Figure 5.10 shows the influence of the SOC of a battery and of the temperature on battery aging. We note that the higher the state of charge, the greater is the loss of capacity.

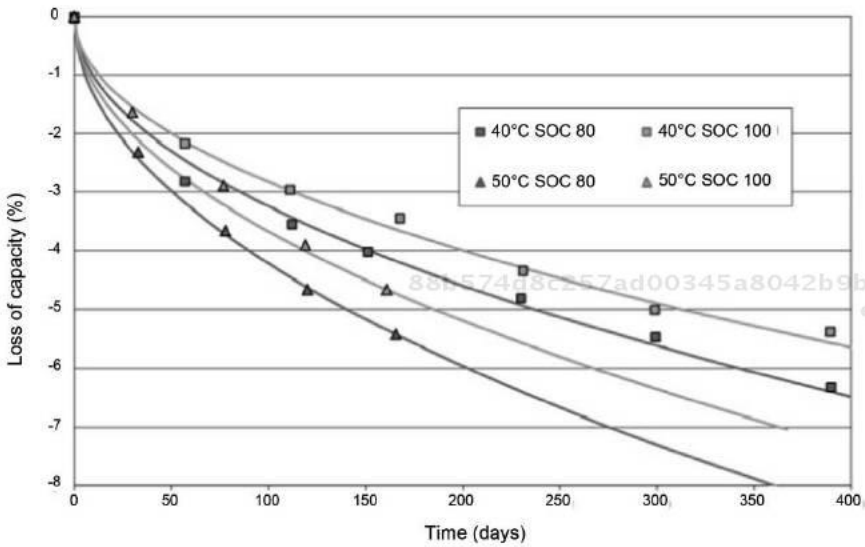

Figure 5.10. *Loss of capacity by a lithium battery as a function of the aging time*

5.8. Exercises

Exercise 1:

Consider a battery of accumulators with the following parameters:

– Nominal voltage 12 V;

– Capacity C_{10} = 150 Ah.

The Peukert effect is neglected (k = 1).

1) Calculate the discharge time for discharge currents of 15 A; 10 A; and 5 A.

2) Determine the energy that can be stored in this component.

3) Calculate the weight of the battery with the following mass energy densities: Technology 1: 50 Wh/kg; technology 2: 100 Wh/kg and technology 3: 200 Wh/kg.

4) Which technology serves best for vehicular applications?

Solution to exercise 1:

1) The capacity of the battery C_{10} is 150 Ah, which means that it can be discharged with a current of 15 A for 10 hours. We can also use the relation $C = It$, where $I = 15$ A, $t = 150/15 = 10$ h, for $I = 10$ A; $t = 150/10 = 15$ hours and for $I = 150/5 = 30$ hours. The weaker the discharge current, the longer the discharge time and the better the lifetime of the battery.

2) The amount of energy that can be stored in this battery is:

E = the capacity (Ah) × the voltage (V) = 150 × 12 = 1800 Wh.

3) The mass energy density = energy/mass; thus, the mass (or weight) = energy / energy density

Technology 1: weight = 1800/50 = 36 kg;

Technology 2: weight = 1800/100 = 18 kg;

Technology 3: weight = 1800/200 = 9 kg.

4) The greater the mass energy density, the lower the weight, and therefore the better the battery for embedded applications (such as in vehicles). Technology 3 is therefore of most interest for vehicular applications.

Exercise 2:

The capacity of a battery of accumulators is given by the following relation:

$$C = I^k t,$$

where k is the Peukert coefficient or index, whose value is between 1.1 and 1.5. The value of k depends on the discharge current of the battery (or the discharge rate).

1) Show that we can write $k = \dfrac{\log t_2 - \log t_1}{\log I_1 - \log I_2}$; where I_1 is the discharge current over time t_1 and I_2 is the discharge current over time t_2.

2) Mathematical application: calculate k for: $I_1 = 15$ A and time $t_1 = 5$ hours; $I_2 = 5$ A and time $t_2 = 20$ hours.

3) For the same battery, the manufacturer states: $C_5 = 75$ Ah with $I_1 = 15$ A and $C_{20} = 100$ Ah (nominal capacity of the battery) with $I_2 = 5$ A. Find the value of k.

Solution to exercise 2:

1) We know that $C = I^k t$; for a discharge current I_1, we have a time t_1; and for I_2 we have t_2. Therefore, we can write:

$$C = I_1^k t_1 = I_2^k t_2 \Rightarrow \left(\frac{I_1}{I_2}\right)^k = \frac{t_2}{t_1} \Rightarrow \log\left(\left(\frac{I_1}{I_2}\right)^k\right) = \log\left(\frac{t_2}{t_1}\right)$$

$$\Rightarrow k \log\left(\frac{I_1}{I_2}\right) = \log\left(\frac{t_2}{t_1}\right) \Rightarrow k(\log(I_1) - \log(I_2)) = \log(t_2) - \log(t_1)$$

$$\Rightarrow k = \frac{\log(t_2) - \log(t_1)}{\log(I_1) - \log(I_2)}$$

2) Mathematical application: $I_1 = 15$ A; $t_1 = 5$ hours; $I_2 = 5$ A; $t_2 = 20$ hours. We get:

$$k = \frac{\log(20) - \log(5)}{\log(15) - \log(5)} = 1.26.$$

3) Considering the data provided by the manufacturer:

$C_5 = 75\ Ah$ means that we can discharge the battery with a current of $I = 15\ A$ for $t_1 = 75/15 = 5$ hours, and for $C_{20} = 100\ Ah$, we have $t_2 = 100/5 = 20$ h. We again find the same data as seen in question 2, so once more, $k = 1.26$.

Exercise 3:

Consider a motorhome equipped with a starter battery (a power battery) and an energy battery used to supply the cabins (light points, PC chargers, refrigerators, etc.) on the same onboard grid. This second battery is charged by photovoltaic panels. The consumption is estimated at 500 Wh for a day. Give the sizing of the energy battery to deliver a 3-day autonomy with a DOD of 100% and another of 70%; assume the panels to be appropriately sized for this purpose.

Solution to exercise 3:

The daily consumption of the motorhome is 500 Wh. Thus, if we consider an autonomy of 3 days, the energy needed is $3 \times 500 = 1500$ Wh. The voltage of the battery is 12 V, which is the typical voltage level for modern onboard grids. Thus, we can write:

Capacity (Ah) = (stored energy (Wh/day) × autonomy (days))/(DOD × voltage (V))

Mathematical application: for a DOD of 100%, we get $C = (500 \times 3)/(1 \times 12) = 125$ Ah; and for a DOD of 70%, we get $C = (500 \times 3)/(0.7 \times 12) = 178.5$ Ah.

We know that the lesser the depth of discharge, the longer the lifetime of the battery will be. Hence, we have a greater capacity. The depth of discharge is an important criterion in this type of application.

Chapter 6

Hybrid Electrical System

6.1. Introduction

This chapter is intended, in a manner of speaking, to give a summary of the elementary concepts discussed in the previous chapters. Our aim, once we have defined the meaning of the term "hybrid", is to offer an overview of hybrid electrical systems intended for applications in the transport or stationary domains. We shall also briefly look at the fact that if we want to speak of the sizing and design of such hybrid systems, we necessarily have to ask questions about the management of the energy flows within these systems: which solutions are appropriate to serve which objectives and which constraints? One section of this chapter will, naturally, be given over to the examination, in perspective, of pertinent solutions for the management (if not optimal, then at least optimized) of these energy flows.

6.2. Definitions

6.2.1. *General points*

If we refer to its etymology (in Latin, *hybrida* means "mixed blood"), the term "hybridization" evokes a fertilization which does not follow the laws of nature: i.e. the fact of crossing two different species or genres to create specimens which, to a greater or lesser extent, bring together specific characteristics of the two parents.

This formal definition gives an excellent account of the advantage to hybridization in the electrical sense of the term: to preserve characteristics specific to the parents (obviously normally strong points in the sense of energy supply or storage) and ensure that the "hybrid" system thus created offers overall performances (yield, specific energy, specific power, cost, durability, etc.) which are more advantageous in relation to the intended application. Here we see what Prof. C.C. Chan [CHA 07] calls the philosophy of hybrid engineering: "1 + 1 > 2", i.e. that the hybridization of elements must create a device whose performances are better than the mere sum of the initial elements (see Figure 6.1).

Figure 6.1. *Concept of a hybrid vehicle*

6.2.2. *Particular case of a hybrid electric vehicle*

In this section, we shall continue with our definitions, focusing on a hybrid electric vehicle, which is presently a source of enormous attention on a global scale. Both their technical and economic potential appear to be significant.

Referring to the remarks in the above section, the simplest definition of a hybrid vehicle is a vehicle which uses two sources of energy. A hybrid electric vehicle is therefore, logically, a vehicle in which a source, an energy storage component or an energy converter is capable of delivering electrical energy.

A *hybrid electric vehicle* (see Figure 6.2) will therefore combine a combustion engine with an electric motor (*a minima*) with the aim of enhancing the performances of purely internal-combustion-based and/or purely electric vehicles (see the philosophy of hybrid engineering mentioned above). With regard to purely internal-combustion-based vehicles, the major goal for hybrid electric vehicles will be to reduce *in situ* emissions of pollutants. With regard to purely electric vehicles, the major goal will be to increase their range.

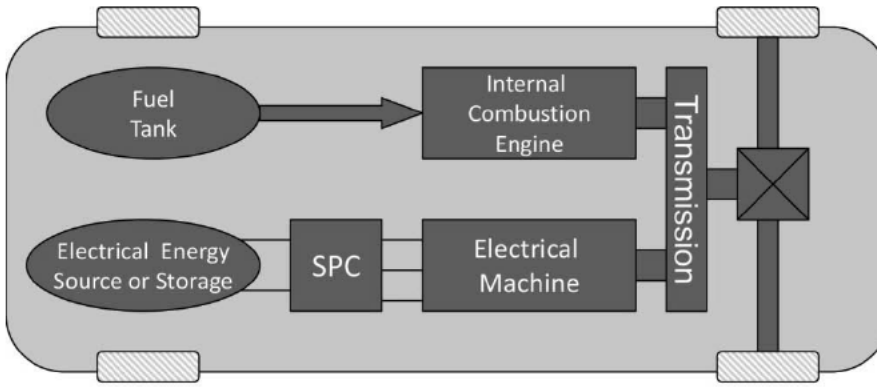

Figure 6.2. *Parallel hybrid electric vehicle*

6.2.3. *Hybrid electric system*

Beyond the very particular application of hybrid electric vehicles, the electricity storage or production devices described in the previous chapters can also be combined to create a *hybrid electric system*, marrying certain advantageous performances (lifetime, efficiency, energy density, power density, etc.) from each of the elements taken separately. In this case, the applications are – of course – not limited only to vehicles or to the transport domain. Such electricity storage systems are to be found in the domain of stationary applications – particularly with the emergence of electrical energy production from renewable energies, which are obviously often intermittent in nature. Still in the stationary domain, these electricity storage systems may be on a large scale (in terms of power or time, etc.), and will also play a major role in the "Smart Grids" of the future.

6.3. Advantages to hybridization

Before highlighting the advantage of hybridization, it is useful to introduce the criteria which will be used to measure the performances of the hybrid power system but also the intrinsic performances of the unitary elements. Conventionally, there are six criteria that can be used [BEN 05; ALL 10]:

– *specific power (expressed in W/kg)*: this reflects the capacity for a given storage device or source weighing 1kg to generate a given level of power;

– *specific energy (expressed in Wh/kg)*: this represents the energy stored or supplied per unit mass. It should be noted that this specific energy constitutes a

theoretical maximum value, which in practice is often unattainable, because of the charge and discharge efficiencies of the storage devices and the fact that certain types of storage devices can never be totally discharged;

– *durability*: the durability is generally characterized by the number of charge/discharge cycles that can be considered for electrochemical or electrostatic storage devices (batteries and supercapacitors). For external storage systems (electrolyzers and/or fuel cell), it is preferable to quantify this durability in terms of the number of hours of acceptable operation (i.e. until the degradation observed is no longer compatible with the operational needs). Irrespective of the definition used, it is tricky to quantify, as it depends on a great many operational parameters (the dynamics of the cycles, excursion in terms of state of charge, temperature, etc.);

– *cost (in €/kWh)*: in general, this represents the cost observed for the initial investment and for operation;

– *recyclability*: this parameter enables us, in evaluating the element, to take account of the proportion of that element which can be recycled at end of life;

– *safety*: as one might imagine, this is an indicator of the risks associated with a storage device or a source of electrical energy.

6.3.1. *Ragone plot*

6.3.1.1. *General description*

Generally, engineers use the Ragone plot [RAG 68] to present the performances of electricity storage devices. This plot traces the specific energy of the element as a function of its specific power, both on a log/log scale. Of the six relevant criteria mentioned above, this method considers only the first two, which are essentially linked to the initial performances of the elements and the technological aspects.

The efficiency of an electricity storage device is generally dependent on its given operating point. This means that such a storage device corresponds not only to a point on the Ragone plot, but rather to a curve. These curves enable us to identify the maximum power limit and the optimal working zone (i.e. the zone wherein the specific energy and power are high). The shape of the curve obtained depends on the physical limits (maximum and minimum) of discharge of the electricity storage device in question. This curve is, of course, specific to the type of storage device. Figure 6.3 shows a typical curve of an electrical energy storage device. We note a limitation in energy, a limitation in power, and two particular zones: one limiting the energy at low power (this phenomenon is due to the self-discharge of the storage devices), and the other limiting the power (this phenomenon is due to the presence of an internal resistance).

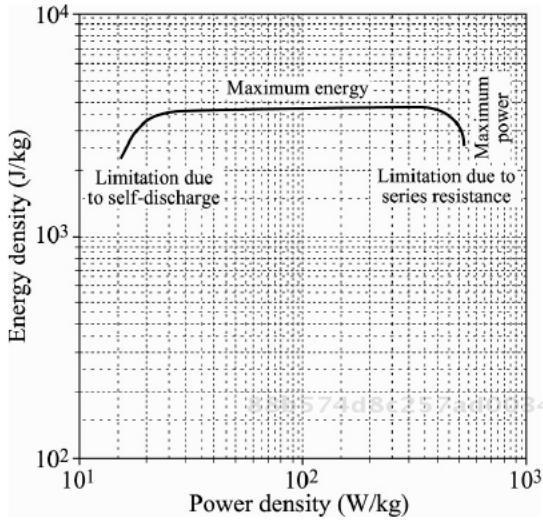

Figure 6.3. *Ragone plot typical of an electricity storage device*

Such a Ragone plot also clearly shows the range of operation which should be reached for a given electricity storage device. Indeed, the optimal working zone highlights the fact that the total energy can only be extracted within a certain range of power.

6.3.1.2. *Tracing of the plot in a generic case [CHR 00]*

To trace the Ragone plot in a generic case, let us take the example given in Figure 6.4. In this scheme, the energy storage device feeds a charge with a constant (active) power $P \geq 0$.

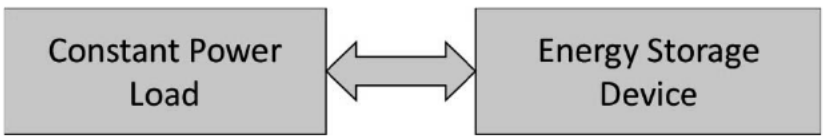

Figure 6.4. *Generic circuit associated with the tracing of the Ragone plot*

By way of illustration, if we consider an energy storage device (which may represent a large number of practical scenarios, considering analogies with the electrical domain) as being made up of a voltage source $V(Q)$ – dependent on the stored charge which is notated as Q –, an internal resistance (notated as R) and an internal inductance (notated as L). If the power is P, the overall voltage U of the

storage device and the current I passing through it are linked by the relation $P = U.I$. Very conventionally, it is also possible to write:

$$I = \frac{dQ}{dt} = \dot{Q} \qquad [6.1]$$

If we consider initial conditions $Q(0) = Q_0$ and $\dot{Q}(0) = \dot{Q}_0$, the equation governing the dynamics of the system in question can be written as:

$$L\ddot{Q} + R\dot{Q} + V(Q) = -\frac{P}{\dot{Q}} \qquad [6.2]$$

At time $t = 0$, the storage system contains the stored energy given by equation [6.3] (where $W(Q_0)$ represents the energy initially stored in the voltage source):

$$E_0 = L\frac{\dot{Q}^2}{2} + W(Q_0) \qquad [6.3]$$

For $t \geq 0$ and a constant power P required by the charge, the stored charge $Q(t)$ follows the evolution defined by equation [6.2]. For finite values of the energy E_0 initially stored in the energy storage device under consideration (a hypothesis which is at least realistic), it is clear that the power will only be able to be supplied by that storage device for a finite period of time, depending on the power requirement. This time-period is notated as $t = t_\infty(P)$. As the power P is time-independent, the energy available in the storage device can be written, using:

$$E(P) = P.t_\infty(P) \qquad [6.4]$$

Tracing equation [6.4] on a log/log scale gives us the Ragone plot, which is generally normalized by dividing by the mass of the component under examination. This is particularly useful during the sizing phases of a hybrid electricity storage system, where the performances often need to be limited because of constraints in terms of mass and/or volume.

It should also be noted that the approach discussed in this section is independent of the type of storage device. As mentioned above, this may not necessarily be electrical in nature, but if need be, similarities can be drawn with the electrical domain.

6.3.1.3. *Location of the plots obtained*

Proceeding in the way described above for different types of energy storage devices, we can localize the curves obtained, here expressed in energy density and power density, as shown in Figure 6.5 below. The spatial location shown here is relative to the "nominal" usage zone for the storage device in question. It is noteworthy that, on the one hand, there are components which present a high specific power and a relatively low specific energy (typically supercapacitors or flywheels); and on the other hand, there are components which exhibit a potentially high specific energy for a low specific power (such is the case, notably, for fuel-cell systems and internal combustion engines). It is also important to stress that with these elements, as demonstrated in Figure 6.5, the very notion of specific energy is tricky to apprehend, in that the available energy relates not only to the element itself, but also to the fuel tank to which it is connected.

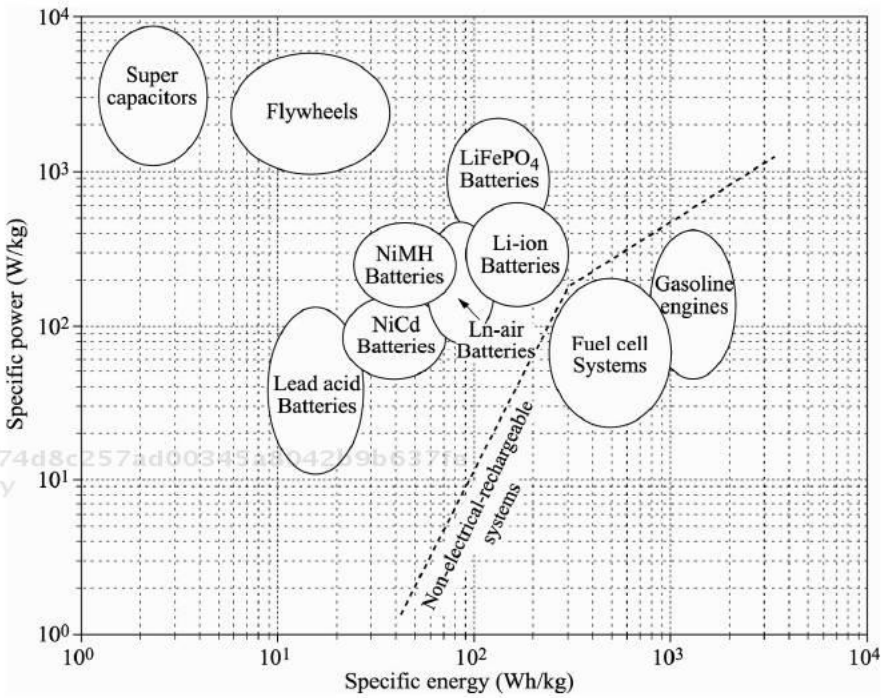

Figure 6.5. *Location of the different traces obtained on the Ragone plot*

Between these two extremes, in particular we find the different types of electrochemical batteries, whose performances vary by a factor 10 depending on the technologies in question.

6.3.2. *Different types of energy?*

Looking at the comparative Ragone plot shown in Figure 6.5, we note that all the electricity storage devices presented in this book (batteries, supercapacitors, flywheels, fuel cells, etc.) do of course store energy, but with constraints on the storage and also the restitution of that energy, which differ significantly.

With regard to the storage constraints, let us take the example of a small electric vehicle, which we wish to imbue with an autonomous range of 100 km. It is useful to envisage an energy supply of around 15 kWh. If we neglect the efficiencies of the converters, and the charge/discharge efficiencies of the different electricity storage devices (which may, depending on the case, constitute a "rough" approximation), the efficiencies of the different auxiliary subsystems needed for the storage devices to operate, we get the following (embedded, etc.) masses:

– around 50 kg for a PEM fuel cell (PEMFC) connected with a storage tank of compressed hydrogen;

– around 75 kg for Li-ion batteries;

– around 375 kg for lead-acid batteries;

– around 1500 kg for a flywheel; and

– nearly 3000 kg if we wish to store this energy using supercapacitors.

Thus, it goes without saying that just on this criterion of embedded mass, certain solutions (flywheel, supercapacitors) appear totally unrealistic. However, does this mean we need to dismiss them totally out of hand? The answer is obviously no, as will be explained in the following sections.

Let us return now to our example of a small electric vehicle. Typically the power of a small vehicle such as this is around 50 kW (which is around 68 hp). Again, if we neglect the efficiencies of the electric traction chain, the electricity storage system in question therefore needs to be able to provide such levels of power. In view of the mass power of the storage devices under consideration, we now get the following results:

– around 500 kg for the PEMFC combined with its compressed hydrogen storage tank;

– around 500 kg for lead batteries;

– around 170 kg for Li-ion batteries;

– around 25 kg for a flywheel;

– only around 15 kg for supercapacitors.

We note that now the advantage is completely reversed, which suggests that for the criterion of mass alone, it is best to favor supercapacitors. Of course, in reality, the solution is not unique, but rather is hybrid, so as to best reconcile the requirements of the technical specifications with the intrinsic characteristics of the components. We shall come back to this later on.

Another interesting way of looking at these results is to combine them with the notion of time. In practice, a given element is capable of furnishing a given level of power for a specific length of time. Of course, with this approach, we see the notions of power and energy implicitly re-emerge. Notably going back to the electricity storage devices presented hitherto, we therefore get Figure 6.6. In this figure, taken from [AMI 07], we can see not only the target zone of power for each element, but also the "nominal" operating time at that power level. This operating time can also be considered as a "time constant" [MUL 04] and is therefore denoted as τ (the unit is the second). This time constant is defined as being the relation between the energy capacity of the storage device in question (here notated as E_{store} and expressed in Wh) and the maximum power for the charging or discharging of that element (notated as $P_{\max}$) (see equation [6.5]). Often, though, electricity storage devices cannot be completely discharged; therefore there is a difference between the exploitable energy and the stored energy. The time constant mentioned above can therefore be defined in relation to this value of truly usable energy, denoted as E_{usable} (see equation [6.5]).

$$\tau = \frac{E_{store}}{P_{\max}} \quad \text{or} \quad \tau = \frac{E_{usable}}{P_{\max}} \qquad [6.5]$$

Thus, Figure 6.6 enables us to quickly find technological solutions for the design of a hybrid electrical system, on the basis of the power/time constraints of the intended application.

If we consider for instance (and without loss of genericity) a hybrid electricity storage system intended for an onboard application, the criterion governing the design is the requirement in terms of power and operating time (in other words, the power and energy requirements). However, this need for electrical power and for operating time is directly dependent on the function that the vehicle is intended to serve (civilian use, military, etc.), the environmental constraints associated with that function (urban or peri-urban usage for a car; slope and route for a locomotive; takeoff and landing for an airplane, etc.), the level of electrification and the intermittence of the onboard auxiliary components, etc.

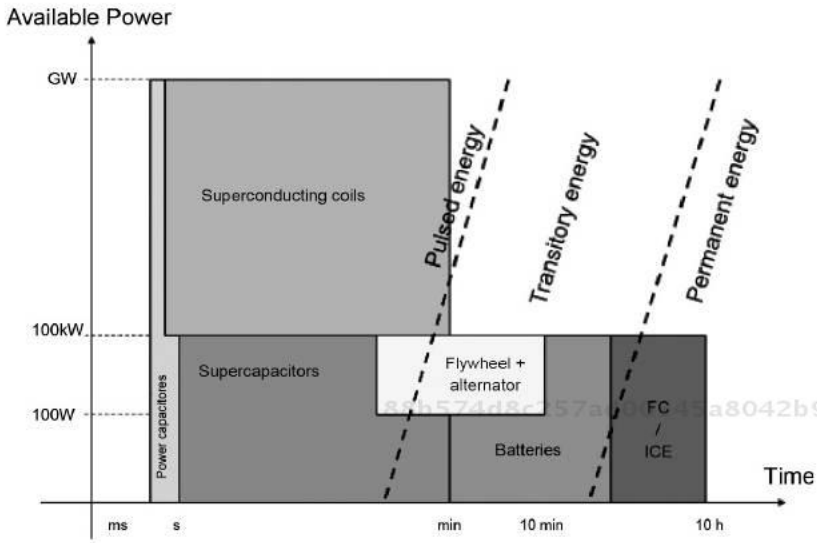

Figure 6.6. *Location of the different electricity storage devices on a power/time plot*

On the basis of this observation, Michel Amiet [AMI 07] therefore put forward what he calls the "Three E Theory", whereby the energy requirement is divided into three "types" of energies: permanent energy (average power needing to be supplied for a relatively long period of time), transitory energy (higher power needing to be provided for a duration of a few minutes) and pulsed energy (very great power needing to be supplied for only a few seconds).

$$E = E_P + E_T + E_I \qquad [6.6]$$

This theory leads us to select the available energy sources on the basis of the specific need of the component that is to be supplied. Of course, this immediately implies the need to "manage" this energy as intelligently as possible, using strategies rooted in mathematics, automation engineering and artificial intelligence, and by way of power electronics. We shall return to this point later on in this chapter.

If we attempt to identify the storage solutions combined with these different types of energy (see Figure 6.6):

– fuel-cell systems and internal combustion engines are generally dedicated to supplying "average" power presenting only very slight fluctuations. In general, therefore, we shall consider these components as permanent energy providers;

– batteries are generally used over shorter durations and with more significant dynamics: hence, they will generally be considered as transitory energy providers;

– power capacitors, supercapacitors, flywheels and superconducting coils are, for their part, usually drawn upon for very short periods of time and often provide very high levels of power. Hence, they will be considered as pulsed energy providers.

However, two remarks must be made here:

– firstly, this division, although it does show the major tendencies, may be subject to certain small adjustments on the basis of the application in question; this is represented in Figure 6.6 by oblique separating lines rather than vertical ones;

– secondly, in our discussion here we have considered only the supply of energy. Of course, for components which are able to be recharged electrically, these considerations are also valid in receiver mode.

6.3.3. *Taking account of non-energy-related criteria in the choice of a hybrid electricity storage solution*

Hitherto, we have only taken account, so to speak, of energy-related criteria (mass power, mass energy, power/time plots) to qualify, compare and select the electricity storage solutions. Of course, other criteria (durability, cost, recyclability, safety, etc.) – some of which are more subjective – also need to be taken into consideration when defining a hybrid architecture for electricity storage.

One interesting way of quickly (and therefore graphically) comparing electricity storage systems on the basis of these four new criteria in combination with the previous two, is to use radar charts. This approach was also advanced by Anne-Laure Allègre in her doctoral thesis [ALL 10]. It consists of representing these six criteria (modalities), say, according to five levels of performance (numbered from 1 to 5, with 5 being the best result). Table 6.1 presents the meaning of each of these performance levels, on the basis of the modalities proposed.

Performance levels	Mass energy (Wh/kg)	Mass power (W/kg)	Cost (€/kWh)	Durability (number of cycles)	Safety	Recyclability (in %)
Level 1	5–10	50–100	$> 10^6$	$10–10^2$	Very poor	0–20
Level 2	11–50	101–500	$10^5–10^6$	$10^2–10^3$	Poor	21–40
Level 3	51–100	501–1000	$10^4–10^5$	$10^3–10^4$	Average	41–60
Level 4	101–500	1001–5000	$10^3–10^4$	$10^4–10^5$	Good	61–80
Level 5	> 500	> 5000	$10^2–10^3$	$> 10^5$	Very good	81–100

Table 6.1. *Performance levels according to six criteria*

Figure 6.7 shows the radar charts thus obtained for the three electricity storage devices studied in this book: batteries, electrolyzer/fuel cell assemblies and supercapacitors. However, in order to illustrate the diversity of the performances achieved by electrochemical accumulators, we shall also discuss the results for a lead-acid battery and for a $LiFePO_4$ battery.

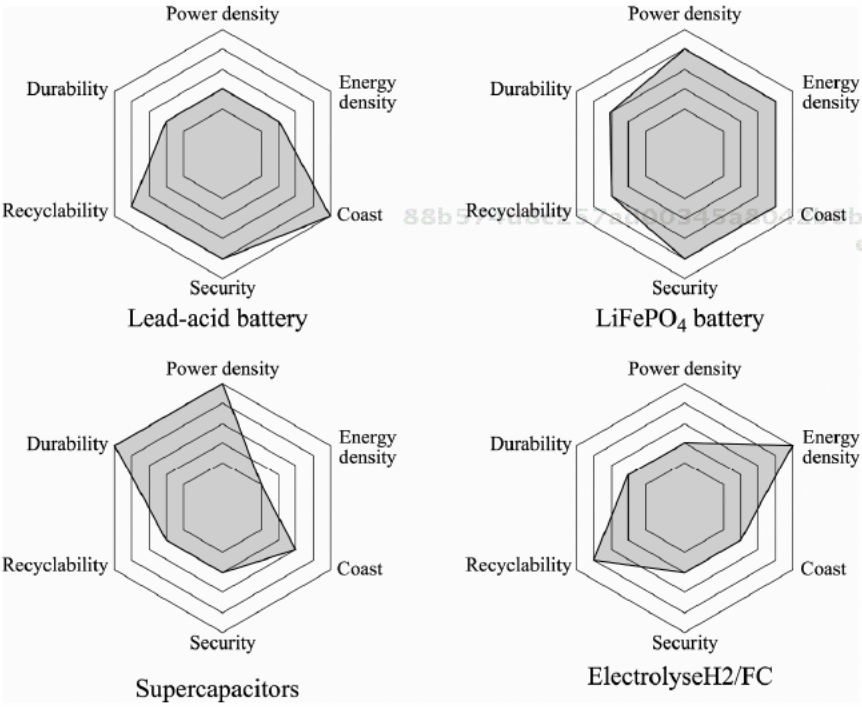

Figure 6.7. *Radar charts comparing different electricity storage technologies*

For the lead-acid battery, if we now look at the non-energy-related criteria, its durability will be arbitrary, between 500 and 1000 charge/discharge cycles, depending on its usage. The cost is very low – typically around €200/kWh. Recycling procedures for this type of battery are now very firmly in place (with over 90% of batteries recycled in France); in addition, nearly 80% of their constitutive materials are recycled. In terms of safety, the main two dangers presented by these batteries are the electrolyte used (sulfuric acid) and the release of hydrogen that occurs during the charge-up phase. All told, if certain precautions are taken, these safety constraints are not unreasonable.

For the $LiFePO_4$ battery, the durability is a little better than the lead-acid battery (typically around 2000 charge/discharge cycles). The price of these batteries is

reasonable – around €1000/kWh. With regard to the recyclability of this type of accumulator, the sticking point at present lies essentially in the collection of them, which is a service that is as yet very underdeveloped. On a safety level, this lithium battery technology is probably the safest available at present, as there is no risk of explosion or fire.

For supercapacitors, the *forte*, besides the specific power, is undeniably the durability, with the possibility of achieving more than a million charge/discharge cycles. The prices are as yet very high, particularly when expressed per Wh – around €10–15 k/kWh. In terms of recyclability, the service is still in its infancy, particularly because of the poor market penetration of this technology. For its part, the safety of this type of storage device is still problematic, due largely to the risk of explosion and the presence of acetonitrile in the electrolyte.

Finally, the "hydrogen battery" (i.e. the combination of an electrolyzer and a fuel cell) for electricity storage is as yet of little interest in terms of the number of charge/discharge cycles – particularly because of the relatively short lifetime of each of the organs (a few thousand hours only, when considering PEM (Proton Exchange Membrane) technology especially). Given that this technology is less mature than the previous ones, it is difficult to quote a guideline price. However, what is likely is that this technology will remain more expensive than the previous ones, owing to the energy conversion chain involved. On the other hand, still on a prospective level, the recyclability should be very good. Finally, as regards safety, the presence of hydrogen and oxygen together, combined at a sometimes high level of pressure as well, remains and will remain a risk factor.

Analyzing these radar charts, we are led to two conclusions:

– there is no single solution for electricity storage which is able to deliver high levels of performance for all of the six criteria under consideration;

– it will therefore be necessary to combine (i.e. hybridize) two or more of these unitary elements to create a hybrid electricity storage system which (at least theoretically) exhibits better performances than those of each of its constituent parts taken in isolation.

6.4. Management of the energy flows in a hybrid system

The previous section illustrated the performances of electricity storage systems and laid the foundations for an objective comparison of such systems. The design of the "hybrid" electricity storage system will essentially stem from that analysis.

The question which we now need to ask ourselves is that of the management (generally in real time) of the energy flows taking place in such hybrid systems.

Indeed, regardless of the quality of the initial design of the hybrid system, if this management of the energy flows is not appropriate, the system's performances will remain limited. The energy-flow management strategy therefore needs to be chosen so as to make optimal use of each of the subsystems for electricity storage making up the hybrid system.

A simple way of classifying these energy flow management strategies is to divide them into two groups [ALL 10]:

– optimization-based strategies;

– rule-based strategies.

Detailed analysis of these strategies would go far beyond the mandate of this book. Hence, here, we shall content ourselves with a description of the major principles and refer readers to works in the bibliography for additional elements – particularly regarding the application of such strategies.

6.4.1. *Optimization-based strategies*

These strategies can themselves be subdivided into two categories: those using global optimization and those which are applicable in real time.

6.4.1.1. *Methods using global optimization*

In the first case, we seek to minimize one or more criteria (for instance, we could cite the minimization of the hydrogen consumption for a fuel cell/battery vehicle) expressed in the form of mathematical function(s). In order to carry out this minimization, the dynamic programming method based on Bellman's principle of optimality [BEL 55]:

> *"A sub-trajectory of an optimal trajectory is itself optimal for the objective function restricted to trajectories sharing the origin of that sub-trajectory"*

is often used [SCO 04; BER 07; HAN 08]. This principle facilitates the use of an ascending resolution method, which determines an optimal solution to a problem on the basis of the solutions of all the sub-problems.

In the same spirit, it is also possible to use optimal control, which is based on Pontryagin's minimum principle [PON 62], which aims to find the control signal which is capable of switching a dynamic system from one state to another, in the presence of constraints on the state or the control signals [DEL 02; HAN 08].

The advantage to this type of approach lies in the fact that the solution obtained is theoretically optimal. The process of optimization takes account of the physical constraints on the components; however, it may be very costly in terms of computation time (and therefore often incompatible with the real-time requirement that is usually the rule in a hybrid storage system) and also requires prior knowledge of the profile of the load required over time, in order to be able to deliver an overall optimization.

6.4.1.2. *Methods applicable in real time*

In the face of these difficulties in the practical use of these methods, adaptations of these strategies have been put forward, but which are therefore necessarily sub-optimal. The advantage here is twofold: adaptation to the temporal constraints associated with real-time operation, and the lack of need for prior knowledge of the load profile.

In general, therefore, the solutions proposed involve "adapting" the above strategies (particularly the optimal control theory) with a view to "predicting" the future energy requirement applied to the system over a finite temporal horizon [KER 09]. Of course, this is particularly tricky. The proposed methods seek to identify, from the past (and therefore known) energy demand, certain "constants" (e.g. frequency ranges, amplitude ranges, etc.) that can be used to make this "prediction". There are a number of different methods which can be envisaged to do this – particularly neural networks, fuzzy logic, wavelet decomposition, etc. [LEN 03].

6.4.2. *Rule-based strategies*

So-called rule-based strategies are based on expert knowledge of the behavior expected of the storage system. It is important to stress that they merely give linguistic expression to this expert knowledge. They exhibit the major advantage of having operation which is almost always compatible with the temporal requirements associated with real-time operation.

The rules used may be deterministic or non-deterministic. For instance, for an FC system, we know that an open-circuit operation is to be avoided if we wish to increase the durability of the system. Thus, one rule might be to prohibit this open-circuit operation.

With the same spirit, we can also perform frequency filtering. This involves arbitrarily defining one or more limit frequencies and, on the basis of the frequency of the power load demanded by the charge in comparison to these limit frequencies, adjusting the power demand to one storage device or another (typically high

frequencies on pulsed energy storage devices, medium frequencies on transitory energy storage devices and low frequencies on permanent energy storage devices) [CHA 99]. Implicitly, this again is a rule-based strategy.

We can also use "fuzzy" rules (based on fuzzy logic theory) to produce excellent results [TEK 07; SOL 11], or indeed neural networks, adaptive or otherwise [MOR 06].

An example of a definition for some of these fuzzy rules might be as follows, in the context of a vehicle supplied by a fuel cell and supercapacitors (where P_{dem} denotes the power demanded on the DC bus of the vehicle and $dP_{PAC}^{\max}$ is the maximum acceptable variation in power on the FC system):

Rule 1: IF $P_{dem} < 0$ THEN (recharge the supercapacitors).

Rule 2: IF $P_{dem} > 0$ AND IF $\left(dP_{dem}/dt < dP_{PAC}^{\max}\right)$ THEN (provide the required power using the fuel-cell system).

Rule 3: IF $P_{dem} > 0$ AND IF $\left(dP_{dem}/dt > dP_{PAC}^{\max}\right)$ THEN (provide the maximum possible power using the fuel-cell system and the remainder using the supercapacitors).

Rule 4: etc.

As we can see from this little example, these rules are very easy to define, and they can also be easily supplemented if necessary. By way of illustration, rule 1 above can obviously be envisaged only within the maximum acceptable limit of the supercapacitors. It can therefore be built upon by limiting the validity of that rule as follows (with SOC_{SCAP} denoting the state of charge of the supercapacitors):

Rule 1 *bis*: IF $P_{dem} < 0$ AND IF $\left(SOC_{SCAP} < SOC_{SCAP}^{\max}\right)$ THEN (recharge the supercapacitors).

As we have seen, the definition of these fuzzy rules is very easy, and is based directly on human expertise about the procedure. Computerized processing of all these rules, which can operate in parallel to one another, is governed by fuzzy logic theory and is entirely compatible with real-time requirements.

6.4.3. *Criteria for the supervision of the energy flows*

Regardless of the strategy envisaged for the supervision of the energy flows in a hybrid electric system, we generally seek to optimize one of the criteria mentioned

above. This optimization is sometimes explicit – e.g. in the case of optimal control – and sometimes implicit, as in the case of fuzzy rules. Of the optimization criteria used, we can cite the following in particular (although this is by no means an exhaustive list):

– the "fatal" energy consumption (heat losses to be minimized, fossil fuel consumption in a hybrid vehicle to be minimized, hydrogen consumption in a fuel-cell-based installation to be minimized, etc.);

– the mass and/or volume of the electricity storage system;

– the dynamic performances of the electrical storage system;

– the cost of the system;

– its lifetime;

– its safety.

We can also seek to optimize several of these criteria simultaneously. In this case, we can use a composite criterion, defined as a function of the relative weight of each of the initial criteria.

6.5. Example of application in the domain of transport: the ECCE platform (*Evaluation des Composants d'une Chaine de traction Electrique* – Evaluation of the Components in an Electric Powertrain)

Here we are going to illustrate hybridization in electricity storage systems using an applied example taken from transport. In order to do so, we could have focused on different prototypes of vehicles offered by almost all manufacturers the world over. As we did not wish to make a (necessarily arbitrary) choice between these different prototypes, we have chosen to present a mobile platform for evaluating and testing components (particularly for onboard storage of electrical energy) in an electric traction chain.

Electric vehicles offer far better dynamic performances than those of vehicles driven by an internal combustion engine, but are heavily penalized by their limited range. In France, the *Direction Générale de l'Armement* (DGA – General Directorate for Armament) was therefore particularly interested in testing the different structures and electricity storage devices in a high-power hybrid vehicle. In view of the potential applications, serial hybridization is the most advantageous option in this case. This approach led to the design, construction and testing of the ECCE platform (see Figure 6.8), which was the fruit of a collaboration under the auspices of the DGA between industrialists and university and public research laboratories [KAU 11]. From the very beginning, this platform was designed in a

modular manner, so that it could be used to test different electrical storage devices on a full-size scale and in onboard conditions. Here, we shall focus on the particular case of energy supply to the DC bus, by a PEMFC system combined with supercapacitors and lead-acid accumulators. Thus, it uses a configuration combining permanent, pulsed and transitory energy storage. The diagram of the principle of the configuration considered for the vehicle is given in Figure 6.9.

ECCE in road tests ECCE equipped with a FC system

Figure 6.8. *ECCE mobile platform / equipped with a PEMFC system*

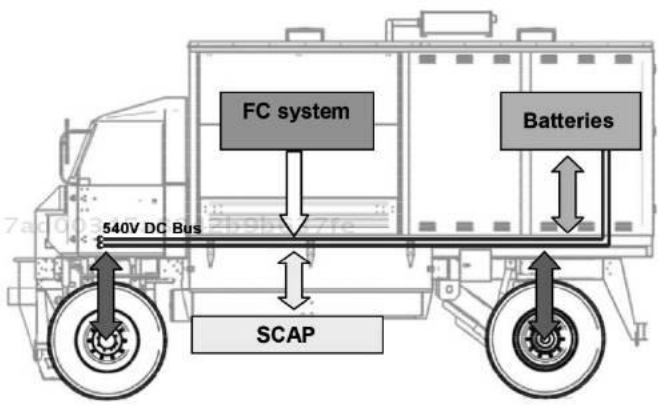

Figure 6.9. *Diagram of the principle behind ECCE in its FC / SCap / Batteries configuration*

Energy distribution takes place around a 540 V (± 270 V) DC bus, which is directly connected to the batteries. In view of the quantity of energy needed and the cost of the batteries, the decision was made to use energy-type lead-acid batteries. 90 elements (6 V; 98 Ah) were serialized, forming two groups, and the common point was linked to the bulk of the chassis. The batteries determined the maximum

current (462 A; 1min) in the charges and the recharging current (20 A) was chosen with a view to ensuring satisfactory battery life.

Up to four electric motors, each comprising 30 kW, were used to drive the vehicle. Each wheel had a converter feeding a motor to drive the wheel directly. As it was a mobile testing array, all four motors were of different types but all had the same nominal power of 30 kW. Thus, at the front, there was a permanent-magnet wheel motor with sine control and a permanent-magnet wheel motor with trapeze control. The magnets in these motors were mounted on the surface. At the rear, there was an induction motor with vector control and a synchronous claw-pole motor with sine control. The converters were adapted to the type of motor, with only the level of control in terms of torque, and therefore current, being pre-defined. It was the front motors which offered the best performances, particularly for the startup torque, which reaches up to six times the nominal torque of 700 N.m.

The fuel-cell system comprised two PEMFC stacks of 110 cells with an active surface area of 760 cm^2. Each fuel cell (FC) was supplied with air and hydrogen. An internal controller managed the FC system in its entirety (stacks, air compressor, flow meter, valves, etc.). A water cooling system was used and heat exchanges with the outside environment took place through an air/water exchanger. The FC system was connected to the 540 V bus via a DC/DC converter. The nominal electrical power that the FC system could deliver was 35 kW. Hydrogen was supplied from a rack of six canisters of compressed hydrogen (200 bars) installed behind the exchangers. Hydrogen sensors were of course installed to ensure safety in case of a leak.

The energy stored in the supercapacitors was sufficient to maintain the voltage on the DC bus following a demand for 40 kW of power for 9 seconds.

A fuzzy-logic-type strategy for management of the energy flows was put in place on this vehicle. More detailed information about this strategy is to be found in [SOL 12]. The on-road experimental results (see Figure 6.10) highlight the participation of the three energy sources (fuel-cell system, supercapacitors, batteries) in energy supply to the vehicle. Thus, we note that the bus voltage was properly maintained around the 540 V mark, although some fluctuations are observed which are attributable to the charging/discharging of the lead batteries (directly connected to the DC bus). The supercapacitors responded to the dynamic loading and were able to recover energy during braking. The fuel-cell system, for its part, provided power with a dynamic that was compatible with the supply of the reagent gases (particularly the supply of oxygen from the air, supplied by the air-compressor group).

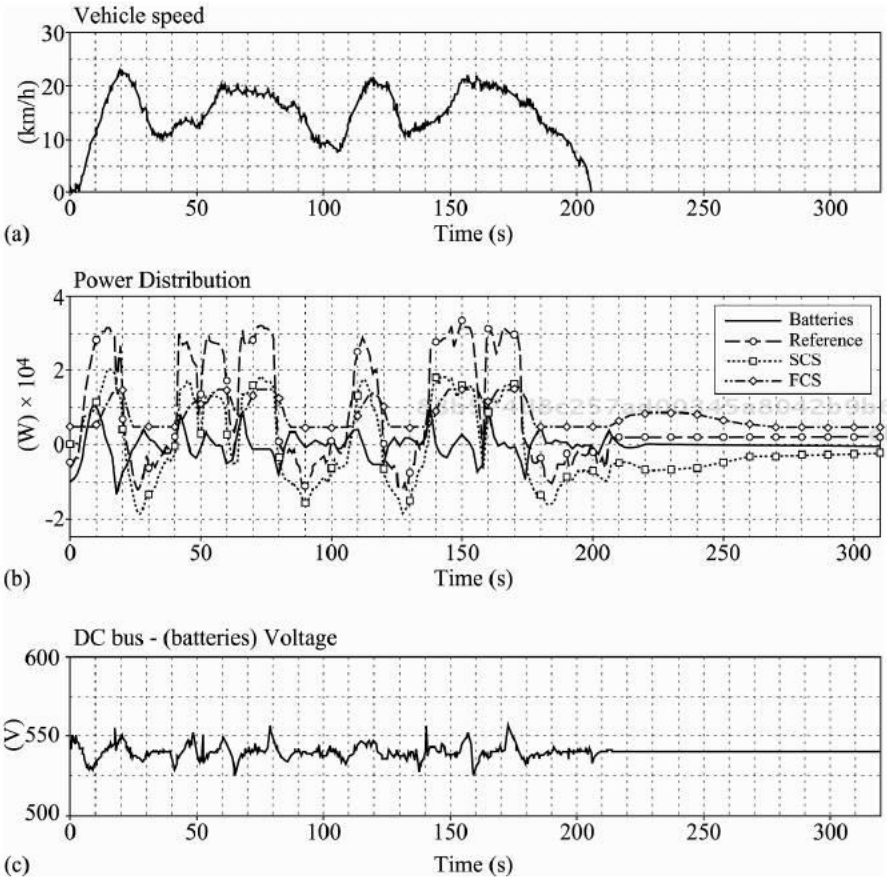

Figure 6.10. *On-road test results for ECCE in its FC / SCap / Batteries configuration*

6.6. Corrected exercises

6.6.1. *Ragone plot of an ideal battery*

We are interested here in tracing the Ragone plot for an "ideal" battery (meaning no inductive effect is taken into account, no frequency-dependency of the values, no intrinsic nonlinearity of the component). The battery is assumed to present a charge Q_0 at the initial time and an internal resistance of value R. It is connected to a charge/discharge system with constant power P (see the diagram below).

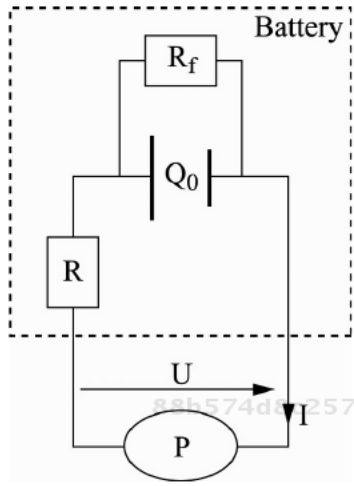

Figure 6.11. *Connection of an ideal battery to a charge with constant power*

1) Trace the Ragone plot for this ideal battery, assuming there to be no leakage resistance ($R_f = \infty$ on the diagram above).

2) Then trace the plot in the case where the leakage resistance has a finite value notated as R_f.

Solution

1) Here the battery is considered with a constant voltage (independent of the charge), given by:

$$\begin{cases} V = U_0 & \text{if} \quad Q_0 \geq Q > 0 \\ V = 0 & \text{if} \quad Q = 0 \end{cases}$$

Equation [7.2] is now written thus (with $I = \dot{Q}$):

$$P = U.I = (U_0 - RI)I$$

The solutions to this equation are written as:

$$I_{\pm} = \frac{U_0}{2R} \pm \sqrt{\frac{U_0^2}{4R^2} - \frac{P}{R}}$$

In order to identify the appropriate value of I, we focus on the case where $P \to 0$. In this case, two possibilities can be envisaged: $I_+ \to U_0 / R$ (which in practice corresponds to a short-circuited operation) and $I_- \to 0$ (which in practice corresponds to an open-circuit operation). Clearly, in the context of tracing the Ragone plot, only the second scenario here is of interest to us, so $I = I_-$.

The battery will be discharged after time $t_\infty = Q_0 / I$. The initial charge is linked to the initial energy according to: $E_0 = Q_0 U_0$. Thus, we can describe the energy available for the charge by writing:

$$E_{batt}(P) = P.t_\infty = \frac{2R.P.Q_0}{U_0 - \sqrt{U_0^2 - 4R.P}}$$

This last equation corresponds to the characteristic Ragone curve for the ideal battery. It can usefully be expressed in a dimensionless manner by setting $p = 4R.P / U_0^2$ and $e_{batt} = E_{batt} / (Q_0 U_0)$. Then we get:

$$e_{batt}(p) = \frac{1}{2} \frac{p}{1 - \sqrt{1-p}}$$

We can easily show that $\lim_{p \to 0} e_{batt}(p) = 1$ and that $e_{batt}(1) = 1/2$. The curve thus obtained is shown as a solid line in Figure 6.12.

2) If we wish to take account of a leakage resistance with a finite value R_f, the reasoning is exactly the same, but it is helpful to add to the previous discharge current a leakage current with the value U_0 / R_f. Thus, we obtain the following equation:

$$e_{batt}(p) = \frac{1}{2} \frac{p}{1 - \sqrt{1-p} + 2R / R_f}$$

We can see that in this case, $e_{batt}(0) = 0$ and that $e_{batt}(1) \cong 1/2$ (because we assume the leakage resistance to be significantly less significant than the internal resistance). We can also show that, here, the Ragone curve attains a maximum for a value of $p \approx \sqrt{\frac{8R}{R_f}}$.

The curve thus obtained is shown as a dotted line in Figure 6.12.

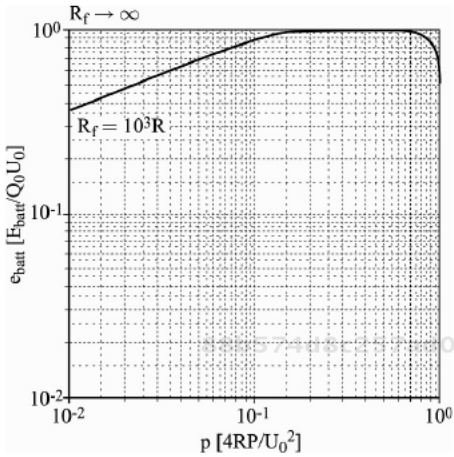

Figure 6.12. *Ragone plot of an ideal battery*

6.6.2. *Ragone plot of an ideal capacitor*

Draw the Ragone plot for an "ideal" capacitor, whose capacity C is supposed to be constant and whose only imperfection is an internal series resistance R. The initial voltage at the edges of the capacity is notated as $U_{C,0}$. The ensemble is connected to a charge/discharge system with constant power P (see the diagram below).

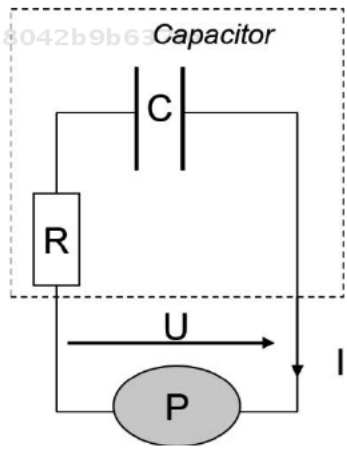

Figure 6.13. *Connection of an ideal capacitor to a charge with constant power*

Solution

By substituting the expression of $V(Q) = Q / C$ into equation [6.2], we can write:

$U = P / I = Q / C - RI$; here $I = -\dot{Q}$.

By deriving this equation in relation to time, we get:

$$\frac{dU}{dt} = \frac{1}{C}\frac{dQ}{dt} - R\frac{dI}{dt} = \frac{-P}{CU} + R\frac{P}{U^2}\frac{dU}{dt}$$

or indeed:

$$\left(1 - \frac{R.P}{U^2}\right)\frac{d\left(U^2\right)}{dt} = -\frac{2P}{C}$$

By integrating this last equation and noting that C, R and P are constants, we finally get:

$$t(U) = \frac{C}{2P}\left\{R.P \ln\left(\left(\frac{U}{U_0}\right)^2\right) + U_0^2 - U^2\right\}$$

The (theoretical) plot of this last curve demonstrates first a discharge of the capacitor, associated with an increase in time, followed by a discharge with a time that begins to decrease, which is physically impossible [SAI 04]. The result of this is the existence of a maximum (denoted $t_\infty = t(U_\infty)$ for a limited voltage value notated as U_∞) defined by $dt/dU = 0$ – for this maximum, the capacitor is no longer capable of providing the required power. We have:

$$\frac{dt}{dU} = \frac{C}{P}\left(R.P\frac{1}{U} - U\right)$$

Thus, $U_\infty = \sqrt{R.P}$ and:

$$t_\infty = \frac{C}{2P}\left\{R.P \ln\left(\frac{R.P}{U_0^2}\right) + U_0^2 - R.P\right\}$$

Indeed, regardless of the quality of the initial design of the hybrid system, if this management of the energy flows is not appropriate, the system's performances will remain limited. The energy-flow management strategy therefore needs to be chosen so as to make optimal use of each of the subsystems for electricity storage making up the hybrid system.

A simple way of classifying these energy flow management strategies is to divide them into two groups [ALL 10]:

– optimization-based strategies;

– rule-based strategies.

Detailed analysis of these strategies would go far beyond the mandate of this book. Hence, here, we shall content ourselves with a description of the major principles and refer readers to works in the bibliography for additional elements – particularly regarding the application of such strategies.

6.4.1. *Optimization-based strategies*

These strategies can themselves be subdivided into two categories: those using global optimization and those which are applicable in real time.

6.4.1.1. *Methods using global optimization*

In the first case, we seek to minimize one or more criteria (for instance, we could cite the minimization of the hydrogen consumption for a fuel cell/battery vehicle) expressed in the form of mathematical function(s). In order to carry out this minimization, the dynamic programming method based on Bellman's principle of optimality [BEL 55]:

> *"A sub-trajectory of an optimal trajectory is itself optimal for the objective function restricted to trajectories sharing the origin of that sub-trajectory"*

is often used [SCO 04; BER 07; HAN 08]. This principle facilitates the use of an ascending resolution method, which determines an optimal solution to a problem on the basis of the solutions of all the sub-problems.

In the same spirit, it is also possible to use optimal control, which is based on Pontryagin's minimum principle [PON 62], which aims to find the control signal which is capable of switching a dynamic system from one state to another, in the presence of constraints on the state or the control signals [DEL 02; HAN 08].

The advantage to this type of approach lies in the fact that the solution obtained is theoretically optimal. The process of optimization takes account of the physical constraints on the components; however, it may be very costly in terms of computation time (and therefore often incompatible with the real-time requirement that is usually the rule in a hybrid storage system) and also requires prior knowledge of the profile of the load required over time, in order to be able to deliver an overall optimization.

6.4.1.2. *Methods applicable in real time*

In the face of these difficulties in the practical use of these methods, adaptations of these strategies have been put forward, but which are therefore necessarily sub-optimal. The advantage here is twofold: adaptation to the temporal constraints associated with real-time operation, and the lack of need for prior knowledge of the load profile.

In general, therefore, the solutions proposed involve "adapting" the above strategies (particularly the optimal control theory) with a view to "predicting" the future energy requirement applied to the system over a finite temporal horizon [KER 09]. Of course, this is particularly tricky. The proposed methods seek to identify, from the past (and therefore known) energy demand, certain "constants" (e.g. frequency ranges, amplitude ranges, etc.) that can be used to make this "prediction". There are a number of different methods which can be envisaged to do this – particularly neural networks, fuzzy logic, wavelet decomposition, etc. [LEN 03].

6.4.2. *Rule-based strategies*

So-called rule-based strategies are based on expert knowledge of the behavior expected of the storage system. It is important to stress that they merely give linguistic expression to this expert knowledge. They exhibit the major advantage of having operation which is almost always compatible with the temporal requirements associated with real-time operation.

The rules used may be deterministic or non-deterministic. For instance, for an FC system, we know that an open-circuit operation is to be avoided if we wish to increase the durability of the system. Thus, one rule might be to prohibit this open-circuit operation.

With the same spirit, we can also perform frequency filtering. This involves arbitrarily defining one or more limit frequencies and, on the basis of the frequency of the power load demanded by the charge in comparison to these limit frequencies, adjusting the power demand to one storage device or another (typically high

frequencies on pulsed energy storage devices, medium frequencies on transitory energy storage devices and low frequencies on permanent energy storage devices) [CHA 99]. Implicitly, this again is a rule-based strategy.

We can also use "fuzzy" rules (based on fuzzy logic theory) to produce excellent results [TEK 07; SOL 11], or indeed neural networks, adaptive or otherwise [MOR 06].

An example of a definition for some of these fuzzy rules might be as follows, in the context of a vehicle supplied by a fuel cell and supercapacitors (where P_{dem} denotes the power demanded on the DC bus of the vehicle and $dP_{PAC}^{\max}$ is the maximum acceptable variation in power on the FC system):

Rule 1: IF $P_{dem} < 0$ THEN (recharge the supercapacitors).

Rule 2: IF $P_{dem} > 0$ AND IF $\left(dP_{dem}/dt < dP_{PAC}^{\max}\right)$ THEN (provide the required power using the fuel-cell system).

Rule 3: IF $P_{dem} > 0$ AND IF $\left(dP_{dem}/dt > dP_{PAC}^{\max}\right)$ THEN (provide the maximum possible power using the fuel-cell system and the remainder using the supercapacitors).

Rule 4: etc.

As we can see from this little example, these rules are very easy to define, and they can also be easily supplemented if necessary. By way of illustration, rule 1 above can obviously be envisaged only within the maximum acceptable limit of the supercapacitors. It can therefore be built upon by limiting the validity of that rule as follows (with SOC_{SCAP} denoting the state of charge of the supercapacitors):

Rule 1 *bis*: IF $P_{dem} < 0$ AND IF $\left(SOC_{SCAP} < SOC_{SCAP}^{\max}\right)$ THEN (recharge the supercapacitors).

As we have seen, the definition of these fuzzy rules is very easy, and is based directly on human expertise about the procedure. Computerized processing of all these rules, which can operate in parallel to one another, is governed by fuzzy logic theory and is entirely compatible with real-time requirements.

6.4.3. *Criteria for the supervision of the energy flows*

Regardless of the strategy envisaged for the supervision of the energy flows in a hybrid electric system, we generally seek to optimize one of the criteria mentioned

above. This optimization is sometimes explicit – e.g. in the case of optimal control – and sometimes implicit, as in the case of fuzzy rules. Of the optimization criteria used, we can cite the following in particular (although this is by no means an exhaustive list):

– the "fatal" energy consumption (heat losses to be minimized, fossil fuel consumption in a hybrid vehicle to be minimized, hydrogen consumption in a fuel-cell-based installation to be minimized, etc.);

– the mass and/or volume of the electricity storage system;

– the dynamic performances of the electrical storage system;

– the cost of the system;

– its lifetime;

– its safety.

We can also seek to optimize several of these criteria simultaneously. In this case, we can use a composite criterion, defined as a function of the relative weight of each of the initial criteria.

6.5. Example of application in the domain of transport: the ECCE platform (*Evaluation des Composants d'une Chaine de traction Electrique* – Evaluation of the Components in an Electric Powertrain)

Here we are going to illustrate hybridization in electricity storage systems using an applied example taken from transport. In order to do so, we could have focused on different prototypes of vehicles offered by almost all manufacturers the world over. As we did not wish to make a (necessarily arbitrary) choice between these different prototypes, we have chosen to present a mobile platform for evaluating and testing components (particularly for onboard storage of electrical energy) in an electric traction chain.

Electric vehicles offer far better dynamic performances than those of vehicles driven by an internal combustion engine, but are heavily penalized by their limited range. In France, the *Direction Générale de l'Armement* (DGA – General Directorate for Armament) was therefore particularly interested in testing the different structures and electricity storage devices in a high-power hybrid vehicle. In view of the potential applications, serial hybridization is the most advantageous option in this case. This approach led to the design, construction and testing of the ECCE platform (see Figure 6.8), which was the fruit of a collaboration under the auspices of the DGA between industrialists and university and public research laboratories [KAU 11]. From the very beginning, this platform was designed in a

modular manner, so that it could be used to test different electrical storage devices on a full-size scale and in onboard conditions. Here, we shall focus on the particular case of energy supply to the DC bus, by a PEMFC system combined with supercapacitors and lead-acid accumulators. Thus, it uses a configuration combining permanent, pulsed and transitory energy storage. The diagram of the principle of the configuration considered for the vehicle is given in Figure 6.9.

ECCE in road tests ECCE equipped with a FC system

Figure 6.8. *ECCE mobile platform / equipped with a PEMFC system*

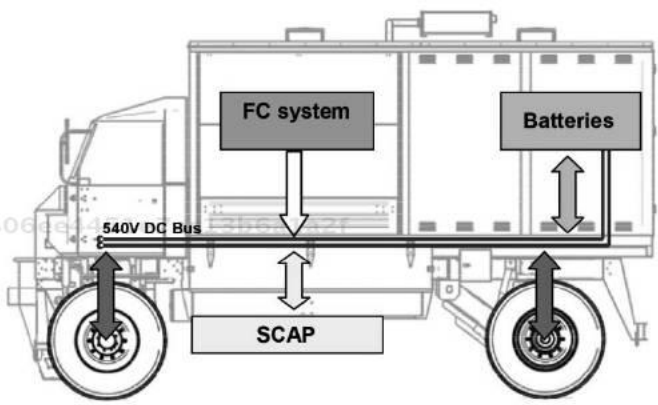

Figure 6.9. *Diagram of the principle behind ECCE in its FC / SCap / Batteries configuration*

Energy distribution takes place around a 540 V (± 270 V) DC bus, which is directly connected to the batteries. In view of the quantity of energy needed and the cost of the batteries, the decision was made to use energy-type lead-acid batteries. 90 elements (6 V; 98 Ah) were serialized, forming two groups, and the common point was linked to the bulk of the chassis. The batteries determined the maximum

current (462 A; 1min) in the charges and the recharging current (20 A) was chosen with a view to ensuring satisfactory battery life.

Up to four electric motors, each comprising 30 kW, were used to drive the vehicle. Each wheel had a converter feeding a motor to drive the wheel directly. As it was a mobile testing array, all four motors were of different types but all had the same nominal power of 30 kW. Thus, at the front, there was a permanent-magnet wheel motor with sine control and a permanent-magnet wheel motor with trapeze control. The magnets in these motors were mounted on the surface. At the rear, there was an induction motor with vector control and a synchronous claw-pole motor with sine control. The converters were adapted to the type of motor, with only the level of control in terms of torque, and therefore current, being pre-defined. It was the front motors which offered the best performances, particularly for the startup torque, which reaches up to six times the nominal torque of 700 N.m.

The fuel-cell system comprised two PEMFC stacks of 110 cells with an active surface area of 760 cm^2. Each fuel cell (FC) was supplied with air and hydrogen. An internal controller managed the FC system in its entirety (stacks, air compressor, flow meter, valves, etc.). A water cooling system was used and heat exchanges with the outside environment took place through an air/water exchanger. The FC system was connected to the 540 V bus via a DC/DC converter. The nominal electrical power that the FC system could deliver was 35 kW. Hydrogen was supplied from a rack of six canisters of compressed hydrogen (200 bars) installed behind the exchangers. Hydrogen sensors were of course installed to ensure safety in case of a leak.

The energy stored in the supercapacitors was sufficient to maintain the voltage on the DC bus following a demand for 40 kW of power for 9 seconds.

A fuzzy-logic-type strategy for management of the energy flows was put in place on this vehicle. More detailed information about this strategy is to be found in [SOL 12]. The on-road experimental results (see Figure 6.10) highlight the participation of the three energy sources (fuel-cell system, supercapacitors, batteries) in energy supply to the vehicle. Thus, we note that the bus voltage was properly maintained around the 540 V mark, although some fluctuations are observed which are attributable to the charging/discharging of the lead batteries (directly connected to the DC bus). The supercapacitors responded to the dynamic loading and were able to recover energy during braking. The fuel-cell system, for its part, provided power with a dynamic that was compatible with the supply of the reagent gases (particularly the supply of oxygen from the air, supplied by the air-compressor group).

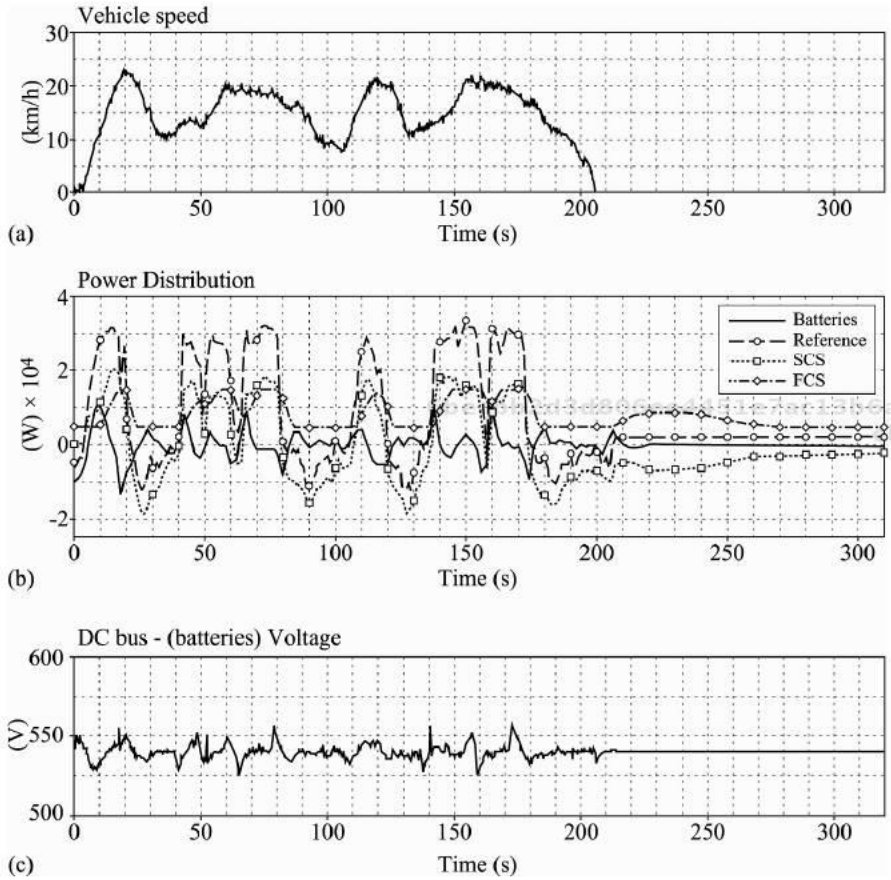

Figure 6.10. *On-road test results for ECCE in its FC / SCap / Batteries configuration*

6.6. Corrected exercises

6.6.1. *Ragone plot of an ideal battery*

We are interested here in tracing the Ragone plot for an "ideal" battery (meaning no inductive effect is taken into account, no frequency-dependency of the values, no intrinsic nonlinearity of the component). The battery is assumed to present a charge Q_0 at the initial time and an internal resistance of value R. It is connected to a charge/discharge system with constant power P (see the diagram below).

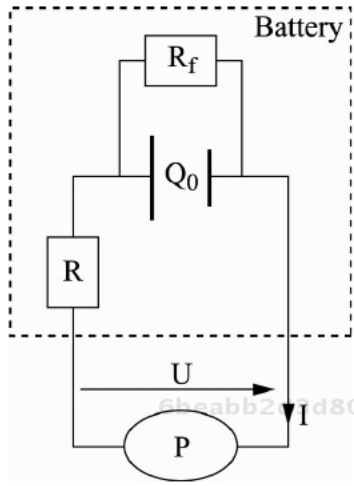

Figure 6.11. *Connection of an ideal battery to a charge with constant power*

1) Trace the Ragone plot for this ideal battery, assuming there to be no leakage resistance ($R_f = \infty$ on the diagram above).

2) Then trace the plot in the case where the leakage resistance has a finite value notated as R_f.

Solution

1) Here the battery is considered with a constant voltage (independent of the charge), given by:

$$\begin{cases} V = U_0 & \text{if} \quad Q_0 \geq Q > 0 \\ V = 0 & \text{if} \quad Q = 0 \end{cases}$$

Equation [7.2] is now written thus (with $I = \dot{Q}$):

$$P = U.I = (U_0 - RI)I$$

The solutions to this equation are written as:

$$I_{\pm} = \frac{U_0}{2R} \pm \sqrt{\frac{U_0^2}{4R^2} - \frac{P}{R}}$$

In order to identify the appropriate value of I, we focus on the case where $P \to 0$. In this case, two possibilities can be envisaged: $I_+ \to U_0 / R$ (which in practice corresponds to a short-circuited operation) and $I_- \to 0$ (which in practice corresponds to an open-circuit operation). Clearly, in the context of tracing the Ragone plot, only the second scenario here is of interest to us, so $I = I_-$.

The battery will be discharged after time $t_\infty = Q_0 / I$. The initial charge is linked to the initial energy according to: $E_0 = Q_0 U_0$. Thus, we can describe the energy available for the charge by writing:

$$E_{batt}(P) = P.t_\infty = \frac{2R.P.Q_0}{U_0 - \sqrt{U_0^2 - 4R.P}}$$

This last equation corresponds to the characteristic Ragone curve for the ideal battery. It can usefully be expressed in a dimensionless manner by setting $p = 4R.P / U_0^2$ and $e_{batt} = E_{batt} / (Q_0 U_0)$. Then we get:

$$e_{batt}(p) = \frac{1}{2} \frac{p}{1 - \sqrt{1-p}}$$

We can easily show that $\lim_{p \to 0} e_{batt}(p) = 1$ and that $e_{batt}(1) = 1/2$. The curve thus obtained is shown as a solid line in Figure 6.12.

2) If we wish to take account of a leakage resistance with a finite value R_f, the reasoning is exactly the same, but it is helpful to add to the previous discharge current a leakage current with the value U_0 / R_f. Thus, we obtain the following equation:

$$e_{batt}(p) = \frac{1}{2} \frac{p}{1 - \sqrt{1-p} + 2R / R_f}$$

We can see that in this case, $e_{batt}(0) = 0$ and that $e_{batt}(1) \cong 1/2$ (because we assume the leakage resistance to be significantly less significant than the internal resistance). We can also show that, here, the Ragone curve attains a maximum for a value of $p \approx \sqrt{\frac{8R}{R_f}}$.

The curve thus obtained is shown as a dotted line in Figure 6.12.

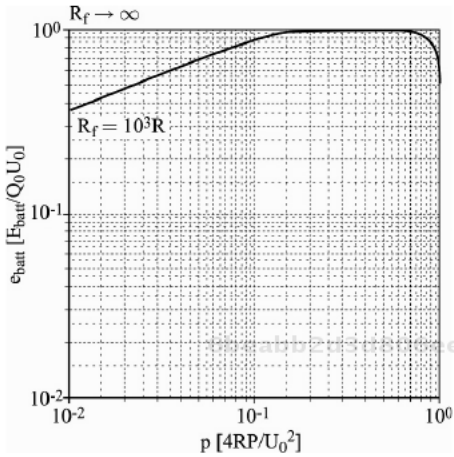

Figure 6.12. *Ragone plot of an ideal battery*

6.6.2. *Ragone plot of an ideal capacitor*

Draw the Ragone plot for an "ideal" capacitor, whose capacity C is supposed to be constant and whose only imperfection is an internal series resistance R. The initial voltage at the edges of the capacity is notated as $U_{C,0}$. The ensemble is connected to a charge/discharge system with constant power P (see the diagram below).

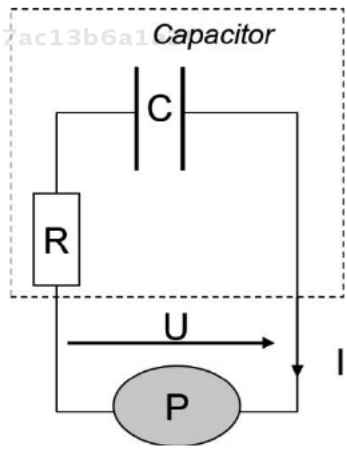

Figure 6.13. *Connection of an ideal capacitor to a charge with constant power*

Solution

By substituting the expression of $V(Q) = Q / C$ into equation [6.2], we can write:

$U = P / I = Q / C - RI$; here $I = -\dot{Q}$.

By deriving this equation in relation to time, we get:

$$\frac{dU}{dt} = \frac{1}{C}\frac{dQ}{dt} - R\frac{dI}{dt} = \frac{-P}{CU} + R\frac{P}{U^2}\frac{dU}{dt}$$

or indeed:

$$\left(1 - \frac{R.P}{U^2}\right)\frac{d\left(U^2\right)}{dt} = -\frac{2P}{C}$$

By integrating this last equation and noting that C, R and P are constants, we finally get:

$$t(U) = \frac{C}{2P}\left\{R.P \ln\left(\left(\frac{U}{U_0}\right)^2\right) + U_0^2 - U^2\right\}$$

The (theoretical) plot of this last curve demonstrates first a discharge of the capacitor, associated with an increase in time, followed by a discharge with a time that begins to decrease, which is physically impossible [SAI 04]. The result of this is the existence of a maximum (denoted $t_\infty = t(U_\infty)$ for a limited voltage value notated as U_∞) defined by $dt/dU = 0$ – for this maximum, the capacitor is no longer capable of providing the required power. We have:

$$\frac{dt}{dU} = \frac{C}{P}\left(R.P\frac{1}{U} - U\right)$$

Thus, $U_\infty = \sqrt{R.P}$ and:

$$t_\infty = \frac{C}{2P}\left\{R.P \ln\left(\frac{R.P}{U_0^2}\right) + U_0^2 - R.P\right\}$$

The required Ragone plot is therefore given by the following formula:

$$E_{cap}(P) = P.t_{\infty} = \frac{C}{2}\left\{R.P \ln\left(\frac{R.P}{U_0^2}\right) + U_0^2 - R.P\right\}$$

In this last equation, however, it is useful to be vigilant about the dependency of U_0 on the power required P. Indeed, we have $U_C = U + RI = U + R.P/U$. Therefore, we can calculate the initial voltage on the whole storage device U_0 as a function of the initial voltage at the edges of the capacity U_{C0} using the following equation:

$$U_0 = \frac{U_{C0}}{2} + \sqrt{\frac{U_{C0}^2}{4} - R.P}$$

From this, we can also deduce the final voltage (i.e. when the storage device is no longer able to provide the required power) at the edges of the capacity:

$$U_{C,\infty} = U_{\infty} + R.P/U_{\infty} = 2\sqrt{R.P}$$

Therefore, we know that there is a residual energy in the capacitor, calculable as:

$$E_{C,\infty} = 2.R.C.P$$

The maximum power that this storage device can supply and for which $E_{cap} \to 0$ is therefore linked to the energy initially stored by the relation:

$$P_{\max} = \frac{E_0}{2.R.C} = \frac{1/2C.U_{C,0}^2}{2.R.C} = \frac{U_{C,0}^2}{4R}$$

Finally, when tracing the Ragone plot (see Figure 6.14), it is helpful to switch to using dimensionless values, with $p = 2R.C.P/E_0$ and $e_{cap} = 2E_{cap}/(C.U_{C,0}^2)$. We then obtain the following expression:

$$e_{cap}(p) = \frac{1}{4}\left\{\left(1+\sqrt{1-p}\right)^2 - p - p\ln\left(\frac{\left(1+\sqrt{1-p}\right)^2}{p}\right)\right\}$$

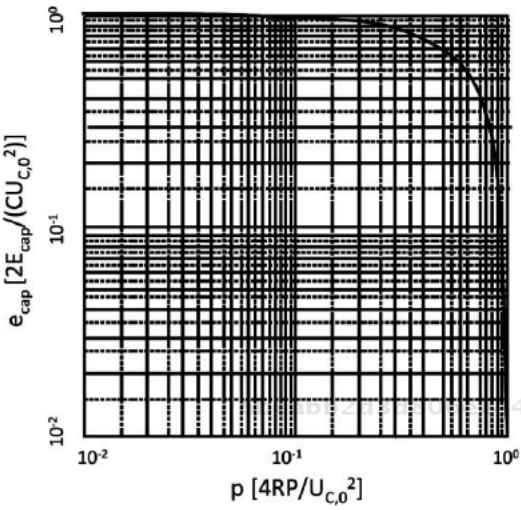

Figure 6.14. *Ragone plot for an ideal capacitor*

6.6.3. *Design of an electric vehicle*

We are interested in the traction chain of a small electric vehicle (segment A), whose efficiency (from the output of the electricity storage devices to the wheels) is assumed to be constant, equal to 0.8. Besides this efficiency, this vehicle's energy consumption is assumed to be served exclusively by aerodynamic friction, rolling friction and the onboard auxiliaries (particularly the air conditioning).

We assume that the mass of the vehicle is 600 kg (without the electricity storage devices, which we are attempting to design in this exercise).

The constraints set for the vehicle are as follows:

– facilitate driving at a stable speed of 130 km/h for at least 1 hour;

– be able to offer acceleration from 0 to 50 km/h in 8 seconds maximum;

– the electric traction chain intended here is based on the use of a fuel cell in conjunction with supercapacitors (whose lowermost voltage will be limited to 50% of their maximum voltage);

– the FC system (low-temperature PEMFC) in question exhibits limited dynamics (because of its auxiliaries) at 1 kW/s.

1) To simplify our calculations, we shall here consider the consumption of the onboard auxiliaries to be constant and equal to 3 kW. In view of these data and

constraints, suggest the most appropriate dimensions for the vehicle (mass of the fuel cell, mass of the supercapacitors). What is the mass of the vehicle thus obtained?

2) We now consider auxiliaries which no longer exhibit constant power demand, but rather a power level which can evolve by steps between the 3 kW and 9 kW levels. The 9 kW levels correspond to very short usage times. How does the sizing of the vehicle change in this case? What is the new mass of the vehicle thus obtained?

Additional data:

– the aerodynamic force is given by $F = \frac{1}{2}\rho.S.C.v^2$, where ρ is the density of air (1.2 kg/m^3, here assumed to be constant); S is the reference surface area (here supposed to be 1.8 m^2 for this small car); C is the aerodynamic coefficient (here taken as 0.35); and v is the velocity of the vehicle expressed in m/s;

– the rolling friction is given by $F = b.m.g$, with $m.g$ being the weight of the vehicle and b a friction coefficient, here taken to be constant and equal to 0.012 (vehicle with well-inflated tires).

Solution

1) Power demanded by the auxiliaries is supposed to be constant

* Calculate the vehicle's energy consumption at a stabilized speed of 130 [km/h].

– The aerodynamic force is therefore given by:

$$F_1 = \frac{1}{2}\rho.S.C.v^2 \cong 492.6\,[N]$$

The power consumed at the level of the energy storage device, which is related to this aerodynamic force, is therefore $P_1 = F_1.v/0.8 \cong 22.2\,[kW]$.

– The mass of the "bare" vehicle (i.e. without the addition of an energy storage device) is given as equal to 600 kg. The mass of the storage devices is *a priori* non-negligible, so we shall add to this vehicular mass an unknown mass notated as x corresponding to those storage devices. The rolling friction is given by:

$$F_2 = b.m.g = 0.012.(600+x)\times 9.81\,[N]$$

The power consumed at the level of the energy storage device, associated with this rolling friction, is given by:

$$P_2 = F_2.v/0.8 \cong \left(5.31\times10^{-3}\times x + 3.19\right)[kW]$$

The power consumed at the level of the energy storage device, associated with the consumption of the onboard auxiliaries is constant and equal to $P_3 = 3[kW]$ (NB: the efficiency of the powertrain is not taken into account here).

The power summoned by the energy storage devices at a stabilized velocity of 130 [km/h] is therefore:

$$P_{stab} = P_1 + P_2 + P_3 = \left(28.39 + 5.31\times10^{-3}\times x\right)[kW]$$

In view of the technical specifications, this power needs to be continuously furnished for at least 1 hour; therefore, it has to be supplied by a "permanent energy" source (here the fuel-cell system). If we refer to the Ragone plot shown in Figure 6.5, we note that a fuel-cell system presents a specific power of around $100[W/kg]$, which gives us:

$$\left(28.39 + 5.31\times10^{-3}x\right) = 0.1x$$

From this, we deduce the mass of the fuel-cell system that is needed: $x \cong 300[kg]$.

We note at this stage that the power associated with the rolling friction is equal to 28.39 [kW] if we do not take account of the mass of the fuel-cell system, as compared to 29.98 [kW] if we do take it into account. Hence, this represents only a slight increase in the power required (around 5%). For the dimensions of the supercapacitors (see below), this means we shall neglect (though this hypothesis needs to be verified later on) the increase in power requirement associated with the additional mass introduced by these supercapacitors.

* Now let us calculate the energy constraints associated with the accelerations prescribed in the technical specifications.

Assuming the acceleration to be constant, if we refer to Figure 6.15, the vehicle's velocity will follow a linear evolution over time. The energy that will be needed by the vehicle to take it from 0 to 50 [km/h] is therefore given by:

$$E = \frac{1}{2}.m.v^2 \cong 86800[J]$$

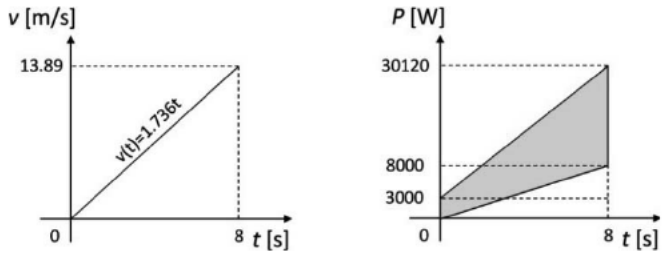

Figure 6.15. *Temporal characteristics from the technical specifications*

This means an average power required from the energy storage device of $\bar{P} = 13560\,[W]$ and a peak power of $P_{\max} = 27120\,[W]$. To these values, we need to add the 3 [kW] constant requirement of the vehicle's auxiliaries. Out of this power requirement, $8000\,[W]$ can be supplied by the fuel cell at $t = 8$ s (in view of the limitation of dynamics imposed on the fuel cell by the technical specifications). The rest of the power needed at $t = 8$ s therefore needs to be provided by the supercapacitors. Similarly, the energy corresponding to the shaded area in Figure 6.15 cannot be provided by the fuel cell and therefore must be supplied by the supercapacitors. Thus, this corresponds to two criteria for the dimensioning of the supercapacitors.

– Thus, in terms of power, the maximum power demand of the supercapacitors will therefore be $22120\,[W]$. Given the Ragone plot shown in Figure 6.5, if we consider a specific power of 3 kW/kg for the supercapacitors, this gives us approximately 7.4 kg of supercapacitors to satisfy the design criterion in terms of power;

– in terms of energy, the shaded area in Figure 6.15 corresponds to an energy of 100480 [*J*]. As the supercapacitors can only be discharged by 75% at most (see the design constraint in the statement of the question), they therefore need to be able to contain a level of energy of around 134000 *J*, which is approximately 37.2 [W.h]. Once again referring to the Ragone plot in Figure 6.15 and for a mass energy of 2.5 Wh/kg, we need around 14.9 kg of supercapacitors. Thus, here, the energy criterion is inflated in relation to the power criterion, so we shall use it.

* Finally, the dimension design proposed is therefore as follows:

– 300 kg for the fuel-cell system (whose power density is 100 W/kg);

– 14.9 kg of supercapacitors (for an energy density of 2.5 Wh/kg and a power density of 3 kW/kg); and so

– the total mass of the vehicle obtained is therefore 914.9 kg.

It is noteworthy that the increase in the mass of the vehicle associated with the supercapacitor is negligible in relation to that resulting from the use of the FC system. The hypothesis made earlier about the non-increase in the power requirement because of rolling friction is therefore vindicated.

2) Alteration of the dimensions in the case of peaks of power requirements by the vehicle's auxiliaries.

In this case, the base (3 kW of power needed by the auxiliaries) corresponds to the previous dimensions. The only difference lies in the necessity – specifically for the supercapacitors, given the stepped nature of the demand – to cater for an additional 6 kW of power requirement. We must stress here that it is a demand for additional power, not energy, because the duration of this demand is defined as being "very short".

Given that power is produced at a rate of 3 kW/kg, in order to supply an additional 6 kW for a few moments, we need to add 2 kg of supercapacitors to the result obtained previously for the power dimensions of the component. Thus, we get 9.4 kg instead of the previous 7.4 kg. Given the energy dimensions relative to these supercapacitors (still equal to 14.9 kg), it results that the array of supercapacitors defined in the previous exercise will be perfectly capable of catering for this additional indicial power requirement. Hence, obviously, the mass of the vehicle will not change.

6.6.4. *Energy management in an electric vehicle*

In this exercise, we return to the applied case of the mobile testing array described in section 6.5 above (the ECCE vehicle: *Evaluation des Composants d'une Chaine de traction Electrique*). The configuration under study is still the configuration combining fuel cells, supercapacitors and lead batteries.

1) Considering the technical data given about the ECCE vehicle and the fuel-cell system, give an estimation of the efficiency of the auxiliaries of the fuel-cell system.

2) Suggest a strategy to change the reference state of charge for the supercapacitors (notated as $SOC_{ref}(t)$), as a function of time and the change in the state of the vehicle.

3) As mentioned in section 6.5, the energy management proposed is based on fuzzy logic. For this fuzzy controller, two input variables are considered: the difference between the power demanded by the DC bus and the power supplied by the fuel-cell system (notatedas $\Delta P(t)$); and the change over time in the state of

charge of the supercapacitors (notated $\Delta SOC_{SCAP}(t)$). These two variables are defined by the following equations:

– $\Delta P(t) = P_{ref}(t) - P_{FC}(t)$

– $\Delta SOC_{SCAP}(t) = SOC_{ref}(t) - SOC_{SCAP}(t)$

The output variable of the fuzzy controller is the increment in power required of the fuel-cell system (denoted $\Delta P_{FC}(t)$) (see Figure 6.16)

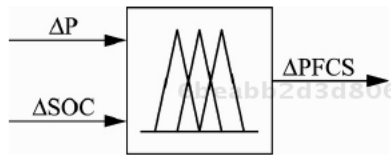

Figure 6.16. *Diagram of the principle behind the fuzzy controller in question*

Assuming that each input variable can be qualified by five "linguistic" states – NH (Negative High), NL (Negative Low), AZ (Almost Zero), PL (Positive Low), PH (Positive High) – and that the output variable can also be qualified by five "linguistic" states – HD (High Decrease in output Power), LD (Low Decrease in output Power), H (Hold the output Power), LI (Low Increase in output Power), HI (High Increase in output Power) – suggest realistic (fuzzy) rules for the management of the energy flows on board the vehicle.

Solution

1) The fuel-cell system under discussion comprises two stacks of 110 cells with 760 cm^2 active surface area. As we are dealing with a PEM fuel cell, a nominal current density of 0.5 A/cm^2 is usual. Therefore we shall retain this value. Similarly, a nominal voltage per cell of around 0.7 V is generally found. On the basis of these data, each stack therefore exhibits a nominal voltage of 77 V and a nominal current of 380 A, for a nominal raw power of 29.26 kW. The nominal power of the entire fuel-cell system (thus including the auxiliaries) is given as 35 kW. This enables us to determine that the efficiency of the auxiliaries of the fuel cell is around 60%.

2) In this application, the supercapacitors primarily serve during the phases of acceleration (providing power) and braking (absorbing power).

Thus, when the vehicle is stopped (velocity of zero), it seems obvious that the next phase of operation of the vehicle will be an acceleration. The SOC of the supercapacitors therefore needs to be as close as possible to the maximum SOC (typically for supercapacitors, $SOC_{ref} = 90\%$).

Similarly, when the vehicle reaches is maximum speed, it seems obvious that the next phase of its operation will be braking. The SOC of the supercapacitors therefore needs to be as close as possible to the minimum SOC (typically for supercapacitors, $SOC_{ref} = 25\%$).

Between these two extreme points, we can suggest a linear evolution of the SOC as a function of the vehicle's speed, as shown in Figure 6.17.

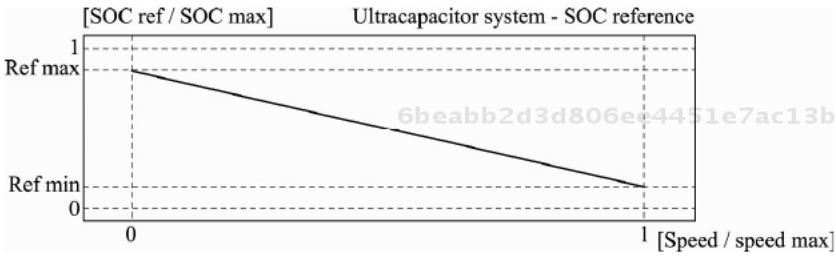

Figure 6.17. *Suggested dynamic evolution of SOC_{ref} of the supercapacitors, as a function of the vehicle's speed*

3) The fuzzy rules associating the five linguistic states of each input to the fuzzy controller with the five linguistic states of the output can be represented by an inference table (assuming an "and" between the predicates of each rule, and an "OR" between each of the rules thus defined). This inference table is obtained by expert knowledge of the system. One possible suggestion is formulated in the table below.

If ΔP is, etc. / and if ΔSOC is, etc. / Then ΔP_{FCS} is, etc.	NH	NL	AZ	PL	PH
NH	HD	HD	HD	LD	H
NL	HD	HD	LD	H	LI
AZ	HD	LD	H	LI	HI
PL	LD	H	LI	HI	HI
PH	H	LI	HI	HI	HI

Table 6.2. *Fuzzy inferences for energy management*

Bibliography

[AGB 12] AGBLI K.S., Modélisation multiphysique des flux énergétiques d'un Couplage Photovoltaïque-Electrolyseur PEM–Pile à Combustible PEM en vue d'une application stationnaire, Doctoral thesis, University of Franche-Comté, 2012.

[ALL 10] ALLÈGRE A.L., Méthodologies de modélisation et de gestion de l'énergie de systèmes de stockage mixtes pour véhicules électriques et hybrides, Doctoral thesis, University of Lille 1, 2010.

[ALL 11a] ALLEAU T., "Les programmes hydrogène et piles à combustible au Japon", *Mémento de l'hydrogène*, fiche 8.5, Association Française de l'Hydrogène, 2011.

[ALL 11b] ALLEAU T., "L'historique de l'hydrogène", *Mémento de l'hydrogène*, fiche 1.1, Association Française de l'Hydrogène, 2011.

[ALL 11c] ALLEAU T., "L'historique de l'hydrogène", *Mémento de l'hydrogène*, fiche 3.2.1, Association Française de l'Hydrogène, 2011.

[ALS 10] AL-SAKKA M., Supercondensateurs et convertisseurs DC/DC pour véhicule à pile à combustible, Doctoral thesis, Vrije Universiteit Brussel and University of Technology of Belfort-Montbéliard, 2010.

[AMI 07] AMIET M., "La théorie des 3^E", *Revue Enseigner l'Electrotechnique et l'Electronique Industrielle*, no. 48, pp. 30–35, 2007.

[AND 12] ANDERSON E., "Recent advances in PEM electrolysis and their implications for hydrogen energy markets", *Symposium Water Electrolysis and Hydrogen as Part of the Future Renewable Energy System*, Copenhagen, Denmark, May 2012.

[AND 09] ANDRIEUX J., Stockage de l'hydrogène dans les borohydrure salcalins hydrolyse du borohydrure de sodium, Doctoral thesis, University of Lyon 1, 2009.

[ATK 96] ATKINS P.W., *The Elements of Physical Chemistry*, 2nd edition, Oxford University Press, 1996.

[BAD 12] BADEY Q., Étude des mécanismes et modélisation du vieillissement des batteries lithium-ion dans le cadre d'un usage automobile, Doctoral thesis, University of Paris-Sud, 22 March 2012.

[BEG 08] BEGOT S., HAREL F., KAUFFMANN J.M., *et al.*, "Freeze-thaw ageing effects on PEM fuel cells", *FDFC'2008 Fundamentals and Developments of Fuel Cells*, 8 pp., Nancy, France, 2008.

[BEL 01] BELHACHEMI F., Modélisation et caractérisation des supercondensateurs à couche double électrique utilisés en électronique de puissance, Doctoral thesis, Institut National Polytechnique de Lorraine, 2001.

[BEN 05] BEN AHMED H., MULTON B., ROBIN G., *et al.*, "Le stockage de l'énergie dans les applications stationnaires", *Revue Technologie – Sciences et Techniques Industrielles*, no. 136, pp. 60–66, 2005.

[BER 07] BERNARD J., Véhicules hybrides à pile à combustible: dimensionnement et stratégies de commande, Doctoral thesis, University of Valenciennes and of Hainaut-Cambrésis, 2007.

[BON 97] BONERT R., ZUBIETA L., "Measurement techniques for evaluation of double-layer power capacitors", *IEEE-Industry Application Society '97*, vol. 2, New Orleans, USA, pp. 1097–1100, October 1997.

[BON 98] BONERT R., ZUBIETA L., "Characterization of double-layer capacitors for power electronics applications", *IEEE-Industry Application Society '98*, St. Louis, USA, pp. 1149–1154, October 1998.

[BOU 08] BOULON L., PÉRA M.C., DELARUE P., *et al.*, "Causal fuel cell system model suitable for transportation simulation applications", *ASME Journal of Fuel Cell Science and Technology*, vol. 49, pp. 880–895, 2008.

[BOU 06] BOURGEOIS R., "Advanced Alkaline Electrolysis", *General Energy Global Research Center*, http://www.hydrogen.energy.gov/pdfs/review06/pd_8_bourgeois.pdf, 2006.

[BOU 07] BOURGEOIS R., "Advanced Alkaline Electrolysis", *General Energy Global Research Center*, http://www.hydrogen.energy.gov/pdfs/review07/pdp_16_bourgeois.pdf, 2007.

[BRA 79] BRAUN M., *Wasserelektrolyse – Basis einer künftigen Wasserstoffwirstschaft*, Chimia, 3, pp. 99–104, 1979.

[BUR 00] BURKE A., "Ultracapacitor: why, how, and where is the technology", *Journal of Power Sources*, no. 91, pp. 37–50, 2000.

[BUS 03] BUSQUET S., Etude d'un système autonome de production d'énergie couplant un champ photovoltaïque, un électrolyseur et une pile à combustible: réalisation d'un banc d'essai et modélisation, Doctoral thesis, Ecole des mines de Paris, 2003.

[CAI 01] CAILLON G., "Accumulateurs portables", *Technique de l'Ingénieur, Traité d'Electronique*, p. 34, 2001.

[CAM 07] CAMARA M.B., Supercondensateurs pour échange dynamique d'énergie à bord des véhicules électriques hybrides : modélisation, étude des convertisseurs et commande, Doctoral thesis, University of Franche-Comté, 2007.

[CAN 07] CANDUSSO D., GLISES R., HISSEL D., *et al.*, "Piles à combustible PEMFC et SOFC Description et gestion du système", *Techniques de l'Ingénieur Génie Energétique*, pp. 1–18, October 2007.

[CEZ 02] CEZARD A., COLLAS F., MARECHE J.F., *et al.*, "Porous electrodes-based double-layer supercapacitors: pore structure versus series resistance", *Journal of Power Sources*, pp. 1–10, 2002.

[CHA 99] CHAPOULIE P., Modélisation systémique pour la conception de véhicules électriques multi-sources, Doctoral thesis, Institut National Polytechnique de Toulouse, 1999.

[CHA 07] CHAN C.C., "The state of the art of electric, hybrid, and fuel cell vehicles", *Proc. of the IEEE*, vol. 95, no. 4, pp. 704–718, April 2007.

[CHA 09] CHARLOU J.-L., "Hydrates de Gaz et Hydrogène : ressources de la mer du futur ?", in *La chimie et la mer: Ensemble au service de l'homme*, Edition Broché, 2009.

[CON 99] CONWAY B.E., *Electrochemical supercapacitors – Scientific fundamentals and technological applications*, Kluwer Academic/Plenum Publishers, New York, 1999.

[CHR 00] CHRISTEN TH., CARLEN M.W., "Theory of Ragone plots", *Journal of Power Sources*, vol. 91, pp. 210–216, 2000.

[CHR 08] CHRENKO D., PÉRA M.C., HISSEL D., *et al.*,"Macroscopic modeling of a PEFC system based on equivalent circuits of fuel and oxidant supplying", *ASME Journal of Fuel Cell Science and Technology*, vol. 5, no. 1, pp. 011015-1/011015-8, 2008.

[CLE 05] CLEFS CEA, *Le stockage embarqué de l'hydrogène*, no. 50/51, winter 2004–2005.

[DAR 10a] DARRAS C., SAILLER S., THIBAULT C., *et al.*, "Sizing of photovoltaic system coupled with hydrogen/oxygen storage based on the ORIENTE model", *International Journal of Hydrogen Energy*, vol. 35, no. 8, pp. 3322–3332, 2010.

[DAR 10b] DARRAS C., Modélisation de systèmes hybrides Photovoltaïque / Hydrogène : Applications site isolé, micro-réseau, et connexion au réseau électrique dans le cadre du projet PEPITE (ANR PAN-H), Doctoral thesis, University of Corsica, 2010.

[DEL 97] DELFOSSE F., Détermination de l'état de charge des batteries d'un véhicule électrique, University of Liège, Faculty of Applied Sciences, academic year 1997–1998.

[DEL 02] DELPRAT S., Elaboration de stratégies de commande pour véhicules hybrides parallèle, Doctoral thesis, University of Valenciennes and Hainaut-Cambrésis, 2002.

[DEM 07] DEMKOWICZ P., MEDVEDEV P., DEWALL K., *et al.*, *Materials degradation studies for high temperature steam electrolysis systems*, International Topical Meeting on the Safety and Technology of Nuclear Hydrogen Production, Control, and Management, June 2007.

[DEM 10] DE MAEYER R., *HySTAT™ on site hydrogen*, Hydrogenics – Visit to Waterstofregio to Oevel, http://www.waterstofnet.eu/upload/File/presentatiehydrogenics/OSG_Presentation%20may%2027%202010.pdf, 27 May 2010.

[DER 05] DERBAL H., MIRI R., M'RAOUI A., "Etude d'un système de production d'hydrogène par voie solaire. Application sur l'électrolyse de la vapeur d'eau à très hautes températures", *Revue des Energies Renouvelables*, vol. 8, pp. 137–156, 2005.

[DEV 12] DEVILLERS N., Caractérisation et modélisation de composants de stockage électrochimiques et électrostatiques, Doctoral thesis, University of Franche-Comté, 2012.

[DIA 96] DIARD J.P., GORREC B.L., MONTELLA C., *Cinétique électrochimique*, Hermann, Paris, 1996.

[DO 10] DO D.V., Diagnostic de batteries Lithium ion dans des applications embarquées, Doctoral thesis, University of Technology of Compiègne, 5 July 2010.

[DOE 82] DOENITZ W., SCHMIDBERGER R., "Concepts and design for scaling up high temperature water vapour electrolysis", *International Journal of Hydrogen Energy*, vol. 7, no. 4, pp. 321–330, 1982.

[DOE 85] DOENITZ W., ERDLE E., "High temperature electrolysis of water vapour – Status of development and perspectives for application", *International Journal of Hydrogen Energy*, vol. 10, pp. 291–295, 1985.

[EIA 11] International Energy Outlook 2011, U.S. Energy Information Administration EIA, DOE/EIA-0484(2011), September 2011.

[ENC 08] "Ritter, Johann Wilhelm", *Complete Dictionary of Scientific Biography*, Encyclopedia.com: http://www.encyclopedia.com/doc/1G2-2830903689.html, 2008.

[FEI 06] FEIDT M., *Energétique Concepts et Applications*, Dunod, Paris, 2006.

[FUS 09] FUSALBA F., MARTINET S., "Stockage électrochimique: piles et batteries", in *Problématiques du stockage d'énergie*, Chapter 8, Hermes-Lavoisier, France, pp. 205–227, 2009.

[GAI 11] GAILLY F., Alimentation électrique d'un site isolé à partir d'un générateur photovoltaïque associé à un tandem électrolyseur/pile à combustible (batterie H_2/O_2), Doctoral thesis, Institut National Polytechnique de Toulouse, 2011.

[GAI 12] GAILLY F., TURPIN C., ASTIER S., *et al.*, "Stand-alone site power supply based on a photovoltaic generator and a H2/O2 battery", *International Conference on Power and Energy Systems*, Hong-Kong, April 2012.

[GAY 12] GAY C., **Amélioration de l'efficacité énergétique des systèmes de micro-cogénération : association pile à combustible SOFC / Moteur Stirling**, Doctoral thesis, University of Franche-Comté, 2012.

[GEN 09] GENOVESE J., HARG K., PASTER M., *et al.*, "**Current (2009) State-of-the-Art hydrogen production cost estimate using water electrolysis**", *Independent Review published for the U.S. Department of Energy Hydrogen Program*, National Renewable Energy Laboratory, NREL/BK-6A1-46676, September 2009.

[GER 10] GÉRARD M., POIROT-CROUVEZIER J.P., HISSEL D., *et al.*, "**Oxygen starvation analysis during air feeding faults in PEMFC**", *International Journal of Hydrogen Energy*, vol. 35, no. 22, pp. 12295–12307, 2010.

[GER 11] GÉRARD M., POIROT-CROUVEZIER J.P., HISSEL D., *et al.*, "**Ripple current effects on PEMFC aging test by experimental and modeling**", *ASME Journal of Fuel Cell Science and Technology*, vol. 8, pp. 021004-1/021004-5, April 2011.

[GHO 03] GHOSH P.C., EMONTS B., JANßEN H., *et al.*, "**Ten years of operational experience with a hydrogen-based renewable energy supply system**", *Solar Energy*, vol. 75, no. 6, pp. 469–478, 2003.

[GLA 12] GLAIZE C., GENIÈS S., *Les accumulateurs électrochimiques au plomb et au nickel*, Hermès/Lavoisier, 2012.

[GLA 13] GLAIZE C., GENIÈS S., *Accumulateurs électrochimiques au lithium, haute température et à circulation d'électrolyte*, Hermès/Lavoisier, 2013.

[GOF 08] GOFFÉ B., "**Des sources d'énergie au fond des mers**", *CNRS Le journal*, no. 216, 2008.

[GON 12] GONI-URTIAGA A., PRESVYTES D., SCOTT K., "**Solid acids as electrolyte materials for proton exchange membrane (PEM) electrolysis: Review**", *International Journal of Hydrogen Energy*, no. 37, pp. 3358–3372, 2012.

[GUA 07] GUALOUS H., GALLAY R., "**Applications des supercondensateurs**", *Techniques de l'Ingénieur*, D3335, 2007.

[GUA 11] GUALOUS H., LOUAHLIA-GUALOUS H., GALLAY R., "**Supercapacitors characterization and thermal modelling with reversible and irreversible heat effect**", *IEEE Transactions on Power Electronics*, vol. 26, no. 11, pp. 3402–3409, 2011.

[HAH 04] HAHN M., BAERTSCHI M., BARBIERI O., *et al.*, "**Interfacial capacitance and electronic conductance of activated carbon double-layer electrodes**", *Electrochemical and Solid State Letters*, vol. 7, no. 2, pp. A33–A36, 2004.

[HAH 05] HAHN M., WÜRSIG A., GALLAY R., *et al.*, "**Gas Evolution in Activated Carbon / Propylene Carbonate Based Double-Layer Capacitors**", *Electrochemical Communication*, vol. 5, pp. 925–930, 2005.

[HAL 1919] HALE A.J., "**The manufacture of chemicals by electrolysis**", *A treatise of electro-chemistry*, edition B. Blout, London, Constable & Company, 1919.

[HAM 11] HAMDAN M., *PEM electrolysis*, GINER Inc./GES, available at http://www1.eere.energy.gov/hydrogenandfuelcells/pdfs/webinarslides052311_pemelectrolysis_hamdan.pdf, 23 May 2011.

[HAM 06] HAMMAR A., Modélisation du superconducteur et étude de son vieillissement: utilization dans les applications de transport ferroviaire, Doctoral thesis, University Claude Bernard Lyon, 2006.

[HAN 08] HANKACHE W., Gestion optimisée de l'énergie électrique d'un groupe électrogène hybride à pile à combustible, Doctoral thesis, Institut National Polytechnique de Toulouse, 2008.

[HAU 86] HÄUSSINGER P., LOHMÜLLER R., WATSON A.M., "Hydrogen", Ullmann's Encyclopedia of Industrial Chemistry, Wiley-VCH, online library, 1986.

[HGM 11] "Hydrogen Generation Market - by Merchant & Captive Type, Distributed & Centralized Generation, Application & Technology - Trends & Global Forecasts (2011 – 2016)", *EP 1708*, marketsandmarkets.com, 2011.

[HIN 04] HINO R., HAGAA K., AITAB H., *et al.*, "R&D on hydrogen production by high-temperature electrolysis of steam", *Nuclear Engineering and Design*, vol. 233, pp. 363–375, 2004.

[HIS 09] HISSEL D., PÉRA M.C., CANDUSSO D., "Pile à combustible : aspect système", *Problématique du stockage d'énergie*, Chapter 7, Hermes-Lavoisier, France, pp. 205–227, 2009.

[HYD] "Fiches techniques de la série HySTAT", available at: http://www.hydrogenics.com/hydro/brochure/IndustrialBrochure_EN/index.html#/6/

[IEA 11] Energy balances, International Energy Agency, Edition 2010.

[IFR 11] SYNTHÈSE COLLECTIVE, *Les resources minérales marines profondes* – Synthèse d'une étude prospective à l'horizon 2030, IFREMER, 2011.

[IVY 04] IVY J., "Summary of Electrolytic Hydrogen Production", National Renewable Energy Laboratory, NREL/MP-560–36734, 2004.

[JAN 12] "La Croix Valmer, commune pilote d'un projet d'autonomie énergétique innovant", *Dossier de presse*, 10 July 2012.

[JEN 08] JENSEN J.O, BANDUR V., BJERRUM N.J., *et al.*, Pre-investigation of water electrolysis, Report PSO-F&U 2006-1-6287, available at: http://www.energinet.dk/SiteCollectionDocuments/Danske%20dokumenter/Forskning%20-%20PSOprojekter/6287%20-%20Elektrolyse%20ved%20over%20100%20gr.%20C.pdf, version as at 4 February 2008.

[JON 92] JONSSON V.K., GUNNASSON R.L., ARNASON B., *et al.*, "The feasability of using geothermal energy in hydrogen production", *Geothermics*, vol. 21, no. 5/6, pp. 673–681, 1992.

[KAU 11] KAUFFMANN J.M., HISSEL D., AMIET M., "ECCE véhicule hybride: du militaire vers le civil", *Journal 3EI*, vol. 64, pp. 74–81, 2011.

[KER 09] KERMANI S., Gestion énergétique des véhicules hybrides : de la simulation à la commande temps réel, Doctoral thesis, University of Valenciennes and Hainaut-Cambrésis, 2009.

[KLE 69] KLEIN M., ASTRIN R., *Hydrogen-oxygen electrolytic regenerative fuel cells*, NASA CR-1244, February 1969.

[KOL 09] KOLIATENE F., Contribution à l'étude de l'existence des décharges dans les systèmes de l'avionique, Doctoral thesis, University of Toulouse, 2009.

[KOT 00] KOTZ R., CARLEN M., "Principles and applications of electrochemical capacitors", *Electrochimica Acta*, no. 45, pp. 2483–2498, 2000.

[KRO 06] KROPOSKI B., LEVENE J., HARRISON K., *et al.*, Electrolysis: Information and Opportunities for Electric Power Utilities, National Renewable Energy Laboratory, NREL/TP-581-40605, September 2006.

[KRU 02] KRUSE B., GRINNA S., BUCH C., Hydrogen – Status og mulugheter, Bellona report no. 6, www.bellona.org/filearchive/fil_Hydrogen_6-2002.pdf, 2002.

[LAG 12] LAGUNA-BERCERO M.A., "Recent advances in high temperature electrolysis using solid oxide fuel cells: A review", *Journal of Power Sources*, vol. 203, pp. 4–16, 2012.

[LAR 09] LARGEOT C., Développement de supercondensateurs carbone/carbone: relation entre la taille des ions de l'électrolyte et la taille des pores de la matière active, Doctoral thesis, University of Toulouse, 2009.

[LAR 00] LARMINIE J., DICKS A., *Fuel cell systems explained*, John Wiley & Sons, 2000.

[LAF 08] LAFFLY E., Modélisation d'une pile à combustible de type PEMFC intégrant les phénomènes de vieillissement, Doctoral thesis, University of Franche-Comté, 2008.

[LEF 09] LEFROU C., FABRY P., POIGNET J.C., *Electrochimie approche des fondamentaux*, EDP Sciences, Paris, 2009.

[LEF 11] LEFEBVRE-JOUD F., MOUGIN J., PETITJEAN M., "Degradation issues in High Temperature Steam Electrolyzers", *2nd International Workshop on Degradation Issues of Fuel Cells*, Thessaloniki, Greece, September 2011.

[LEN 03] LENDASSE A., *Analyse et prédiction de séries temporelles par méthodes non linéaires – Application à des données industrielles et financières*, Presses Universitaires de Louvain, 2003.

[LEV 67] DE LEVIE R., *Advances in Electrochemistry and Electrochemical Engineering*, vol. 6, pp. 329–397, 1967.

[LEV 99] DE LEVIE R., "The electrolysis of water", *Journal of Electroanalytical Chemistry*, no. 476, pp. 92–93, 1999.

[MAM 10] MAMADOU K., Prévision de la disponibilité énergétique des accumulateurs électrochimiques par estimation d'états d'énergie (S.O.E.), Doctoral thesis, University of Grenoble, 2010.

[MAR 04a] MARIE-FRANÇOISE J.N., Contribution à la commande neuronale et à la gestion de l'énergie d'un système hybride batterie - supercondensateurs: Application aux transports terrestres, Doctoral thesis, University of Franche-Comté, 2004.

[MAR 04b] MARTINET S., ROUAULT H., POINSO J.Y., "Nouvelles voies dans les accumulateurs lithium et les électrolytes de batteries", *Clefs CEA*, no. 50/51, 2004.

[MAS 86] MASKALICK N.J., "High temperature electrolysis cell performance characterization", *International Journal of Hydrogen Energy*, vol. 11, no. 9, pp. 563–570, 1986.

[MAX 12] http://www.maxwell.com/

[MIL] MILLER T.B., Nickel-Hydrogen Battery Cell Life Test Program Update for the International Space Station, http://www.grc.nasa.gov/WWW/RT/RT1999/5000/5420miller.html.

[MIL 07] MILLET P., "Electrolyseurs de l'eau à membranes acides", *Techniques de l'ingénieur*, J4810, 2007.

[MIT 97] MITLITSKY F., "The unitized regenerative fuel cell", *Science & Technology Review*, May 1997.

[MIT 98] MITLITSKY F., MYERS B., WEISBERG A.H., "Regenerative Fuel Cell Systems R & D", Lawrence Livermore National Laboratory, UCRL-JC-131087, June 1998.

[MIT 11] MITTELSTEADT C., "Regenerative fuel cells for energy storage", *Giner, Inc, Giner Electrochemical Systems*, http://www1.eere.energy.gov/hydrogenandfuelcells/pdfs/rev_fc_wkshp_mittelsteadt.pdf, April 2011.

[MON 09] Montaru M., Contribution à l'évaluation du vieillissement des batteries de puissance utilisées dans les véhicules hybrides selon leurs usages, Doctoral thesis, Institut National Polytechnique de Grenoble, 2009.

[MOR 06] MORENO J., ORTUZA M.E., DIXON J.W., "Energy management system for a hybrid electric vehicle, using ultracapacitors and neural networks", *IEEE Trans. on Industrial Electronics*, vol. 53, no. 2, pp. 614–623, 2006.

[MUL 04] MULTON B., ROGIN G., ERAMBERT E., *et al.*, "Stockage de l'énergie dans les applications stationnaires", *Colloque Energie et Transport Terrestre*, p. 12, Belfort, France, 2004.

[MUL 08] MULOT J., NIETHAMMER M., MUKERJEE S., *et al.*, "Development update on Delphi's solid oxide fuel cell systems", *Fundamentals and Development in Fuel Cells FDFC 2008*, Nancy, 2008.

[MYR] Website for the MYRTE (Mission hYdrogène Renouvelable pour l'inTégration au réseau Electrique) platform, http://myrte.univ-corse.fr/.

[NOS 12] NOSHIN O., Assessment of rechargeable energy storage systems for plug-in hybrid electric vehicles, Doctoral thesis, Vrije Universiteit Brussel (VUB), Brussels, September 2012.

[OUS 97] OUSTALOUP A., MOREAU X., MATHIEU B., Commande CRONE : Principe et exemple d'applications. *Techniques de l'ingénieur,* Mesures mécaniques et dimensionnelles, 1997.

[PER 06] PÉRA M.C., Modélisation de systèmes de conversion d'énergie électrique complexes, Accreditation to Supervise Research, University of Franche-Comté, 2006.

[PER 07] PÉRA M.C., CANDUSSO D., HISSEL D., *et al.*, "Power generation by fuel cells", IEEE-Industrial Electronics Magazine, vol. 1, no. 3, pp. 28–37, 2007.

[PER 08] PÉRA M.C., CHRENKO D., HISSEL D., "De la pile à combustible à son integration système", *3EI Enseigner l'Electrotechnique et l'Electronique Industrielle*, no. 55, pp. 38–42, 2008.

[PHL 09] PHLIPPOTEAU V., Outils et Méthodes pour le diagnostic d'un état de santé d'une pile à combustible, Doctoral thesis, Institut National Polytechnique de Toulouse, 2009.

[POW 10] "Powergenix", www.powergenix.com, 2010.

[PY] PY J.P, CAPITAINE A., Hydrogen production by high temperature electrolysis of water vapour and nuclear reactors, http://www.cder.dz/A2H2/Medias/Download/Proc%20PDF/PARALLEL%20SESSIONS/%5BS05%5D%20Production%20-%20Water%20Electrolysis/15-06-06/414.pdf.

[QUA 86] QUANDT K.H., STREICHER R., "Concept and design of a 3.5 MW pilot plant for high Temperature electrolysis of water vapor", *International Journal of Hydrogen Energy*, vol. 11, no. 5, pp. 309–315, 1986.

[RAF 07] RAFIK F., Caractérisation et modélisation des supercondensateurs: Application aux systèmes d'automatismes 'pick and place', Doctoral thesis, University of Franche-Comté, 2007.

[RAG 68] RAGONE D.V., "Review of battery systems for electrically powered vehicles", *Mid-year meeting of the society of automotive engineers*, Detroit, USA, 1968.

[RAL 11] RALLIERES O., Modélisation et caractérisation de piles à combustible et électrolyseurs PEM, Doctoral thesis, Institut National Polytechnique de Toulouse, 2011.

[RAN 98] RAND D.A.J., WOOD R., *Batteries for electric vehicles*, Research Studies Press Ltd, 1998.

[RAS 03] RASTEN E., HAGEN G., TUNOLD R., "Electrocatalysis in water electrolysis with solid polymer electrolyte", *Electrochimica Acta*, vol. 48, pp. 3945/3952, 2003.

[REL] http://www.relhy.eu/

[ROB 04] ROBERT J., ALZIEU J., "Accumulateurs, considérations théoriques", *Techniques de l'ingénieur*, D3351, 2004.

[ROB 05] ROBERT J., ALZIEU J., "Accumulateurs, Accumulateurs à oxyde de Nickel", *Techniques de l'ingénieur*, D3353, 2005.

[SAI 04] SAISSET R., Contribution à l'étude systémique de dispositifs énergétiques à composants électrochimiques, Doctoral thesis, Institut National Polytechnique de Toulouse, 2004.

[SAU 08] SAUR G., "Wind-To-Hydrogen Project: Electrolyzer Capital Cost Study", National Renewable Energy Laboratory, NREL/TP-550-44103, December 2008.

[SCH 00] SCHUCAN T., "Case studies of integrated hydrogen energy systems", Paul Scherrer Institute, Final report IEA/H2/T11/FR1-2000, 2000.

[SCO 04] SCORDIA J., Approche systématique de l'optimisation du dimensionnement et de l'élaboration de lois de gestion d'énergie de véhicules hybrides, Doctoral thesis, Henri Poincaré University – Nancy 1, 2004.

[SMO 12] SMOLINKA T., GARCHE J., HEBLING C., *et al.*, Overview on water electrolysis for hydrogen - Production and storage, Symposium - Water electrolysis and hydrogen as part of the future Renewable Energy System, Copenhagen, Denmark, 12 May 2012.

[SOL 11] SOLANO-MARTINEZ J., HISSEL D., PÉRA M.C., *et al.*, "Practical control structure and energy management of a testbed hybrid electric vehicle", *IEEE Trans. on Vehicular Technology*, vol. 60, no. 9, pp. 4139–4152, 2011.

[SOL 12] SOLANO-MARTINEZ J., Modélisation et supervision des flux énergétiques à bord d'un véhicule hybride lourd: approche par logique floue de type 2, Doctoral thesis, University of Franche-Comté, 2012.

[STE 00] STEVENS P., NOVEL-CATTIN F., HAMMOU A., *et al.*, "Piles à combustibles", *Techniques de l'ingénieur - Traité de Génie Electrique*, vol. D3 - D3340, pp. 1–28, 2000.

[STO 10a] STOLTEN D., *Hydrogen and fuel cells: fundamentals, technologies and applications*, Wiley-VCH, July 2010.

[STO 10b] STOLTEN D., KRIEG D., WEBER M., "An Overview on Water Electrolysis", *International Workshop on Hydrogen and Fuel Cells - WICaC 2010,* Campinas, Brazil, October, 2010.

[STR 08] STRAND A., WEYDAHL H., "Regenerative fuel cell systems for satellites", *CMR Prototech*, www.prototech.no/doc/PDF%20files/RFCS%20artikkel.pdf, 2008.

[STU 98] STUCKI S., SCHERER G.G., SCHLAGOWSKI S., *et al.*, "PEM water electrolysers: evidence for membrane failure in 100 kW demonstration plants", *Journal of Applied Electrochemistry*, vol. 28, no. 10, pp. 1041–1049, 1998.

[SUN 12] SUNDE S., "Water electrolysis technology – concepts and performance", *Sushgen Spring School Fuel Cells and Hydrogen Technology*, Newcastle, March 2012.

[SUR 07] SURESH B., YONEYAMA M., SCHLAG S., "CEH marketing research report abstract – hydrogen", *Chemical Industries Newsletter*, SRI Consulting, October 2007.

[SUT 12] SUTHERLAND E., "Overview of water electrolysis and renewable hydrogen activities in the US DOE portfolio, U.S. Department of Energy", *Symposium Water Electrolysis and Hydrogen as Part of the Future Renewable Energy System*, Copenhagen, Denmark, May 2012.

[SWA 08] SWALLA D., Advanced Alkaline Electrolysis, General Energy Global Research Center, http://www.hydrogen.energy.gov/pdfs/review08/pdp_14_swalla.pdf, 2008.

[TEK 07] TEKIN M., HISSEL D., PÉRA M.C., *et al.*, "Energy management strategy for embedded fuel cell system using fuzzy logic", *IEEE Trans. on Industrial Electronics*, vol. 54, no. 1, pp. 595–603, 2007.

[THA 03] THALLER L.H., ZIMMERMAN A.H., "Overview of the design, development, and application of nickel-hydrogen batteries", *NASA/TP-2003-211905*, 2003.

[TRA 99] TRASATTI S., "Water electrolysis: who first?", *Journal of Electroanalytical Chemistry*, vol. 476, pp. 90–91, 1999.

[TSI 12] TSIPLAKIDES D., PEM water electrolysis fundamentals, http://research.ncl.ac.uk/sushgen/docs/summerschool_2012/PEM_water_electrolysisFundamentals_Prof.Tsiplakides.pdf, 2012.

[TUR 08] TURPIN C., Piles à combustible et composants électrochimiques de stockage : caractérisation, modélisation et mise en œuvre dans des systèmes énergétiques, Accreditation to Supervise Research, Institut National Polytechnique de Toulouse, January 2008.

[VAN 06] VAN DEN BOSSCHE P., VERGELS F., VAN MIERLO J., *et al.*, "SUBAT: an assessment of sustainable battery technology", *Journal of Power Sources*, vol. 162, pp. 913–919, 2006.

[VER 11] VERDU O., "High Power PEMFC Backup Power Systems - Field test experiment feed-back", *Fundamentals and Development in Fuel Cells FDFC 2011*, Grenoble, 2011.

[WAH 07] WAHDAME B., CANDUSSO D., FRANÇOIS X., *et al.*, "Comparison between two PEM fuel cell durability tests performed at constant current and under solicitations linked to transport mission profile", *International Journal of Hydrogen Energy*, vol. 32, no. 17, pp. 4523–4536, 2007.

[WAN 11] WANG K., HISSEL D., PÉRA M.C., *et al.*, "A review on solid oxide fuel cell models", *International Journal of Hydrogen Energy*, vol. 36, no. 12, pp. 7212–7228, 2011.

[WIK 13a] Wikipedia, Chronologie des technologies de l'hydrogène: http://fr.wikipedia.org/wiki/Chronologie_des_technologies_de_l%27hydrog%C3%A8ne. Accessed on 25 April 2013.

[WIK 13b] Wikipedia, Electrolysis of water: http://en.wikipedia.org/wiki/Electrolysis_of_water. Accessed on 25 April 2013.

[WIK 13c] Wikipedia, Gramme Machine: http://en.wikipedia.org/wiki/Gramme_machine. Accessed on 25 April 2013.

[WIK 13d] Wikipedia, Johann Wilhelm Ritter: http://en.wikipedia.org/wiki/Johann_Wilhelm_Ritter. Accessed on 25 April 2013.

[WIK 13e] Wikipedia, Voltamètre de Hofmann, http://fr.wikipedia.org/wiki/Voltam%C3%A8tre_d'Hofmann. Accessed on 25 April 2013.

[WIK 13f] Wikipedia, Nickel de Raney, http://fr.wikipedia.org/wiki/Nickel_de_Raney. Accessed on 25 April 2013.

[WIK 13g] Wikipedia, NASA Pathfinder, http://en.wikipedia.org/wiki/NASA_Pathfinder. Accessed on 25 April 2013.

[WIK 13h] Wikipedia, Christian Schönbein, http://fr.wikipedia.org/wiki/Christian_Schönbein. Accessed on 25 April 2013.

[WIK 13i] Wikipedia, Gaston Planté, http://fr.wikipedia.org/wiki/Gaston_Planté. Accessed on 25 April 2013.

[ZEI 11] ZEIDAN M., Etude expérimentale et modélisation d'une micropile à Combustible à respiration, Institut National Polytechnique de Toulouse, 2011.

[ZEN 10] ZENG, K., ZHANG, D., E., "Recent progress in alkaline water electrolysis for hydrogen production and applications", *Progress in Energy and Combustion Science* 36, pp. 307–326, 2010.

[ZOU 06] ZOULIAS E., VARKARAKI E., LYMBEROPOULOS N., *et al.*, A Review on Water Electrolysis, Project report "Cluster pilot project for the integration of renewable energy sources into European energy sectors using hydrogen", *Centre for Renewable Energy Sources (CRES)*, Pikermi, Greece, 2006.